THE UNIVERSITY
of EDINBURGH

The origin and maintenance of Kupffer Cells in homeostasis and liver injury

Catherine Alice Hawley

THE UNIVERSITY *of* EDINBURGH

Submitted for the degree of Doctor of Philosophy

The University of Edinburgh

2019

Acknowledgements

Firstly I must thank my primary supervisor Steve Jenkins, for all of his guidance and support throughout the 5 years I have been working on this PhD, and especially for sticking with me over the two years it has taken to write the thesis. Also to my second supervisor Ian Dransfield for his advice during my 3 years in the lab, particularly with how to get started on putting the thesis together.

Thanks to the Lab Legends, Fiona, Joanne, Ruairi, Anna and Calum for their help, support and friendship across my 3 years in the lab. You guys kept me sane, and I especially remember our coffee breaks with much fondness. Anna, thanks for being a great friend, for your help in the lab, and for keeping me calm before my RIPs. Ruairi, thanks for your help with harvests and liver preps on big experiment days. Calum, thank you for all of your guidance, help and support, as a friend and a mentor. You helped me find my feet, and taught me the ropes when it comes to flow cytometry. Thanks also for the post-work pub trips, I certainly needed them!

Thank you to my parents and parents-in-law for all of their continuing love and support throughout my time in Edinburgh, and since moving to York to write the thesis. Special thanks to Sue for all of your help looking after Reuben every week – without it I don't know how I would have managed to write this thesis, so a huge thank you!

Finally, the biggest thanks is to my husband, Andrew. Thank you doesn't seem like enough to describe how much your unwavering support means to me. You've been there all the way – picking me up from work when I finished on the flow cytometer at late at night, listening to me practise my presentations, listening to me talk about work for hours at a time and sharing in my highs and lows. You supported me throughout my pregnancy and as we welcomed Reuben into the world, and then continually encouraged and supported me to finish writing, taking Reuben away for days and weekends so I could focus. I absolutely could not have achieved this without you, and the completion of this thesis is truly a joint triumph.

Table of Contents

Declaration

I declare that this thesis has been composed by myself and that the work has not be submitted for any other degree or professional qualification except as specified. I confirm that the work submitted is my own, except where indicated in the text. Work which has formed part of jointly-authored publications has also been included. My contribution and those of the other authors to this work have been explicitly indicated below. I confirm that appropriate credit has been given within this thesis where reference has been made to the work of others.

Some of the work presented in Chapter 3 was previously published in The Journal of Leukocyte Biology as part of the article 'An efficient method to isolate Kupffer Cells eliminating endothelial cell contamination and selective bias' by Ruairi W Lynch*, Catherine A Hawley*, Antonella Pellicoro, Calum C Bain, John P Iredale and Stephen J Jenkins (supervisor). This study was conceived by all of the authors. I designed, performed and analysed experiments, and wrote the manuscript with Ruairi Lynch. All figures presented in chapter 3 are my own work, and although many of the figure panels are included in the publication, they have not been directly lifted from the published article. The paper is included at the back of this thesis as an appendix.

The work presented in Chapter 4 was previously published in The Journal of Immunology as '*Csf1r*-mApple transgene expression and ligand binding in vivo reveal dynamics of CSF1R expression within the mononuclear phagocyte system' by Catherine A Hawley*, Rocio Rojo*, Anna Raper*, Kristin A Sauter, Zofia M Lisowski, Kathleen Grabert, Calum C Bain, Gemma M Davis, Pieter A Louwe, Michael C Ostrowski, David A Hume, Clare Pridans and Stephen J Jenkins (supervisor). This study was conceived by all of the authors. I performed and analysed experiments, and created figures as indicated in chapter 4. The paper is included in the chapter.

Catherine Hawley

Abstract

Evaluation of liver resident Kupffer Cells (KC) has shown that in mouse these cells derive from a population of foetal liver monocytes that seed the tissues during embryogenesis and maintain themselves in steady state conditions independently of circulating monocytes, via local proliferation. The factors which regulate this KC autonomy have not yet been determined, but likely comprise both biochemical and physical factors which form their 'niche'. Furthermore, their regulation, and specifically whether they retain total autonomy from monocyte-derived macrophages following liver injury has not been extensively studied. In this thesis I aimed to address the role of availability of the macrophage growth factor CSF1 in maintenance of KC and their autonomy from monocytes in homeostasis, and the roles and long-term fate of KC and monocyte-derived macrophages following acute and chronic liver injury.

An optimal method for isolation and identification of F4/80^{hi}CD11b^{lo} KC for flow cytometric analysis was first established. To explore the role of CSF1 in maintenance of KC, *Csf1r*-mApple mice were generated which revealed that KC expressed the highest levels of the *csf1r*-mApple transgene compared with other leukocytes in the liver. *In vivo* administration of fluorescently-labelled CSF1-Fc^{AF647} revealed that KC captured 10x more circulating CSF1 per cell than other myeloid cells in the liver and lung, suggesting efficient capture of CSF1 may be one mechanism that allows KC to regulate differentiation of monocytes in the liver. Delivery of CSF1-Fc to chimeric mice led to an increase in proliferation and accumulation of resident KC and a transient increase in the number of bone marrow-derived F4/80^{hi}CD11b^{lo} cells in the liver, which were lost by 2 weeks following withdrawal of CSF1-Fc. These bone-marrow derived macrophages did not express the putative KC marker Tim4, indicating that they did not fully adopt a KC phenotype.

Acute CCl_4-driven liver injury resulted in a transient loss of approximately 50% of the resident KC population which recovered in number by 6 days post injury, through proliferation of the remaining KC. This was despite the fact that injury led to the massive recruitment of monocyte-derived macrophages some of which matured into an F4/80^{hi}CD11b^{lo} population, but which also lacked Tim4 expression. These cells were spatially distinct from KC and were found clustered around blood vessels, presumed to be the region of necrotic damage. Comparison of gene expression was consistent with their involvement in tissue repair. Following CCl_4-driven chronic liver injury, KC were depleted in number, but unlike in acute

injury, the population did not return to normal numbers even 8 weeks following cessation of treatment. This time, the recruited macrophages these were not found in clusters but alongside resident KC in the parenchyma. However, in both acute and chronic injury, monocyte-derived macrophages could no longer be seen 8 weeks after injury, and did not mature into long-lived, self-renewing KC.

In conclusion I found that CSF1 is one of the major limiting factors that dictates the size of the KC niche, but additional factors are required to fully support monocyte engraftment to the KC population. Following CCl_4-driven acute liver injury, monocyte-derived macrophages do not contribute long-term to the KC population despite exhibiting a F4/80^{hi}CD11b^{lo} phenotype during the latter stages of liver repair. KC are depleted long-term following CCl_4-driven chronic liver injury, but monocyte-derived macrophages remain unable to replenish the population, indicating that damage to a physical component of the KC niche may have occurred

Lay Summary

Macrophages are cells of the immune system present in every organ in the body. They maintain tissue health by clearing dead and dying cells, and also switch on other immune cells when there is injury or infection.

Liver disease represents a serious global health and economic burden and macrophages are involved in disease progression and repair and regeneration. In the healthy liver there is one population of macrophages but during liver disease these cells are out-numbered by an additional population of macrophages which are recruited from the bone marrow.

These two populations of macrophages have differing roles and to target them for therapeutics we must first understand the differences between them. Additionally, macrophages which arrive in the liver during disease may replace the resident population that was present in the healthy liver. This may have long-term adverse consequences for liver function.

I aimed to understand how macrophages are maintained in healthy and damaged liver using animal models and markers to distinguish between the resident and recruited macrophages. I found that the resident macrophages present in the healthy liver are very separate from the recruited macrophages, and were not replaced by them following acute or chronic liver injury. I found that multiple factors contribute to the maintenance of the healthy liver, including a growth factor, and possibly being in direct contact with other cell types in the liver. The recruited macrophages honed to the area of injured liver and may play a role in tissue repair. Increased understanding of the relationship between these two types of macrophage may help with developing new therapies to treat liver injury and disease.

List of abbreviations

α-SMA	α-smooth muscle actin
4-OHT	4-hydroxytamoxifen
7-AAD	7-amino-actinomycin D
AF700	Alexafluor 700
AGM	Aorta-gonad-mesonephros
ALT	Alanine aminotransferase
AM	Alveolar macrophage
APAP	N-acetyl-p-aminophenol (acetaminophen/paracetamol)
APC	Allophycocyanin
AST	Aspartate aminotransferase
BM	Bone marrow
CCL	Chemokine ligand
CCl_4	Carbon tetrachloride
CCR	Chemokine receptor
CD	Cluster of differentiation
cDC	Classical dendritic cell
CLEC4f	C-type lectin 4f
CMoP	Common monocyte progenitor
CSF1	Colony stimulating factor 1
CSF1R	Colony stimulating factor 1 receptor
DAMP	Damage associated molecular pattern
DAPI	4'6-diamidino-2-phenylindole
DMEM	Dulbecco's modified eagle medium
DT	Diphtheria toxin
DTR	Diphtheria toxin receptor

EDTA	Ethylenediaminetetraacetic acid
EMP	Erythromyeloid progenitor
FACS	Flow Assisted Cell Sorting
FCS	Foetal calf serum
FITC	Fluorescein isothyocyanate
FMO	Fluorescence minus one
GeoMFI	Geometric mean fluorescence intensity
GFP	Green fluorescent protein
H2B	Histone 2B
HBSS	Hank's balanced salt solution
HCC	Hepatocellular carcinoma
HFD	High fat diet
HLA	Human leukocyte antigen
HMGB-1	High mobility group box 1
HSC	Haematopoietic stem cell
HSP	Heat shock protein
Ig	Immunoglobulin
IL	Interleukin
iNOS	Inducible nitric oxide synthase
ip	Intra peritoneal
ISI	Ischaemia reperfusion injury
iv	Intra venous
KC	Kupffer Cell
LC	Langerhans cell
LPS	Lipopolysaccharide
LSEC	Liver sinusoidal endothelial cell

Mϕ	Macrophage
MCD	Methionine- and choline- deficient diet
MDP	Monocyte and dendritic cell precursor
MHC	Major histocompatibility complex
MMP	Matrix metalloproteinase
MPS	Mononuclear phagocyte system
NAFLD	Non-alcoholic fatty liver disease
NGS	Normal goat serum
NK cell	Natural Killer cell
OCT	Optimal cutting temperature compound
PAMP	Pattern associated molecular pattern
PAS	Periodic acid schiff
PBS	Phosphate buffered saline
pDC	Plasmacytoid dendritic cell
PDL1	Programmed death ligand 1
PE	Phycoerythrin
Pen/strep	Penicillin/Streptavidin
PFA	paraformaldehyde
PO	Peroxidase
PRR	Pattern recognition receptor
RBC	Red blood cell
RPMI	Rosewell Park Memorial Institute medium
SA	Streptavidin
sc	Sub cutaneous
TGF-β	Transforming growth factor β
TLR	Toll like receptor

TNF-α	Tumour necrosis factor α
WT	Wild type
YFP	Yellow fluorescent protein

List of publications

Stutchfield BM, Antoine DJ, Mackinnon AC, Gow DJ, Bain CC, Hawley CA, Hughes MJ, Francis B, Wojtacha D, Man TY, Dear JW, Devey LR, Mowat AM, Pollard JW, Park BK, Jenkins SJ, Simpson KJ, Hume DA, Wigmore SJ, Forbes SJ, (2015), CSF1 restores innate immunity after liver injury in mice and serum levels indicate outcomes of patients with acute liver failure, *Gastroenterology*, **149 (7):** 1896-1909

Bain CC, Hawley CA, Garner H, Scott CL, Schridde A, Steers NJ, Mack M, Joshi A, Guilliams M, Mowat AM, Geissmann F, Jenkins SJ, (2016), Long-lived self-renewing bone marrow-derived macrophages displace embryo-derived cells to inhabit adult serous cavities, *Nature Communications*, **7:** ncomms11852

Hawley CA*, Rojo R*, Raper A*, Sauter KA, Lisowski ZM, Grabert K, Bain CC, Davis GM, Louwe PA, Ostrowski MC, Hume DA, Pridans C, Jenkins SJ, (2018), Csf1r-mApple transgene expression and ligand binding reveal dynamics of CSF1R expression within the mononuclear phagocyte system, *Journal of Immunology*, **200 (6):** 2209-2223

Lynch RW*, Hawley CA*, Pellicoro A, Bain CC, Iredale JP, Jenkins SJ, (2018), An efficient method to isolate Kupffer cells eliminating endothelial cell contamination and selective bias, *Journal of Leukocyte Biology*, **104 (3):** 579-586

*denotes joint first authorship

Table of figures

Chapter 1: Introduction

1.1 General overview

Immunology is a broad term that encompasses the study of immune responses to injury, infection and disease, to self-antigens resulting in allergy, auto-immunity or cancer, but also the homeostatic role of innate immune cells in maintaining tolerance to food, pollen and microbiota antigens, in clearance of dead and dying cells, and tissue remodelling. At the heart of these homeostatic immune functions are macrophages, which are present in vast numbers in all tissues of the body. Cells with macrophage-like morphology and function appear across both vertebrate and invertebrate species including worms, molluscs and sponges (Buchmann 2014), indicating that they have highly conserved and indispensable functions. Elie Metchnikoff noted macrophages first in 1882 when he described their phagocytic functions within tissues. Macrophages are an extremely diverse group of cells which maintain tissue health, initiate inflammatory immune responses, but conversely also dampen inflammation and contribute to tissue repair. They can be short-lived and recruited from bone marrow precursors in times of inflammation or stress, or they can be very long lived, surviving in the tissue from before birth and into adulthood, proliferating *in situ*. Thus the term 'macrophage' encompasses a great number of distinct cell populations, of which the roles and developmental relationships between them are still to be fully understood; the major paradigm that in adults macrophages are continually replenished by their precursors monocytes from a pool of haematopoietic stem cells, which has largely governed our understanding of macrophage biology for the last century and a half, is currently being rewritten. In this introduction I will first summarise the roles of monocytes and macrophages, and will then examine in detail what was known about their origins and developmental relationships at the point at which I commenced this project. I will then focus on the resident macrophages of the liver, Kupffer Cells (KC), as the maintenance and origin of KC forms the focus of this thesis.

1.2 Tissue macrophages and the mononuclear phagocyte system

1.2.1 Traditional view of the mononuclear phagocyte system

After their initial discovery, the cellular origin of macrophages was heavily debated in the earlier half of the 20th century, driven by a desire within the scientific community to classify macrophages into their correct 'system'. Aschoff observed in 1924 that endothelial cells were also capable of phagocytosis and grouped the two cell types into what he called the 'reticuloendothelial system' (Aschoff 1924). This term was used by immunologists and clinicians until van Furth and Cohn proposed that macrophages be grouped into the 'mononuclear phagocyte system' (MPS) along with their pre-cursors monocytes (van Furth et al. 1972). This new classification was made on the basis that tissue macrophages were observed to be replenished by blood monocytes after lethal irradiation, and that monocytes were also capable of phagocytosis (van Furth et al. 1972). Thus it became dogma that all macrophages present in the steady state and during infection and inflammation are derived from bone marrow haematopoietic stem cell (HSC) precursors via a circulatory monocytic intermediary. Although some aspects of this original proposal have been demonstrated to hold true, the linear description that bone marrow precursors give rise to monocytes which give rise to macrophages is overly simplistic, and will be discussed in further detail later in this introduction.

1.2.2 Monocytes subsets and function

Adult monocytes are circulating cells which mature in the bone marrow (BM) from HSCs via a series of progenitors: first the Common Myeloid Progenitors (CMP), which give rise to Monocyte and Dendritic Cell Precursors (MDP) and then the Common Monocyte Progenitor (CMoP) (Hettinger et al. 2013). In mice, monocytes can be split into two subtypes, delineated on the basis of Ly6C expression: Ly6C^{hi}, or classical monocytes, and Ly6C^{lo}, or non-classical monocytes. These subsets parallel CD14^{+}CD16^{-} and CD14^{-}CD16^{+} monocytes in humans respectively (Ziegler-Heitbrock et al. 2010). The murine subsets can be further defined by their expression of chemokine receptors; Ly6C^{hi} monocytes express CCR2, but express only low levels of CX3CR1, whilst Ly6C^{lo} monocytes are CCR2^{-} but express high levels of CX3CR1. Ly6C^{hi} monocytes require CCR2 to emigrate from the bone marrow into the blood, and they accumulate in the bone marrow of *Ccr2*$^{-/-}$ mice (Serbina and Pamer, 2006). Studies that used adoptive transfer of both monocyte subsets from CX3CR1$^{+/GFP}$ mice suggested that the role

of classical monocytes was to emigrate from the circulation to tissues during inflammation, whilst non-classical monocytes were recruited to tissues under homeostatic conditions (Geissmann et al. 2003). However, more recent studies indicate that the two subsets represent a developmental sequence, with short-lived Ly6C^{hi} monocytes, which have a half-life of around 20 hours (Yona et al. 2013), giving rise to the more long-lived (4-10 days) Ly6C^{lo} monocytes (Varol et al. 2007; Yona et al. 2013). An additional heterogenous 'transitional' or Ly6C^{int} subset (or CD14^{lo}CD16^{+} in humans) has also been defined (Ziegler-Heitbrock et al. 2010; Mildner et al. 2017), further supporting their developmental relationship. Whilst Ly6C^{hi} monocytes very clearly do give rise to macrophages in both homeostasis and inflammation (Guilliams et al. 2018), the role of monocytes is now thought to stretch beyond simply that of a precursor to macrophages, as they also have important functions in their undifferentiated state. For example, Ly6C^{lo} monocytes have been observed to patrol the lumen of blood vessels, and have even been termed the 'resident macrophage' of the circulatory system (Hanna et al. 2011; Carlin et al. 2013; Auffray et al. 2007), as in homeostatic conditions they remove cell debris, phagocytose apoptotic cells, and present antigen which may also lead to tolerogenic responses (Thomas et al. 2015).

1.2.3 Roles of tissue macrophages

Macrophages are large, highly differentiated myeloid cells found in every tissue in the body. They have protrusions which allow them to 'feel' into the tissue, giving them a stellate, or star-like appearance. The name macrophage translates literally from Greek as 'big eater', an accolade to their highly efficient phagocytic ability. However, their roles are many and diverse, contributing to maintenance of healthy tissue, responding to infection or injury and subsequent tissue repair. Additionally, inappropriate activation of macrophages can lead to autoimmunity and cancer.

In the steady state, macrophages perform a host of functions including tissue surveillance, phagocytosis of dead and dying cells, tissue remodelling, and providing cytokines and chemokines. The precise nature of the role of macrophages is specific to the tissue in which they reside, and although core shared functions of macrophages across tissues are programmed by macrophage lineage transcription factors such as PU.1 (Lavin et al. 2014), they also exhibit transcriptional identities that arise in response to local microenvironmental signals (Lavin et al. 2014; Epelman et al. 2014b), resulting in highly specialised functions. For

example, alveolar macrophages (AM) clear excess surfactant in the alveolar space, and AM depletion either directly or as a result deficiency in their main growth factor GM-CSF leads to pulmonary alveolar proteinosis (Dranoff et al. 1994; Forbes et al. 2007; Trapnell et al. 2009). In the brain, microglia (the resident macrophage population) are required for efficient synaptic pruning, and CX3CR1-knock out mice which have a severe reduction in microglia demonstrate delayed pruning and immature synapses (Paolicelli et al. 2011). Splenic red pulp macrophages are efficient at recycling iron from senescent red blood cells which filter through the spleen (Kohyama et al. 2009), whilst peritoneal macrophages can respond to local retinoic acid signals to control IgA production by B1 cells (Okabe and Medzhitov 2014).

Macrophages are also professional antigen presenting cells, expressing MHCII on their surface (Hume 2008), and their presentation of self-antigen along with innocuous particles breathed in the air or ingested in food, appears to actively suppress T cell-specific responses, resulting in peripheral tolerance (Heymann et al. 2015; Munn et al. 1996). The pan macrophage marker F4/80 appears to be required for this tolerogenic response as mice deficient in functional F4/80 fail to develop $CD8^+$ T regulatory cells capable of suppressing an antigen-specific delayed-type hypersensitivity reaction (Lin et al. 2005).

In addition to their steady state roles, macrophages are a critical part of the innate immune response to infection and injury. They are activated very early in the immune response through their recognition of damage associated molecular patterns (DAMPs) and pattern-associated molecular patterns (PAMPs) via pattern recognition receptors (PRRs). DAMPs are released by dying cells and include molecules such as heat shock protein 60 (hsp60) – which is detected by the toll-like receptors TLR2 and TLR4 resulting in TNF-α secretion and nitric oxide production (Ohashi et al. 2000) – or ATP which acts as a 'find-me' signal, promoting their phagocytosis of apoptotic cells by macrophages (Elliott et al. 2009). PAMPs are conserved moieties derived from pathogens, for example LPS, which is sensed by TLR4 leading to a proinflammatory response via an IL-6 pathway (Greenhill et al. 2011). Once activated, macrophages can also recruit additional immune cells via chemokine secretion. Neutrophils are recruited first, for example to the spleen at the onset of *Candida* infection due to CXCL1 and CXCL2 production by splenic red pulp macrophages (Kanayama et al. 2015). Monocytes are then recruited to tissues and rapidly differentiate into macrophages where they also contribute to the inflammatory immune response but then switch to a pro-restorative phenotype, contributing to wound healing (Minutti et al. 2017). Thus resident macrophages and monocyte-derived macrophages very often co-exist during the

inflammation and repair phases of injury or infection, although in many injury and infection models their exact differing roles are still to be clearly defined. For example, although use of LysMCre-DTR mice to delete macrophages clearly demonstrated delayed wound closure in a skin inflammation model compared to control mice (Lucas et al. 2010), this model could not distinguish between resident and recruited macrophages since LysM is universally expressed by macrophages and monocytes as well as neutrophils (Orthgiess et al. 2016). However, tools to better distinguish between resident and recruited macrophages, and monocytes are currently available and are detailed below.

1.2.4 Tools to assess the relationship between monocytes and macrophages

There are a range of tools available to investigate the relationship between monocytes and macrophages, allowing researchers to deplete specific macrophage or monocyte populations, and trace their differentiation, proliferation and survival. Total body, lethal irradiation of mice leads to severe depletion of bone marrow cells, and of many radio-sensitive immune cell populations in tissues, including resident macrophages in most organs. Reconstitution with bone marrow from a congenic mouse strain produces a chimera in which HSCs are of donor bone marrow origin, allowing their fates in tissues to be tracked using flow cytometry or imaging methods. Although irradiation chimeras have been used for decades in macrophage research, the improvement in multi-colour flow cytometry over the last 10 years or so has allowed for much more detailed and sophisticated analysis of the monocyte and macrophage compartments in more recent studies. Currently, the most commonly used system in mouse takes advantage of CD45.1 and CD45.2, which are naturally occurring isoforms of CD45, for which there are very good commercially available antibodies, to distinguish between host and donor cells. A variation of this protocol is to shield the organs of interest with a lead brick to prevent damage to, or loss of the resident cells in the tissue. These ‘partially irradiated’ or ‘protected’ chimeras therefore allow tracking of monocytes (or other precursor cells of interest) into tissues without disrupting the incumbent resident macrophage population. Similarly, parabiosis, which is the joining of two mice via their circulatory systems can be used to track recruitment of circulating cells from one parabiotic partner to the tissues of the other partner, again allowing researchers to determine the level of recruitment of monocytes to macrophage populations. Knock out mice have been available for decades, and can be effectively used to deplete a precursor population to look

at the effect on the mature populations they normally differentiate into. However, a global knockout deletes the gene in all cells which express it, which may have major functional consequences in cell types other than those of direct interest. Fluorescent reporter mice are widely available for many genes of interest, but all cells expressing the gene of interest will be labelled, and they only label current gene expression. Thus the Cre-lox system is very often used in which a specific gene promoter drives Cre expression, resulting in excision of a stop codon upstream of the gene for a fluorescent reporter. Constitutive Cre mice, in which there is constant Cre expression, can be used to label current and historic gene expression, but does not allow distinction between the two. Inducible Cre systems, usually requiring tamoxifen administration to activate Cre expression, can be used to label cells within a specific time window to trace their fate, and the fate of their progeny. Yona and colleagues used CX3CR1$^{gfp/+}$, constitutive CX3CR1$^{Cre/+}$:R26-yfp and inducible CX3CR1$^{CreER/+}$:R26-yfp mice side by side. The reporter (CX3CR1^{GFP}) demonstrated that most tissue macrophages don't express CX3CR1, but come from a precursor which expressed CX3CR1 at some point in its development (shown by the constitutive Cre), but largely persist independently of CX3CR1^{+} monocytes (shown by the inducible Cre) (Yona et al. 2013).

An overview of the tools currently available to researchers in the macrophage field are detailed in table 1.1

Table 1.1 Tools to investigate the relationships between monocytes and macrophages in mouse

Tool	Pros	Cons	References
Total body irradiation chimeras	Can be reconstituted with bone marrow from wild type mice, reporter/Cre mice; Can make competitive bone marrow chimeras	Irradiation damages populations of interest; Can only study from 8 weeks onwards; Irradiation may mobilise; Animals given antibiotics; Potential inflammatory response to irradiation	(Klein et al. 2007; Bain et al. 2014; Molawi et al. 2014; Merad et al. 2002; Guilliams et al. 2013)
Partially protected irradiation chimeras	Protects the population of interest from irradiation; Reduces inflammatory response to irradiation; Can be reconstituted with bone marrow from wild type mice, reporter/Cre mice; Can make competitive bone marrow chimeras	Can only study from 8 weeks onwards; Animals given antibiotics; Systemic effects of irradiation of extremities unknown	(Jenkins et al. 2011)
Parabiosis	Exchange of circulating cells, antigens and immune factors without triggering an immune reaction; Can stitch partners of different strains/gender/age	Ethically questionable; Animals given antibiotics; Risk of death through wound infection	(Hashimoto et al. 2013; Bain et al. 2014; Guilliams et al. 2013; Molawi et al. 2014; Merad et al. 2002)
Knock out	Does not require tamoxifen administration; Highly efficient way to silence a gene	May universally knock out gene from all populations - cannot study knock out on only specific populations; Gene redundancy means population of interest may still persist	(Bain et al. 2014)
Fluorescent reporter	Widely available for lots of genes; Multiple fluorescent colours available; No requirement for tamoxifen	May label multiple populations in addition to population of interest; Only reports current gene expression (this could also be a pro)	(Yona et al. 2013)
Constitutive Cre	No requirement for tamoxifen administration – cheaper/easier; Can study fate from embryogenesis	Can have low recombination efficiency; Overlap in gene expression means multiple populations may be labelled; No control over when populations become labelled; Possible Cre toxicity	(Hashimoto et al. 2013; Yona et al. 2013; Gomez Perdiguero et al. 2014; Bain et al. 2014)
Inducible Cre	Labels cells within specific time-frame; Can study different populations depending on timing of tamoxifen; Can study cell fate from embryogenesis	Can have low recombination efficiency; Overlap in gene expression means multiple populations may be labelled even with single tamoxifen dose;	(Yona et al. 2013; Bain et al. 2014; Gomez Perdiguero et al. 2014; Hoeffel et al. 2015; Schulz et al.

		Must administer tamoxifen – could have side effects; Possible Cre toxicity	2012; Ginhoux et al. 2010)

1.3 Macrophage self-renewal and embryonic origin

1.3.1 Embryonic myelopoiesis

The traditional view of the MPS that all tissue macrophages require replenishment by adult circulating monocytes has recently been challenged. However, before I explore what is now known about the relationship between monocytes and macrophages, I will first look at how myelopoiesis occurs in the embryo, as this is when the very first macrophage populations are formed. Tissue macrophage populations are established in the embryo before the onset of mature haematopoietic stems cells. In mouse, the first blood cells are produced within blood islands that begin to form in the extraembryonic yolk sac from gestational day E7-E7.5 (Haarl and Adolph, 1970), and it is here that primitive erythropoiesis is established (Silver and Palis 1997). The additional presence of macrophages in the yolk sac was first recorded over a century ago, and early studies in the 70s and 80s consolidated this work, identifying F4/80^{+} cells of macrophage morphology in the yolk sac from day 10 of gestation (Cline and Moore 1972; Takahashi et al. 1989). These studies provided evidence that the very first macrophages were developmentally distinct from those described by the MPS.

Until recently, and when I started my PhD, two waves of haematopoiesis had been described during development, with the first, 'primitive' wave of progenitors capable of giving rise to primitive macrophages in the yolk sac, followed by the onset of 'definitive' haematopoiesis with the generation of HSCs in the aorta-gonad-mesonephros (AGM) (see Ginhoux & Jung 2014 for a review). However, there have been some discrepancies with regard to how the terms primitive and definitive are used (Frame et al. 2013). In part, this may be due to the fact that multiple waves of haematopoiesis have been described in the yolk sac (Palis et al. 1999; Palis et al. 2001; Bertrand et al. 2005; Hoeffel et al. 2015), and multipotent precursors, capable of giving rise to erythrocytes as well as macrophages (and granulocytes) have been considered 'definitive' in the erythrocyte field, but 'primitive' in the macrophage field (Frame et al. 2013). Additionally, studies over the years have assigned different names to what are most probably the same cells and the subject of macrophage ontogeny is still being actively researched which is constantly refining the way we identify and define macrophage precursors and their progeny. However, I will summarise what is currently known about myelopoiesis during development below.

There is consensus that the first primitive wave of myelopoiesis occurs in the yolk sac from as early as E7.5 in mouse, with the emergence of a precursor with a largely macrophage-

restricted potential, which have been termed Mac-CFCs (Palis et al. 1999), or 'early' erythromyeloid progenitor cells (EMPs) (Hoeffel et al. 2015). These cells mature into primitive macrophages *in situ* in the yolk sac, bypassing any pro-monocyte or monocyte intermediary (Hoeffel et al. 2015), which aligns them with the 'foetal macrophages' described earlier by Takahashi and colleagues, who found no evidence for monocytic peroxidase (PO) activity in this lineage (Takahashi et al. 1989; Naito et al. 1990). These early precursors are defined by their reliance on the transcription factor PU.1, and a CD45$^-$c-Myb$^-$c-kit$^+$ phenotype. The designation of these progenitor cells by Hoeffel *et al.* as 'EMPs' is arguable, since they do not possess granulocyte potency (McGrath et al. 2015), and as such they will be referred to as yolk sac macrophage precursors, as proposed previously (Bertrand et al. 2005).

A second wave of development in the yolk sac occurs at around E8.5 with the emergence of a multipotent progenitor defined as 'late' EMPs (Hoeffel et al. 2015a), which are probably the cells designated as HPP-CFCs, observed at E8.25 in earlier studies by Palis *et al.* (2001), or Ys-EMPs by Bertrand *et al.* (2005). These cells have been defined as PU.1$^-$CD45$^-$c-Myb$^+$c-kit$^+$. These c-Myb$^+$ EMPs can give rise to macrophages directly in the yolk sac, but also enter the embryo proper from around E8.5 when the circulatory system becomes established (McGrath et al. 2003), and enter the foetal liver between E9.5 and E10.5 (Hoeffel et al. 2015; Gomez Perdiguero et al. 2015). Here they seed the liver with foetal monocytes via a c-Myb$^+$CSF1R$^+$ myeloid progenitor (Hoeffel et al. 2015; Gomez Perdiguero et al. 2015). It is only recently that primitive macrophages and their precursors, and c-Myb$^+$ EMPs have been considered developmentally distinct, as historically they had been referred to collectively as 'primitive'. However, the wave of c-Myb$^+$ 'late' EMPs is now often referred to as 'transient definitive' (Hoeffel and Ginhoux 2018), given their ability to disseminate into the embryo proper and seed the foetal liver with foetal monocytes.

Much later, at around developmental day 10.5, the first immature haematopoietic stem cells (HSCs) arise in the embryo proper within the AGM, originally identified by their ability to repopulate lethally irradiated mice in sex-mismatched transplants with cultured AGM tissue (Medvinsky and Dzierzak 1996). Immature HSCs then migrate to the foetal liver where they mature fully (Kieusseian et al. 2012). HSCs can give rise to an additional population of foetal monocytes in the liver by around E14.5 via a Flt3$^+$ progenitor (Gomez Perdiguero et al. 2015), and this was thought to be the major pathway by which tissue macrophages arose (reviewed in Ginhoux & Jung 2014), but this has since been largely disproven, as discussed below.

1.3.2 Embryonic origin of tissue macrophages

The discovery that there are distinct waves of macrophage progenitors arising during embryogenesis raises the question of which of the early macrophage progenitors give rise to the macrophage populations which are present in the tissues at birth, and whether this differs between tissue macrophage populations.

Expression of transcription factors is tightly regulated during embryogenesis, and recent research has focussed on exploiting temporal gene expression patterns to differentially label primitive and definitive waves of macrophage precursors to determine their fate. In particular, tamoxifen-inducible Cre-lox labelling systems have been utilised, in which an injection of 4-hydroxytamoxifen (4-OHT) is used to label a specific population and their progeny. Recombination time is limited to under 24 hours, allowing labelling within a short developmental window (Samokhvalov et al. 2007). Using this approach, several research groups have labelled cells expressing Runx1 at E7.25-E7.5, a time point at which Runx1 is restricted to the yolk sac (Ginhoux et al. 2010). Labelling of $Runx1^{+}$ yolk sac macrophages resulted in YFP labelling in microglia at E10.5 (Ginhoux et al. 2010; Hoeffel et al. 2015) indicating that primitive macrophages seeded the microglia population, whilst there was no labelling of alveolar or dermal macrophages (Ginhoux et al. 2010), but a small contribution of primitive macrophages to Langerhans cells (LC) was seen (Hoeffel et al. 2012). Later labelling at E8.5 resulted in little labelling in primitive macrophages, or in microglia, but approximately 30% labelling in macrophage populations in the liver, skin, kidney and lung which was maintained into adulthood (Hoeffel et al. 2015).

Similarly, $CSF1R^{MerCreMer}Rosa26^{YFP}$ mice have been used to label $CSF1R^{+}$ primitive macrophages in the yolk sac at E8.5. In one prominent study, YFP expression was found in macrophages populations in the skin, liver, spleen, pancreas, lung and kidney 4 weeks after birth, suggesting that these populations were derived from yolk sac macrophages (Schulz et al. 2012). However, the efficiency of YFP labelling was not shown. A later study demonstrated that labelling at E8.5 did indeed lead to YFP expression in all tissue macrophages at E13.5, but that the extent of labelling diminished and was almost negligible by birth, with the clear exception of microglia which were still 60% YFP^{+} 6 weeks post birth (Hoeffel et al. 2015). This was confirmed in another study which found maximal YFP labelling of 30% in the adult brain, a small contribution of YFP^{+} cells to macrophage populations in the heart and liver, but

minimal labelling in the skin, kidney, spleen, peritoneum and lung 10 weeks after birth (Epelman et al. 2014a), whilst initial labelling in the gut rapidly declined following birth (Bain et al. 2014). Together, these studies suggest that although primitive macrophages seed macrophage populations in all tissues, they are largely displaced by a later lineage of cells, with the exception of microglia. Another study, again labelling CSF1R^{+} cells in CSF1R^{MerCreMer}Rosa26^{YFP} mice with a 4-OHT pulse at E8.5 found YFP^{+} cells in the foetal liver at E10.5 which were also AA4.1^{+}c-Kit^{+}CD45^{lo} (Gomez Perdiguero et al. 2015) suggesting they are likely to be the 'late' EMPs which were described to migrate from the yolk sac to the foetal liver to give rise to foetal monocytes (Hoeffel et al. 2015). YFP^{+}F4/80^{bright} cells were subsequently found in the liver, skin and lung (Gomez Perdiguero et al. 2015). Critically, at E10.5 there were no YFP^{+} cells within the AGM region indicating that the F4/80^{bright} cells had not come from early definitive HSCs within the embryo proper (Gomez Perdiguero et al. 2015). Although these data would appear to conflict the findings by Hoeffel and colleagues (2015) that CSF1R-YFP^{+} cells are displaced by a later lineage of cells, again, the labelling efficiency in this study was not shown, and may simply represent a small remaining contribution of primitive macrophages to some tissue macrophage populations.

Taking the converse approach, Flt3^{Cre}Rosa26^{YFP} mice, in which there is constitutive YFP expression in all foetal and adult HSC-derived cells and their progeny, were used to determine whether the early primitive macrophage lineage was displaced by definitive HSC-derived macrophages. In some tissues, Flt3-YFP^{+} cells largely did not contribute to tissue macrophage populations apart from small contributions to liver (14%), brain (2%) and LC (30%) which plateaued at around 8 days post birth which did not further increase over one year. However, 60% of dermal macrophages were YFP^{+} at birth (Gomez Perdiguero et al. 2015) and 35% of gut macrophages were YFP^{+} at 8 weeks of age (Bain et al. 2014). Labelling was initially low in AM and brain macrophages, but gradually increased over one year indicating that HSC-derived cells gradually replenished the population in these tissues with age (Gomez Perdiguero et al. 2015). Induction of labelling of Tie2, which is expressed in the yolk sac, foetal liver, AGM and by HSCs, as well as endothelial cells, at E7.5, E8.5, E9.5 and E10.5 demonstrated that the earlier the tamoxifen pulse, the greater the labelling in microglia, confirming that this population arises from the earliest primitive yolk-sac derived macrophages, and by comparing levels of labelling across the time points the authors also deduced that labelling of KC, AM, LCs and F4/80^{hi} cells in the spleen occurred independently of the HSC lineage (Gomez Perdiguero et al. 2015).

Further study using the Runx1-labelling system found that labelling at E7.5 labelled primitive macrophages, E8.5 labelled EMPs and E9.5 labelled HSCs. This revealed that apart from microglia, the most efficient labelling of tissue macrophages arose with labelling at E8.5, indicating EMPs as the main precursor (Hoeffel et al. 2015). These EMPs express c-Myb, which is a master regulator of haematopoiesis (Ferrero et al. 2018). In disagreement with this study, F4/80^{hi} macrophages could still be detected in c-Myb$^{-/-}$ mice which lack c-kit^{+} EMPs (Schulz et al. 2012). However, the fact that in this model the F4/80^{hi} macrophages of primitive origin were not replaced does not preclude the fact that EMP-derived cells could displace them in normal development. In agreement with this, foetal monocytes were shown to be the main precursor for AM, which colonize the lung and develop into mature AM during the first week post birth, at the time that there is a 'boost' in production of their growth factor GM-CSF (CSF2) (Guilliams et al. 2013). Primitive foetal macrophages (likely of yolk sac origin) are also found in the lung during embryogenesis, but Guilliams et al did not find these to give rise to the mature AM population, using a series of foetal macrophage and foetal monocyte transfer experiments to look at their long term potential to become AM (Guilliams et al. 2013). They argue that these primitive foetal macrophages are probably the F4/80^{hi} cells observed in c-Myb$^{-/-}$ embryos studied by Schulz *et al.* (Schulz et al. 2012), but that since the c-Myb$^{-/-}$ animals die before full term, Schulz and colleagues could not prove the conclusion that these primitive macrophages give rise to the mature AMs seen in adult mice.

The exact signals which mediate recruitment of embryonic macrophages to the organs are not fully elucidated. The establishment of the circulation appears to be absolutely critical to allow access to the tissues. Indeed, there were no skin-infiltrating macrophages (Hoeffel et al., 2012) or microglia (Ginhoux et al., 2010) present in Ncx1$^{-/-}$ embryos, which lack a heartbeat and therefore have no blood circulation. The formation of the blood brain barrier occurs around the same time as foetal monocytes emerge from the foetal liver, which may prevent their recruitment, perhaps explaining why microglia remain of primitive origin, unlike other tissues (Hoeffel et al., 2015). Whilst the circulatory system provides a means for macrophage precursors to disseminate around the developing foetus, it is likely that additional chemotactic signals are required for precursors to extravasate into tissues. CSF1 and its interaction with its receptor are highly implicated in recruitment of monocytes to tissues in adult mice (Tagliani et al., 2011; Jenkins et al., 2013). However, whilst microglia are absent from CSF1R deficient mice, they are present in normal numbers in CSF1 deficient mice (Hoeffel et al., 2015). Likewise, absence of the CSF1R did not affect the subsequent

recruitment of foetal monocytes to the developing dermis, although it did affect their differentiation into LC (Hoeffel et al., 2012). Thus other signals must be responsible for macrophage recruitment during embryogenesis, and signalling axes such as CX3CR1-CX3CL1 is one such potential candidate (Hoeffel et al., 2010).

Together, these studies demonstrate that primitive yolk sac-derived macrophages arising as early as E7.5 colonise all tissues and form the initial macrophage population resident in developing tissues. With the exception of microglia, which maintain this heritage, these early primitive macrophages are displaced by a later lineage of cells during embryogenesis, but these are not of definitive HSC origin. Instead, most tissue macrophage populations at birth originate from c-Myb^{+} EMPs in the liver which differentiate into tissue macrophages via a foetal monocyte intermediate.

1.3.3 Maintenance of tissue macrophage populations in adult mice

Many studies have attempted to determine whether the resident macrophages seeded during embryogenesis survive long term in adult mice under steady state conditions, and to what degree recruitment and differentiation of monocytes contributes to maintenance of resident macrophage populations. These studies have demonstrated that dependent on tissue, resident macrophages can be maintained either through local proliferation, longevity or through replenishment by circulating adult monocyte-derived macrophages recruited to the tissue in steady state conditions, or following injury or inflammation. These modes of maintenance are not mutually exclusive, as populations of macrophages of multiple ontogenies co-exist within most tissues, and even populations that exhibit the same basic phenotype can represent a mix of embryonically-derived and monocyte-derived cells. Furthermore, the extent to which a population is maintained independently of monocytes, or depends on monocyte replenishment can change with time.

Early studies that appeared to support the notion that all macrophages required continual replenishment by monocytes generally involved total body irradiation to fate map transferred donor bone marrow, which lead to replacement of the incumbent macrophage populations. Chromosomal labelling of bone marrow and use of lethal irradiation chimeras was used to demonstrate that macrophages from various tissues were of donor and therefore haematopoietic origin (Virolainen 1968; Goodman 1964; Hess et al. 2004). Later studies using whole body irradiation chimeras reconstituted with congenic WT- or

competitive WT and CCR2$^{-/-}$ -donor bone marrow confirmed that Ly6C^{hi} monocytes from the circulation are certainly capable of replenishing macrophage populations in the lung (Guilliams et al. 2013), liver (Klein et al. 2007), heart (Molawi et al. 2014) and gut (Bain et al. 2014). However, two studies looking across multiple organs were published just before I started my PhD, which challenged the notion that tissue macrophages are dependent on monocytes. Using s100a4^{Cre}R26^{tomato} and Flt3^{Cre} mice to track monocytes, Hashimoto and colleagues concluded that resident macrophages in the lung, spleen, peritoneal cavity, bone marrow and brain did not rely greatly on adult monocytes or their progenitors, and their own parabiosis experiments further supported this conclusion (Hashimoto et al. 2013). At the same time, Yona and colleagues used an inducible Cx3cr1^{CreER}R26^{YFP} system that labels monocytes (albeit with very low efficiency), which indicated minimal contribution of monocytes to macrophage populations in the liver, spleen, lung, peritoneal and to LC in the skin (Yona et al. 2013). Further studies focussing on individual tissues have revealed in greater detail which macrophage populations rely on monocyte replenishment and which rely on proliferation, and which are maintained through a combination of the two in the steady state.

The Runx1 and CSF1R inducible Cre methods used to fate map primitive embryonic macrophages, described above, provide some of the strongest evidence that microglia maintain their embryonic lineage in adult mice and are not replenished by monocytes. In further confirmation of this, there was no emergence of non-host cells in the microglial compartment of each parabiotic mouse pair over a 5 month period (Ajami et al. 2007). Even following microgliosis caused by facial nerve ataxotomy or in a chronic mouse model of ALS, parabiosis revealed no evidence of monocyte recruitment and differentiation into microglia (Ajami et al. 2007). In experimental autoimmune encephalitis (EAE), the murine model of multiple sclerosis, monocytes were recruited to the brain and gave rise to macrophages which were phenotypically indistinct from resident microglia. These cells were transient and did not survive long-term in the brain following resolution of disease (Ajami et al. 2011). Together these studies demonstrate that microglia maintain tight autonomy from the HSC lineage, even during acute and chronic brain injury. In stark contrast, although CSF1R-labeling at E8.5 led to YFP labelling in the gut in the neonate, this rapidly declined into adulthood and whole body chimeras and parabionts confirmed that Ly6C^{hi} monocytes largely replenished the population. Microbiota may be signalling their replenishment as continual antibiotic treatment led to reduced chimerism in parabionts compared to those which received

antibiotics for only the first 4 weeks after treatment. (Bain et al. 2014). Although colonic macrophages were found to proliferate in the first 3 weeks after birth, this ability declined as their dependence on BM-derived monocytes increased. As such, *Ccr2*$^{-/-}$ mice had normal colonic macrophage numbers at birth which declined with age (Bain et al. 2014). The absence of colonic macrophages in adult *Ccr2*$^{-/-}$ mice also suggests that dependence of colonic macrophages on monocytes is non-redundant and these cells cannot rely on self-renewal in the absence of monocytes. Microglia and colonic macrophages represent the far extremes of the spectrum of reliance on self-renewal versus monocyte replenishment. All other tissues appear to fall somewhere in between (fig 1.1).

Detailed studies of the heart have revealed multiple populations of cardiac macrophages that exist concurrently. In one study, four populations, defined by their MHCII and CD11c expression profiles displayed varying degrees of monocyte replenishment in parabiotic mice over a 2 week period (Epelman et al. 2014a). When the macrophage populations were depleted by chlodronate liposome injection, bead-labelled Ly6C^{hi} monocytes were able to

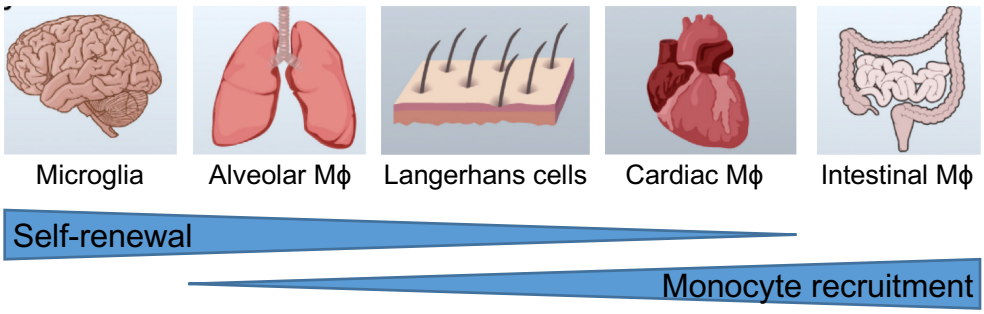

Figure 1.1 Spectrum of tissue macrophage maintenance through self-renewal versus monocyte recruitment. Images adapted from (Epelman et al. 2014b).

contribute to all macrophage populations, whilst during cardiac distress caused by AngII infusion, a combination of monocyte recruitment and *in situ* proliferation caused the macrophage compartments to expand. Notably, once the tissue macrophages had been repopulated by monocytes following artificial depletion or cardiac distress, self-maintenance then resumed with monocytes maturing into self-renewing resident macrophages (Epelman et al. 2014a). Epelman et al (2014a) demonstrated that the MHCII^{+}CD11c^{+} population of cardiac macrophages was the most dependent on circulating monocytes, and consistent with

this, had the highest proportion of $Flt3^{Cre+}$ cells indicative of having come from an HSC precursor, prompting suggestion by others that this is in fact a population of dendritic cells (DC) (Molawi et al. 2014). Molawi and colleagues instead defined four cardiac macrophage populations on the basis of MHCII and CX3CR1 and found using $CX3CR1^{Cre}$-R26-yfp mice that all cardiac macrophages passed through a $CX3CR1^{+}$ stage during embryogenesis, but labelling declined with age, indicating the loss of embryonic-derived cells. (Molawi et al. 2014). Molawi et al also used parabiosis between a WT mouse and a *Ccr2*$^{-/-}$ host to show that 16% of all cardiac macrophages were of non-host origin over a 10 week period, whilst adoptive transfer of YFP-labelled bone marrow into $rag2^{-/-}yc^{-/-}Kit^{w/wv}$ mice which accept grafts without irradiation showed a small but significant contribution of 7% YFP^{+} cells within the total cardiac pool (Molawi et al. 2014). Both studies therefore largely agree that in the steady state cardiac macrophages are gradually replaced by monocytes over time. In the lung parabiosis studies demonstrated that AM were largely self-maintaining, with less than 5% of the population deriving from the parabiotic donor monocyte-derived cells (Guilliams et al. 2013). Chimeras made within 24 hours after birth demonstrated that adult LCs were of host origin up to 7 months after irradiation, and that these cells were largely of foetal liver-derived monocyte origin (adoptive transfer of foetal monocytes at E13.5-E14.5) with a small contribution from yolk sac macrophages (Runx1 labelling at E7.5) (Hoeffel et al. 2012).

Thus some macrophage populations rely heavily on monocytes whilst others do not. What was known about the origin of KC in the steady state is discussed in detail later in section 1.4.2.

1.3.4 Tissue macrophages proliferate *in situ*

So how are fully differentiated, mature tissue macrophage populations maintained if they are not solely reliant on recruitment of monocytes? A pool of highly multipotent long term haematopoietic stem cells (LT-HSC) reside within the bone marrow. These are largely quiescent, which may be to 'protect' stem cells from replication-induced DNA mutations. LT-HSC give rise to rapidly dividing daughter cells (Foudi et al. 2009), and a branching model is generally accepted in which there is progressive loss of proliferative potential and potency as cells differentiate, coinciding with initiation of lineage-specific transcription. Monocytes are generated in the bone marrow from highly proliferative precursors, but they do not proliferate in the circulation because they do not express the necessary transcription factors,

and are not exposed the extrinsic factors which then signal their proliferation upon arrival in tissues (Swirski et al. 2014). Instead, their number is controlled by release from the bone marrow (Swirski et al. 2014). Given that tissue macrophages are mature, terminally differentiated effector cells, it might seem logical that they should not retain capacity to proliferate. Indeed, this is one of the original tenets of the MPS model that accompanies the concept that macrophages are exclusively maintained and replenished by monocytes. However, despite van Furth's conclusion that KC were of monocytic origin, his own papers reported that approximately 1% of the KC population and of the resident peritoneal macrophages were in mitosis during homeostasis, determined by incorporation of radioactively labelled thymidine over one hour (van Furth and Cohn 1968; Crofton et al. 1978). With more sophisticated methods to assess proliferation at the single cell level, including BrdU incorporation, expression of the cell cycle marker Ki67 and cellular dyes and genetic labelling which can trace proliferation history, multiple research groups have shown that resident macrophages in just about every tissue are able to proliferate (Epelman et al. 2014a; Molawi et al. 2014; Hashimoto et al. 2013; Guilliams et al. 2013; Czernielewsk et al. 1985; Chorro et al. 2009; Jenkins et al. 2011, 2013).

During inflammation, resident macrophages are often severely reduced in number, in what has been termed the 'macrophage disappearance reaction' (Nelson and Boyden 1963; Haskill and Becker 1985). Monocytes are recruited to tissues in response to inflammation, but in many cases the remaining resident macrophages have been shown to proliferate during the recovery phase of injury to restore their numbers. In the case of zymosan-induced peritonitis, a small number of resident macrophages survive and analysis of the phosphorylation status of histone H3 showed that these macrophages proliferate to restore normal numbers of resident macrophages (Davies et al. 2011). Colony Stimulating Factor 1 (CSF1) was found to be the major factor controlling proliferation in this scenario and blockade with an anti-CSF1 antibody completely shut off proliferation of resident macrophages (Davies et al. 2013). In the context of a helminth-induced type-2 immune response, proliferation driven predominantly by IL-4 provides a mechanism for the expansion of peritoneal macrophages, overriding CSF1 signalling, allowing expansion of the macrophage population without monocyte recruitment (Jenkins et al. 2011, 2013). Likewise, KC in the liver proliferate following acetaminophen injury to the liver (Zigmond et al. 2014), AM proliferate following influenza infection (Hashimoto et al. 2013) and cardiac macrophages proliferate following cardiac stress (Epelman et al. 2014a). LC in the skin were shown to proliferate in a mouse

model of atopic dermatitis (eczema) (Chorro et al. 2009), and these findings were mirrored in two human skin samples from patients with eczema (Chorro et al. 2009). One clear exception is in the gut, where there was no clear proliferative burst in the macrophage population following inflammation with acute DSS colitis (Bain et al. 2014).

One question raised by the discovery that mature tissue macrophages can proliferate is whether all cells within a population possess equal proliferation potential, or whether there is a hierarchy, akin to that of HSC. Multicolour fate mapping using inducible confetti mice, in which cells can express either GFP, YFP, RFP or CFP suggests within the LC population, proliferation may occur within distinct units, as foci of proliferating cells surrounded by daughter cells expressing the same fluorescent marker emerged following induction of Cre activity (Ghigo et al. 2013). In contrast, two rounds of depletion of AM using CD169-DTR mice, one of which was followed by pulse labelling of proliferating cells with BrdU and the other without labelling revealed that both $BrdU^+$ AM and $BrdU^-$ AM equally expressed Ki67 (a marker cells in active cell cycle). The authors interpreted this as all AM having equal ability to proliferate, or in other words that proliferation of AM was stochastic (Hashimoto et al. 2013). The Jenkins lab used the H2B-GFP labelling system used to identify LT-HSC (Foudi et al. 2009) to look for a local tissue progenitor to peritoneal macrophages (Bain et al. 2016). Although we were unable to identify a clear progenitor, proliferation appeared to be non-stochastic, suggestive that there is some heterogeneity of proliferation in the steady state (Bain et al. 2016). In chapter 5 I attempted to use this same system to look for a local tissue progenitor for KC.

1.3.5 The concept of the macrophage niche

The fact that reliance on monocyte recruitment versus *in situ* proliferation for the maintenance of macrophages is so tissue-specific raises the question of the importance of local environmental factors in defining their size, ontogeny and function. This has resulted in the idea that there is a macrophage 'niche' (Jenkins and Hume 2014), which may comprise both physical and biochemical factors which may dictate physical location of tissue macrophages (Guilliams and Scott 2017). The idea of the macrophage niche will be explored in further detail in chapters 5, 6 and 7.

1.3.6 Comparison of origin in species other than mouse

The majority of studies into macrophage origin have been conducted in mouse due to ease of breeding, availability of reporter strains and a well mapped genome. However, there are many similarities in how macrophage populations are established and maintained across species. For example, the presence of two anatomically distinct sites for haematopoiesis – one in the yolk sac and one in the embryo – appears conserved among species, as shown in early studies on *Xenopus* and chicks (Kau and Turpen 1983; Lassila et al. 1978). Furthermore, a recent study showed that in zebra fish, the earliest primitive macrophages, and not EMPs give rise to microglia (Ferrero et al. 2018). However, unlike in mouse, these primitive macrophage-derived microglia are transient, and are replaced by HSC-derived macrophages, indicating that the maintenance of the embryonic macrophage lineage varies between species.

Despite this, emerging evidence suggests that mice are a relevant model for comparison with human macrophage maintenance. The origins of tissue macrophages are, for obvious reasons, more difficult to study in humans, but patients undergoing tissue or stem cell transplant provide a rare opportunity. Evidence from these types of case studies suggests that dependency of resident macrophages on monocyte replenishment in humans mirrors the tissue-dependent nature seen in mouse. For example, a case study in which a woman who had received a sex-mismatched cord blood stem cell transplant showed that although >99.5% chimerism was maintained for over 2 years in the bone marrow and in the periphery, fewer than 0.1% of microglia in the brain were of donor origin, indicating that microglia persist independently of monocyte recruitment even in the context of chemotherapy which might have disrupted the blood brain barrier (Takahashi et al. 2016). In HLA-mismatched lung transplant patients, the origin of AM in bronchiolar alveolar lavage (BAL) fluid was assessed and greater than 87% of AM remained of donor origin up to 3 ½ years following transplant, indicating that, as in mouse, AM in humans are not rapidly replenished by circulating monocytes (Nayak et al. 2016). In comparison, around 70% of human dermal macrophages were replaced in one year following HSC transplant in a cohort of 52 patients (Haniffa et al. 2009).

1.4 The liver and liver Kupffer Cells

Unlike many other tissue macrophage populations, the origin and maintenance of liver KC in adult mice had been less well studied when I embarked on my PhD, and this became the major focus of my studies. KC are vital for maintenance of both liver tissue health, and for protecting the body from autoimmunity via maintenance of peripheral tolerance. Thus a better understanding how they are maintained, particularly in the context of liver injury or dysfunction, may provide crucial insight into how to manipulate these cells to improve or enhance their function.

1.4.1 Location and role of liver Kupffer Cells

The liver is a highly vascularized tissue, structured into repeating hepatic lobules. Each lobule comprises the portal triad, composed of a portal vein, hepatic artery and bile duct. Blood flows from the portal vein and hepatic artery to the central vein via the sinusoids. KC sit within the sinusoids, spanning their diameter and maintaining close contact with the liver sinusoidal endothelial cells (LSECs) (Burkel and Low 1966; Wisse et al. 1983) (fig. 1.2). In fact, when von Kupffer first identified KC they were mistakenly thought to be endothelial cells until they were subsequently identified as macrophages by Browiecz (reviewed by Dixon et al. 2013). Histologically, KC can be identified by this sinusoidal location, with archetypal processes which stretch from the body of the cell through the vessels giving their distinctive star-shape (Lopez et al. 2011; Sasmono et al. 2003; McCuskey et al. 1990; Movita et al. 2012) described by von Kupffer. In mouse, KC express high levels of the pan macrophage marker F4/80, which has been used for their identification widely in both imaging and flow cytometry; F4/80 immunofluorescence staining alone reveals KC within the liver parenchyma with their typical star-like shape. They are present in both the centrilobular and periportal regions of the liver, but are absent in the area surrounding the central vein. They are most abundant in the periportal region, which could reflect the fact that this is where endotoxin arrives in the liver through the portal vein, and these KC are larger and have a greater phagocytic capacity than those in the centrilobular zone (Bykov et al. 2003).

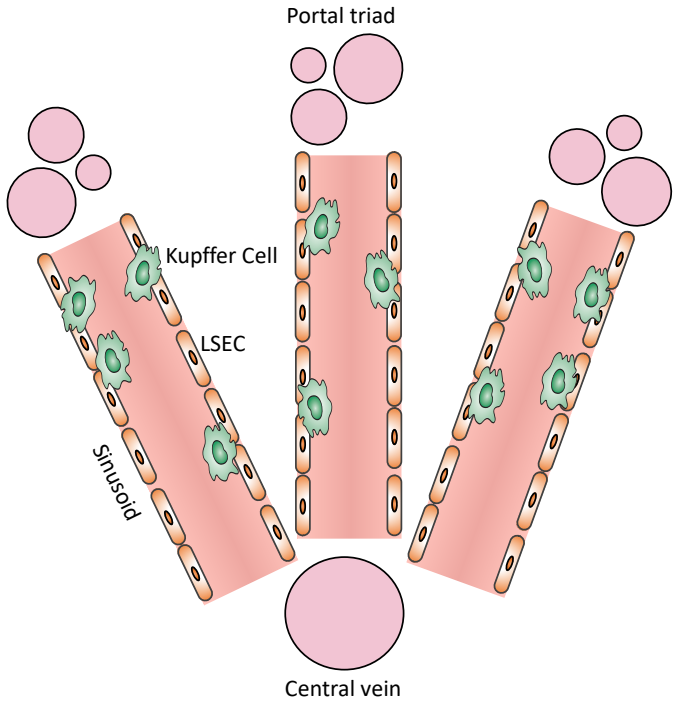

Figure 1.2 Structure of the liver. Blood drains through the sinusoids from the portal triad to the central vein. Kupffer Cells (KC) sit within the sinusoids which are lined with liver sinusoidal endothelial cells (LSECs). KC are absent in the area surrounding the central vein and are most abundant near the portal triad.

Like other tissue resident macrophages, KC express multiple scavenger receptors on their surface (Hughes et al. 1995), allowing them to efficiently sense and respond to factors in their local environment. They can initiate immune responses, for example by upregulating expression of the class A scavenger receptor MARCO in response to bacterial infection (Gordon et al. 1999), leading to endocytosis and production of reactive oxygen species (ROS) (Movita et al. 2012). In other contexts they can dampen immune responses and can produce the anti-inflammatory cytokine IL-10 following signalling through TLR4, TLR7/8 and TLR9 (Movita et al. 2012). They can also protect tissues from injury and express high levels of haemoxygenase 1 (HO-1) which catalyses the degradation of haemoglobin, which was shown to reduce susceptibility of mice to ischaemia reperfusion injury (IRI), through the dampening of inflammation and protection from oxidative stress (Devey et al. 2009; Bauer and Bauer 2002).

KC are crucial for maintaining tissue health, in particular by scavenging and phagocytosing erythrocytes damaged by oxidative stress from the circulation (Terpstra and van Berkel 2000) as well as other apoptotic cells (Dini et al. 2002). They are professional antigen presenting cells (APC), and present scavenged material via MHCII on their surface. However, unlike mature dendritic cells, T-cell priming by KC leads to the induction of $Foxp3^{+}$, IL-10-producing regulatory T cells, which is at least in part through their expression of the suppressive costimulatory marker PDL-1 (Heymann et al. 2015). They are continually exposed to LPS in the circulation from the intestines, but repeated signalling through TLR4 leads to them to display 'endotoxin tolerance' causing a refractory period to subsequent LPS stimulus, preventing potentially harmful overactivation and inappropriate immune response to commensals (Hafenrichter et al. 1994; Liu et al. 2008). The liver as an organ has been described as a second 'firewall', protecting the body from overt responses to endotoxin and other bacterial products during systemic infection or gut mucosal damage, and KC were shown to be an important part of clearing live commensal bacteria from the blood stream (Balmer et al. 2014). Thus, KC are key in maintaining peripheral tolerance and in dampening immune responses to commensal bacteria. However, bacterial clearance by the liver was impaired in the context of liver dysfunction (Balmer et al. 2014), indicating that KC may lose some of this tolerogenic function under ongoing or chronic inflammatory conditions. One possible explanation for this loss of function during liver dysfunction is that KC may be replaced by monocyte-derived macrophages under inflammatory conditions which cannot recapitulate normal KC functions, and this idea is explored in chapter 6.

1.4.2 Maintenance of Kupffer Cells in mouse

As discussed in section 1.3.4, lineage fate mapping studies have revealed that at birth, murine KC are derived largely from a foetal monocyte precursor generated from yolk sac-derived EMP progenitors. Many of these studies additionally looked for retention of CSF1R- driven fluorescent label in macrophage populations in multiple tissues in adult mice. These generally indicated that at least some of the fluorescent label was retained in KC post birth (Schulz et al. 2012; Epelman et al. 2014a). However, the frequency of label-expressing KC was shown to decline with time in some studies, between birth and 6 or 12 weeks of age (Hoeffel et al. 2015; Bain et al. 2014) which would argue that either monocytes were replenishing the population or that non-labelled KC were out-competing labelled KC. $Flt3^{Cre}$-YFP labelling

demonstrated that there appeared to be a small contribution (~15%) of HSC-derived cells to the KC population in the first few weeks after birth (Schulz et al. 2012; Perdiguero et al. 2014). In agreement with this, there was incorporation of monocyte-derived KC during the immediate postnatal phase, accounting for around 40% of the KC population at 8-12 weeks of age in this study. This coincided with an expansion in the total KC population size during which there is also an increase in liver mass (Scott et al. 2016). However, using the $Flt3^{Cre}$-YFP labelling approach, there appeared to be no further incorporation of YFP up to one year in mice, indicating autonomy from cells of HSC lineage in the steady state likely occurs at some point between birth and adulthood (Gomez Perdiguero et al. 2015). In agreement with this, equivalent numbers of KC were found in WT and *Ccr2*$^{-/-}$ mice at 8 weeks of age and very few non-host KC were present in WT and *Ccr2*$^{-/-}$ parabiotic partners following 10 weeks of parabiosis (Bain et al. 2014). Together these studies indicate that in adult mice KC are maintained by self-renewal and are not replenished by monocytes.

The differentiation, proliferation and survival of KC is highly dependent on the growth factor CSF1 and its signalling through the CSF1 receptor (CSF1R). Accordingly, both *op/op* mice, which have a natural mutation in the *csf1* gene (Wiktor-Jedrzejczak et al. 1982; Yoshida et al. 1990), and mice lacking CSF1R activity display a deficit in KC number (Dai et al. 2004; MacDonald et al. 2010). CSF1 availability has been proposed previously as a key factor in defining the macrophage niche (Jenkins and Hume 2014), and signalling through the CSF1R has been shown to be required for conversion of monocytes to tissue macrophages (Hashimoto et al. 2013). Thus CSF1 consumption likely plays a key role in regulating the autonomy and origin of KC. Expression of the CSF1R by tissue macrophages including KC, along with uptake of CSF1 through the CSF1R will be explored further in chapter 4, whilst the role for CSF1 in maintaining the KC niche is discussed in detail in chapter 5. CSF1 and the CSF1R are introduced in more detail in both chapters 4 and 5, and therefore are not discussed further here.

1.5 Kupffer Cells and monocyte-derived macrophages in liver injury

1.5.1 Human liver injury and disease and animal models

Liver injury can be acute or chronic in nature, causing high morbidity and often mortality. Acute liver failure is a rare condition, affecting fewer than 6 in a million people in the developed world, defined by loss of metabolic liver function, systemic inflammation and

possibly multiorgan failure including encephalopathy (Bernal and Wendon 2013). In the US and the UK, paracetamol or acetaminophen (APAP) overdose is the most common cause of acute liver failure, accounting for around 50% of all cases, whilst hepatitis infection is the biggest global cause (Bernal and Wendon 2013). By definition, acute liver injury is the occurrence of apoptosis and necrosis of hepatocytes in previously healthy liver (Forbes and Newsome 2016). This triggers an inflammatory immune response, including the recruitment of neutrophils and monocytes, followed by liver regeneration with the activation of myofibroblasts, and hepatocyte proliferation resulting in wound healing and finally the resumption of steady state metabolic function (Markose et al. 2018; Forbes and Newsome 2016).

Nearly 850 million people are estimated to have chronic lifver disease worldwide, resulting in 2 million deaths each year (Marcellin and Kutala 2018). Chronic liver disease can be caused by alcohol, viral infection or non-alcoholic fatty liver disease, but is generally characterised by progressive fibrosis (Schuppan and Afdhal 2008) resulting from impaired tissue repair under ongoing inflammation (Wick et al. 2010). Uncontrolled, progressive fibrosis eventually results in liver cirrhosis characterised by loss of endothelial fenestration, portal hypertension and loss of metabolic function, and possibly the development of hepatocellular carcinoma (HCC) (Schuppan and Afdhal 2008). Cirrhosis carries a particularly high bacterial infection risk, as the liver in its immunocompromised is unable to effectively deal with bacteria translocated from the gut. Bacterial infection is responsible for up to 50% of all deaths in cirrhosis patients, and infection with *E. coli* is particularly common (Bunchorntavakul *et al.,* 2016). Finally patients reach end stage liver disease, for which the only current treatment is liver transplant, and without which encephalopathy, multiple organ failure and death will result. In rodents there are several liver damage and disease models. APAP overdose is commonly used as an acute liver injury as it closely mimics the injury seen in humans using the same toxic substance. Chronic injury can be modelled through bile duct ligation which results in secondary biliary fibrosis, but has a high mortality rate, through viral hepatitis or *Schistosomiasis* infection or spontaneous mouse models, such as Ob/Ob mice which have a mutation in the gene coding lectin, and become obese, insulin resistant and develop fatty livers. Non-alcoholic fatty liver disease (NAFLD) can also be modelled through diet, such as the methionine- and choline- deficient diet (MCD) or high fat diet (HFD) (Liu et al. 2013). One of the most widely used models for livery injury is the halogenated alkane Carbon tetrachloride (CCl_4), which causes sterile, toxic liver damage. The mechanisms through which

it causes toxicity are many and there is not space to detail them here, but a comprehensive review has been published describing its many actions (Weber et al. 2003). Briefly, cytochrome activity in the liver metabolises CCl_4, producing the free radical $CCl_3^{\bullet}$. In the presence of oxygen $CCl_3^{\bullet}$ becomes the highly reactive radical $CCl_3OO^{\bullet}$ causing major damage to cells (Weber et al. 2003). A single dose of CCl_4 results in acute necrotic damage in the centrilobular region, mimicking that seen with APAP overdose (Weber et al. 2003), which is quickly resolved through a cascade of immune responses, including the recruitment of eosinophils which secrete IL-4, driving the hepatocyte proliferation which is crucial for efficient tissue repair (Goh et al. 2013). Repeated delivery of CCl_4 results in progressive fibrosis with bridging septa and ultimately cirrhosis. The fibrosis caused in this model is spontaneously reversible (Iredale et al. 1998; Ramachandran et al. 2012). CCl_4 is used in this study as provides a unique model in which the same hepatotoxic agent can be administered to achieve either acute or chronic fibrotic injury, and to study the liver following spontaneous recovery.

1.5.2 Kupffer Cells and recruited liver macrophages during liver injury

1.5.2.1 Kupffer cells in liver injury

The role of KC has not always been clearly distinguished from that of monocyte-derived macrophages which arise during inflammation. However, the loss of F4/80^{hi} KC in the early phase post injury has been documented in both acute and chronic models (Zigmond et al. 2014; Heymann et al. 2015; David et al. 2016; Ramachandran et al. 2012). The remaining KC are activated by the release of DAMPs including HMGB-1, HSP-70, histones and free DNA which are released by dying hepatocytes (Sitia et al. 2007; Martin-Murphy et al. 2010; Imaeda et al. 2009; Wen et al. 2013; Tsung et al. 2007). This stimulates KC to produce pro-inflammatory cytokines, and one hour following APAP, FACS-sorted CD45^{+}F4/80^{+}CD11b^{lo} KC were shown to increase production of TNF-α, IL-6 and IL-1β (Martin-Murphy et al. 2010). Activated KC, along with hepatocytes, produce monocyte chemotactic protein (MCP-1), or CCL2 which recruits Ly6C^{hi} monocytes to the liver (Karlmark et al. 2009; Dambach et al. 2002; Martin-Murphy et al. 2010). Depletion of KC prior to ischaemia-reperfusion injury (IRI) using gadolinium chloride has also demonstrated that they attract neutrophils through production of the chemokines CXCL1, CXCL2 and CXCL8 (Mosher et al. 2001). Following this initial inflammatory response, KC may also contribute to resolution of inflammation and injury

through phagocytosis of apoptotic hepatocytes. Depletion of KC using chlodronate liposomes, using a regime which the authors claim did not deplete circulating monocytes, resulted in increased $HMGB1^+$ hepatocytes, which became secondarily necrotic, leading to enhanced DAMP release and increased neutrophil recruitment (Sitia et al. 2011). Interestingly, KC displayed a transcriptional profile which was almost indistinguishable from that of steady state KC 72 hours following APAP-induced acute liver injury (Zigmond et al. 2014), suggesting that they may have resumed their homeostatic functions by this time point.

1.5.2.2 Recruited macrophages in liver injury

In many tissues, populations of both classical $Ly6C^{hi}CCR2^{hi}CX3CR1^{lo}$ and nonclassical $Ly6C^{lo}CCR2^{lo}CX3CR1^{hi}$ 'patrolling' monocytes can be found (Geissmann et al. 2003). Their roles are generally thought to be distinct, with $Ly6C^{hi}$ monocytes contributing to the inflammatory process whist $Ly6C^{lo}$ monocytes appear to be involved in processes such as clearance of endothelial cells, but may also differentiate into more pro-reparative macrophages (Geissmann et al. 2003; Carlin et al. 2013; Auffray et al. 2014). In the liver, however, nonclassical $Ly6C^{lo}$ monocytes could not be detected in the steady state, and instead $Ly6C^{hi}$ monocytes appeared to take on the 'patrolling' role, seen crawling through the sinusoids, along with a population of 'patrolling' natural killer cells (Dal-Secco et al. 2015). The $Ly6C^{hi}$ monocytes are recruited to the liver following both acute or chronic injury, where they mature into hepatic macrophages, identified variously by expression of CD68 (or microsialin) (Dambach et al. 2002; Mitchell et al. 2009), their $CD11b^+F4/80^+GR1^+$ profile (Karlmark et al. 2009), or downregulation of Ly6C (Ramachandran et al. 2012; Dal-Secco et al. 2015). The CCR2/CCL2 chemokine axis has been demonstrated to be crucial for the recruitment of $Ly6C^{hi}$ monocytes following both acute and chronic injury.

In acute injury, there were reduced numbers of $Ly6C^{hi}$ monocytes in *Ccr2*$^{-/-}$ mice following both acute CCl_4 (Karlmark et al. 2009) and APAP (Mossanen et al. 2016; Zigmond et al. 2014). Prior depletion of circulating monocytes (and likely also resident KC) using chlodronate liposomes, did not affect the level of necrotic injury (Karlmark et al. 2009), and serum ALT levels were not affected in *Ccr2*$^{-/-}$ mice (Dambach et al. 2002) following APAP, indicating that monocytes do not contribute to the initial necrosis process. However, $Ly6C^{hi}$ monocyte-derived macrophages do appear to contribute to continuing hepatic injury as *Ccr2*$^{-/-}$ mice

displayed reduced necrotic area and reduced ALT compared with WT mice 12 hours following APAP (Mossanen et al. 2016). However, like KC, monocyte-derived macrophages also contribute to tissue repair following acute injury, congregating at the site of injury (Dal-Secco et al. 2015; Mossanen et al. 2016). Monocyte-derived macrophages have been shown to induce phagocytosis of neutrophils through cell-cell contacts (Holt, Cheng, and Ju 2008), and blockade of monocyte recruitment using MC-21, an α-CCR2 antibody resulted in increased numbers of neutrophils (Graubardt et al. 2017), and prolonged hepatic damage with bridging necrosis at 24 and 48 hours post APAP (Zigmond et al. 2014).

In chronic injury, recruited macrophages are associated with fibrosis progression and *Ccr2*$^{-/-}$ mice displayed reduced levels of fibrosis following 6 weeks of CCl_4 treatment (Mitchell et al. 2009), with reduced staining for collagen, hydroxyproline and α-SMA, a marker of hepatic stellate cell activation (Karlmark et al. 2009). Monocyte-derived macrophages were shown to produce TGFβ (Karlmark et al. 2009) which promotes the differentiation of hepatic stellate cells into myofibroblasts, and PDGFβ which is required for myofibroblast proliferation and survival (Wynn and Barron 2010). However, reversal of fibrosis following cessation of treatment was also delayed in *Ccr2*$^{-/-}$ animals (Mitchell et al. 2009) indicating that recruited macrophages also switch phenotype during the resolution phase following chronic injury. In agreement with this, depletion of recruited macrophages, but not resident KC, in CD11b-DTR mice at 48, 72 and 96 hours post chronic CCl_4 resulted in failure of resolution of fibrosis at 120 hours post injury (Ramachandran et al. 2012). Although the exact mechanism by which recruited macrophages enable fibrosis resolution is not clear, it likely involves their increased production of matrix metalloproteinases such as MMP2 and MMP13 which degrade extra cellular matrix. Consistent with this, there was reduced MMP2 and MMP13 production in *Ccr2*$^{-/-}$ mice following chronic CCl_4 in mice (Mitchell et al. 2009) and *mmp13*$^{-/-}$ mice displayed reduced resolution of fibrosis following chronic CCl_4 in rats (Fallowfield et al. 2007).

1.5.2.3 Fate of Kupffer Cells and recruited macrophages following injury

As described above, both resident KC and recruited macrophages are present during liver injury, and their differing roles have been at least partially elucidated. However, what happens to the two populations following complete resolution from injury is not clear. A key question which remained to be answered when I started my project was whether KC continue to be regulated autonomously and independently of monocyte-derived

macrophages after injury, or whether they are replenished by recruited cells, and if so, whether this affects their long-term function. The loss and replenishment of resident macrophages in other tissues had been addressed in a variety of inflammation scenarios, however. An almost 9-fold loss of LCs was detected 7 days following exposure to UV light, and replenishment occurred through recruitment of bone-marrow derived LCs. Donor LCs were still present 12 weeks after the injury, indicating that they had permanently replenished the LC population (Merad et al. 2002). The identity of the recruited LCs was later shown to be Ly6C^{hi} monocytes (Ginhoux et al. 2006). Interestingly, LC were also reduced in number following inflammation driven by x-irradiation or through topical application of acetone and oil, but there was no replenishment by BM-derived cells in these contexts (Merad et al. 2002). However, the levels of inflammation caused with either x-irradiation or acetone and oil did not result in increased expression of CCL2 and CCL7 as was seen with UV radiation, indicating that monocytes were simply not recruited to the skin in these scenarios (Merad et al. 2002). Resident lung macrophages were depleted following infection with an influenza virus, but recovered to normal numbers 4 weeks later through local repopulation, as there was no evidence of their replacement by tdTomato^{+} monocytes (Hashimoto et al. 2013). However, monocyte-derived macrophages were still present in the lung one year after bleomycin-induced lung fibrosis, and these recruited macrophages acquired a gene-expression pattern which differed by only 330 genes from that of the resident alveolar macrophages (Misharin et al. 2017). In the liver, Zigmond and colleagues concluded that KC replenished though local proliferation following APAP, as they did not see emergence of CX3CR1-GFP^{neg} cells from CX3CR1-GFP^{+} transferred monocytes (Zigmond et al. 2014). However, at the 4 day time point, the donor cells that were present had in fact down regulated Ly6C and upregulated F4/80 (Zigmond et al. 2014), which could be suggestive that they were, in fact, maturing into a KC phenotype. Following chronic CCl_4 injury, labelling of circulating Ly6C^{lo} monocytes with fluorescent latex beads 4 hours after the final CCl_4 injection resulted in a small number of bead^{+} F4/80^{hi}CD11b^{lo} cells indicative of their contribution to the KC population at 168 hours (7 days). However, a major caveat with this method is that bead^{+} KC may simply represent a KC which has phagocytosed a bead^{+} cell. Furthermore, whether the bead^{+} KC remained in the liver long-term, beyond the 7 day time point was not assessed, and could represent a transient emergence of F4/80^{+} recruited cells, which may not permanently replenish the resident KC population.

Thus the question of whether KC remain totally autonomous of monocyte-derived macrophages following acute and chronic liver injury remained to be determined, and is addressed in chapter 6, using more robust fate-mapping methods, and allowing for long-term recovery from injury to assess whether there is any long-term contribution of recruited macrophages to the resident KC compartment.

Collectively, the studies detailed in this introduction which revealed that tissue macrophages are established during embryogenesis, proliferate *in situ* to self-renew and in many tissues require little or no contribution from monocytes to maintain the population were completely ground-breaking (Sieweke and Allen 2013). They significantly challenged the idea of the MPS which had held for decades and there was therefore much excitement to understand the importance of both origin and local tissue factors on macrophage function in both homeostasis and injury (Varol 2015; Ginhoux and Jung 2014; Epelman et al. 2014b; Hoeffel and Ginhoux 2015).

1.6 Thesis aims

Such massive diversity in the functions of tissue macrophages raises questions of the significance of their origin and how they are maintained. Although there was some evidence that KC do not require replenishment from monocytes in the steady state, I hypothesised that disruption of homeostatic conditions through exogenous administration of CSF1-Fc, or through acute or chronic liver injury would lead to their long-term replacement by circulating Ly6C^{hi} monocytes. To test my hypothesis, my aims were as follows:

- Establish a protocol to efficiently isolate liver leukocyte populations for flow cytometry.
- Investigate the role of competition for CSF1 in the maintenance of KC autonomy.
  - Characterise the newly generated *Csf1r*-mApple mice and use a fluorescently labelled CSF1-Fc^{AF647} fusion protein to determine comparative CSF1R transgene expression and CSF1 uptake across liver populations.
  - Administer CSF1-Fc to explore whether CSF1 availability is a limiting factor in determining KC population size and ability of monocytes to convert to long-lived KC.

- ❖ Establish whether monocyte-derived macrophages permanently replenish resident KC following liver injury, and if so, whether this leads to long-term changes in function of the population.

These aims fall within the broader question of whether the functions of resident macrophages are defined by their genetic programming or by local tissue-specific factors, or both. To answer this over-arching question we must understand in detail the mechanisms which maintain tissue macrophage populations, focussing on individual tissues and populations within tissues in both homeostatic and infection/inflammation scenarios. This thesis adds to the emerging body of work by exploring parameters which surround maintenance of liver Kupffer Cells in both homeostatic and inflammation and repair scenarios.

Chapter 2: Materials and methods

2.1 Mice

All mice were maintained in house under specific pathogen free (SPF) conditions at Little France Phase 1 (LF1) or Phase 2 (LF2) or Ann Walker units, with exceptions listed below. Transgenic mouse lines used in this study – *Ccr2*$^{-/-}$, *Csf1r*-EGFP (MacGreen), *Csf1r*-mApple were bred and housed in the clean LF1 facility at Little France, and transferred to LF2 for experimental procedures and necropsies, except where specified otherwise. For *Csf1r*-mApple or *Csf1r*-EGFP experiments conducted at Little France, WT littermate (C57BL/6) controls were used whilst for *Ccr2*$^{-/-}$ experiments, C57BL/6JCrl mice were obtained from Charles River and kept in house for 2 weeks prior to use in the same room as their transgenic counterparts. All other chimeric and C57BL/6 mouse studies were carried out in the Ann Walker animal facility on the King's Buildings campus using mice bred in house. Part way through the study the Ann Walker facility switched from maintaining a C57BL/6JOlaHsd colony to a C57BL/6J colony. Anecdotally, there was no noted effect of this switch to results or their interpretation. All experiments were carried out under license granted by the UK Home Office and approved by the University of Edinburgh Animal Welfare and Ethical Review Body

Table 2.1 Mouse strains and source

Strain (alternative names)	**Source**
C57BL/6J (CD45.2^{+}, Ly5.2)	Bred in house in Ann Walker. Originally from Harlan UK (first half of study) or The Jackson Laboratory (second half of study)
Ly5.1 Het (CD45.1^{+}CD45.2^{+})	Bred in house in Ann Walker by crossing C57BL/6J with Ly5.1 Hom

Ly5.1 Hom (B6.SJL-*Ptprc*^{a} *Pepc*^{b}/BoyJ, CD45.1^{+})	Bred in house in Ann Walker. Originally from Harlan UK (first half of study) or The Jackson Laboratory (second half of study)
C57BL/6JCrl	Obtained from Charles River and kept in LF2 alongside transgenic mice for 2 weeks prior to use
C57BL/6OlaHsd	Obtained from Harlan UK for breeding with *Csf1r*-mApple mice
Csf1r-mApple (*Csf1r*-mApple/*Csf1r-rtTA)*	Generated in collaboration with David Hume by pronuclear injection and bred in house in LF1. Bred with C57BL/6OlaHsd to generate negative littermate controls
MacGreen (B6.Cg-Tg(Csf1r-EGFP)1Hume/J, c-*fms*-EGFP, *Csf1r*-EGFP)	Kindly provided by Prof. Philippa Saunders and Dr Takanori Kitamura (housed in LF1).
Ccr2$^{-/-}$ (B6.129S4-*Ccr2*^{tm1Ifc}/J)	Originally obtained from Jackson Laboratories and maintained in LF2. *Or* Kindly provided by Prof. Allan Mowat (The University of Glasgow) for one aged experiment
H2B-GFP (B6;129S4-*Gt(ROSA)26Sor*$^{tm1(rtTA*M2)Jae}$ *Col1a1*$^{tm7(tet0-HIST1H2BJ/GFP)Jae}$/J)	Bred in house in LF1

2.2 Generation of protected, partially irradiated bone marrow chimeras

Ly5.1 Hom or Ly5.1 Het mice were anaesthetised with 0.008mg/g Domitor (Medetomidine) and 0.8mg/g Veletar (Ketamine) mixed in sterile dPBS given sub-cutaneously (sc) in the flank of the animal (at a volume of 0.008ml/g). Mice were put into bubble wrap 'sleeping bags' to

maintain core body temperature during the irradiation process. The lower limbs and lower portion of the abdomen were exposed to 9.5Gy γ irradiation for 19 minutes and 30 seconds, whilst the rest of the body, including the liver was shielded by a 2 inch thick lead block. For experiments where the resident macrophages of the peritoneal cavity were to be studied, less of the abdomen was exposed to the irradiation, to protect the cavity. Mice were given 0.5mg of Antisedan (Atipamezole) in 100μl sterile dPBS sc, and placed into a heat box at 37°C for 10 minutes to aid recovery from anaesthetic. Mice were given broad spectrum antibiotics (Baytril) in their drinking water for 4 weeks post irradiation to reduce risk of bacterial infection, and mash for 2 weeks.

2.3 Preparation of bone marrow cells for reconstitution of irradiated hosts

C57BL/6 (Ly5.2 hom) mice bred in Ann Walker, or MacGreen mice bred in LF1 were culled by cervical dislocation. Skin was removed from the lower abdomen to expose the hind legs. Excess muscle and flesh was cut away, and the tibias and femurs were dissected from the animal, ensuring that bones were kept intact. Bones were discarded if there was any accidental breakage of bones or exposure of bone marrow in order to ensure bone marrow remained sterile. For mice bred in Ann Walker, dissection of the mice was carried out in the SPF dissection room B56, whilst for MacGreen animals, mice were dissected in a class II cell culture hood in LF1. Bones were collected into ice cold dPBS in a bijou.

In sterile conditions, bones were transferred into ice cold 70% ethanol for 2 minutes to sterilize and wash bones. Bones were washed twice in sterile, ice cold dPBS and kept in dPBS on ice. The ends of each bone were removed using sterile scissors and sterile forceps to expose the bone marrow. Using a 23 gauge needle and a 10ml syringe, bone marrow was flushed from each bone with HBSS (Gibco) supplemented with 5% FCS (Gibco). A bone was considered to be fully flushed of its bone marrow when its colour changed from a pale pink to a translucent white.

Flushed bone marrow was gently mixed to a single cell suspension using a 10ml syringe without a needle. The single cell suspension was poured through a sterile 40μm filter (VWR) into a 50ml falcon. Cells were centrifuged at 300g for 5 minutes at 4°C. Supernatant was discarded and cells were lysed in RBC lysis buffer on ice (Sigma; 5ml for 5 minutes). Cells were topped up to 10ml with HBSS + 5% FCS. Cells were centrifuged at 300g for 5 minutes at 4°C.

Supernatant was discarded and cells were resuspended in 10ml HBSS + 5% FCS for counting. Cells were counted using a haemocytometer and a light microscope. See section 2.13 for methods for haemocytometer counts. Cells were resuspended at $25x10^6$/ml (but this could be reduced to $10x10^6$/ml if an insufficient number of cells were recovered) in dPBS.

2.4 Reconstitution of irradiated mice with donor bone marrow

The day after irradiation mice were given 2-$5x10^6$ bone marrow cells from congenic C57Bl/6 mice, or Macgreen mice intra-venously (iv) through the tail vein in a total volume of 200µl sterile dPBS (Gibco).

2.5 Screening of chimeras

Mice were placed into a heat box set at 37°C to ensure adequate vasodilation. The tail vein was punctured using a grey 27 gauge needle (BD) and tail vein blood (20µl) was collected with a pipette for analysis by flow cytometry to test the level of chimerism which had been achieved 6 weeks after reconstitution. Mice were left for a total of 8 weeks after irradiation before commencement of studies. Any mouse with blood chimerism below 10% in the $Ly6C^{hi}$ monocyte compartment was excluded from the study, and was culled.

2.6 Isolation of leukocytes from the liver

Mice were culled by increasing concentrations of CO_2. Mice were slowly perfused through the inferior vena cava with 10ml of PBS. In most cases, 0.5g (±0.05g) of the left lobe of the liver was collected into RPMI for transport. If the left lobe weighed less than 0.45g then an extra piece of liver (usually from the right or caudate lobes) was added. Livers were put into 60mm cell culture dishes (Scientific Laboratory Supplies Ltd.) and finely chopped using a razor blade until homogenised. A 5ml stripette with 5ml of enzyme cocktail (RPMI with 0.625mg.ml^{-1} collagenase D (Roche), 0.85 mg.ml^{-1} collagenase V (Sigma-Aldrich), 1 mg.ml^{-1} dispase (Gibco, Invitrogen) and 30U.ml^{-1} DNase (Roche Diagnostics GmbH)) was used to transfer the liver homogenate to a 50ml conical tube. Livers were digested for 22 minutes at 37°C, 240rpm, with vigorous hand shaking every 5 minutes. Digests were poured through a 100µm strainer, then cells were prepared according to one of the following protocols:

2.6.1 300g centrifugation method

Tubes were topped up to 50ml with ice cold RPMI (Gibco) and centrifuged at 300g, max. break and accelerator for 5 minutes at 4°C. Supernatants were discarded, except when comparing protocols, in which case the supernatants were transferred to a fresh 50ml falcon, centrifuged at 400g and the pellet retained for analysis. Cell pellets were resuspended in 30ml ice cold RPMI and centrifuged at 300g for 5 min. RBC lysis buffer (Sigma; 2ml) was added for 2 minutes and samples were topped up with another 2 ml FACS buffer (PBS supplemented with 0.5% BSA and 2mM EDTA (Life technologies)). Cells were centrifuged at 300g for 5 min and the supernatant discarded. The pellet was resuspended in 2ml FACS buffer, passed through a 40µm strainer with a stripette, and counted using a CASY TT counter (Roche). This method was used for all experiments in this thesis except where clearly indicated in chapter 3.

2.6.2 33% Percoll gradient method

Tubes were topped up to 50ml with liver wash buffer (PBS + 10% FCS) and centrifuged at 443g for 6 min, max. break and accelerator, 4°C. The supernatant was discarded and the process was repeated. The pellet was resuspended in a 33% Percoll gradient (25ml per sample – 8.25ml Percoll, 0.925ml 10X PBS, 15.825ml 1X PBS) and spun at 600g for 12 min, with minimum break and accelerator, at room temperature. The resultant hepatocyte and percoll layers were discarded, except when comparing protocols, in which case they were centrifuged at 400g and the resultant pellet was stained. The leukocyte pellet was transferred to a fresh 50ml falcon and topped up to 30ml with liver wash buffer and centrifuged 300g for 5 min, max. break and accelerator, 4°C. Red blood cells were lysed for 5 min in 5ml RBC lysis buffer (Sigma), topped to 30ml with liver wash buffer and washed at 300g for 5 min. Pellets were resuspended, strained and counted as above.

2.6.3 50g centrifugation method

Tubes were topped up to 50ml with RPMI supplemented with 10% FCS and centrifuged at 50g for 10 min with accelerator set at 3 and breaks set at 1, 4°C. For comparisons of protocols, the pellet (normally discarded) was retained, whilst the supernatant was collected into a fresh tube and was centrifuged at 340g for 10 min, breaks 3;1. The pellet was lysed

with RBC lysis buffer (Sigma; 2ml) for 5 min on ice, topped up with 2ml RPMI + 10% FCS and spun 340g for 10 min, breaks 3;1. Pellets were resuspended, strained and counted as above.

2.7 Isolation of leukocytes from the peritoneal cavity

Mice were culled by increasing concentrations of CO_2. Skin was removed from the abdomen, carefully leaving the peritoneum intact. 5ml syringes were loaded with 3ml RPMI + 2mM EDTA + 10mM HEPES solution, and an extra 1ml of air was drawn into the syringe to aid inflation of the cavity. A 23 gauge (blue) needle (BD) was guided bevel upright into the cavity, taking care not to puncture any organs and the air and RPMI was expelled into the cavity. The needle was withdrawn and the mouse gently shaken to ensure distribution of media throughout the cavity. The needle was inserted to the side of the cavity and media was drawn back into the syringe. This process was carried out 3 times in total, yielding an average of around 8ml of peritoneal wash fluid in total. Cells were centrifuged at 300g, 5 mins, 4°C. The pellet was resuspended in 1ml FACS buffer and samples were counted using a CASY TT counter (Roche).

2.8 Isolation of leukocytes from the lung

Mice were culled by increasing concentrations of CO_2. The thoracic cavity was opened and lungs were gently cut out using scissors. Lungs were not perfused. Lungs were stored in ice cold RPMI, then transferred to a 5ml bijou and cut into small pieces using scissors. Samples were digested in 2ml enzyme mix (see section 2.6) at 37°C, 240rpm for 45 mins with vigorous hand shaking every 10-15 minutes. Digests were pushed through a 100μm strainer using a plunger from a 5ml syringe and tubes were topped up to 10ml with FACS buffer. Samples were centrifuged at 300g, 5 mins, 4°C. The pellets were resuspended in 10ml FACS buffer, strained through a 40μm strainer and counted using a CASY TT counter (Roche).

2.9 Isolation of leukocytes from whole blood

Blood for experimental analysis was collected either by tail vein puncture or cardiac puncture (see section 2.10). Leukocytes were then isolated from blood in two ways. Blood (20μl) was collected into V-bottomed culture plates (VWR) containing 180μl blood buffer (HBSS + 5%

FCS + 2mM EDTA). Samples were washed once in PBS before staining. After staining, RBC were lysed using 200µl 1X RBC lysis buffer (BD Biosciences) diluted in water for 8 minutes at room temperature.

Alternatively, blood (100µl) was collected into 10µl of EDTA in a 15ml falcon tube. RBC were lysed twice in 1ml of 1X RBC lysis buffer diluted in water (Biolegend) for 5 mins on ice. Cells were washed in 9ml FACS buffer (PBS + 2mM EDTA + 0.5% BSA). Cells were plated into 96-well V-bottomed tissue culture plates for staining with antibodies for flow analysis.

Both methods anecdotally gave roughly equivalent ratios of different leukocyte populations, but the latter method gave far superior yields, and was used for all experiments performed by me in chapters 4 and 6.

2.10 Processing of blood for serum analysis

After euthanasia by increasing concentrations of CO_2, cardiac puncture directly through the ribcage was used to collect large volumes of blood. The ribcage was steadied using the free hand, and a 1ml syringe with a grey 27 gauge needle (BD) was guided between ribs into the heart. The plunger was gently pulled to draw blood into the syringe. The needle can be moved gently in and out until the needle is in a chamber and blood can be drawn easily into the syringe. If no blood can be drawn on the first attempt, the needle can be withdrawn and the process attempted again. Blood was transferred to a microtainer tube (BD) and left at room temperature for 30 minutes to 2 hours. Blood was centrifuged at 100g for 1.5 min at room temperature. The serum was transferred to a 1.5ml microfuge tube and stored at -80°C. Samples were analysed for serum ALT and AST levels by Dr Forbes Howie at the SURF service based at QMRI.

2.11 Flow cytometry

2.11.1 Surface staining

$2x10^6$ liver cells, $5x10^6$ lung cells, $1x10^6$ peritoneal cavity cells were added to a 96 well V bottomed cell culture plate (VWR). If cells were to be stained with Zombie Aqua fixable viability dye (Biolegend) they were first washed in PBS to remove any protein (a wash indicates a spin at 300g for 5 minutes at 4°C). 10µl Zombie Aqua (see table 2.2 for all antibody

dilutions) was added for 10 minutes at room temperature, and samples were wrapped in foil to protect them from light. Cells were then incubated in the dark with 10μl anti-CD16/CD32 + 10% mouse serum (Life technologies) referred to as 'block', for 10 minutes on ice. Cells were then incubated with a mix of primary antibodies (30μl) for 30 minutes in the dark on ice. Cells were washed twice in FACS buffer. If required, cells were incubated with fluorochrome-conjugated streptavidin (50μl) for 20 minutes on ice, and washed twice in FACS buffer. Cells were resuspended in FACS buffer for acquisition on the same day. All samples were run live, the same day as necropsy throughout the study, unless they were to be fixed for additional intracellular staining. In this instance, pellets were resuspended in 100μl Foxp3/transcription factor staining fixation reagent, diluted 1:3 with permeabilization reagent (eBioscience). Samples were left overnight at 4°C. The following morning, samples were washed into 1X Foxp3/transcription factor permeabilization buffer in dH_2O (eBiosicence) and stored at 4°C for a maximum of one week before intracellular staining. Fluorescence minus one controls were used to determine gates, and where indicated isotype matched controls were used to determine specificity of binding. For some experiments, 7AAD (Biolegend; 20μl for liver/lung samples; 10μl for blood/peritoneal cavity samples added to 150μl cells in FACS buffer) was added either alongside, or instead of, Zombie Aqua 5 minutes before acquisition. Samples were run on either a 5 or 6 laser LSR Fortessa flow cytometer (BD). Samples that formed part of a time course were always run on the same machine, using the same set up parameters. Data were analysed in FlowJo v9.9

2.11.2 Ki67 and BrdU intracellular staining

For Ki67 and BrdU staining, surface markers were stained and cells were fixed as detailed above. Cells were incubated at 37°C for 30 minutes with 100μl DNase mixture (master mix = 30μl DNase [Sigma] + 970μl dPBS + 10μl $MgCl_2$ [Sigma; from hexahydrate powder]). A no DNase control well was included for setting BrdU gating, and an isotype matched control was used to set the Ki67 gate. Cells were washed twice with 1X permeabilization buffer. BrdU and Ki67 antibodies diluted in 1X permeabilization buffer were added to samples (20μl) and incubated for 30 minutes at room temperature in the dark. Cells were washed twice with 1X permeabilization buffer and resuspended in FACS buffer. Samples were immediately analysed by flow cytometry.

2.11.3 Clec4f staining for flow

For Clec4f staining, a polyclonal goat anti-mouse Clec4f antibody was included in the normal surface antibody cocktail. After washes, cells were incubated with a donkey anti-goat-AF647 antibody for 20 minutes on ice in the dark. If necessary, the donkey anti-goat secondary was added at the same time as a streptavidin secondary to reduce the number of staining steps.

2.11.4 Single stained control beads

To generate a compensation matrix in the FACSDiva software (BD), single stained control beads were used. A few drops of Ultra-comp beads (eBioscience) were added to FACS buffer, and 100µl of this was added to 12x75mm polystyrene tubes (SLS Falcon). 0.5µl of a single fluorochrome-conjugated antibody was added to each tube and incubated in the fridge for 30 minutes. Beads were washed with FACS buffer. For biotinylated primary antibodies, the streptavidin conjugated fluorochrome (0.5µl) was incubated at the same time.

2.12 Flow assisted cell sorting

For FACS, livers were split into two sections, each of which were digested with 5ml of enzyme cocktail and processed according to the standard liver protocol (see sections 2.6 and 2.6.1). Split livers were pooled in 5ml total volume prior to counting. The whole liver (40-50x10^6 cells) was stained according to the surface staining protocol (see section 2.11.1) in 12x75mm polystyrene tubes (SLS Falcon). The total staining volume was scaled up to 1ml to account for the increased number of cells. 400µl block and 600µl antibody cocktail were added. 1ml of streptavidin secondary was added where appropriate. DAPI was added at 1:1000 immediately prior to running of samples to exclude dead cells. FMO controls were used to set gates. Cells were sorted using a FACS Fusion (BD) sorter with a 70µm nozzle attachment.

2.13 Haemocytometer counts

10µl of cell suspension was mixed with 10µl 0.4% Trypan Blue and 20µl of this cell suspension was loaded into a haemocytometer. The total number of cells within the central 5x5 grid was counted. This number was multiplied by 20000 to find the total number of cells per ml.

2.14 CASY TT cell counter counts

Cells were counted according to manufacturer's instructions. 5μl cell suspension was added to 5ml of CASY ton in a CASY cup and gently shaken to mix. Cells were then run through CASY's automated cell counting system. A size threshold was set from 5.3μm-15μm to exclude red blood cells and small bits of debris, and large clumps of cells.

2.15 Storage of CSF1-Fc, IL-4 and anti-IL-4 Ab

CSF1-Fc was given to the Jenkins lab by David Hume. When it arrived it was at a concentration of 3.96mg/ml in a total volume of 1ml. Vials were resuspended at 1mg/ml in sterile dPBS (Gibco) and aliquotted into 100μl aliquots, giving a total of 100μg of CSF1-Fc protein per aliquot. Both stock CSF1-Fc at 3.96mg/ml and aliquotted CSF1-Fc at 1mg/ml was stored at -80°C.

Recombinant murine IL-4 protein was bought from Peprotech and resuspended in dPBS to give a stock concentration of 1mg/ml, stored in 50μl aliquots at -80°C. Anti-IL-4 antibody (IIBII) was bought from Bio X Cell and resuspended in dPBS to give a stock concentration of 7mg/ml, which was stored in 36μl or 72μl aliquots at -80°C.

2.16 Administration of CSF1-Fc and IL-4c *in vivo*

CSF1-Fc was resuspended in dPBS and mice were given 1μg/g sc in a volume of 5μl/g of dPBS. Recombinant murine IL-4 was mixed with recombinant anti-IL-4 (IIBII) in sterile conditions to form an IL-4 complex (IL-4c) at a ratio of 1:5 IL-4:anti-IL-4. Mice were given 0.05μg IL-4 + 0.25μg anti-IL-4/g in a volume of 5μl/g of dPBS.

2.17 Administration of carbon tetrachloride

One part Carbon tetrachloride (CCl_4, Sigma) was mixed with 3 parts olive oil (low endotoxin, Sigma) in a glass bottle in a fume cupboard. Male mice were treated with 1μl/g of body weight of the CCl_4 in olive oil mixture ip to give a final dose of 0.25μl/g of CCl_4. Control animals received 1μl/g olive oil ip. Mice received either one dose of CCl_4 (acute model), or two doses

a week for 4 weeks (chronic model), in which case doses were given alternately 3 or 4 days apart.

100μl Hamilton syringes were used allowing accurate dosing to the nearest 1μl, and separate Hamilton syringes were used for olive oil control and CCl_4 treated mice to prevent any cross contamination. Control and CCl_4 treated animals were kept in separate cages due to anecdotal evidence by pers. com. with others in the department that CCl_4 can be excreted by animals through urine, which can contaminate bedding, leading to transfer of CCl_4 to control animals via the inhalation route.

Syringes and glass bottles were washed 5 times in 100% ethanol followed by 5 times with water, and were autoclaved after each day of injections.

2.18 Administration of BrdU

BrdU (Sigma) (1mg in 100μl dPBS) was administered sc in the flank 2 hours prior to necropsy. Cells were stained following the protocol in section 2.11.2.

2.19 RNA extraction and quantification

50,000 cells were FACS purified directly into 0.5ml RLT buffer (Qiagen) in RNase free 1.5ml eppendorfs (Qiagen) and kept on ice until RNA extraction. RNA was extracted the same day as the sort to avoid freeze-thaw. The sort volume was 200μl, giving a total volume of 0.7ml per sample. An additional 200μl RLT buffer was added, giving a final volume of 0.9ml per sample. 9μl β-mercaptoethanol (Sigma) was added and tubes were gently mixed. RNA was extracted using reagents from the RNeasy plus Micro kit, according to manufacturer's instructions (Qiagen), following the 'purification of total RNA from animal cells' protocol, with exceptions: gDNA eliminator columns were not used, and no DNase step was performed. RNA was quantified by Pamela Brown using the Perkin Elmer Labchip GX24 gel quantification. 2μl was loaded per sample, leading to one freeze-thaw cycle. Samples were run using the pico chip with a detection range of 5-50000pg/μl. Many of the samples had an RNA concentration greater than this maximum, but pers. com. with Pamela indicated that this should not greatly affect the accuracy of the predicted concentrations or the quality scores. Samples were also quantified using the Nanodrop 1000 (Thermo) and for this

purpose separate 1.5µl aliquots were used which had been taken prior to freezing of the main sample, avoiding an additional freeze-thaw cycle.

2.20 NanoString analysis

RNA samples were delivered on frozen ice to the NanoString facility at the MRC Institute of Genetics and Molecular Medicine (IGMM), University of Edinburgh. Alison Munro performed hybridization reactions and ran 8µl per sample through the nCounter platform using the nCounter Mouse myeloid innate immunity panel (NanoString Technologies).

The sample reporter code count (RCC) files were uploaded to nSolver Analysis Software v4.0.70 (NanoString Technologies) and quality checked using default settings. Tim4^{hi}post replicate 1 exhibited an imaging QC flag due to a borderline "fields of view" success rate of 70%. Alison Munro suggested this was acceptable, and further analysis showed near-perfect positive pairwise correlations (all correlations: $r>0.99$; $p < 0.0001$). Samples were individually normalised for background noise using the geometric means of negative controls, and sample-based variation using the geometric means of positive control RNA spike-ins and all housekeeping genes. Following the recommendations of the NanoString Gene Expression Data Analysis Guidelines (NanoString Technologies, 2017), fold change significance values were not corrected for multiple testing. Data were further explored using the nCounter Advanced Analysis Software v2.0.115 (NanoString Technologies) using R v3.3.2 (R Core Team).

Volcano plots were generated using fold change for all assayed gene targets. Data were $\log_2$ transformed and the top fifty genes with greatest absolute fold change between Tim4^{hi} post and Tim4^{lo} post populations were used to construct a heatmap (Morpheus, 2019). Samples were grouped using hierarchical clustering with Euclidean distance and average linkage. Gene function was annotated using information provided by the nCounter® Mouse myeloid innate immunity panel. Bioinformatic analysis was carried out by Dr Andrew Mason.

2.21 Preparation of tissues for histological assessment

2.21.1 Fixation in 4% paraformaldehyde

This method was used to preserve EGFP fluorescence in MacGreen whole mice, and chimeras with MacGreen donor bone marrow. 4% paraformaldehyde (PFA) was prepared in the lab, and stored at -20°C until use. A lobe of liver was fixed for 2 hours in 10ml 4% PFA on a roller in a cold room at 4°C. Livers were washed twice in dPBS. 10ml 15% sucrose in dPBS was added for 1 hour at room temperature. The 15% sucrose was drained and 10ml 30% sucrose in dPBS was added. Livers were left overnight at 4°C. The 30% sucrose was drained and livers were air dried. Livers were embedded into OCT (Fisher Scientific) in Peel-A-Way embedding molds (SLS). The OCT-embedded samples were snap frozen in a 100% ethanol + dry ice slurry. Blocks were stored at -80°C.

2.21.2 Fixation in 10% formalin

This method was used to fix livers before embedding in paraffin. A lobe of liver was fixed for 12 hours in 10% formalin (3.7% formaldehyde) (diluted 1:10 in PBS from 37% formaldehyde solution; Sigma) at room temperature. Livers were washed twice in 70% ethanol and sent to The University of Edinburgh SURF histology service based at QMRI to be paraffin embedded and cut.

2.21.3 Snap freezing of liver into OCT on dry ice

This method was used to freeze livers due for cryosectioning, followed by fixation and immunofluorescence. A lobe of liver was immediately embedded in OCT in Peel-A-Way molds and snap frozen on dry ice within a minute of being removed from the animal. Blocks were stored at -80°C.

2.22 Cryosectioning

Samples were brought to -20°C at least 24 hours prior to cryosectioning. Blocks were removed from the molds and mounted on the cryostat chuck. 9μm sections were taken onto standard glass microscope slides (Leica). If tissues had already been fixed with 4% PFA, slides were immediately stored at -20°C for up to one week before staining. If tissues had been directly snap frozen, sections were allowed to air dry for one hour. Sections were fixed in ice

cold 1:1 acetone:methanol for 5 minutes. Slides were dabbed dry and stored at -20°C for up to one week before staining.

2.23 Periodic acid-Schiff staining

10% formalin fixed, wax embedded tissues were used. PAS staining was carried out by staff at SURF histology service, following their standard protocols.

2.24 Immunofluorescence

Cryosectioned tissues were used. Slides from the freezer were air dried for 30 minutes and samples were drawn around with a hydrophobic pen (ImmEdge, Vector Labs). Slides were placed into a humidity chamber. Slides were washed twice in 120µl dPBS. Slides were blocked in 120µl 20% normal goat serum (NGS) (In-Vitro Diagnostics) in PBS for one hour at room temperature. The block was tipped off and the slides dabbed dry. Primary antibodies were diluted in antibody staining diluent (Invitrogen) at the relevant concentrations, and slides were incubated with 100µl antibody for 2 hours at room temperature (see table 2.3 for details of dilutions). Slides were washed twice in dPBS. Fluorochrome-conjugated secondary antibodies were diluted in 20% NGS and 100µl was added for 30 minutes at room temperature. Slides were washed twice in dPBS and mounted in Vectashield hard set antifade mounting medium with DAPI (Vector labs). Slides were sealed with clear nail varnish and stored wrapped in foil at 4°C for up to one week before imaging.

2.25 Imaging

PAS stained slides were imaged on a light microscope with 80X total magnification. Images were processed using Fiji ImageJ v 2.0.0.

For immunofluorescence, stained slides were imaged using a LSM780 confocal microscope (Zeiss) with Zen Black software (Zeiss). All images from within the same data set were imaged with the exact same acquisition settings. Images were processed and analysed using Fiji ImageJ v 2.0.0. Where brightness and contrast was edited, this kept consistent across all images within a data set.

2.26 Calculation for contribution of endogenous KC to total proliferation rate (discussed in Chapter 5)

To determine the proportion of the total KC proliferation that was attributable to endogenous, tissue-resident KC (of host origin) the following calculation was used: $\%\ proliferation\ in\ host\ KC - (\%\ chimerism\ in\ KC\ population\ x\ \frac{\%\ proliferation\ in\ donor\ KC}{100})$

2.27 Statistical analysis

Data were analysed in Prism 6 (GraphPad), and significance in cell frequencies was determined by One-way ANOVA with Tukey's multiple corrections, Two-way ANOVA with Tukey's multiple corrections, student's t-test, multiple t-tests with Holm-Sidak correction applied or a paired t-test where appropriate and as indicated throughout the text.

Table 2.2 Primary, secondary and streptavidin-conjugated antibodies used for flow cytometry

Antibody	**Clone**	**Dilution**	**Supplier**
7AAD	n/a	10-20µl/sample	Biolegend
BrdU	Bu20a	1.25µl/sample	Biolegend
CD115	AFS98	1:200	Biolegend
CD11b	M1/70	1:200	Biolegend/eBioscience
CD11c	N418	1:200	Biolegend
CD19	6D5	1:200	Biolegend
CD26	H194-112	1:200	Biolegend
CD3	17A2	1:200	Biolegend
CD31	MEC13.3	1:200	Biolegend
CD43	S11	1:200	Biolegend
CD45.1	A20	1:200	Biolegend
CD45.2	104	1:200	Biolegend
CD64	X54-4/7.1	1:200	Biolegend
CD80	16-10A1	1:200	Biolegend

Clec4f	polyclonal	1:100	R&D
DAPI	n/a	1:1000	Biolegend
Donkey anti-goat AF647	polyclonal	1:1000	Thermofisher
F4/80	BM8	1:200	Biolegend
Ki67	B56	7.5µl/sample	BD Bioscience
Ly6C	HK1.4	1:400/1:200	Biolegend/eBioscience
Ly6G	1A8	1:200	Biolegend
PDCA-1	927	1:200	Biolegend
PDL1	10F.9G2	1:200	Biolegend
SiglecF	E50-2440	1:200	BD Pharmingen
SiglecF - biotin	ES22-10D8	1.7µl/sample	Miltenyi Biotech
Streptavidin-BV650	n/a	1:200 (0.1mg/ml vial)	Biolegend
Tim4	RMT4-54	1:200	Biolegend
Zombie Aqua viability dye	n/a	1:100	Biolegend

Table 2.3 Primary and secondary antibodies used for immunofluorescence staining

Antibody	Clone	Dilution	Supplier
F4/80	A3-1	1:100	Abcam
Tim4	RMT4-54	1:50	Biolegend
Goat anti-rat IgG AF488	polyclonal	1:200	Thermofisher
Goat anti-rat IgG AF594	polyclonal	1:200	Thermofisher

Chapter 3: Establishment of a robust method for the unbiased isolation of Kupffer Cells, removing any endothelial cell contamination

3.1 Introduction

In order to explore the origin and maintenance of liver Kupffer Cells during homeostasis and liver injury I first needed to develop robust and sensitive techniques to isolate and analyse leukocytes in the liver. Flow cytometry is a powerful tool, as it provides a method to evaluate changes in frequency, number and phenotype of multiple cell populations in parallel, and is the main method used to analyse samples in this thesis. However, the accuracy and validity of the conclusions made from flow cytometric studies depends on both the process used to isolate and prepare a single cell suspension, and the choice of markers and fluorochrome combinations used to identify populations of interest.

The isolation of leukocyte populations from solid tissue which faithfully represented the ratios and phenotypes of the populations present *in vivo* was an important consideration before embarking on further study. There are multiple protocols published for the preparation of a single cell suspension of leukocytes from murine liver. Common to these methods is the manual and enzymatic digestion of solid tissue to release leukocytes from the parenchymal structure of the tissue. When I joined the Jenkins lab, we favoured a protocol employing a 33% Percoll gradient separation step designed to remove hepatocytes and debris from the liver digestion soup, which has been used previously (Phythian-Adams et al. 2010). However, other members within the department were using an alternative protocol employing an initial 50g centrifugation step to pellet and discard hepatocytes and other parenchymal cells (Ramachandran et al. 2012). Additionally, Dr Calum Bain had recently joined the Jenkins lab as a post-doc and had previously published a study using a more simple method of multiple 300g centrifugation steps (Bain et al. 2014). Thus, comparison of these methods was a critical first step to determine the optimal method for my studies.

At the time that I started my PhD, the most universally accepted marker for liver KC was F4/80, which was first identified for use as a general macrophage marker in mouse (Austyn et al. 1981) and the use of an F4/80^{hi}CD11b^{lo} gate to identify KC had remained the gold

standard despite a further 30 years of research in the macrophage field (Heymann and Tacke 2016). During the course of the project, CLEC4F, a C-type lectin, was shown to be expressed specifically by KC (Scott et al. 2016; Yang et al. 2013; Lavin et al. 2014), whilst I and others found that Tim4, a phosphatidylserine receptor (Miyanishi et al. 2007) was useful in distinguishing KC from other myeloid cells in the liver (Beattie et al. 2016; Scott et al. 2016). In parallel to my studies, Dr Ruairi Lynch, another PhD student in the Jenkins lab, discovered what appeared to be a significant contamination of the F4/80^{hi}CD11b^{lo} KC gate with endothelial cells using a tamoxifen inducible fluorescent reporter system to label cells expressing the endothelial marker CDH5. These findings, together with the data presented in this chapter were published in The Journal of Leukocyte Biology (Lynch et al. 2018). The experiments presented in this chapter were all performed by me, with the exception of one of the two repeat experiments that form figure 3.4B, which was carried out by Dr Calum Bain, and that the 50g spin protocol was performed by Dr Antonella Pellicoro for the steps after digestion of tissue up until the point of counting of cell suspensions.

3.2 Identification of liver leukocytes by flow cytometry

As flow cytometry was to be the major mode of analysis of liver KC in this project, it was first important to devise a robust gating strategy. Live, single cells were identified using viability markers and a FSC-A v FSC-H singlets gate. CD45^{+} leukocytes were then further divided into F4/80^{hi}CD11b^{lo} KC and putative F4/80^{lo}CD11b^{hi} cells as described by Schulz and colleagues (Schulz et al. 2012) (fig. 3.1A). The subdivision of this F4/80^{lo}CD11b^{hi} population is further examined in chapter 4 (Hawley et al. 2018), but for simplicity is considered as a single population in this chapter. The marker CD31 was included in the staining panel for the majority of experiments which is examined in more detail later in this chapter. A ‘dump’ gate including CD3, CD19, Ly6G and Siglec F was used primarily for the exclusion T cell, B cell, neutrophil and eosinophil populations, although each population could be rudimentarily identified within the dump gate on the basis of their side scatter, and CD11b and MHCII expression (fig. 3.1A). Fluorescence minus one (FMO) controls were used to determine where gates should be set (fig. 3.1B).

3.3 Comparison of 3 protocols for the preparation of murine liver leukocytes for flow cytometry

Before beginning to investigate parameters of liver KC origin and self-renewal, I first set about establishing the optimal method of isolating and analysing leukocytes in the liver for my studies. I compared the use of a 33% Percoll gradient, a 50g spin, or a 300g spin method to determine which would be most suitable for the study of KC biology. Full details of the methods used can be found in chapter 2. The criteria for appraisal of methods were multiple: cell yield and viability, amount of debris in the preparation, how well the cells recovered represented the *in vivo* population and how this affected interpretation of aspects of KC biology.

3.3.1 Choice of method for isolation of liver leukocytes affects cell viability and retention of cell debris

Cell debris can be a significant problem with solid tissue digests as preparations full of debris can easily block the flow cytometer, making assessment of cell yield problematic; unless a size threshold is set, events relating to debris can vastly outnumber cells of interest during sample acquisition. These events tend to be small and of low complexity, falling in the bottom left hand corner of a forward scatter versus side scatter (FSC-A v SSC-A) flow plot. Following enzymatic digestion, livers were processed following one of the 3 methods described briefly above, stained and run through the flow cytometer. Comparison of FSC-A v SSC-A, with a 'cells' gate set at FSC-A greater than 25K, below which, no events were positive for the leukocyte marker CD45 (data not shown), revealed that the 50g centrifugation protocol retained the greatest proportion of debris, whilst the Percoll gradient had produced the preparation with the highest ratio of cells to debris. The 300g spin protocol fell in between (fig. 3.2A & 3.2B).

To assess what proportion of the 'cells' gate was alive, two viability markers were included: 7AAD which binds DNA of cells with compromised membranes, and Zombie Aqua which binds primary amine groups of proteins, such as the abundant intracellular protein accessible in dead and dying cells. After debris and doublets had been removed from analysis (fig. 3.2A & 3.2C), the proportion of cells which were negative for both 7AAD and Zombie Aqua was assessed (fig. 3.2D). There was only a small, albeit significant, difference in viability between

the Percoll and 300g centrifugation methods, with high viability found with both methods. However, there were significantly more dead cells with the 50g centrifugation protocol than with either other protocol, with less than 50% of cells viable (fig 3.2E). As it is impossible to exclude cell debris solely by FSC vs SSC characteristics, these data are consistent with a large amount of cell debris in the 50g preparation.

3.3.2 Greater yield of KC and no selective enrichment of KC with 300g spin method

Given the complex and intricate nature of interactions between immune cell subsets, I wanted to use a protocol which isolated immune cells in proportions which were representative of their relative abundances *in vivo,* and which was not selective for a specific immune cell type. I therefore considered the composition of the live cells recovered by each method. Leukocytes were identified using a $CD45^{+}CD31^{-/lo}$ gate (fig. 3.3A) and there were no significant differences in the overall proportion of $CD45^{+}$ cells as a frequency of the total live, single cell population between methods (fig. 3.3B). However, there were clear differences in the relative abundance of $F4/80^{hi}CD11b^{lo}$ KC, comprising ~35% of the total leukocyte population isolated with the 300g spin protocol, ~18% with the Percoll protocol and ~10% with the 50g spin method (fig. 3.3C). The frequency of $F4/80^{lo}CD11b^{hi}$ cells was more consistent between methods making up around 10-15% of the total leukocyte population (fig. 3.3C). With any protocol, there is an inevitable loss of the cells of interest during processing of samples. To determine whether this could account for the differences in the relative abundance of KC recovered with each method, the supernatant after the first centrifugation of the multiple 300g spin method, the discarded fraction after the Percoll gradient, and the pellet from the 50g spin – all of which would normally be discarded when processing livers – were retained, stained and run through the flow cytometer alongside the normal isolates. KC and $F4/80^{lo}$ cell populations could be identified in the discards (fig. 3.3D) using the same live, $CD45^{+}CD31^{-/lo}$ gating strategy as used for the isolates. B cells, T cells, neutrophils and eosinophils could also be identified in both the isolates and the discards from a single lineage gate containing CD3, CD19, Ly6G and Siglec F, along with side scatter profiles CD11b and MHCII expression (gated following the strategy set out in fig. 3.1). Comparing the frequency of each cell type in the isolate to the frequency in the discard for each mouse demonstrated that there were no differences in relative abundance of any leukocyte population between the isolate and the discard using the 300g spin method (fig. 3.3E). This

indicated that this method did not select or enrich for any specific cell type. In contrast, KC were significantly enriched in the discards of both the Percoll gradient and 50g spin methods (fig. 3.3F & 3.3G). In other words, KC were being selectively lost using these protocols.

In addition, cell suspensions were counted using a CASY TT cell counter which determines numbers of live cells on the basis of electrical resistance and a size exclusion threshold of 5.3µm. This revealed that the 300g spin method yielded around 7-fold more KC than with the Percoll gradient (fig. 3.3H). Accurate cell counts could not be obtained from the 50g spin method due to the large proportion of debris, which the cell counter was unable to distinguish from live cell events. However, far fewer live cell events were acquired when running these 50g samples through the flow cytometer indicating that it is very likely that fewer live cells are recovered with this protocol.

3.3.3 Choice of method affects biological interpretation of proliferation and origin of KC

Finally, we investigated whether choice of protocol affected measures of KC biology. Two key readouts for my studies were macrophage proliferation and origin, and I noted that recent studies examining aspects of KC ontogeny and self-renewal had mainly used either Percoll gradient (Yona et al. 2013; Jenkins et al. 2011) or conventional centrifugation (Bain et al. 2014; Schulz et al. 2012; Gomez Perdiguero et al. 2015; Scott et al. 2016). I therefore compared these readouts in the KC populations recovered by the Percoll and 300g spin methods respectively. The 50g spin was not considered further given the poor yield, low viability and high amount of debris obtained with this method.

There was a significant difference in the proportion of KC that expressed the cell cycle marker Ki67 between methods, with higher levels of proliferation among the KC from the Percoll gradient method (fig. 3.4A), indicating that the Percoll gradient enriched for KC that were actively in cell cycle.

To assess cell origin, I used partially irradiated bone marrow chimeras that will be used extensively later in my thesis. In this system, $CD45.1^{+}CD45.2^{+}$ host mice are irradiated with the lower abdomen and legs shielded by a lead brick, then reconstituted with $CD45.2^{+}$ only donor bone marrow (or fluorescent reporter bone marrow where relevant) to achieve partial chimerism which in blood $Ly6C^{hi}$ monocytes reaches a maximum of 20-30%. The level of

chimerism seen within individual populations in the tissues can then be assessed to measure the contribution of bone marrow derived cells to those populations. There was no difference in the non-host chimerism in the F4/80^{lo} population between methods (fig. 3.4B), which is consistent with the short half-life and bone marrow origin of this population reported previously (Schulz et al. 2012). However, there was a significantly higher proportion of donor cells in the KC population isolated by the Percoll gradient compared with the 300g spin method (fig. 3.4B), showing that the Percoll gradient enriched for KC of the CD45.2 homozygous donor origin over CD45.2 heterozygous host cells, which would grossly affect conclusions about whether bone marrow derived cells contribute to this population or not.

In summary, whilst the Percoll gradient method produced a cell isolate with the greatest proportion of viable cells, the 300g spin method was superior to the 50g spin and Percoll gradient methods in terms of total numbers of cells recovered and in not being selective for any one population of leukocytes, thus allowing for a more accurate and unbiased analysis of KC biology. Hence, the 300g method was chosen as the superior method to be used in this project.

3.3.4 Contamination of F4/80^{hi}CD11b^{lo} KC gate with CD31^{+} cells

The routine use of CD31 to exclude endothelial cells from the gating strategy (fig. 3.1) was introduced after another PhD student in the lab, Dr Ruairi Lynch, noted EGFP expression in a proportion of cells in the F4/80^{hi}CD11b^{lo} KC gate in mice which express a tamoxifen inducible Cre recombinase under the control of the cadherin-5 (Cdh5) promoter. Cdh5 is more typically associated with endothelial cells (Zhang et al. 2016), and indeed these cells were also positive for another endothelial cell marker CD31 (or PECAM-1) (Lynch et al. 2018). This suggested that the GFP^{+}CD31^{+} cells found in the KC gate may be endothelial cell contaminants. To confirm that this was the case, I performed flow cytometry with additional KC markers.

Interestingly, cell surface staining for KC-specific markers CLEC4F or Tim4 was not able to adequately differentiate between CD31^{lo} KC and CD31^{hi} contaminants, even when compared to FMO controls (fig. 3.5A & 3.5B), which appeared at first to contradict the theory that the CD31^{hi} cells were endothelial contaminants. In contrast, comparison of mApple fluorescence in transgenic mice which express mApple under the control of a *Csf1r* promoter (see chapter 4; Hawley et al. 2018) with a negative littermate control mouse, revealed CD31^{lo} KC to be very bright for the fluorescent reporter, whilst CD31^{hi} cells were much lower, with only a

small shift in fluorescence compared to the control (fig. 3.5C), suggesting that they were not of myeloid origin.

Liver sinusoidal endothelial cells (LSECs) have been demonstrated to bind small immune complexes via their high expression of the FcγRIIb (CD32b), (Ganesan et al. 2012) which might lead to non-specific binding to the CD45 and F4/80 flow antibodies. However, the expression of CD45 and F4/80 was shown to be specific in comparison to isotype control antibodies (fig. 3.5D), and titration of the anti-CD16/CD32 blocking antibody, which was added to cells prior to staining with fluorochrome-conjugated antibodies to reduce non-specific background staining did not affect the mean fluorescence intensity of F4/80-PE on the $CD31^{hi}$ contaminating cells (fig. 3.5E). This confirmed that the F4/80 staining was not due to inefficient blocking of Fc receptors on the prepared single cell isolate.

Finally, fluorescence microscopy of FACS-sorted $F4/80^{hi}CD11b^{lo}$ cells carried out by Dr Lynch revealed that some of the $CD31^{hi}$ contaminants were doublets with $F4/80^{hi}CD31^{lo}$ KC, whilst the rest appeared to be $CD31^{hi}$ cells with small areas of punctate F4/80 and CD45 staining (Lynch et al. 2018). Hence, we found no solid evidence that the contaminating $CD31^{hi}$ cells were macrophages. These cells were therefore excluded from analysis of the $F4/80^{hi}CD11b^{lo}$ KC population in all experiments subsequent to this finding by first gating out all $CD31^{hi}$ cells.

3.4 Contamination of $F4/80^{hi}CD11b^{lo}$ KCs with $CD31^{hi}$ endothelial cells is apparent regardless of protocol used to isolate cells

The discovery that $CD31^{hi}$ endothelial cells were contaminating the $F4/80^{hi}CD11b^{lo}$ gate was made using the 300g centrifugation method and it was possible that this endothelial cell contamination could be an artefact specific to this protocol. However, $CD31^{hi}$ cells were present in the KC gate when cells were prepared with any 3 of the methods, forming around 8% of the total $F4/80^{hi}$ population with the 300g centrifugation and Percoll gradient methods, and over 20% of the population with the 50g centrifugation method (fig. 3.6A & 3.6B)

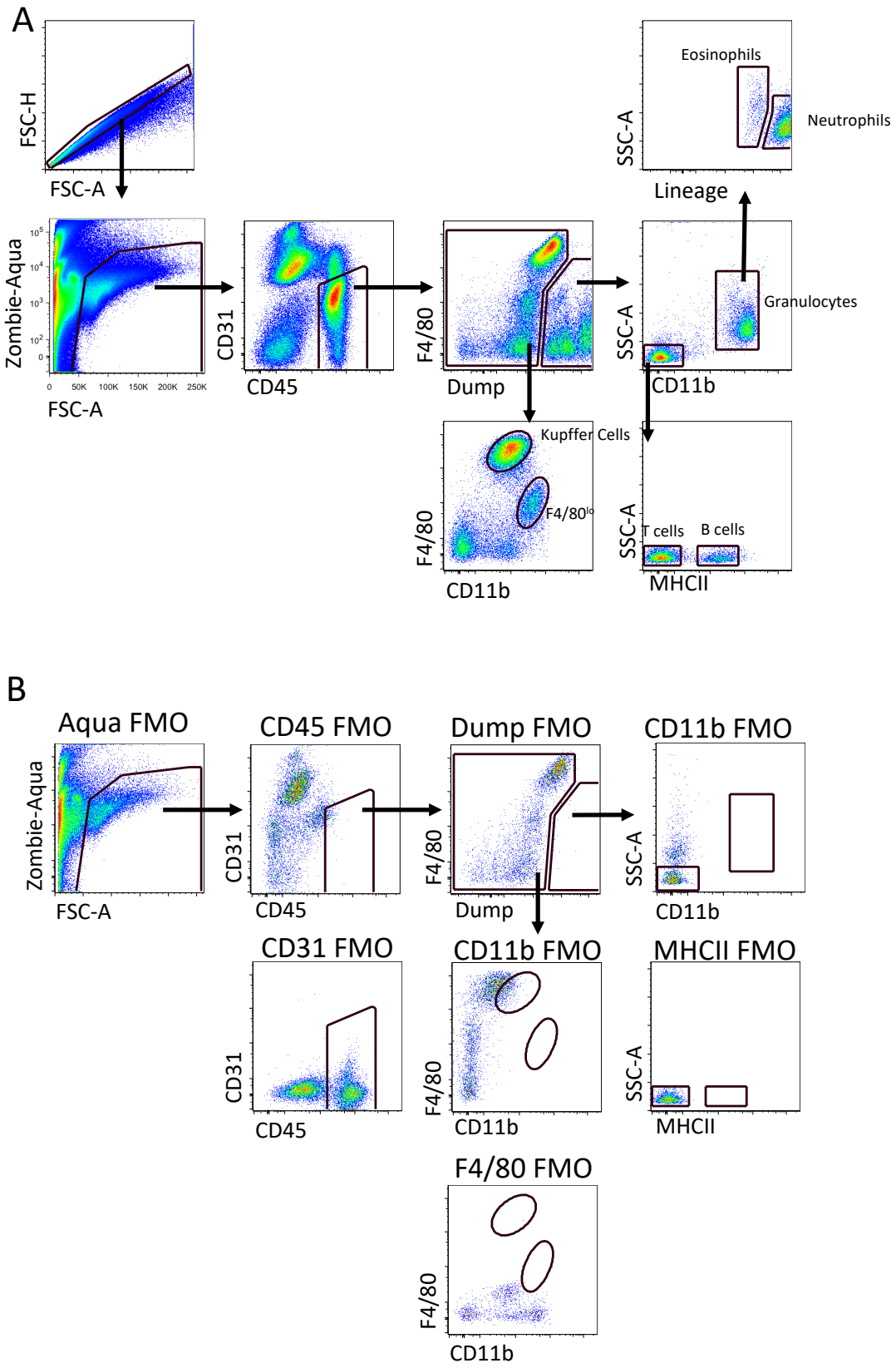

Figure 3.1 Gating strategy for the identification of murine leukocytes in liver. (A) Standard gating strategy used to identify murine leukocyte populations in the liver for this study and **(B)** fluorescence minus one (FMO) controls used to set gates for the identification of liver populations.

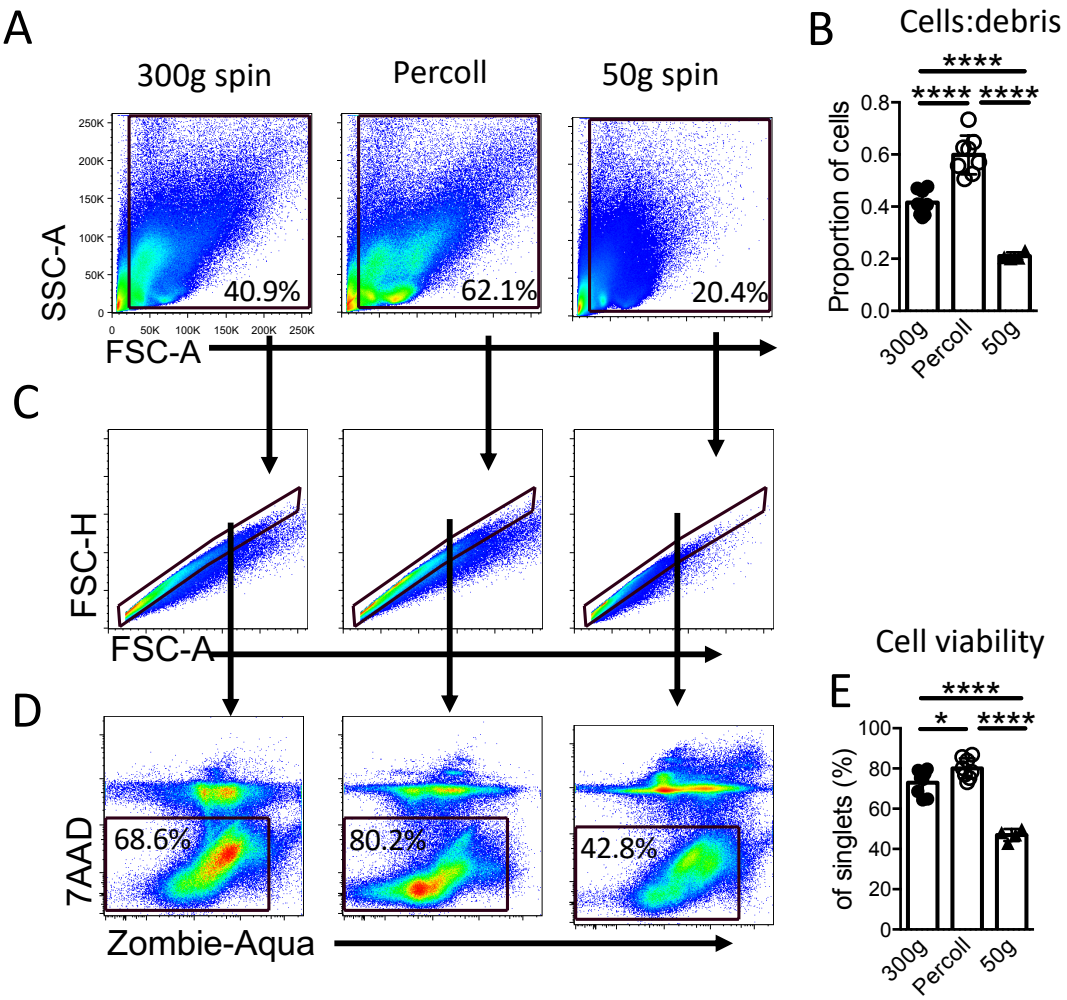

Figure 3.2 Comparison of debris retention and cell viability between the 3 methods for isolation of murine leukocytes in liver. (A) Representative plots of FSC-A versus SSC-A of samples from each of the three protocols compared. Gates show the proportion of all events that were considered to be cells. **(B)** Replicate data showing the proportion of events that were cells for each method. **(C)** Representative plots showing the singlets gate used to exclude doublets from the analysis of liver prepared with each of the 3 methods. **(D)** Representative plots of two viability markers Zombie-aqua and 7AAD. Gates show the proportion of single cells which were negative for both markers and **(E)** replicate data showing proportion of single cells which were live for each method. Two experiments were carried out in which the 3 protocols were compared side-by-side. In the first experiment, technical difficulties led to no data from the 50g spin method, but these issues were resolved by the preparation being performed by Dr A. Pellicoro for the repeat experiment. n=8 for 300g and Percoll gradient methods pooled from 2 independent experiments and n=4 for 50g spin from one experiment. Significance determined by One-way Anova with multiple comparisons where **** p<0.0001 * p<0.05.

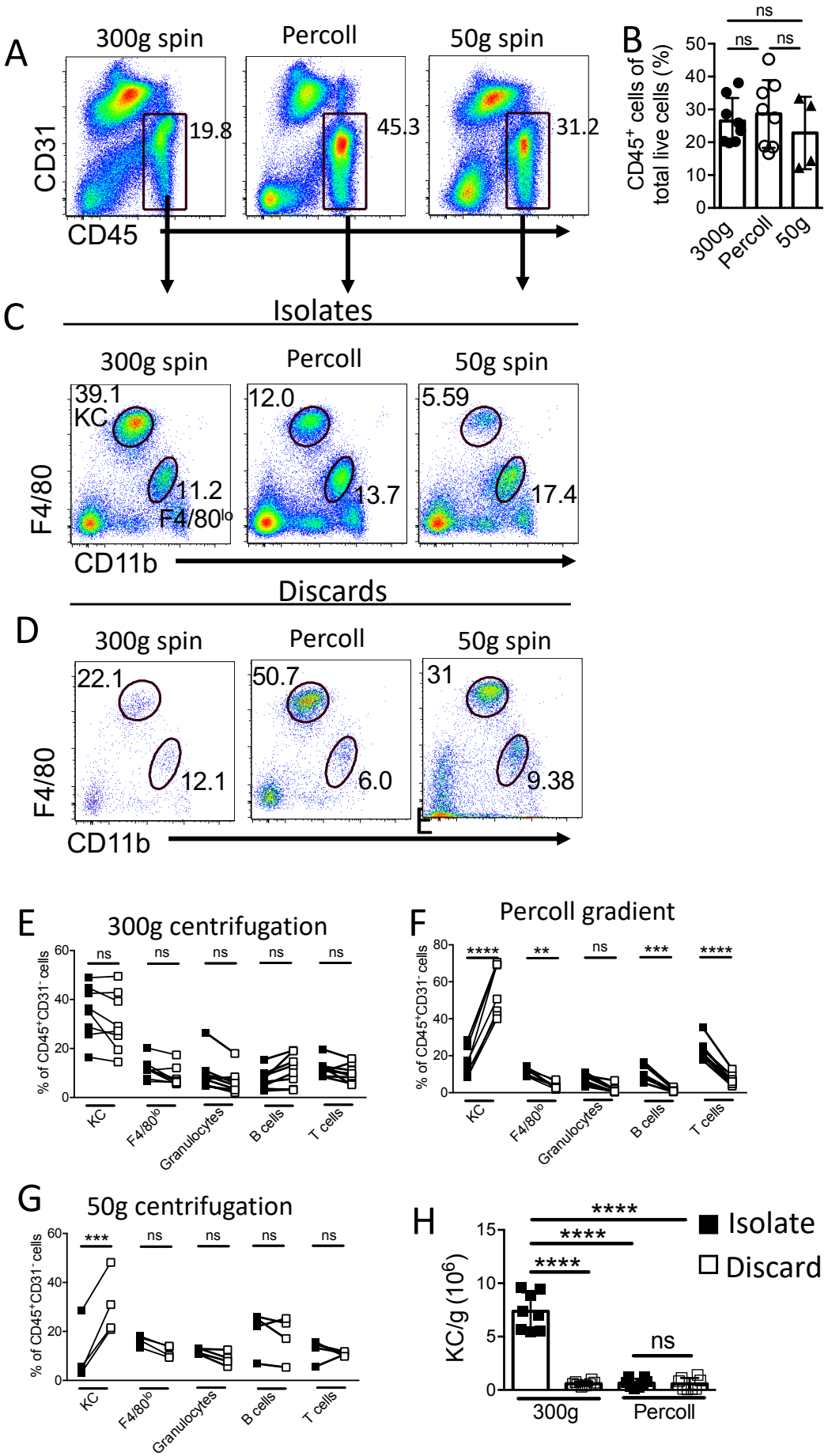
A
300g spin
Percoll
50g spin
CD31
CD45
19.8
45.3
31.2
B
CD45+ cells of total live cells (%)
ns
300g
Percoll
50g
C
Isolates
F4/80
CD11b
39.1
KC
11.2
F4/80lo
12.0
13.7
5.59
17.4
D
Discards
22.1
12.1
50.7
6.0
31
9.38
E
300g centrifugation
% of CD45+CD31- cells
KC
F4/80lo
Granulocytes
B cells
T cells
F
Percoll gradient
G
50g centrifugation
H
KC/g (10^6)
Isolate
Discard
300g
Percoll

Figure 3.3 300g spin recovers the most KC and is not selective for the KC population. (A) Representative plots showing the $CD45^{+}CD31^{lo/-}$ gate used to determine leukocyte populations for each of the 3 methods and **(B)** replicate data showing the proportion of $CD45^{+}CD31^{lo/-}$ cells of the total single cell population. **(C)** Representative plots of F4/80 versus CD11b showing the proportion of $F4/80^{hi}CD11b^{lo}$ KC and $F4/80^{lo}CD11b^{hi}$ myeloid cells of the total $CD45^{+}CD31^{lo/-}$ population. **(D)** Representative plots of CD11b versus F4/80 from the discarded fractions of each of the 3 methods. **(E)** The frequency of cell subsets in the cell isolate (black squares) linked to the frequency in the discard for the same sample (open squares) as a proportion of the total leukocyte population for the 300g spin method, **(F)** the Percoll gradient method and **(G)** the 50g spin method. **(H)** The total number of $F4/80^{hi}CD11b^{lo}$ KC per gram of liver tissue for the isolates and discards of the 300g spin method and the Percoll gradient method. Significance determined by One-way Anova with multiple comparisons. * p<0.05 ** p<0.01 ****P<0.0001 **(B, H)**, or multiple t-tests comparing the cells to the discard for each cell type, with the Holm-Sidak method applied to determine significance. *p<0.05 **p<0.01 ***p<0.001 ****p<0.0001 (**E, F, G)**. n=4 (50g spin) or 8 (Percoll and 300g spin) per group from the same experiments as figure 3.2

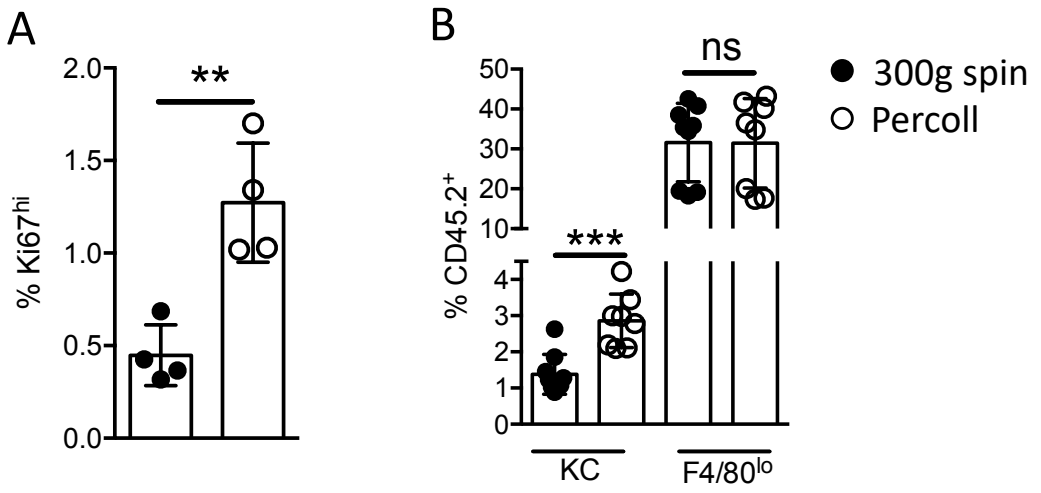

Figure 3.4 Choice of method affects interpretation of KC biology. (A) The frequency of the KC population that had high expression of the cell cycle marker Ki67 in the 300g and Percoll gradient preps. n=4, data are representative of 2 independent experiments. Significance determined using a Student's t-test, ** $p<0.01$. **(B)** The proportion of the F4/80^{hi}CD11b^{lo} KC and F4/80^{lo}CD11b^{hi} populations that were CD45.2^{+} donor cells in a partially irradiated congenic bone marrow chimera system 8 weeks post reconstitution where the host mice were CD45.1^{+}CD45.2^{+} genotype. n=8, pooled from 2 independent experiments, one repeat was performed by Dr Calum Bain. Significance determined by Student's t-test for each cell type. *** $p<0.001$.

Gated: CD45^{+} → lineage^{-} → F4/80^{hi}CD11b^{lo}

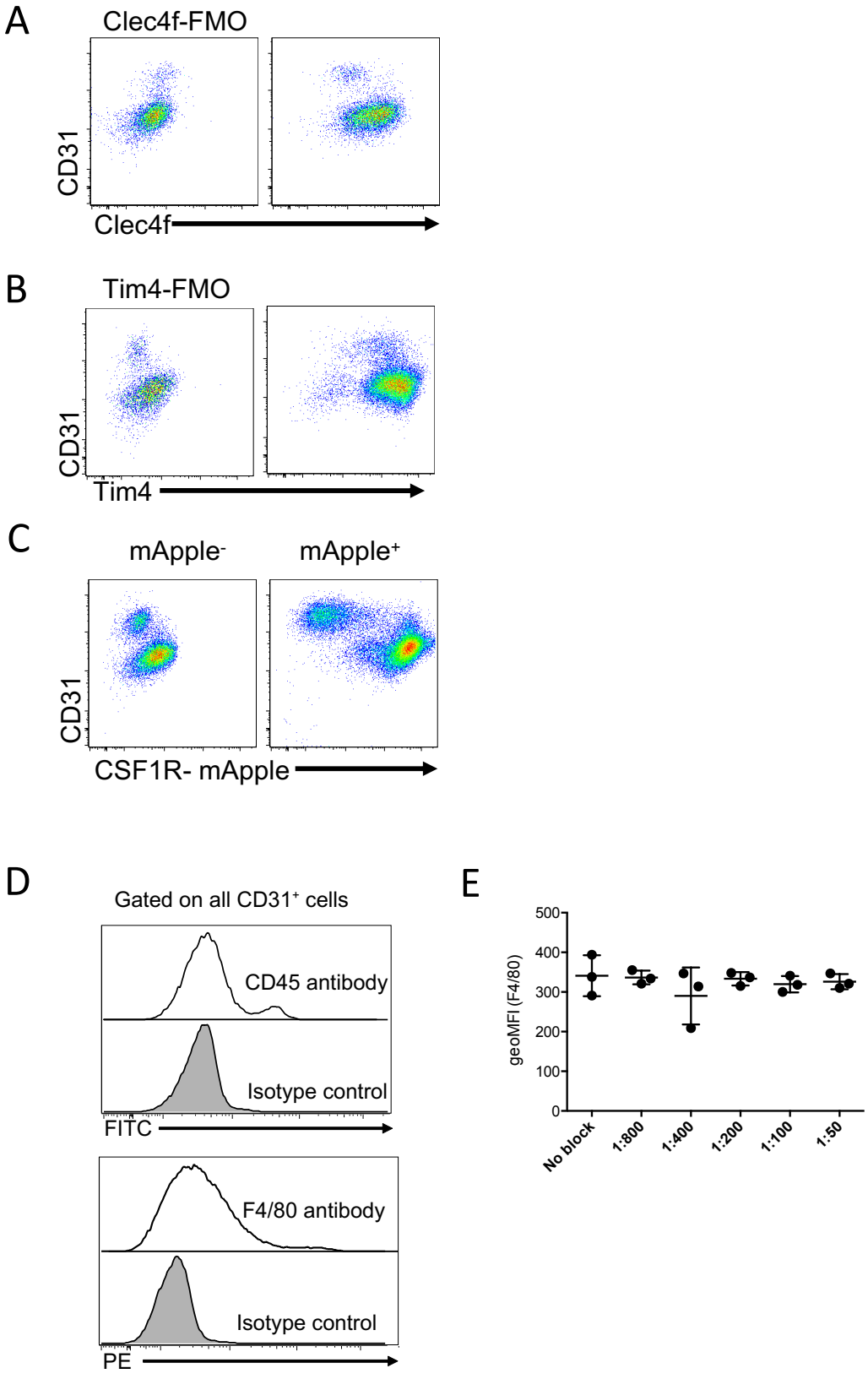

Figure 3.5 Phenotype of CD31^{+} endothelial cells contaminating F4/80^{hi}CD11b^{lo} gate. (A) Representative plot of Clec4f, **(B)** Tim4 and **(C)** *Csf1r*-mApple vs CD31 expression and their relevant controls. All representative of at least 3 independent experiments. **(D)** Representative histograms showing CD45-FITC and F4/80-PE binding profile of the bulk CD31^{+} population (no prior gating apart from to attain single, live cells) compared with the binding profile for isotype matched controls for each antibody. **(E)** The geometric mean fluorescence intensity (geoMFI) of F4/80 within the contaminating F4/80^{hi}CD31^{hi} population when anti-CD16/CD32 blocking antibody is titrated. Plots are representative of two independent experiments with total n=6 per group.

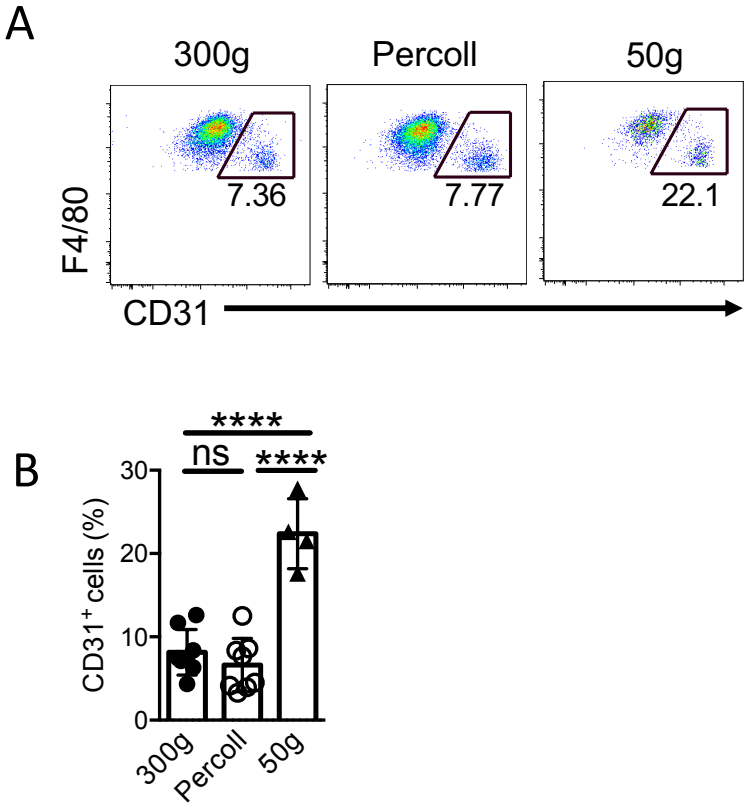

Figure 3.6 CD31^{hi} endothelial cell contamination present with all 3 methods (A) representative plots and **(B)** replicate data showing the proportion of F4/80^{hi}CD11b^{lo} cells which were CD31^{hi} for each of the 3 methods compared. Significance determined by One-way Anova with multiple comparisons where ****P<0.0001. Data from the same experiments as figure 3.2.

3.5 Discussion

In this chapter I set out to establish the optimal method to isolate and analyse liver leukocytes for my study. I compared the cell isolates produced from three protocols for the preparation of liver leukocytes for flow cytometry, which were considered to be representative of the three main methods used in the literature. The Percoll gradient separates cells on the basis of density, giving a distinct hepatocyte layer which can be easily discarded and separated from the leukocyte pellet following centrifugation (Stijlemans et al. 2015), and it was therefore unsurprising that this method gave the preparation with the least debris. In my hands, two 300g spin steps removed more debris than the 50g spin protocol which comprised a 50g spin followed by a 340g spin. There were no significant differences in the frequency of leukocytes (defined as $CD45^{+}CD31^{lo/-}$) as a proportion of live, single cells between methods, which was surprising given that the slower spin was intended to pellet large parenchymal cells such as hepatocytes whilst leaving leukocytes in the supernatant, as has been shown with human liver preparations (Kegel et al. 2016). However, as frequency is a relative measure, differences in the proportions of other cell types, for example $CD31^{hi}$ endothelial cells isolated with each method could explain this finding.

Whilst comparing the methods, it also became clear that there were differences in the ratios of leukocyte populations isolated from each method, with a greater frequency of KC isolated with the 300g spin method. Analysis of the discarded fractions for each method (the supernatants from the 300g spins, the pellet after the 50g spin and middle layers from after the Percoll density gradient separation) revealed that the Percoll and 50g spin methods led to the selective loss of KC. Further comparison of the 300g with the Percoll gradient revealed that a higher level of proliferation and increased non-host chimerism in those KC isolated with the Percoll method. It has been shown in yeast cells that cell density increases as a cell enters S-phase (Bryan et al. 2010), so it seems feasible that the density gradient preferentially isolated KC in cell cycle due to increased density, resulting in a higher overall readout for proliferation compared to the population isolated with the 300g spin method. A lower percentage of Percoll in the density column might rectify this problem. Likewise, it is possible that there are differences in density between donor and host cells in the chimeric system, perhaps due to differences in maturity or differentiation status between recently recruited donor cells and tissue-resident host cells, that meant that the ratio was affected by Percoll separation. Therefore, the method of isolation chosen significantly affected the

interpretation of KC biology. However, the fact that the 300g spin method recovered a significantly higher total number of cells, together with the fact that there was no selective loss of KC meant that I am confident that this method gives the cell isolate that is most representative of that found *in vivo.* Additionally, the 300g spin method was the simplest and fastest method to perform, thereby allowing more livers to be processed on a single day, facilitating the processing of large sample sizes critical throughout my project.

It must be noted that I only compared one Percoll density, and the fact that the sum of the number of KC in the isolate and the discard with this method was significantly less than the total number isolated with the 300g spin method suggests that a large number of KC were retained in the Percoll itself. With careful optimization, it is possible that this method could be used to isolate representative samples of liver leukocytes with high viability, good yields and less debris than the 300g method, which could be more useful and suitable for alternative applications such as cell culture but this was not explored within the realms of this project.

Alongside comparison of methods, it was important to establish a robust gating strategy to faithfully identify KC. As part of this work, it was discovered in the lab that the KC population identified using the F4/80^{hi}CD11b^{lo} gating strategy contained a subset of cells which were CD31^{hi}, compared to the bulk of the population which was CD31^{lo}. Staining for markers that have subsequently be found to be more specific to KC in the liver, such as Clec4f and Tim4 revealed that whilst the CD31^{lo} population was very bright for these markers, the CD31^{hi} cells also exhibited only slightly lower intensity of staining which was insufficient to distinguish between the two populations. This suggested that the CD31^{hi} cells could in fact be macrophages, which supported RNA-seq data which identified the liver sinusoidal endothelial cell (LSEC) marker CDH5 (Zhang et al. 2016) as a 'KC-specific' gene (Lavin et al. 2014; Scott et al. 2016). However, the fact that the *Csf1r*-mApple reporter system was able to clearly distinguish between CD31^{hi} cells and CD31^{lo} cells indicated that the CD31^{hi} cells did not express this typical myeloid cell marker. Furthermore, imaging revealed that the F4/80^{hi}CD11b^{lo}CD31^{hi} cells were actually either doublets of F4/80^{-}CD31^{hi} endothelial cells with an F4/80^{hi}CD11b^{lo} KC, or were F4/80^{-}CD31^{hi} endothelial cells with what is likely to be a fragment of F4/80^{hi}CD11b^{lo} KC still bound. KC have been shown to be relatively sessile (Lee & Kubes, 2008), supporting the notion that they are strongly adhered to one another *in vivo*. The exact identity of these adhesion molecules are yet to be identified, but endothelial cells constitutively express intercellular adhesion molecule 1 (ICAM1, or CD54) (Sorensen *et al.*,

2015), which may be involved in anchoring KC to the sinusoids through interaction with intergrins.

In summary, I have extensively compared protocols for the isolation of murine liver leukocytes and determined that a simple 300g spin protocol gave a superior yield of cells which gave a true representation of the ratios of immune cell populations found *in vivo*. Additionally, I demonstrated that the use of CD31 to exclude endothelial cell contamination should be used routinely in the gating strategy to identify KC, as additional KC markers Clec4f and Tim4 were not sufficient to discriminate between these populations. With a robust method for identification of KC in place, I was equipped to begin exploring the factors that affect their origin and maintenance in more detail, starting with the role of CSF1 and its receptor.

Chapter 4: Expression of CSF1R and uptake of CSF1 by liver leukocytes

4.1 Introduction

Having established a robust method to isolate liver leukocytes, and identify liver KC which were free from endothelial cell contamination, I could begin to investigate parameters surrounding KC maintenance. The macrophage colony stimulating factor receptor (CSF1R) is a type III tyrosine kinase receptor (Bonifer and Hume 2008) and binding with its ligands results in dimerization and autophosphorylation of up to 8 tyrosine residues which create docking sites for signalling molecules (Yu et al. 2012; Stanley and Chitu 2014). Many tissue resident macrophage populations are highly dependent on signalling through the CSF1R with its ligands CSF1 and IL-34 to regulate their differentiation and survival (Jenkins and Hume 2014). Both antibody blockade of the CSF1R (MacDonald et al. 2010) and inactivation of the *Csf1r* gene in knock out mice (Dai et al. 2002) results in reduced tissue resident macrophage numbers in multiple tissues including the peritoneal cavity and liver. The *Csf1r*-EGFP or MacGreen mouse line which expresses the EGFP protein under the control of a transgenic *Csf1r* promoter region (Sasmono et al. 2003) has been used extensively to identify and image mononuclear phagocytes across tissues. However, EGFP is widely used in other fluorescent reporter lines, limiting the possibility to cross MacGreen mice with other reporters to analyse multiple cell lineages simultaneously or answer more complex experimental questions; thus *Csf1r*-mApple mice were generated in collaboration with David Hume which express the bright red fluorochrome mApple under the control of the same *Csf1r* transgene as was used for MacGreen mice.

I took the opportunity to use the *Csf1r*-mApple mice to compare *Csf1r* transgene expression between discrete myeloid populations across blood, peritoneal cavity, lung and liver and explore whether the level of expression differed between populations, and what this could reveal about their biology. Of particular interest to me was the identity of the F4/80^{lo}CD11b^{hi} population in the liver which has not been clearly defined, but has been previously assumed to be a macrophage population in line with CD11b^{+} macrophage populations present in other tissues (Schulz et al. 2012; Yona et al. 2013). Others have further defined at least a fraction of these as monocytes on the basis of Ly6C expression (Ramachandran et al. 2012). I

therefore used the *Csf1r*-mApple mice in combination with staining for macrophage- and DC-associated cell surface markers to more clearly define the mononuclear phagocyte populations present in the liver in steady state. Alongside these experiments, another lab member analysed the origin of different macrophage populations using tissue protected chimeras given *Ccr2*$^{+/+}$ or *Ccr2*$^{-/-}$ bone marrow to confirm the identity of CCR2-dependent populations indicating they are monocyte-derived, CCR2-independent cells of bone marrow origin likely to be DC and bone marrow independent tissue resident macrophages.

Macrophages are reliant on CSF1 for differentiation, survival and proliferation, and CSF1R signalling also contributes to recruitment and chemotaxis. However, the level of signalling through the CSF1R receptor affects the signalling outcome. By adding varying concentrations of CSF1 to the media of cultured bone marrow derived macrophages it has been demonstrated that lower concentrations are required for survival whilst higher concentrations induce proliferation in a dose-dependent manner (Tushinski et al. 1982). Differing levels of signalling resulting in pleiotropic effects is not unique to the CSF1R, and is also known to occur within the EGF-EGFR signalling pathway (Krall et al. 2011). Thus, in addition to CSF1R expression, understanding how much CSF1 a cell is able to capture and utilize may give insight into how it may function, survive and compete with other CSF1R-expressing cells. To explore this, we used injection of a CSF1-Fc conjugated to the fluorochrome alexa fluor 647 (AF647) to determine uptake of CSF1 on a per cell basis *in vivo*. CSF1-Fc is a fusion protein of porcine CSF1 conjugated to the Fc region of pig IgG1a which is more stable than CSF1 alone and has a longer half-life (Gow et al. 2014), and is used extensively in chapter 5 to study the effects of exogenous CSF1 on KC origin and maintenance and conversion of monocytes to macrophages. As with analysis of *Csf1r*-mApple expression, CSF1-Fc^{AF647} uptake was analysed in conjunction with a staining panel that would allow distinction between resident macrophages, monocytes, monocyte-derived macrophages and dendritic cells.

These studies formed the backbone of a paper published in The Journal of Immunology, of which I am joint first author, and which forms this chapter. In this paper I performed experiments and analysed data for all of figure 2, figure 3 (except fig. 3E & F), figure 4 (except fig. 4B), and figure 5 (except fig. 5E). I contributed extensively to figure 6A-C and I performed experiments for all of supplementary figure 2. This work allowed comparison of *Csf1r* transgene expression across various tissues, exploration of how this related to CSF1R protein expression and, in conjunction with data from BM chimeras, how this related to cell lineage.

Through this analysis, I provide a more clear definition of leukocyte populations in the liver, and demonstrate differences in their ability to capture and utilise CSF1.

Csf1r-mApple Transgene Expression and Ligand Binding In Vivo Reveal Dynamics of CSF1R Expression within the Mononuclear Phagocyte System

Catherine A. Hawley,*[,1] Rocio Rojo,[†,1] Anna Raper,[†,1] Kristin A. Sauter,[†] Zofia M. Lisowski,[†] Kathleen Grabert,[†] Calum C. Bain,* Gemma M. Davis,[†,‡] Pieter A. Louwe,* Michael C. Ostrowski,[§] David A. Hume,*[,†,¶] Clare Pridans,*[,†] and Stephen J. Jenkins*

CSF1 is the primary growth factor controlling macrophage numbers, but whether expression of the CSF1 receptor differs between discrete populations of mononuclear phagocytes remains unclear. We have generated a *Csf1r*-mApple transgenic fluorescent reporter mouse that, in combination with lineage tracing, Alexa Fluor 647–labeled CSF1-Fc and CSF1, and a modified Δ*Csf1r*-enhanced cyan fluorescent protein (ECFP) transgene that lacks a 150 bp segment of the distal promoter, we have used to dissect the differentiation and CSF1 responsiveness of mononuclear phagocyte populations in situ. Consistent with previous *Csf1r*-driven reporter lines, *Csf1r*-mApple was expressed in blood monocytes and at higher levels in tissue macrophages, and was readily detectable in whole mounts or with multiphoton microscopy. In the liver and peritoneal cavity, uptake of labeled CSF1 largely reflected transgene expression, with greater receptor activity in mature macrophages than monocytes and tissue-specific expression in conventional dendritic cells. However, CSF1 uptake also differed between subsets of monocytes and discrete populations of tissue macrophages, which in macrophages correlated with their level of dependence on CSF1 receptor signaling for survival rather than degree of transgene expression. A double Δ*Csf1r*-ECFP-*Csf1r*-mApple transgenic mouse distinguished subpopulations of microglia in the brain, and permitted imaging of interstitial macrophages distinct from alveolar macrophages, and pulmonary monocytes and conventional dendritic cells. The *Csf1r*-mApple mice and fluorescently labeled CSF1 will be valuable resources for the study of macrophage and CSF1 biology, which are compatible with existing EGFP-based reporter lines. ***The Journal of Immunology*****, 2018, 200: 2209–2223.**

The mononuclear phagocyte system (MPS) is a family of functionally related myeloid cells comprising progenitor cells, monocytes, macrophages, and conventional dendritic cells (cDC) (1–5). Macrophages resident in tissues may be derived from definitive hematopoiesis via circulating monocytes or by self-renewal from cells seeded during embryonic or early postnatal life (1, 2, 4, 5). cDCs have been classified as those cells deriving from common dendritic cell (DC) progenitors via circulating pre-DC (1, 6, 7). Regardless of their developmental origin, macrophages and their precursors express the M-CSF receptor CSF1R, and depend upon signals from two ligands, CSF1 or IL34, for proliferation, differentiation, and survival (2, 3). Receptor-mediated internalization and destruction of CSF1 controls its availability (8) and provides a homeostatic control on macrophage numbers (3). Accordingly, administration of recombinant CSF1 (9) or a more stable CSF1-Fc fusion protein (10–12) to mice produces expansion of blood monocyte and tissue macrophage populations, yet the degree to which CSF1R expression and activity differ between populations of mononuclear phagocytes is unclear.

cDC express high levels of a related tyrosine kinase receptor, Fms-like tyrosine kinase 3 (Flt3). Their numbers are greatly increased following treatment of mice with Flt3 ligand (Flt3L), and depleted in Flt3L-deficient animals (7, 13–17). Two subsets of cDC, cDC1 and cDC2, appear to differ in their expression of *Csf1r*. cDC1 are not generally dependent upon CSF1 and lack *Csf1r* mRNA (14). cDC2 have been more difficult to define because of major overlaps in cellular phenotype with other $CD11b^+$ $CD11c^+$MHC class II $(MHCII)^+$ monocyte-derived APCs (18–20). Genuine Flt3-dependent cDC2 of common DC progenitor origin have been defined based upon migratory behavior and the lack of the macrophage markers CD64 and F4/80 (6, 15, 21, 22). With this definition, cDC2 in various tissues expressed lower levels of

*Medical Research Council Centre for Inflammation Research, University of Edinburgh, Edinburgh EH16 4TJ, United Kingdom; [†]The Roslin Institute, University of Edinburgh, Midlothian EH25 9RG, United Kingdom; [‡]Faculty of Life Sciences, The University of Manchester, Manchester M13 9PL, United Kingdom; [§]Hollings Cancer Center, Medical University of South Carolina, Charleston, SC 29425; and [¶]Mater Research–University of Queensland, Translational Research Institute, Woolloongabba, Queensland 4104, Australia

[1]C.A.H., R.R., and A.R. contributed equally to this work.

ORCIDs: 0000-0001-9686-3377 (R.R.); 0000-0003-0949-9963 (A.R.); 0000-0002-1323-9593 (Z.M.L.); 0000-0001-8884-327X (C.C.B.); 0000-0001-8323-5013 (G.M.D.); 0000-0001-9423-557X (C.P.); 0000-0002-0233-5424 (S.J.J.).

Received for publication October 30, 2017. Accepted for publication January 17, 2018.

This work was supported by Medical Research Council Grant MR/L008076/1. P.A.L. was supported by a Wellcome Trust Ph.D. studentship.

Address correspondence and reprint requests to Dr. Stephen J. Jenkins, University of Edinburgh, Queens Medical Research Centre, 47 Little France Crescent, Edinburgh EH16 4TJ, U.K. E-mail address: stephen.jenkins@ed.ac.uk

The online version of this article contains supplemental material.

Abbreviations used in this article: AF647, Alexa Fluor 647; BM, bone marrow; cDC, conventional dendritic cell; DC, dendritic cell; ECFP, enhanced cyan fluorescent protein; Flt3, Fms-like tyrosine kinase 3; Flt3L, Flt3 ligand; KC, Kupffer cell; MFI, median fluorescence intensity; MHCII, MHC class II; MPS, mononuclear phagocyte system; pDC, plasmacytoid DC; WT, wild type.

www.jimmunol.org/cgi/doi/10.4049/jimmunol.1701488

Csf1r mRNA than monocyte-derived APC (15, 22) and have been considered CSF1R independent (1). The levels of surface CSF1R largely distinguish Flt3L-dependent cDC2 from short-lived monocyte-derived CD11c$^{+/-}$ MHCII^{+} cells in the serous cavities (23, 24). However, cDC2 isolated from spleen express high levels of both *Csf1r* and *Flt3* mRNA (www.biogps.org) and their numbers are controlled by CSF1 in vivo (25). Therefore, it remains unclear whether there is a genuine dichotomy between Csf1r and Flt3-dependent myeloid APC.

CSF1R on macrophages is continuously removed from the cell surface by endocytosis and degraded following ligand binding. For that reason, the detection of CSF1R protein by immunohistochemistry or flow cytometry does not provide a clear indication of functional expression. To identify Csf1r-expressing cells in situ, regulatory elements of the murine *Csf1r* locus, including a 150 bp segment of the distal promoter, were used to produce *Csf1r*-EGFP reporter mice (26). The same promoter construct was used to drive constitutive (27) and inducible cre-recombinase to support macrophage-specific conditional mutations (28) as well as lineage tracing (29), and these tools have been widely distributed among the research community. However, new resources are required to verify with single-cell resolution the extent to which *Csf1r* transgene expression reflects that of functional CSF1R protein.

In addition to aiding our understanding of the regulation of myeloid cells, visualization of *Csf1r* gene and protein expression may also be useful to study cell interactions in vivo due to the lack of tools to identify discrete MPS populations during multicolor imaging. A binary enhanced cyan fluorescent protein (ECFP) reporter (Δ*Csf1r*-Gal4VP16/UAS-ECFP) transgene with a 150 bp segment of the distal Csf1r promoter deleted, termed Δ*Csf1r*-ECFP, has provided a novel tool to support in vivo imaging of monocyte trafficking (30, 31), because expression was lost from the large majority of tissue macrophages but remained in blood monocytes, microglia, Langerhans cells, and cDC2 (32). In particular, dual reporter mice, such as those generated by crossing the *Cx3cr1*-EGFP and *Ccr2*-RFP mice, have been valuable tools for visualizing monocyte subsets and their differentiation in the brain and liver (33), findings that would not have been obtainable using single reporter mice. However, many other macrophage and nonmacrophage reporter genes use EGFP, rendering the original *Csf1r*-EGFP transgene of limited use for this purpose. Thus, additional monocyte/macrophage reporter mice that are compatible with existing EGFP-based reporters are needed.

Hence, we have created new tools and assays to image and assess *Csf1r* gene and protein expression that can be combined conveniently with common fluorophores, EGFP transgenes, and the Δ*Csf1r*-ECFP transgene for use in imaging and flow cytometry. In particular, we characterize a new *Csf1r*-mApple line expressing the red reporter gene *mApple* under the same promoter used in the *Csf1r*-EGFP reporter, and apply this in combination with the Δ*Csf1r*-ECFP transgene, lineage tracing, and labeled CSF1-Fc and CSF1 proteins to distinguish different cellular compartments within the MPS, and to dissect the homeostatic roles of CSF1.

Materials and Methods

Plasmid constructs

The 7.2 kb *Csf1r* reporter construct previously used to generate the *Csf1r*-EGFP mice (26) was digested with ApaI and SalI (NEB) to remove EGFP before gel purification using the QIAquick gel extraction kit (Qiagen). Overhangs were removed with Mungbean nuclease (NEB) and DNA was purified using QIAGEN MinElute columns (Qiagen), then dephosphorylated using thermosensitive alkaline phosphatase (Promega). A construct encoding the fluorescent protein *Csf1r*-mApple (34) was digested with SmaI and AflII, similarly purified, and overhangs removed before both constructs were precipitated with EtOH/NaOAc and then ligated with T4 ligase (NEB) at 16°C overnight. The resulting *Csf1r*-mApple construct was transformed into DH5α competent cells. The *Csf1r-rtTA-M2* construct utilizing the same 7.2 kb mouse *Csf1r* promoter region was used previously to generate *Csf1r-rtTA* transgenic mice (35) For generation of transgenic mice, plasmid backbones were removed by digestion with DrdI/PvuI (*Csf1r*-mApple, NEB) and SalI/MluI (*Csf1r*-rtTA, Promega/NEB) and then gel-purified using a QIAquick gel extraction kit. DNA was then further purified using AMPure XP beads (Agencourt) according to the instructions.

Generation of transgenic mice and animal maintenance

Animal experiments were permitted under license by the U.K. Home Office, and were approved by the University of Edinburgh Animal Welfare and Ethical Review Body. All mice including wild-type (WT) C57BL/6JOlaHsd CD45.2^{+}, congenic CD45.1^{+}CD45.2^{+}, *Csf1r*-EGFP (26), Δ*Csf1r*-Gal4VP16/UAS-ECFP (36), and Ccr2$^{-/-}$ (37) lines were bred and housed in specific-pathogen free facilities at the University of Edinburgh. *Csf1r-mApple/Csf1r-rtTA* transgenic mice were generated at the University of Edinburgh's Central Biological Services Transgenic Core facility by microinjection of transgenes into the pronuclei of fertilized oocytes from C57BL/JOlaHsd mice. The integration of the transgenes was determined by PCR analysis of genomic DNA isolated from ear biopsy using primers that amplified a 565 bp product between the c-fms promoter and rtTA gene, and a 507 bp product between the c-fms promoter and *Csf1r-mApple* gene, using primers 5′-TTC CAG AAC CAG AGC CAG AG-3′ (forward) and 5′-CTG TTC CTC CAA TAC GCA GC-3′ (reverse), and 5′-CCT ACA TGT GTG GCT AAG GA-3′ (forward) and 5′-CTT GAA GTA GTC GGG GAT GT-3′ (reverse), respectively, and amplification temperatures of 35 cycles of 30 s at 94, 55, and 72°C, after an initial denaturing step of 94°C for 5 min. Expression of *Csf1r-mApple* was verified by screening 10 μl blood for the presence of *Csf1r*-mApple fluorescence by flow cytometry. One founder positive for both transgenes transmitted the transgenes to progeny and established the *Csf1r*-mApple/*Csf1r-rtTA* line (referred to as *Csf1r*-mApple). The *Csf1r*-mApple line was maintained by breeding to C57BL/6JOlaHsd mice, or where specified, bred to the Δ*Csf1r*-ECFP line, for which subsequent analysis was performed on F1 progeny. For maintenance of the *Csf1r*-mApple line, transgenic progeny were initially identified by PCR analysis of genomic DNA and flow-cytometric assessment of the presence of *Csf1r*-mApple in blood cells, and subsequently by flow cytometry alone. For identification of myeloid populations replenished by CCR2-dependent bone marrow (BM) precursors, tissue-protected BM chimeric mice were generated as previously described (23). Briefly, anesthetized C57BL/6 CD45.1^{+}CD45.2^{+} congenic mice were exposed to a single dose of 9.5 Gy γ-irradiation, while all but the hind legs and lower abdomen were protected by a 2 inch lead shield. Animals were subsequently given 2–5 × 10^{6} BM cells from CD45.2^{+} C57BL/6J mice or *Ccr2*$^{-/-}$ animals by i.v. injection before being left for 8 wk prior to analysis of chimerism in the tissue compartments. All experiments were performed with age- and sex-matched littermate control mice and approved by the University of Edinburgh Animal Welfare and Ethical Review Body under license granted by the U.K. Home Office.

Tissue digestion and FACS analysis

Unless otherwise stated, mice were culled by a rising concentration of CO_2. Then 100 μl of blood was collected by cardiac puncture into EDTA tubes. The peritoneal cavity was lavaged with RPMI 1640 containing 2 mM EDTA and 10 mM HEPES (Invitrogen). Cadavers were subsequently perfused and lung and liver removed and chopped finely, and digested in prewarmed collagenase mixture [0.625 mg ml^{-1} collagenase D (Roche), 0.85 mg ml^{-1} collagenase V (Sigma-Aldrich), 1 mg ml^{-1} dispase (Life Technologies, Invitrogen), and 30 U ml^{-1} DNase (Roche Diagnostics) in RPMI 1640] for 22 and 45 min respectively in a shaking incubator at 37°C before being passed through a 100 μm filter. Lung preparations were washed in PBS containing 2 mM EDTA (Life Technologies, Invitrogen) and 0.5% BSA (Sigma-Aldrich), termed FACS buffer, followed by centrifugation at 300 g for 5 min, whereas liver preparations were washed in 50 ml then 30 ml of ice-cold RPMI 1640 followed by centrifugation at 300 g for 5 min. Erythrocytes in tissues and blood were lysed using RBC lysis buffer from Sigma-Aldrich or BioLegend, respectively. All cells were maintained on ice until further use. Cellular content of the preparations was assessed by cell counting using a CASY TT counter (Roche). Equal numbers of cells or equivalent volumes of blood were stained with Zombie Aqua viability dye (Invitrogen) blocked with 0.025 μg anti-CD16/32 (2.4G2; BioLegend) and 1:10 heat-inactivated mouse serum (Invitrogen), and then surface stained with a combination of Abs in FACS buffer. The following Abs were used: F4/80 (BM8), Siglec-F (E50-2440), Siglec-F (ES22-10D8), Ly6C (HK1.4), CD11b (M1/70), CD11c (N418), MHCII

(M5/114.15.2), CD19 (6D5), CD3 (17A2), CD3 (17A2), CSF1R (AFS98), CD45.1 (A20), CD45.2 (104), CD226 (10E5), CD64 (X57-5/7), Ly6G (1A8), CD26 (H194-112), and PDCA-1 (927) (eBioscience, Miltenyi Biotec, or BD Europe). Where applicable, cells were subsequently stained with streptavidin-conjugated fluorochromes. Fluorescence minus one controls confirmed gating strategies, whereas discrete populations within lineage-negative cells were confirmed by omission of the corresponding population-specific Ab. Samples were acquired on an LSRFortessa flow cytometer (Becton Dickinson) at the Queens Medical Research Institute Flow Cytometry and Cell Sorting Facility and resulting data were analyzed using FlowJo V9 software. $CD45^+$ cells were identified as live single cells by excluding $7AAD^+$ or Zombie $Aqua^+$ cells and using forward scatter area versus forward scatter height characteristics. Cells positive for CD19, CD3, Ly6G, and SiglecF, or CD19, CD3, and Ly6G were referred to as $Lineage^+$ and were excluded prior to analysis of liver, blood and cavity cells, or lung cells, respectively, as shown in the respective figures.

For the processing of brain tissue, double transgenic mice were perfused transcardially with physiological saline and brains were removed for regional dissection into cerebellum, cortex, hippocampus, and striatum. Mixed brain cell homogenates were prepared as described (32). The single-cell suspension of each region was incubated with 1 μg ml^{-1} anti-CD16/32 and subsequently stained with rat anti-mouse/human CD11b (M1/70) and rat anti-mouse CD45 (BioLegend). Flow cytometry was acquired using the Fortessa ×20 (Becton Dickinson) and resulting data were analyzed using FlowJo V10 software.

Inhibition of CSF1R signaling

The CSF1R kinase inhibitor GW2580 (LC Laboratories) was suspended in 0.5% hydroxypropylmethylcellulose and 0.1% Tween 20 using a Teflon glass homogenizer. Diluent control or 160 mg/kg GW2580 was administered daily for 4 d by oral gavage before mice were culled on day 5.

Alexa Fluor 647–labeled CSF1 and anti-CSF1R mAb

Preservative-free sterile anti-CSF1R mAb (clone AFS98) was purchased from Bioserv (Sheffield, U.K.). Porcine CSF1 and CSF1-Fc was prepared as described previously (12). CSF1 and CSF1-Fc were conjugated to Alexa Fluor 647 (AF647) using the AF647 Microscale Protein labeling kit from Thermo Fisher Scientific according to manufacturer's instructions, and sodium azide subsequently removed using 7k MWCO Pierce polyacrylamide spin desalting columns (Thermo Fisher Scientific). Mice were injected i.v. with 0.5 mg anti-CSF1R mAb or PBS vehicle control, followed by 5 μg $CSF1\text{-}Fc^{AF647}$ or PBS vehicle i.v. 10 min later. After a further 10 min, 60 μl of blood was removed by tail venipuncture, with the animals then immediately culled by cervical dislocation, and tissues perfused with PBS through the inferior vena cava. For study of CSF1 uptake in the peritoneal cavity, mice were injected i.p. with or without 0.5 mg AFS98 followed by 0.5 μg $CSF1^{AF647}$ or PBS vehicle 2 min later, and then culled 10 min later by exposure to increasing levels of CO_2. The degree of CSF1R-dependent uptake of $CSF1^{AF647}$ or $CSF1\text{-}Fc^{AF647}$ is presented as the Δ median fluorescence intensity (MFI) calculated as the MFI for individual samples from mice given labeled CSF1 minus the average MFI from all samples pretreated with AFS98.

Imaging of tissues and cells

Whole-mount imaging of freshly isolated tissues from transgenic and WT littermate control mice aged 12–15 wk was performed using a Zeiss AxioZoom.V16 fluorescence microscope. Immediately after excision, tissues were kept at 4°C and protected from light. The fluorescent signal was acquired at 500–550 and 590–650 nm for EGFP and *Csf1r*-mApple, respectively. Acquisition of tissue background signal was performed by imaging WT tissue with the filter used for detection of the *Csf1r*-mApple protein.

Ex vivo confocal imaging of tissues

Male transgenic or WT male littermates were anesthetized, as per regulations, and intravenously injected in the tail vein with 5 μg/g of weight of Lectin-I [from *Griffonia* (*Bandeiraea*) *simplicifolia*] tagged with FITC (Vector Labs). After 10 min, mice were perfused transcardially with HBSS (Thermo Fisher Scientific), at a rate of 10 ml per min, and the left lobe of the liver was excised. Lungs were inflated with a solution containing 1% low melting-point agarose (Sigma-Aldrich) and, upon agarose solidification, the left lung was excised. Detection of functional CSF1R in lung myeloid subsets was performed by administering 5 μg $CSF1\text{-}Fc^{AF647}$ and 5 μg/g of weight of Lectin-I via i.v. injection. Mice were perfused with HBSS, previous to lung excision and inflation with agarose, as described. After dissection, liver and lung were placed on coverslip-bottom chambers and covered with a sufficient volume of HBSS to prevent the surface of tissues from drying. Chambers were kept on ice and protected from light until tissues were imaged on a Zeiss LSM 710 microscope. Laser wavelengths for ECFP, FITC, and mApple were 405, 488, and 543 nm, respectively. Fluorescence acquisition for ECFP, FITC, and mApple signals in liver and lung was 400–480, 525–600, and 602–758 nm, respectively. Acquisition settings for lung tissue treated with $CSF1\text{-}Fc^{AF647}$ were 400–479, 525–583, 593–651, and 651–755 nm for ECFP, FITC, mApple, and AF647, respectively. Postprocessing of images was performed by adjusting the black/white thresholds in the software ZEN 2012 (blue edition) developed by Carl Zeiss as follows: ECFP: 0–175, FITC: 0–100, mApple: 0–75, AF647: 0–200.

Statistics

Statistical tests detailed in the figure legends were performed using GraphPad Prism 6. Where necessary, data were log-transformed to achieve equal variance.

Results

Generation of Csf1r-mApple mice

C57BL/6 mouse embryos were comicro-injected with a construct containing the 7.2 kb *Csf1r* promoter region used to create the *Csf1r*-EGFP mice (26) upstream of *mApple*, along with a construct encoding the reverse tetracycline inducible transactivator *rtTA-m2* under control of the same promoter (*Csf1r*-rtTA), previously used to generate a *Csf1r*-driven Tet-on system (35). mApple was used because it is brighter than its parent mCherry, refractory to photobleaching (38), suffers little from background autofluorescence, and previously enabled whole-mount imaging of the avian response to CSF1 in *Csf1r*-mApple reporter chickens (39). A single founder positive by PCR for both transgenes and for mApple protein in blood cells by flow cytometry was mated with a WT C57BL/6 mouse to establish the *Csf1r*-mApple line. PCR analysis across 77 mice revealed that *Csf1r*-mApple and *Csf1r*-rtTA transgenes were exclusively coinherited, suggesting cointegration (data not shown). PCR and flow cytometry analysis of blood demonstrated the *Csf1r*-mApple transgene to be inherited at a frequency of 44.0% (n = 207). The utility of the cointegrated Tet-on cassette is under investigation and is not considered further in this study but preliminary data demonstrate *rtTA-m2* mRNA is expressed in peritoneal cells (data not shown).

Comparison of Csf1r-EGFP and Csf1r-mApple expression across tissue

In whole-mount fluorescence microscopy of live organs from *Csf1r*-mApple mice expression patterns of mApple recapitulated EGFP in *Csf1r*-EGFP transgenic mice (Fig. 1A–F). Large stellate $mApple^+$ cells were observed throughout the liver, lung, epidermis, and cardiac muscle. Both transgenic strains highlighted the abundant macrophage populations of the intestinal lamina propria (Fig. 1E), and the red pulp of spleen (Fig. 1F) (26). Background fluorescence in littermate control mice was negligible (Fig. 1A–F, left panel). The *Csf1r*-EGFP and Δ*Csf1r*-ECFP transgenes have been used extensively for in vivo imaging with multiphoton and spinning disc microscopes (e.g., Refs. 20, 30, 31, 40–43), providing high-resolution analysis of macrophage motility and the extent of their ramified processes. Multiphoton imaging of whole mounts of the muscularis externa of the intestine demonstrated the high signal-to-noise ratio obtainable with the *Csf1r*-mApple reporter (Fig. 1G), enabling visualization of the regular network of microglial-like macrophages in this site (44, 45). Furthermore, the impact of exogenous CSF1-Fc, which regulates the function of these cells (44), could be directly visualized as an increase in cell size.

Csf1r-mApple expression by blood myeloid cells

To determine efficiency, reliability, and specificity of transgene expression, flow cytometry was performed on the blood of a

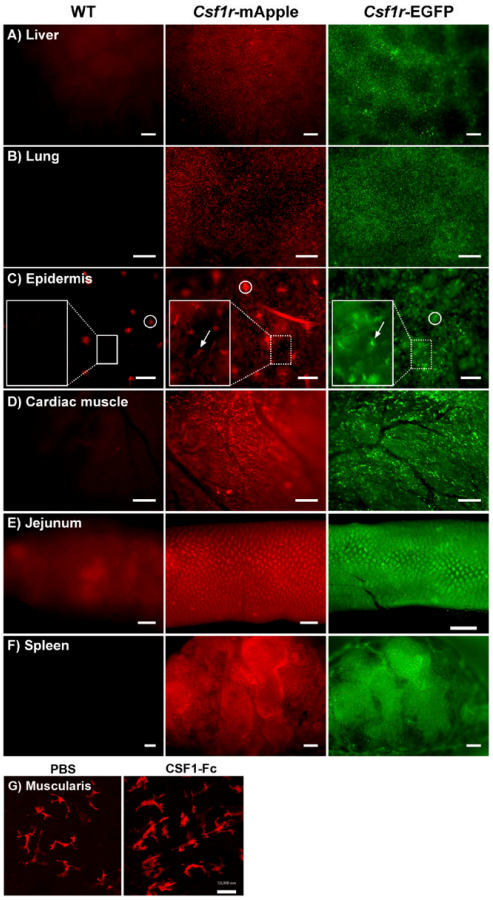

FIGURE 1. Distribution of the *Csf1r*-mApple and *Csf1r*-EGFP transgenes is similar throughout tissues. Whole-mount imaging of freshly isolated liver (**A**), lung (**B**), skin epidermis (**C**), cardiac muscle (**D**), jejunum (**E**), and cross-section of spleen (**F**) from WT (left panel), *Csf1r*-mApple (central), and *Csf1r*-EGFP (right panel) mice, or from muscularis (**G**) of *Csf1r*-mApple mice treated with PBS (left panel) or CSF1-Fc (right panel). In (C), a region of interest has been further magnified to better show Langerhans cells (white arrows), and hair follicles can be detected as highly autofluorescent structures (white circles). Scale bars in skin represent 100 μm; 200 μm in liver, spleen, and cardiac muscle; 500 μm in lung and jejunum; and 10 μm in the muscularis.

cohort of *Csf1r*-mApple mice and littermate controls. Circulating CSF1R$^+$CD11b$^+$ monocytes (Fig. 2A) were uniformly *Csf1r*-mApple$^+$ in both Ly6C$^+$ and Ly6C$^-$ subsets (Fig. 2B, 2C). As reported for the expression of EGFP in *Csf1r*-EGFP mice, neutrophils and eosinophils, which express *Csf1r* mRNA but not protein (46), were also *Csf1r*-mApple positive (Fig. 2B, 2C). The *Csf1r* promoter is active in B cells, which like macrophages, express the key transcription factor, PU.1, albeit at lower levels (47). Accordingly, ~70% of B cells had very low, but detectable, *Csf1r*-mApple (Fig. 2B, 2C). Similar expression of EGFP in *Csf1r*-EGFP mice is not detectable by confocal microscopy on spleen sections (46). The intensity of *Csf1r*-mApple expression was consistent between animals, with equivalent levels expressed by monocytes and neutrophils and lower levels in eosinophils and B cells (Fig. 2D). Hence, the pattern of *Csf1r*-mApple expression reproduced that reported for EGFP in *Csf1r*-EGFP mice.

The level of Csf1r-mApple expression distinguishes monocytes, macrophages, and cDC in different tissues

To determine if transgene expression distinguished cDC and macrophages across multiple tissues, we first confirmed the identity of marker-defined MPS populations before surveying transgene expression in *Csf1r*-mApple mice. In the peritoneal cavity, we have demonstrated that recruited monocytes continuously replenish rare short-lived F4/80^{lo} MHCII$^+$ macrophages that include both CD11c$^+$ and CD11c$^-$ cells (23), although only slowly replacing the more abundant F4/80^{hi} resident macrophages of embryonic origin (23). Both CD11c$^+$ and CD11c$^-$ short-lived and F4/80^{hi} peritoneal macrophage populations express detectable surface CSF1R. In contrast, Flt3-dependent cavity cDC of non-monocyte BM origin also express CD11c$^+$ and MHCII$^+$ and can be found among F4/80$^{lo/-}$ cells, but can be distinguished as CSF1R$^-$ (23, 24, 48, 49). Based upon this published gating strategy and previously assigned ontogenies (Fig. 3A) (23), *Csf1r*-mApple was detected in Ly6C$^+$ monocytes, all macrophage populations, and in CD11b$^-$ cDC1 and CD11b$^+$ cDC2 (Fig. 3B, 3C) (24). There was a progressive increase in *Csf1r*-mApple intensity between Ly6C$^+$ monocytes, CD11c-defined subsets of short-lived F4/80^{lo}MHCII$^+$ macrophages, and long-lived F4/80^{hi} macrophages (Fig. 3D), consistent with the linear developmental relationship between these populations and monocytes in adult mice (23, 48, 50). *Csf1r*-mApple fluorescence in both CD11b$^-$ cDC1 and CD11b$^+$ cDC2 was lower than in monocytes (Fig. 3D), consistent with the lack of surface CSF1R (Fig. 3A). EGFP expression in *Csf1r*-EGFP mice replicated this pattern (Fig. 3E, 3F).

In the lung, alveolar macrophages are readily identified based upon high levels of CD11c and SiglecF (Fig. 4A) (51, 52). Interstitial cells are more heterogeneous. Some MHCII$^+$ cells with varying levels of CD11c have been defined as macrophages based upon their expression of the Fc receptor CD64 and CSF1R dependence (51, 53), which contrasts the Flt3 dependence of CD64$^-$ interstitial cDC2 (15). To verify that CD64 expression distinguishes pulmonary interstitial macrophages from CD11b$^+$ cDC2, we assessed the turnover kinetics of CD64-defined MHCII$^+$ cells and their dependence on CCR2, an established method for determining the likely monocyte dependence of tissue MPS cells (23, 54). We used a BM chimeric system in which WT mice were irradiated with organs of interest shielded to prevent irradiation-induced injury and reconstituted with congenic WT or *Ccr2*$^{-/-}$ BM. This approach results in stable nonhost chimerism in blood leukocytes of ~30% in recipients of WT BM (23, 55) (Fig. 4B, short-dashed line) and allows the turnover kinetics of tissue populations to be assessed. Importantly, in recipients of *Ccr2*$^{-/-}$ BM chimerism in monocytes (Fig. 4B, long-dashed line) but not other circulating leukocytes is largely abolished (23). Notably, putative CD64$^-$CD11b$^+$MHCII$^+$ cDC2 were completely replaced within 8 wk, consistent with the short half-life of DCs (14). This occurred in a completely CCR2-independent manner, with identical chimerism in recipients of WT and *Ccr2*$^{-/-}$ BM (Fig. 4B). In contrast, relatively few CD64$^+$MHCII$^+$ cells were replaced over 8 wk, although this was completely dependent on CCR2, suggesting slow replenishment from monocytes. Thus, consistent with previous work (15), CD64 accurately defines distinct CD11b$^+$ MPS populations. Alveolar macrophages showed no evidence of chimerism (Fig. 4B), consistent with self-maintenance (52, 56, 57). Surprisingly, replenishment of cells

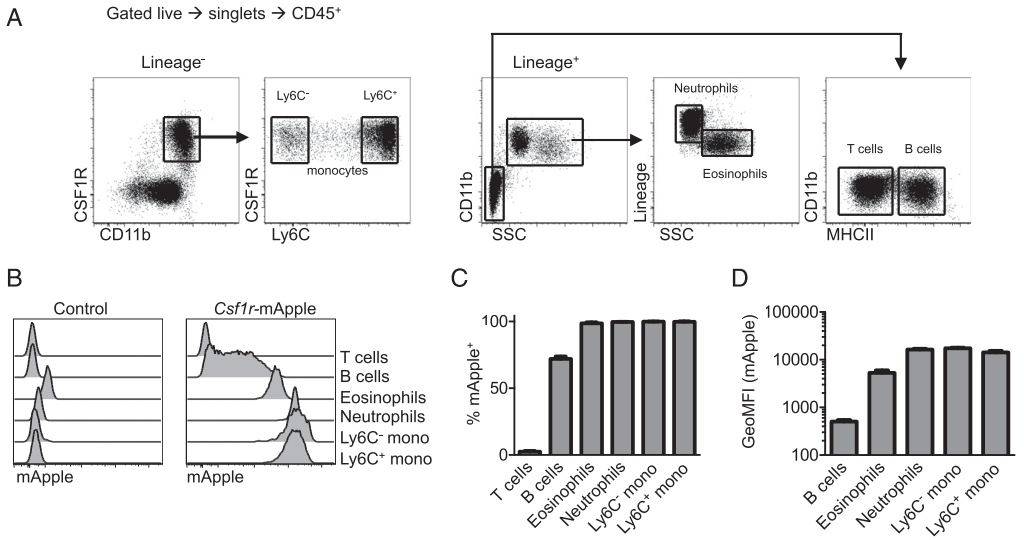

FIGURE 2. *Csf1r*-mApple transgene expression in blood leukocytes. (**A**) Flow cytometric strategy to identify blood leukocytes. (**B**) Expression of *Csf1r*-mApple in venous blood leukocytes from a representative *Csf1r*-mApple (right) and WT littermate control (left) mouse. (**C**) Frequency of cells positive for *Csf1r*-mApple and (**D**) geometric mean fluorescence intensity (GeoMFI) of *Csf1r*-mApple gated on *Csf1r*-mApple$^+$ cells for different blood leukocytes. (B–D) Representative data from one of three experiments. Data are presented as mean ± SD of four mice (C and D).

defined as cDC1 was also dependent upon CCR2. However, these cells express CCR2 within the lung environment (58) and thus may require this receptor for tissue retention. Based upon the verified ontogenies, Ly6C$^+$ monocytes, CD64$^+$ interstitial macrophages, and alveolar macrophages in the lungs were all *Csf1r*-mApple$^+$ (Fig. 4C, 4D), but expression increased progressively between monocytes and mature macrophages (Fig. 4C, 4E). Both cDC populations also expressed *Csf1r*-mApple, but at lower levels than monocytes (Fig. 4C–E).

In the liver, the largest phagocyte population is the Kupffer cells (KC), but a minority CD11b$^+$F4/80^{lo} BM-derived population may include monocytes, cDC2, and possibly F4/80^{lo} BM-derived macrophages (14, 29, 57). KCs [F4/80^{hi}CD11b^{lo} (29, 59, 60)] (Fig. 5A) exhibited uniformly high expression of *Csf1r*-mApple (Fig. 5B–D). The minority CD11b$^+$F4/80^{lo} compartment was subdivided based upon Ly6C and MHCII (Fig. 5A). The Ly6C$^+$ cells and Ly6C$^-$MHCII$^-$ cells resembled Ly6C$^+$ and Ly6C$^-$ blood monocytes in size and marker expression (Fig. 5F). Unlike blood monocytes, MHCII$^+$ cells among CD11b$^+$F4/80^{lo} cells were larger, exhibited high levels of CD11c, and must include the Flt3-dependent CSF1R-independent CD11b$^+$ cDC2 described previously (14); hence, we provisionally assigned these cDC2 (Fig. 5F). All CD11b$^+$ populations expressed high levels of *Csf1r*-mApple (Fig. 5B, 5C). In the same CCR2-dependent tissue-protected BM chimera system used for the lung, the putative CD11b$^+$ cDC2 population was replenished almost entirely by CCR2-independent BM precursors (Fig. 5E). They also expressed the highest levels of CD26, a marker of cDC conserved across species (61), and were negative for CD64 (Fig. 5F), confirming them as cDC2. CD11b$^{-/lo}$ F4/80$^-$ cells were also positive for *Csf1r*-mApple, but expressed markers of cDC1 (Ly6C$^-$MHCII$^+$CD11c$^+$CD26$^+$) and plasmacytoid DC (pDC) (Ly6C$^+$MHCII$^+$PDCA-1$^+$) (Fig. 5A, 5F), and were replenished by CCR2-independent precursors (Fig. 5E). Hence, in liver the *Csf1r* transgene did not distinguish cDC from monocytes, but was highest in mature macrophages.

Detection of functional CSF1R using fluorescent CSF1-Fc

Csf1r mRNA may be posttranscriptionally regulated (62) and the protein may be cleaved from the cell surface in response to TLR signals (63). To assess functional CSF1R expression, we investigated the ability of MPS cells to take up labeled pig CSF1-Fc fusion protein, which produces a large increase in tissue macrophage populations when injected into mice (12) or pigs (64). CSF1-Fc conjugated with AF647 (CSF1-Fc^{AF647}) was found to bind specifically to monocytes in vitro (65). CSF1-Fc^{AF647} was injected intravenously 10 min before mice were sacrificed. In the liver, the uptake of CSF1-Fc^{AF647} was detected in KC, monocytes, and cDC2, but not in cDC1, pDC (Fig. 6A, 6B), or neutrophils (data not shown). Within cDC2, CSF1-Fc^{AF647} binding was prevalent in CD11c^{hi} cells (Fig. 6C) precluding any possible confusion with the CD11c^{dim} MHCII$^+$ subcapsular macrophages described recently (42). In the lung, the majority of Ly6C$^+$ monocytes and interstitial macrophages bound CSF1-Fc^{AF647}, whereas both cDC populations were negative (Fig. 6A, 6B). Uptake of labeled CSF1-Fc by myeloid populations was reduced or abolished by the anti-CSF1R Ab, AFS98 (Fig. 6A, 6B), a weak inhibitor of receptor-ligand binding (66), and an identical labeling profile was observed following injection of a non–Fc-fused AF647-labeled porcine CSF1 (CSF1^{AF647}) (data not shown). No detectable CSF1-Fc^{AF647} was bound by alveolar macrophages (Fig. 6A, 6B) and these cells also failed to bind appreciable levels in vitro (data not shown). Labeled anti-CD45 Ab was able to access all other myeloid populations in lung (data not shown) (67) and liver (Fig. 6D), suggesting a lack of CSF1-Fc^{AF647} or CSF1^{AF647} uptake by certain cDC reflects an absence of surface CSF1R expression rather than the inaccessibility of the sites they may occupy (31, 53).

Consistent with previous population-level data on CSF1 clearance (68), KC bound the highest level of labeled CSF1 per cell in a receptor-dependent manner (Fig. 6B), and considerably more per

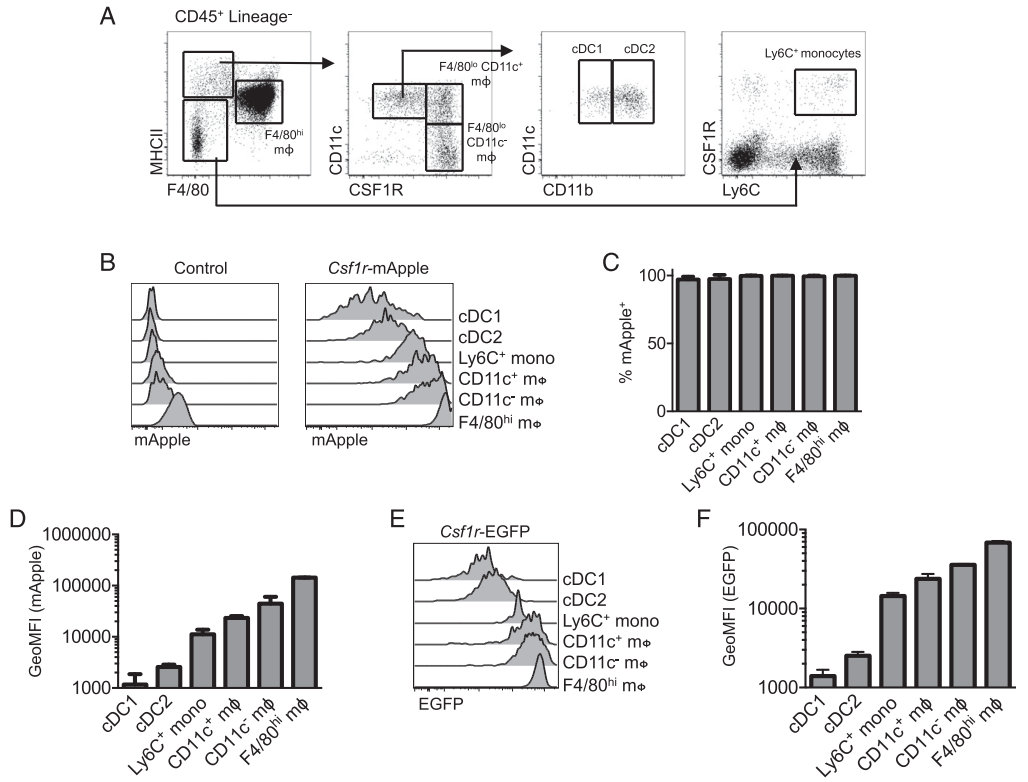

FIGURE 3. *Csf1r* transgene and CSF1R protein expression in the peritoneal cavity. (**A**) Flow cytometric strategy to identify peritoneal cavity myeloid cells as recently described (23). (**B**–**D**) Expression of *Csf1r*-mApple in peritoneal cavity myeloid populations determined by flow cytometry, showing a representative WT littermate control (left) and *Csf1r*-mApple (right) mouse (B), and graphs depicting the mean frequency of *Csf1r*-mApple$^+$ cells in each population (C) and geometric mean fluorescence intensity (GeoMFI) of *Csf1r*-mApple for different peritoneal leukocytes gated on *Csf1r*-mApple$^+$ cells (D). (**E** and **F**) Expression of *Csf1r*-EGFP in peritoneal cavity myeloid populations from *Csf1r*-EGFP mice, showing a representative flow cytometric overlay (E) and graphs depicting the frequency and GeoMFI of *Csf1r*-EGFP$^+$ cells in each population (F) across multiple mice. Representative data from one of three experiments (B–D) or a single experiment (E and F). Data are presented as mean ± SD of four mice (C, D, and F).

cell than blood monocytes (Fig. 6E). In turn, Ly6C$^+$ monocytes in lung and liver were more intensely labeled than interstitial lung macrophages or liver CD11b$^+$ cDC2 and liver Ly6C$^-$ monocytes (Fig. 6B), although distinct intravascular versus parenchymal locations of these cells (31, 53) means exposure to circulating CSF1 cannot be controlled in this comparison. Of note, Ly6C$^+$ blood monocytes, identified independently of CSF1R expression (Supplemental Fig. 1A), were more intensely labeled than the Ly6C$^-$ subset (Fig. 6E), despite equivalent surface expression of CSF1R (Fig. 6F) (69, 70). Thus, novel differences in capacity to bind CSF1 were revealed using this ligand-binding approach.

The relationship between *Csf1r*-mApple activity and CSF1R-mediated ligand uptake was also examined in the peritoneal cavity following i.p. injection. Monocytes and CD11c$^+$ and CD11c$^-$F4/80^{lo}CD226$^+$ macrophages (49, 50) were identified as described in Supplemental Fig. 1B, avoiding the use of Abs to CSF1R. Neither *Csf1r*-mApple^{lo} cDC population bound appreciable levels of CSF1^{AF647}, whereas all three macrophage populations had higher levels of receptor-dependent uptake of CSF1^{AF647} than Ly6C$^+$ cavity monocytes (Fig. 7A). Surprisingly, the CD11c$^-$F4/80^{lo} macrophages exhibited the greatest uptake. These differences were not explained by differential levels of receptor-independent macropinocytosis as uptake of injected OVA–Texas Red was largely equivalent between populations (Fig. 7B). Anti-CSF1R mAb inhibited CSF1 uptake to a similar degree in each population, with a reduction between 63 and 75%. The difference in receptor activity appeared to have functional significance, as treatment of mice daily for 4 d with a CSF1R kinase inhibitor, GW2580 (71), which has been shown to inhibit proliferation of microglia (41) and pleural macrophages (11), partly depleted the CD11c$^-$ subset of F4/80^{lo}MHCII$^+$ peritoneal macrophages alone (Fig. 7C, left graph), despite inhibiting proliferation (as evidenced by Ki67 staining) of all macrophage populations (Fig. 7C, right graph).

Csf1r-mApple:ΔCsf1r-ECFP mice allow in situ imaging of distinct mononuclear phagocytes

The Δ*Csf1r*-ECFP transgene was crossed previously to the *Cx3cr1*$^{+/gfp}$ or *Itgax* (CD11c)-EYFP mouse to distinguish pulmonary monocytes from other myeloid lung populations (31). To determine the utility of the *Csf1r*-mApple mouse to facilitate in vivo imaging of different myeloid populations, we crossed it to

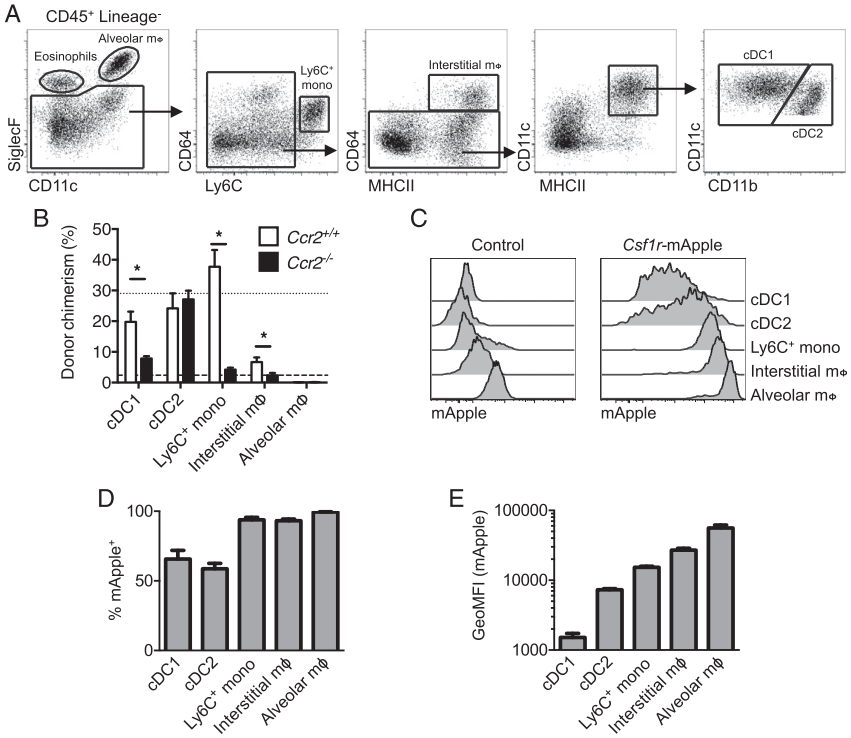

FIGURE 4. Lineage-restricted *Csf1r*-mApple transgene expression in the lung. (**A**) Flow cytometric strategy to identify lung leukocytes. (**B**) Frequency of donor cells within each lung population from tissue protected BM chimeric mice 8 wk after receiving BM from WT (white) or *Ccr2*$^{-/-}$ (black) mice. Mean donor chimerism for circulating Ly6C$^+$ monocytes is presented as short- or long-dashed lines for recipients of WT or *Ccr2*$^{-/-}$ BM, respectively. (**C**) Expression of *Csf1r*-mApple in lung leukocytes from a representative WT littermate control (left) and *Csf1r*-mApple (right) mouse. (**D**) Frequency of cells expressing *Csf1r*-mApple and (**E**) geometric mean fluorescence intensity (GeoMFI) of *Csf1r*-mApple gated on *Csf1r*-mApple$^+$ cells for different lung leukocytes. Data are from one of two independent experiments. Data presented as mean ± SD of four mice (D and E) or mean ± SEM of five mice (B). The asterisk (*) indicates significant differences using multiple *t* tests corrected for multiple comparisons using the Holm–Sidak method.

the Δ*Csf1r*-ECFP line (32, 36). As in the intestine (32), the majority of cDC1, cDC2, and Ly6C$^+$ and Ly6C$^-$ monocytes in the liver expressed high levels of ECFP, whereas pDC expressed intermediate levels. Neutrophils, eosinophils, and lymphocytes were negative (data not shown) as were F4/80^{hi} KC (Supplemental Fig. 2A). All ECFP$^+$ cells expressed intermediate levels of mApple (Supplemental Fig. 2B, cyan gate), whereas all mApple^{hi} cells were ECFP$^-$ and represent KC (Supplemental Fig. 2B, red gate). We combined the two *Csf1r* reporters with detection of endothelial cells by injection of FITC-labeled Lectin I. In confocal images the mApple$^+$ cells were almost completely restricted to the liver sinusoids (e.g., pink boxes), consistent with KC (Fig. 8). In contrast, ECFP$^+$mApple$^+$ double-positive cells were rarely detected (e.g., white box), despite the presence of numerous ECFP$^+$ mApple$^-$ cells (e.g., yellow box) (Fig. 8). These data suggest the intermediate levels of *Csf1r*-mApple expressed in ECFP$^+$ cDC and monocytes (Fig. 5B, Supplemental Fig. 2A) are apparently below the threshold of detection of confocal imaging. This conclusion was supported by only weak detection of mApple expression when peripheral blood was imaged using identical microscope settings (Supplemental Fig. 3A). The *Csf1r*-ECFP$^+$ cells in the liver (e.g., yellow box) were mainly detected outside the sinusoids and likely include the subcapsular liver macrophages that also express the Δ*Csf1r*-ECFP transgene (42). The high level of mApple expression in KC therefore allows imaging of these cells without detection of monocytes and other mApple$^+$ cells in the liver.

In the lung, interstitial macrophages and DC were ECFP negative (Supplemental Fig. 2C) whereas the majority of alveolar macrophages and Ly6C$^+$ monocytes expressed ECFP, as reported previously (31, 32). Combined, all ECFP$^+$ cells were mApple$^+$ (Supplemental Fig. 2D, cyan gate) and encompassed alveolar macrophages and Ly6C$^+$ and Ly6C$^-$ monocytes, whereas ECFP$^-$ mApple^{hi} cells (Supplemetal Fig. 2D, red gate) comprised CD64$^+$ interstitial macrophages and a minor fraction of ECFP$^-$ alveolar macrophages. In confocal images of transverse lung sections, parenchymal populations broadly divided into rounded ECFP$^+$mApple$^+$ cells (Fig. 9, yellow box) consistent with alveolar macrophages or interstitial migratory monocytes (31, 67) and elongated stellar-shaped ECFP$^-$mApple$^+$ cells (Fig. 9, white box). Injection of CSF1-Fc^{AF647} into the double transgenic mice selectively labeled the extravascular interstitial ECFP$^-$mApple$^+$ cells (Supplemental Fig. 4, white box), visible as punctate staining indicative of internalization of labeled ligand,

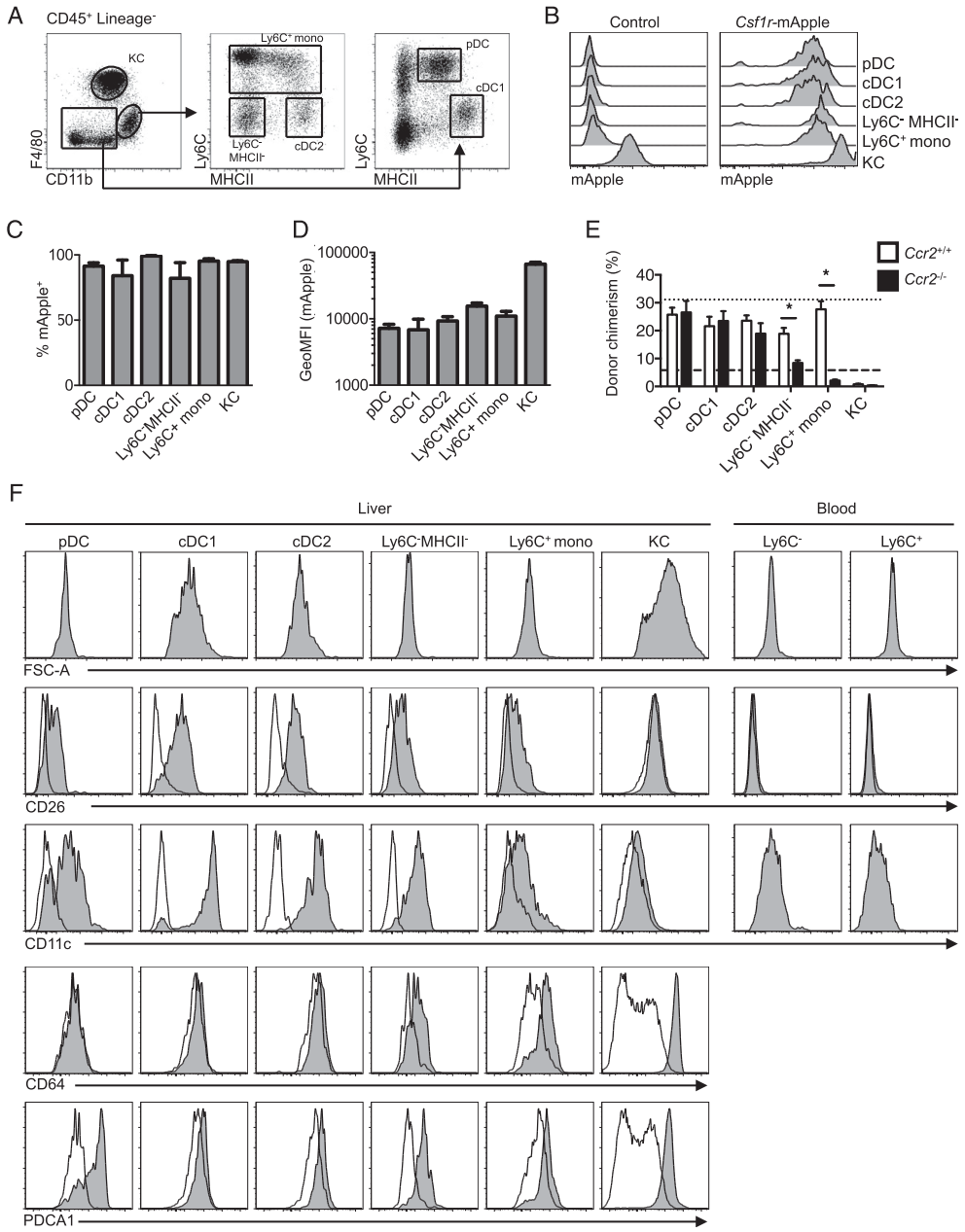

FIGURE 5. *Csf1r*-mApple transgene expression in the liver. (**A**) Flow cytometric strategy to identify liver leukocytes. (**B**) Expression of *Csf1r*-mApple in liver leukocytes with histograms from a representative *Csf1r*-mApple (right) and WT littermate control (left) mouse. (**C**) Frequency of cells expressing *Csf1r*-mApple and (**D**) geometric mean fluorescence intensity (GeoMFI) of *Csf1r*-mApple gated on *Csf1r*-mApple$^+$ cells for different liver leukocytes. (**E**) Frequency of donor cells within each hepatic population from tissue protected BM chimeric mice 8 wk after receiving BM from WT (white) or *Ccr2*$^{-/-}$ (black) mice. Mean donor chimerism for blood Ly6C$^+$ monocytes is presented as short- or long-dashed lines for recipients of WT or *Ccr2*$^{-/-}$ BM, respectively. (**F**) Representative histograms showing forward scatter area (FSC-A) characteristics and CD26, CD11c, CD64, and PDCA1 expression (tinted) overlayed with FMO controls (open) for liver leukocytes and blood monocytes. (B–D) Representative data from one of three or (E) two experiments, with data presented as mean ± SD of four mice (C and D) or mean ± SEM of five (E) mice. The asterisk (*) indicates significant differences using multiple *t* tests corrected for multiple comparisons using the Holm–Sidak method.

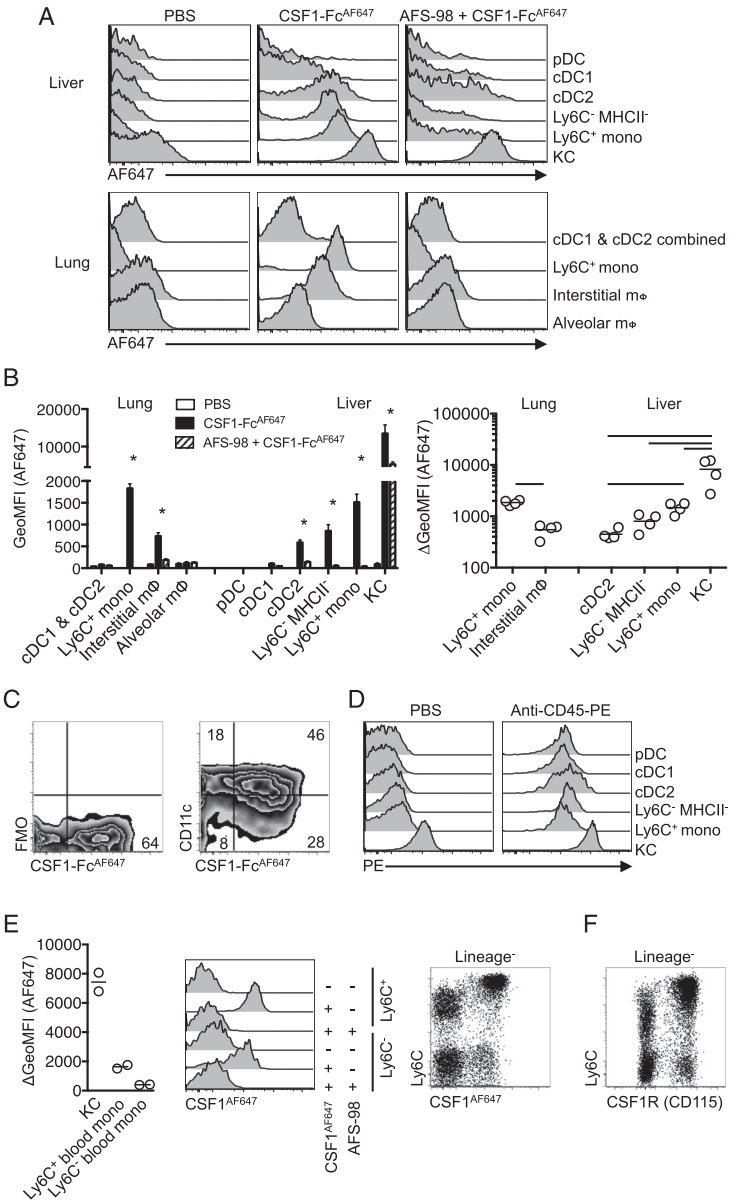

FIGURE 6. Tissue-specific consumption of CSF1 by cDC2 in vivo. (**A**) Histograms of AF647 fluorescence of leukocyte populations from lung and liver following i.v. injection of anti-CSF1R mAb AF-S98 or PBS vehicle before subsequent i.v. delivery of CSF1-Fc^{AF647} or PBS vehicle. (**B**) Geometric mean fluorescence intensity (GeoMFI) of AF647 of cells from mice in (A) (left graph) and change in MFI between mice given CSF1-Fc^{AF647} alone or after AFS-98 pretreatment (right graph), with data presented as mean ± SEM of four mice per group (left), or with data points for individual mice shown (right). Data are from one of two repeat independent experiments. (**C**) Representative plots showing CSF1-Fc^{AF647} uptake versus CD11c expression or FMO control on hepatic cDC2 from mice in (A). (**D**) PE fluorescence of liver leukocytes from C57BL/6 mice injected i.v. with anti–CD45-PE mAb or PBS vehicle 2 min prior to necropsy, showing data from one representative mouse of two per group. (**E**) Histograms of AF647 fluorescence of Ly6C$^+$ and Ly6C$^-$ blood monocytes from mice treated as in (A) but given CSF1^{AF647}, and a graph showing change in GeoMFI of blood monocytes and liver KC between mice given CSF1^{AF647} alone or after pretreatment with AFS98, and a dot plot showing Ly6C versus AF647 uptake on all CD3$^-$CD19$^-$Ly6G$^-$ blood cells with data points representing individual mice. (**F**) Conventional surface CSF1R (CD115) and Ly6C staining on CD3$^-$CD19$^-$Ly6G$^-$ blood cells from naive mice. Data are from one representative experiment of two (B–D and F) or three (E) independent repeats. The asterisk (*) indicates significant differences between CSF1-Fc^{AF647} alone and AFS98 + CSF1-Fc^{AF647} using *t* tests corrected for multiple comparisons with the Holm–Sidak method (B, left graph), whereas lines indicate significant differences using one-way ANOVA (B, right graph).

and confirmed them to be interstitial macrophages rather than ECFP$^-$mApple^{lo} pulmonary DC. Many extravascular ECFP$^+$mApple$^+$ cells also took up CSF1-Fc^{AF647} (Supplemental Fig. 4), most likely migratory monocytes identified previously by live imaging (30, 31). In contrast, the most frequent cells observed within the pulmonary capillaries were ECFP$^-$mApple$^+$ (Fig. 9D, cyan box) and failed to label with injected CSF1-Fc^{AF647} (Supplemental Fig. 4), consistent with pulmonary neutrophils (72). Consistent with this, imaging of blood cells at identical power settings confirmed strong detection of mApple in ECFP$^+$ monocytes and ECFP$^-$ neutrophils (Supplemental Fig. 3B).

Heterogeneous expression of Csf1r reporter genes in the brain

Macrophages in the mouse embryo are ECFP positive in the Δ*Csf1r*-ECFP line from their earliest appearance in the yolk sac (32). In addition to alveolar macrophages, one of the few locations in adults in which transgene expression is retained is in microglia.

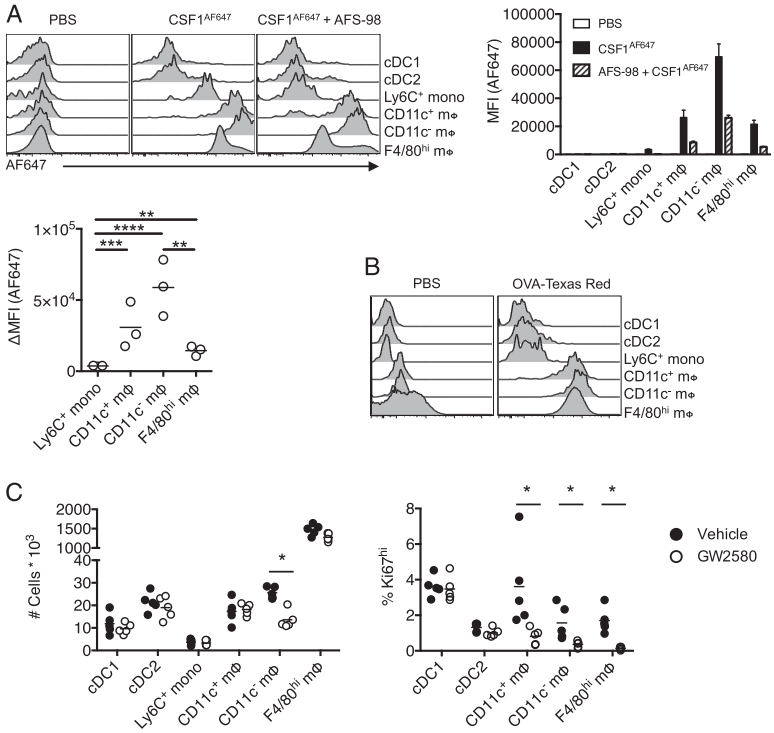

FIGURE 7. Consumption of CSF1 differs between monocytes and resident peritoneal macrophage populations. (**A**) Representative histograms of AF647 fluorescence in cavity leukocytes 10 min after i.p. injection of $CSF1^{AF647}$ or PBS vehicle alone or in combination with pretreatment with AFS98, and graphs showing MFI of AF647 (right of histogram) and change in MFI between mice given $CSF1^{AF647}$ alone or after AFS98 pretreatment (below histogram), with data presented as mean ± SEM of three to four mice per group. Data are from one of three independent repeat experiments. (**B**) Representative histograms of Texas Red fluorescence in cavity leukocytes 10 min after i.p. injection of OVA–Texas Red conjugate from a single experiment. (**C**) Total number of cavity leukocytes and proportion expressing high levels of Ki67 from mice treated for 4 d with GW2580 (open) or vehicle control (closed), with data points depicting individual mice. Data representative of two independent experiments. The asterisk (*) indicates significant differences using multiple *t* tests corrected for multiple comparisons using the Holm–Sidak method.

Grabert et al. (73) reported differences in microglia numbers and gene expression profiles in different mouse brain regions, and changes in gene expression with age. We used the *Csf1r*-mApple: Δ*Csf1r*-ECFP cross to further dissect microglial heterogeneity in different brain regions. $CD45^{lo}CD11b^{+}$ classical microglia were uniformly strongly positive for mApple (Fig. 10A). Like blood monocytes and alveolar macrophages, microglia in cortex, hippocampus, and striatum were largely positive for ECFP, but in the cerebellum the percentage was much lower (37.4%, Fig. 10B). The level of ECFP in these cells was also lower, and lacked a clear peak, reminiscent of the ECFP profiles of macrophages and DC in the gut (32). The brain also contains a separable $CD11b^{+}$, $CD45^{hi}$ macrophage-like microglial population, a subset of which occupies perivascular locations and expresses higher levels of *Csf1r* than monocytes (74). By contrast to the classical microglia and blood monocytes, the $CD11b^{+}CD45^{hi}$ cells were >50% ECFP negative in all brain regions (Fig. 10B).

Discussion

We have developed a novel *Csf1r*-mApple reporter line. The *Csf1r* promoter construct used has been remarkably consistent in generating location and copy-number–independent expression of transgenes (75), further confirmed by the comparable pattern of *Csf1r*-mApple and *Csf1r*-EGFP transgene expression. Expression of *Csf1r*-mApple had no impact on numbers of tissue macrophages or circulating blood leukocytes (data not shown). With optimal microscope settings, the distinct profile of transgene expression across subsets of MPS cells allowed exclusive detection of $mApple^{hi}$ cells. When combined with the Δ*Csf1r*-ECFP reporter gene, which selectively labels subsets of *Csf1r*-positive cells, CSF1-Fc labeled with AF647, and FITC-labeled Lectin, we could identify and image lung interstitial macrophages and liver KC, and distinguish them from other myeloid cells. Despite high levels of *Csf1r*-mApple and *Csf1r*-EGFP (46) transgene expression, neutrophils are identifiable by injection of labeled Abs to Ly6G, a molecule with a negligible role in neutrophil trafficking or function (76, 77). Thus, there are numerous possibilities to produce live images of macrophage behavior and heterogeneity, particularly by combining with other established EGFP-based reporter mice.

In common with the *Csf1r*-EGFP reporter (78), *Csf1r*-mApple expression was uniformly higher in resident macrophages compared with monocytes, a difference reflected in the ability of at

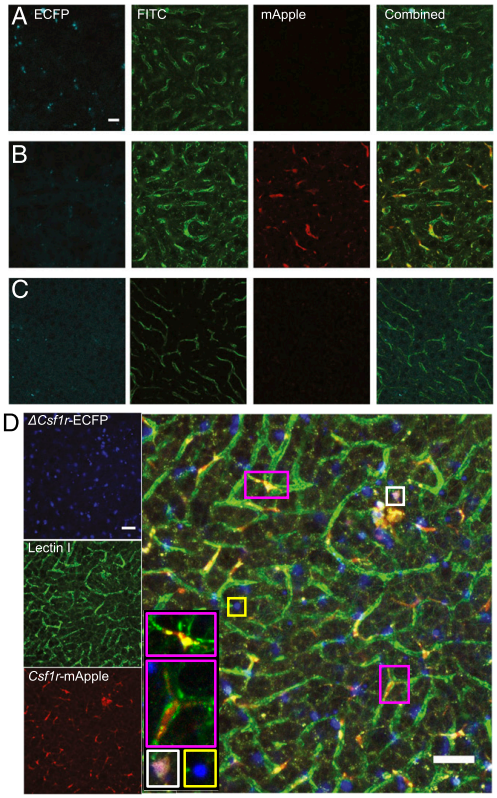

FIGURE 8. *Csf1r*-mApple and Δ*Csf1r*-ECFP transgenes allow imaging of distinct lineages of hepatic myeloid cells. Confocal image of the surface of the left lobe of the liver of a Δ*Csf1r*-ECFP (**A**), *Csf1r*-mApple (**B**), WT (**C**), and *Csf1r*-mApple/Δ*Csf1r*-ECFP (**D**) mouse imaged ex vivo. FITC-Lectin I was injected i.v. to reveal liver sinusoidal endothelium. Scale bars represent 20 μm (A–C) or 50 μm (D).

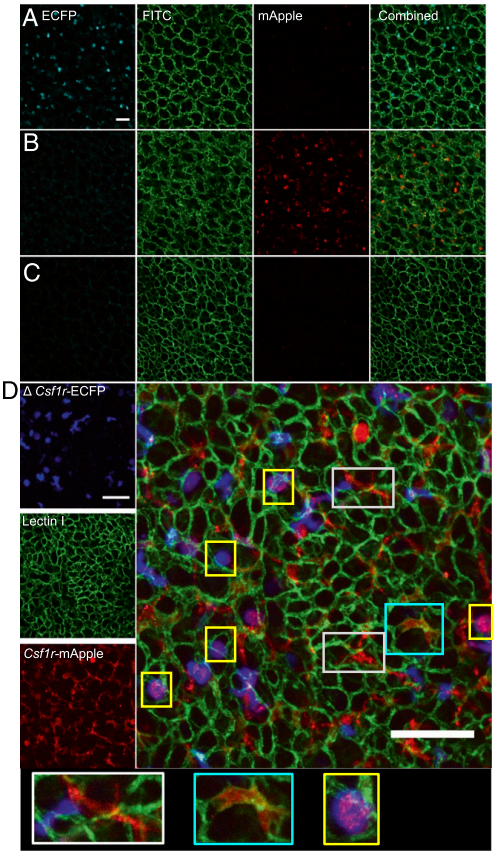

FIGURE 9. *Csf1r*-mApple and Δ*Csf1r*-ECFP transgenes allow imaging of distinct lineages of pulmonary myeloid cells. Confocal image of a transverse section of lung from a Δ*Csf1r*-ECFP (**A**), *Csf1r*-mApple (**B**), WT (**C**), and *Csf1r*-mApple/Δ*Csf1r*-ECFP (**D**) mouse imaged ex vivo. FITC-Lectin was injected i.v. to reveal pulmonary vasculature. Scale bars in all panels represent 50 μm.

least liver and cavity macrophages to capture more CSF1 on a per-cell basis than monocytes in vivo. Consistently, peritoneal macrophages compete effectively for available CSF1 in mixed culture with proliferating BM-derived macrophages (79). The rapid uptake of $CSF1^{AF647}$ by KC is consistent with their role in regulating the circulating CSF1 concentration (68). Hence, upregulation of CSF1R expression may be a general feature of macrophage differentiation that allows them to compete for or control bioavailable CSF1. The apparent inability of alveolar macrophages to capture CSF1 is a notable departure from this tenet. However, alveolar macrophages are unaffected in adult CSF1-deficient op/op mice (80) and their replenishment from BM following irradiation is largely independent of CSF1R (81). Thus, our data are consistent with a lack of role for CSF1 in maintenance of the alveolar macrophage niche. However, it remains unclear why both alveolar macrophages and granulocytes express high levels of *Csf1r* transgene despite lacking a surface receptor. In the blood, $Ly6C^+$ monocytes more readily took up CSF1 than their $Ly6C^-$ progeny, a feature consistent with the suggestion that $Ly6C^+$ monocytes regulate the availability of CSF1, thereby controlling the lifespan of the $Ly6C^-$ population (57). Interestingly, higher consumption of CSF1 by classical monocytes is also evident in PBMCs from *Csf1r*-EGFP transgenic sheep (65), suggesting this feature is conserved across species.

Intensity of fluorescence in *Csf1r*-mApple mice also largely distinguished long-lived tissue-resident macrophages (KC, alveolar macrophages, and $F4/80^{hi}$ peritoneal macrophages) from those of more recent monocyte-origin ($F4/80^{lo}$ resident peritoneal and lung interstitial macrophages) but was not correlated with the ability to take up labeled CSF1. In the peritoneal cavity, the receptor activity was greatest in $F4/80^{lo}CD11c^-$ cells. Notably, these cells were selectively depleted following treatment with the CSF1R kinase inhibitor GW2580. Dynamics of loss of labeled histone 2B-GFP from peritoneal $F4/80^{lo}$ macrophages places the half-life for replenishment of both $CD11c^+$ and $CD11c^-$ subsets from monocytes at around 2 wk (23), much longer than the 4 d treatment regimen in this study. Hence, selective loss of $F4/80^{lo}$ $CD11c^-$ cells likely results from reduced survival or retention in

A

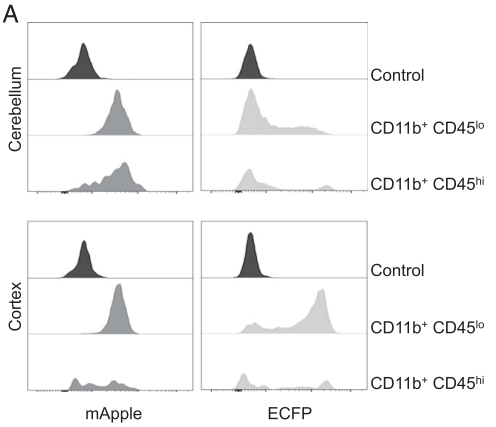

B

Region	Average % of mApple x ECFP double positive cell populations	
	CD11b$^+$CD45^{lo} (microglia)	CD11b$^+$CD45^{hi}
Cerebellum	37.4%	28.9%
Cortex	75.2%	36.4%
Hippocampus	72.9%	28.8%
Striatum	68.1%	42.9%

FIGURE 10. The expression of *Csf1r*-mApple and Δ*Csf1r*-ECFP transgenes in regional brain homogenates. Cerebellum, cortex, hippocampus, and striatum were processed to generate a single-cell suspension. (**A**) Compared are CD11b$^+$CD45^{lo} microglia and CD11b$^+$CD45^{hi} cells of the cerebellum and cortex regarding their expression of *Csf1r*-mApple and ECFP. (**B**) Percentage of double transgene positive CD11b$^+$CD45^{lo} and CD11b$^+$CD45^{hi} cell populations across all selected regions.

the cavity rather than a failure of monocytes to differentiate and replenish these cells. Both F4/80^{hi} and F4/80^{lo} populations of peritoneal macrophages are rapidly lost upon Ab-mediated neutralization of CSF1 (24), suggesting only partial blockade of CSF1R signaling occurred with the oral inhibitor used in this study. Higher levels of CSF1R signaling are generally required for proliferation than survival of macrophages (8) and hence the uniform inhibition of Ki67 expression observed across the peritoneal macrophage compartment is consistent with a reduction of high-level CSF1R-signaling by GW2580 treatment. In light of this, our data suggest the F4/80^{lo}CD11c$^-$ subset require a higher threshold of CSF1R signaling for survival and consequently exhibit greater CSF1R activity. Thus, different populations of peritoneal macrophages would appear to pursue distinct survival strategies. Short-lived cells are more reliant on high levels of CSF1 signaling, whereas long-lived cells are better adapted to efficiently use CSF1, possibly explaining the predominance of the latter under homeostatic CSF1-limited conditions (82). Either way, our data reveal fine-tuning of CSF1R activity but not necessarily *Csf1r* transgene or gene expression between distinct macrophage populations.

Relatively low, or absent, expression of the *Csf1r*-mApple reporter also provided a useful marker delineating peritoneal and pulmonary CCR2-independent cDC from CCR2-dependent CD11c$^{+/-}$MHCII$^+$ APC, likely of monocyte origin. Monocyte-derived CD11c$^+$ APC have also been described within the dermis, kidney, and gut (6, 21, 54, 83), in which tissue cDC also expressed lower levels of *Csf1r* (22). In the liver, MHCII$^+$ CD11c$^+$ cells were largely replenished by CCR2-independent BM precursors, uniformly expressed the candidate cDC marker CD26, and lacked the candidate macrophage marker CD64. Consistent with a cDC nature, these cells also uniformly express the transcription factor Zbtb46 (84). Nevertheless, these cells showed similar levels of *Csf1r*-mApple transgene expression to monocytes, and the CD11b$^+$ cDC2 fraction bound labeled CSF1-Fc. Although juvenile *Csf1r*$^{-/-}$ mice have normal numbers of hepatic cDC2 (14), unlike in other tissues, these cells also do not require CSF2 for survival (85), indicating possible redundancy between these growth factors. In adult mice the impact of *Csf1* and *Csf1r* mutations are more apparent (86) and anti-CSF1R treatment produced an almost complete depletion of liver cells expressing a *Csf1r*-EGFP transgene (87). Hence, in general, our data do not support an absolute division between Csf1r and Flt3-dependent APC populations. By analogy with the functional diversity of classical macrophages in different organs (51, 88–90), APC differentiation is likely also organ specific. Because CSF1 drives a largely immunoregulatory program (91), the responsiveness of cDC2 to CSF1 may underlie the relatively weak APC activity in liver (92) and contribute to a tolerogenic environment in the liver (93). Similarly, competition of CSF1R$^+$ cDC2 together with KC and classical patrolling monocytes (94) for available CSF1 could provide an explanation for the relative absence of hepatic monocyte-derived MHCII$^+$ APC.

In adult mice, labeling of cDC and macrophages in the Δ*Csf1r*-ECFP reporter is tissue specific (32). Using the Δ*Csf1r*-ECFP transgene, we highlighted the utility of the *Csf1r*-mApple strain to be crossed to existing reporter lines, visualizing distinct MPS populations in the lung and liver. Moreover, combined analysis of the *Csf1r*-mApple and Δ*Csf1r*-ECFP transgenes highlighted heterogeneity among microglia. Intriguingly, the percentages of Δ*Csf1r*-ECFP negative microglia correlated with the retention of microglia in the IL-34–knockout mouse in the same brain regions (95). Similarly, in other tissues, ECFP expression occurs predominantly in locations where macrophages are more reliant on IL-34 (for example, Langerhans cells) or CSF2 (alveolar macrophages). Hence, the graded expression of the Δ*Csf1r*-ECFP transgene in microglia may reflect its induction during differentiation or the proximity of individual cells to the tissue-specific factors that control its expression.

In overview, the *Csf1r*-mApple mouse recapitulates the expression profile of the widely used *Csf1r*-EGFP reporter. In combination with other reporters, and labeled CSF1, the *Csf1r*-mApple mouse provides a new tool to dissect the differentiation and function of the heterogeneous populations of mouse tissue mononuclear phagocytes and the homeostatic roles of CSF1. How different mononuclear phagocytes regulate CSF1R activity remains an important question given the continued interest in macrophages as possible vehicles for delivery of gene therapies and as targets of therapeutics.

Acknowledgments

We thank Miriam Abraham for help with genotyping the *Csf1r*-mApple mice, Judith Allen for critical review of the manuscript, and Marc Vendrell for advice on labeling of CSF1.

Disclosures

The authors have no financial conflicts of interest.

References

1. Guilliams, M., F. Ginhoux, C. Jakubzick, S. H. Naik, N. Onai, B. U. Schraml, E. Segura, R. Tussiwand, and S. Yona. 2014. Dendritic cells, monocytes and macrophages: a unified nomenclature based on ontogeny. *Nat. Rev. Immunol.* 14: 571–578.
2. Hume, D. A. 2006. The mononuclear phagocyte system. *Curr. Opin. Immunol.* 18: 49–53.
3. Jenkins, S. J., and D. A. Hume. 2014. Homeostasis in the mononuclear phagocyte system. *Trends Immunol.* 35: 358–367.
4. Lavin, Y., A. Mortha, A. Rahman, and M. Merad. 2015. Regulation of macrophage development and function in peripheral tissues. *Nat. Rev. Immunol.* 15: 731–744.
5. Okabe, Y., and R. Medzhitov. 2016. Tissue biology perspective on macrophages. *Nat. Immunol.* 17: 9–17.
6. Schraml, B. U., J. van Blijswijk, S. Zelenay, P. G. Whitney, A. Filby, S. E. Acton, N. C. Rogers, N. Moncaut, J. J. Carvajal, and C. Reis e Sousa. 2013. Genetic tracing via DNGR-1 expression history defines dendritic cells as a hematopoietic lineage. *Cell* 154: 843–858.
7. Liu, K., G. D. Victora, T. A. Schwickert, P. Guermonprez, M. M. Meredith, K. Yao, F. F. Chu, G. J. Randolph, A. Y. Rudensky, and M. Nussenzweig. 2009. In vivo analysis of dendritic cell development and homeostasis. *Science* 324: 392–397.
8. Tushinski, R. J., I. T. Oliver, L. J. Guilbert, P. W. Tynan, J. R. Warner, and E. R. Stanley. 1982. Survival of mononuclear phagocytes depends on a lineage-specific growth factor that the differentiated cells selectively destroy. *Cell* 28: 71–81.
9. Hume, D. A., P. Pavli, R. E. Donahue, and I. J. Fidler. 1988. The effect of human recombinant macrophage colony-stimulating factor (CSF-1) on the murine mononuclear phagocyte system in vivo. *J. Immunol.* 141: 3405–3409.
10. Stutchfield, B. M., D. J. Antoine, A. C. Mackinnon, D. J. Gow, C. C. Bain, C. A. Hawley, M. J. Hughes, B. Francis, D. Wojtacha, T. Y. Man, et al. 2015. CSF1 restores innate immunity after liver injury in mice and serum levels indicate outcomes of patients with acute liver failure. *Gastroenterology* 149: 1896–1909.e14.
11. Jenkins, S. J., D. Ruckerl, G. D. Thomas, J. P. Hewitson, S. Duncan, F. Brombacher, R. M. Maizels, D. A. Hume, and J. E. Allen. 2013. IL-4 directly signals tissue-resident macrophages to proliferate beyond homeostatic levels controlled by CSF-1. *J. Exp. Med.* 210: 2477–2491.
12. Gow, D. J., K. A. Sauter, C. Pridans, L. Moffat, A. Sehgal, B. M. Stutchfield, S. Raza, P. M. Beard, Y. T. Tsai, G. Bainbridge, et al. 2014. Characterisation of a novel Fc conjugate of macrophage colony-stimulating factor. *Mol. Ther.* 22: 1580–1592.
13. Waskow, C., K. Liu, G. Darrasse-Jèze, P. Guermonprez, F. Ginhoux, M. Merad, T. Shengelia, K. Yao, and M. Nussenzweig. 2008. The receptor tyrosine kinase Flt3 is required for dendritic cell development in peripheral lymphoid tissues. *Nat. Immunol.* 9: 676–683.
14. Ginhoux, F., K. Liu, J. Helft, M. Bogunovic, M. Greter, D. Hashimoto, J. Price, N. Yin, J. Bromberg, S. A. Lira, et al. 2009. The origin and development of nonlymphoid tissue CD103+ DCs. *J. Exp. Med.* 206: 3115–3130.
15. Schlitzer, A., N. McGovern, P. Teo, T. Zelante, K. Atarashi, D. Low, A. W. Ho, P. See, A. Shin, P. S. Wasan, et al. 2013. IRF4 transcription factor-dependent CD11b+ dendritic cells in human and mouse control mucosal IL-17 cytokine responses. *Immunity* 38: 970–983.
16. Onai, N., A. Obata-Onai, M. A. Schmid, T. Ohteki, D. Jarrossay, and M. G. Manz. 2007. Identification of clonogenic common Flt3+M-CSFR+ plasmacytoid and conventional dendritic cell progenitors in mouse bone marrow. *Nat. Immunol.* 8: 1207–1216.
17. Naik, S. H., P. Sathe, H. Y. Park, D. Metcalf, A. I. Proietto, A. Dakic, S. Carotta, M. O'Keeffe, M. Bahlo, A. Papenfuss, et al. 2007. Development of plasmacytoid and conventional dendritic cell subtypes from single precursor cells derived in vitro and in vivo. *Nat. Immunol.* 8: 1217–1226.
18. Mabbott, N. A., J. Kenneth Baillie, D. A. Hume, and T. C. Freeman. 2010. Meta-analysis of lineage-specific gene expression signatures in mouse leukocyte populations. *Immunobiology* 215: 724–736.
19. Hume, D. A. 2008. Differentiation and heterogeneity in the mononuclear phagocyte system. *Mucosal Immunol.* 1: 432–441.
20. Lohela, M., A. J. Casbon, A. Olow, L. Bonham, D. Branstetter, N. Weng, J. Smith, and Z. Werb. 2014. Intravital imaging reveals distinct responses of depleting dynamic tumor-associated macrophage and dendritic cell subpopulations. *Proc. Natl. Acad. Sci. USA* 111: E5086–E5095.
21. Tamoutounour, S., M. Guilliams, F. Montanana Sanchis, H. Liu, D. Terhorst, C. Malosse, E. Pollet, L. Ardouin, H. Luche, C. Sanchez, et al. 2013. Origins and functional specialization of macrophages and of conventional and monocyte-derived dendritic cells in mouse skin. *Immunity* 39: 925–938.
22. Cerovic, V., S. A. Houston, C. L. Scott, A. Aumeunier, U. Yrlid, A. M. Mowat, and S. W. Milling. 2013. Intestinal CD103(-) dendritic cells migrate in lymph and prime effector T cells. *Mucosal Immunol.* 6: 104–113.
23. Bain, C. C., C. A. Hawley, H. Garner, C. L. Scott, A. Schridde, N. J. Steers, M. Mack, A. Joshi, M. Guilliams, A. M. Mowat, et al. 2016. Long-lived self-renewing bone marrow-derived macrophages displace embryo-derived cells to inhabit adult serous cavities. *Nat. Commun.* 7: ncomms11852.
24. Louis, C., A. D. Cook, D. Lacey, A. J. Fleetwood, R. Vlahos, G. P. Anderson, and J. A. Hamilton. 2015. Specific contributions of CSF-1 and GM-CSF to the dynamics of the mononuclear phagocyte system. *J. Immunol.* 195: 134–144.
25. MacDonald, K. P., V. Rowe, H. M. Bofinger, R. Thomas, T. Sasmono, D. A. Hume, and G. R. Hill. 2005. The colony-stimulating factor 1 receptor is expressed on dendritic cells during differentiation and regulates their expansion. *J. Immunol.* 175: 1399–1405.
26. Sasmono, R. T., D. Oceandy, J. W. Pollard, W. Tong, P. Pavli, B. J. Wainwright, M. C. Ostrowski, S. R. Himes, and D. A. Hume. 2003. A macrophage colony-stimulating factor receptor-green fluorescent protein transgene is expressed throughout the mononuclear phagocyte system of the mouse. *Blood* 101: 1155–1163.
27. Deng, L., J. F. Zhou, R. S. Sellers, J. F. Li, A. V. Nguyen, Y. Wang, A. Orlofsky, Q. Liu, D. A. Hume, J. W. Pollard, et al. 2010. A novel mouse model of inflammatory bowel disease links mammalian target of rapamycin-dependent hyperproliferation of colonic epithelium to inflammation-associated tumorigenesis. *Am. J. Pathol.* 176: 952–967.
28. Qian, B. Z., J. Li, H. Zhang, T. Kitamura, J. Zhang, L. R. Campion, E. A. Kaiser, L. A. Snyder, and J. W. Pollard. 2011. CCL2 recruits inflammatory monocytes to facilitate breast-tumour metastasis. *Nature* 475: 222–225.
29. Schulz, C., E. Gomez Perdiguero, L. Chorro, H. Szabo-Rogers, N. Cagnard, K. Kierdorf, M. Prinz, B. Wu, S. E. Jacobsen, J. W. Pollard, et al. 2012. A lineage of myeloid cells independent of Myb and hematopoietic stem cells. *Science* 336: 86–90.
30. Jacquelin, S., F. Licata, K. Dorgham, P. Hermand, L. Poupel, E. Guyon, P. Deterre, D. A. Hume, C. Combadière, and A. Boissonnas. 2013. CX3CR1 reduces Ly6Chigh-monocyte motility within and release from the bone marrow after chemotherapy in mice. *Blood* 122: 674–683.
31. Rodero, M. P., L. Poupel, P. L. Loyher, P. Hamon, F. Licata, C. Pessel, D. A. Hume, C. Combadière, and A. Boissonnas. 2015. Immune surveillance of the lung by migrating tissue monocytes. *Elife* 4: e07847.
32. Sauter, K. A., C. Pridans, A. Sehgal, C. C. Bain, C. Scott, L. Moffat, R. Rojo, B. M. Stutchfield, C. L. Davies, D. S. Donaldson, et al. 2014. The MacBlue binary transgene (csf1r-gal4VP16/UAS-ECFP) provides a novel marker for visualisation of subsets of monocytes, macrophages and dendritic cells and responsiveness to CSF1 administration. *PLoS One* 9: e105429.
33. Saederup, N., A. E. Cardona, K. Croft, M. Mizutani, A. C. Cotleur, C. L. Tsou, R. M. Ransohoff, and I. F. Charo. 2010. Selective chemokine receptor usage by central nervous system myeloid cells in CCR2-red fluorescent protein knock-in mice. [Published erratum appears in 2017 *PLoS One* 12: e0176931.] *PLoS One* 5: e13693.
34. Balic, A., C. Garcia-Morales, L. Vervelde, H. Gilhooley, A. Sherman, V. Garceau, M. W. Gutowska, D. W. Burt, P. Kaiser, D. A. Hume, and H. M. Sang. 2014. Visualisation of chicken macrophages using transgenic reporter genes: insights into the development of the avian macrophage lineage. *Development* 141: 3255–3265.
35. Connelly, L., W. Barham, H. M. Onishko, L. Chen, T. P. Sherrill, T. Zabuawala, M. C. Ostrowski, T. S. Blackwell, and F. E. Yull. 2011. NF-kappaB activation within macrophages leads to an anti-tumor phenotype in a mammary tumor lung metastasis model. *Breast Cancer Res.* 13: R83.
36. Ovchinnikov, D. A., C. E. DeBats, D. P. Sester, M. J. Sweet, and D. A. Hume. 2010. A conserved distal segment of the mouse CSF-1 receptor promoter is required for maximal expression of a reporter gene in macrophages and osteoclasts of transgenic mice. *J. Leukoc. Biol.* 87: 815–822.
37. Boring, L., J. Gosling, S. W. Chensue, S. L. Kunkel, R. V. Farese, Jr., H. E. Broxmeyer, and I. F. Charo. 1997. Impaired monocyte migration and reduced type 1 (Th1) cytokine responses in C-C chemokine receptor 2 knockout mice. *J. Clin. Invest.* 100: 2552–2561.
38. Shaner, N. C., M. Z. Lin, M. R. McKeown, P. A. Steinbach, K. L. Hazelwood, M. W. Davidson, and R. Y. Tsien. 2008. Improving the photostability of bright monomeric orange and red fluorescent proteins. *Nat. Methods* 5: 545–551.
39. Garceau, V., A. Balic, C. Garcia-Morales, K. A. Sauter, M. J. McGrew, J. Smith, L. Vervelde, A. Sherman, T. E. Fuller, T. Oliphant, et al. 2015. The development and maintenance of the mononuclear phagocyte system of the chick is controlled by signals from the macrophage colony-stimulating factor receptor. *BMC Biol.* 13: 12.
40. Wyckoff, J. B., Y. Wang, E. Y. Lin, J. F. Li, S. Goswami, E. R. Stanley, J. E. Segall, J. W. Pollard, and J. Condeelis. 2007. Direct visualization of macrophage-assisted tumor cell intravasation in mammary tumors. *Cancer Res.* 67: 2649–2656.
41. Askew, K., K. Li, A. Olmos-Alonso, F. Garcia-Moreno, Y. Liang, P. Richardson, T. Tipton, M. A. Chapman, K. Riecken, S. Beccari, et al. 2017. Coupled proliferation and apoptosis Maintain the rapid turnover of microglia in the adult brain. *Cell Rep.* 18: 391–405.
42. Sierro, F., M. Evrard, S. Rizzetto, M. Melino, A. J. Mitchell, M. Florido, L. Beattie, S. B. Walters, S. S. Tay, B. Lu, et al. 2017. A liver capsular network of monocyte-derived macrophages restricts hepatic dissemination of intraperitoneal bacteria by neutrophil recruitment. *Immunity* 47: 374–388.e6.
43. Poché, R. A., C. W. Hsu, M. L. McElwee, A. R. Burns, and M. E. Dickinson. 2015. Macrophages engulf endothelial cell membrane particles preceding pupillary membrane capillary regression. *Dev. Biol.* 403: 30–42.
44. Muller, P. A., B. Koscsó, G. M. Rajani, K. Stevanovic, M. L. Berres, D. Hashimoto, A. Mortha, M. Leboeuf, X. M. Li, D. Mucida, et al. 2014. Crosstalk between muscularis macrophages and enteric neurons regulates gastrointestinal motility. [Published erratum appears in 2014 *Cell* 158: 1210.] *Cell* 158: 300–313.
45. Farro, G., M. Stakenborg, P. J. Gomez-Pinilla, E. Labeeuw, G. Goverse, M. D. Giovangiulio, N. Stakenborg, E. Meroni, F. D'Errico, Y. Elkrim, et al. 2017. CCR2-dependent monocyte-derived macrophages resolve inflammation and restore gut motility in postoperative ileus. *Gut* 66: 2098–2109.
46. Sasmono, R. T., A. Ehrnsperger, S. L. Cronau, T. Ravasi, R. Kandane, M. J. Hickey, A. D. Cook, S. R. Himes, J. A. Hamilton, and D. A. Hume. 2007. Mouse neutrophilic granulocytes express mRNA encoding the macrophage colony-stimulating factor receptor (CSF-1R) as well as many other macrophage-specific transcripts and can transdifferentiate into macrophages in vitro in response to CSF-1. *J. Leukoc. Biol.* 82: 111–123.
47. Ross, I. L., T. L. Dunn, X. Yue, S. Roy, C. J. Barnett, and D. A. Hume. 1994. Comparison of the expression and function of the transcription factor PU.1 (Spi-1

proto-oncogene) between murine macrophages and B lymphocytes. *Oncogene* 9: 121–132.
48. Cain, D. W., E. G. O'Koren, M. J. Kan, M. Womble, G. D. Sempowski, K. Hopper, M. D. Gunn, and G. Kelsoe. 2013. Identification of a tissue-specific, C/EBPβ-dependent pathway of differentiation for murine peritoneal macrophages. *J. Immunol.* 191: 4665–4675.
49. Liao, C. T., M. Rosas, L. C. Davies, P. J. Giles, V. J. Tyrrell, V. B. O'Donnell, N. Topley, I. R. Humphreys, D. J. Fraser, S. A. Jones, and P. R. Taylor. 2016. IL-10 differentially controls the infiltration of inflammatory macrophages and antigen-presenting cells during inflammation. *Eur. J. Immunol.* 46: 2222–2232.
50. Kim, K. W., J. W. Williams, Y. T. Wang, S. Ivanov, S. Gilfillan, M. Colonna, H. W. Virgin, E. L. Gautier, and G. J. Randolph. 2016. MHC II+ resident peritoneal and pleural macrophages rely on IRF4 for development from circulating monocytes. *J. Exp. Med.* 213: 1951–1959.
51. Immunological Genome Consortium. 2012. Gene-expression profiles and transcriptional regulatory pathways that underlie the identity and diversity of mouse tissue macrophages. *Nat. Immunol.* 13: 1118–1128.
52. Guilliams, M., I. De Kleer, S. Henri, S. Post, L. Vanhoutte, S. De Prijck, K. Deswarte, B. Malissen, H. Hammad, and B. N. Lambrecht. 2013. Alveolar macrophages develop from fetal monocytes that differentiate into long-lived cells in the first week of life via GM-CSF. *J. Exp. Med.* 210: 1977–1992.
53. Gibbings, S. L., S. M. Thomas, S. M. Atif, A. L. McCubbrey, A. N. Desch, T. Danhorn, S. M. Leach, D. L. Bratton, P. M. Henson, W. J. Janssen, and C. V. Jakubzick. 2017. Three unique interstitial macrophages in the murine lung at steady state. *Am. J. Respir. Cell Mol. Biol.* 57: 66–76.
54. Tamoutounour, S., S. Henri, H. Lelouard, B. de Bovis, C. de Haar, C. J. van der Woude, A. M. Woltman, Y. Reyal, D. Bonnet, D. Sichien, et al. 2012. CD64 distinguishes macrophages from dendritic cells in the gut and reveals the Th1-inducing role of mesenteric lymph node macrophages during colitis. *Eur. J. Immunol.* 42: 3150–3166.
55. Jenkins, S. J., D. Ruckerl, P. C. Cook, L. H. Jones, F. D. Finkelman, N. van Rooijen, A. S. MacDonald, and J. E. Allen. 2011. Local macrophage proliferation, rather than recruitment from the blood, is a signature of TH2 inflammation. *Science* 332: 1284–1288.
56. Murphy, J., R. Summer, A. A. Wilson, D. N. Kotton, and A. Fine. 2008. The prolonged life-span of alveolar macrophages. *Am. J. Respir. Cell Mol. Biol.* 38: 380–385.
57. Yona, S., K. W. Kim, Y. Wolf, A. Mildner, D. Varol, M. Breker, D. Strauss-Ayali, S. Viukov, M. Guilliams, A. Misharin, et al. 2013. Fate mapping reveals origins and dynamics of monocytes and tissue macrophages under homeostasis. [Published erratum appears in 2013 *Immunity* 38: 1073–1079.] *Immunity* 38: 79–91.
58. Jakubzick, C., F. Tacke, F. Ginhoux, A. J. Wagers, N. van Rooijen, M. Mack, M. Merad, and G. J. Randolph. 2008. Blood monocyte subsets differentially give rise to CD103+ and CD103- pulmonary dendritic cell populations. *J. Immunol.* 180: 3019–3027.
59. Perdiguero, E. G., and F. Geissmann. 2016. The development and maintenance of resident macrophages. *Nat. Immunol.* 17: 2–8.
60. Scott, C. L., F. Zheng, P. De Baetselier, L. Martens, Y. Saeys, S. De Prijck, S. Lippens, C. Abels, S. Schoonooghe, G. Raes, et al. 2016. Bone marrow-derived monocytes give rise to self-renewing and fully differentiated Kupffer cells. *Nat. Commun.* 7: 10321.
61. Guilliams, M., C. A. Dutertre, C. L. Scott, N. McGovern, D. Sichien, S. Chakarov, S. Van Gassen, J. Chen, M. Poidinger, S. De Prijck, et al. 2016. Unsupervised high-dimensional analysis aligns dendritic cells across tissues and species. *Immunity* 45: 669–684.
62. Hiasa, M., M. Abe, A. Nakano, A. Oda, H. Amou, S. Kido, K. Takeuchi, K. Kagawa, K. Yata, T. Hashimoto, et al. 2009. GM-CSF and IL-4 induce dendritic cell differentiation and disrupt osteoclastogenesis through M-CSF receptor shedding by up-regulation of TNF-alpha converting enzyme (TACE). *Blood* 114: 4517–4526.
63. Sester, D. P., S. J. Beasley, M. J. Sweet, L. F. Fowles, S. L. Cronau, K. J. Stacey, and D. A. Hume. 1999. Bacterial/CpG DNA down-modulates colony stimulating factor-1 receptor surface expression on murine bone marrow-derived macrophages with concomitant growth arrest and factor-independent survival. *J. Immunol.* 163: 6541–6550.
64. Sauter, K. A., L. A. Waddell, Z. M. Lisowski, R. Young, L. Lefevre, G. M. Davis, S. M. Clohisey, M. McCulloch, E. Magowan, N. A. Mabbott, et al. 2016. Macrophage colony-stimulating factor (CSF1) controls monocyte production and maturation and the steady-state size of the liver in pigs. *Am. J. Physiol. Gastrointest. Liver Physiol.* 311: G533–G547.
65. Pridans, C., G. M. Davis, K. A. Sauter, Z. M. Lisowski, Y. Corripio-Miyar, A. Raper, L. Lefevre, R. Young, M. E. McCulloch, S. Lillico, et al. 2016. A Csf1r-EGFP transgene provides a novel marker for monocyte subsets in sheep. *J. Immunol.* 197: 2297–2305.
66. Fend, L., N. Accart, J. Kintz, S. Cochin, C. Reymann, F. Le Pogam, J. B. Marchand, T. Menguy, P. Slos, R. Rooke, et al. 2013. Therapeutic effects of anti-CD115 monoclonal antibody in mouse cancer models through dual inhibition of tumor-associated macrophages and osteoclasts. *PLoS One* 8: e73310.
67. Jakubzick, C., E. L. Gautier, S. L. Gibbings, D. K. Sojka, A. Schlitzer, T. E. Johnson, S. Ivanov, Q. Duan, S. Bala, T. Condon, et al. 2013. Minimal differentiation of classical monocytes as they survey steady-state tissues and transport antigen to lymph nodes. *Immunity* 39: 599–610.
68. Bartocci, A., D. S. Mastrogiannis, G. Migliorati, R. J. Stockert, A. W. Wolkoff, and E. R. Stanley. 1987. Macrophages specifically regulate the concentration of their own growth factor in the circulation. *Proc. Natl. Acad. Sci. USA* 84: 6179–6183.
69. Lenzo, J. C., A. L. Turner, A. D. Cook, R. Vlahos, G. P. Anderson, E. C. Reynolds, and J. A. Hamilton. 2012. Control of macrophage lineage populations by CSF-1 receptor and GM-CSF in homeostasis and inflammation. *Immunol. Cell Biol.* 90: 429–440.
70. Swirski, F. K., M. Nahrendorf, M. Etzrodt, M. Wildgruber, V. Cortez-Retamozo, P. Panizzi, J. L. Figueiredo, R. H. Kohler, A. Chudnovskiy, P. Waterman, et al. 2009. Identification of splenic reservoir monocytes and their deployment to inflammatory sites. *Science* 325: 612–616.
71. Conway, J. G., B. McDonald, J. Parham, B. Keith, D. W. Rusnak, E. Shaw, M. Jansen, P. Lin, A. Payne, R. M. Crosby, et al. 2005. Inhibition of colony-stimulating-factor-1 signaling in vivo with the orally bioavailable cFMS kinase inhibitor GW2580. *Proc. Natl. Acad. Sci. USA* 102: 16078–16083.
72. Yipp, B. G., J. H. Kim, R. Lima, L. D. Zbytnuik, B. Petri, N. Swanlund, M. Ho, V. G. Szeto, T. Tak, L. Koenderman, et al. 2017. The lung is a host defense niche for immediate neutrophil-mediated vascular protection. *Sci. Immunol.* 2: eaam8929.
73. Grabert, K., T. Michoel, M. H. Karavolos, S. Clohisey, J. K. Baillie, M. P. Stevens, T. C. Freeman, K. M. Summers, and B. W. McColl. 2016. Microglial brain region-dependent diversity and selective regional sensitivities to aging. *Nat. Neurosci.* 19: 504–516.
74. Goldmann, T., P. Wieghofer, M. J. Jordão, F. Prutek, N. Hagemeyer, K. Frenzel, L. Amann, O. Staszewski, K. Kierdorf, M. Krueger, et al. 2016. Origin, fate and dynamics of macrophages at central nervous system interfaces. *Nat. Immunol.* 17: 797–805.
75. Hume, D. A. 2011. Applications of myeloid-specific promoters in transgenic mice support in vivo imaging and functional genomics but do not support the concept of distinct macrophage and dendritic cell lineages or roles in immunity. *J. Leukoc. Biol.* 89: 525–538.
76. Yipp, B. G., and P. Kubes. 2013. Antibodies against neutrophil LY6G do not inhibit leukocyte recruitment in mice in vivo. *Blood* 121: 241–242.
77. Hasenberg, A., M. Hasenberg, L. Männ, F. Neumann, L. Borkenstein, M. Stecher, A. Kraus, D. R. Engel, A. Klingberg, P. Seddigh, et al. 2015. Catchup: a mouse model for imaging-based tracking and modulation of neutrophil granulocytes. *Nat. Methods* 12: 445–452.
78. Mooney, J. E., B. E. Rolfe, G. W. Osborne, D. P. Sester, N. van Rooijen, G. R. Campbell, D. A. Hume, and J. H. Campbell. 2010. Cellular plasticity of inflammatory myeloid cells in the peritoneal foreign body response. *Am. J. Pathol.* 176: 369–380.
79. Hume, D. A., and S. Gordon. 1984. The correlation between plasminogen activator activity and thymidine incorporation in mouse bone marrow-derived macrophages. Opposing actions of colony-stimulating factor, phorbol myristate acetate, dexamethasone and prostaglandin E. *Exp. Cell Res.* 150: 347–355.
80. Shibata, Y., Z. Zsengeller, K. Otake, N. Palaniyar, and B. C. Trapnell. 2001. Alveolar macrophage deficiency in osteopetrotic mice deficient in macrophage colony-stimulating factor is spontaneously corrected with age and associated with matrix metalloproteinase expression and emphysema. *Blood* 98: 2845–2852.
81. Hashimoto, D., A. Chow, C. Noizat, P. Teo, M. B. Beasley, M. Leboeuf, C. D. Becker, P. See, J. Price, D. Lucas, et al. 2013. Tissue-resident macrophages self-maintain locally throughout adult life with minimal contribution from circulating monocytes. *Immunity* 38: 792–804.
82. Ghosn, E. E., A. A. Cassado, G. R. Govoni, T. Fukuhara, Y. Yang, D. M. Monack, K. R. Bortoluci, S. R. Almeida, L. A. Herzenberg, and L. A. Herzenberg. 2010. Two physically, functionally, and developmentally distinct peritoneal macrophage subsets. *Proc. Natl. Acad. Sci. USA* 107: 2568–2573.
83. Bain, C. C., A. Bravo-Blas, C. L. Scott, E. G. Perdiguero, F. Geissmann, S. Henri, B. Malissen, L. C. Osborne, D. Artis, and A. M. Mowat. 2014. Constant replenishment from circulating monocytes maintains the macrophage pool in the intestine of adult mice. *Nat. Immunol.* 15: 929–937.
84. Meredith, M. M., K. Liu, G. Darrasse-Jeze, A. O. Kamphorst, H. A. Schreiber, P. Guermonprez, J. Idoyaga, C. Cheong, K. H. Yao, R. E. Niec, and M. C. Nussenzweig. 2012. Expression of the zinc finger transcription factor zDC (Zbtb46, Btbd4) defines the classical dendritic cell lineage. *J. Exp. Med.* 209: 1153–1165.
85. Greter, M., J. Helft, A. Chow, D. Hashimoto, A. Mortha, J. Agudo-Cantero, M. Bogunovic, E. L. Gautier, J. Miller, M. Leboeuf, et al. 2012. GM-CSF controls nonlymphoid tissue dendritic cell homeostasis but is dispensable for the differentiation of inflammatory dendritic cells. *Immunity* 36: 1031–1046.
86. Dai, X. M., G. R. Ryan, A. J. Hapel, M. G. Dominguez, R. G. Russell, S. Kapp, V. Sylvestre, and E. R. Stanley. 2002. Targeted disruption of the mouse colony-stimulating factor 1 receptor gene results in osteopetrosis, mononuclear phagocyte deficiency, increased primitive progenitor cell frequencies, and reproductive defects. *Blood* 99: 111–120.
87. MacDonald, K. P., J. S. Palmer, S. Cronau, E. Seppanen, S. Olver, N. C. Raffelt, R. Kuns, A. R. Pettit, A. Clouston, B. Wainwright, et al. 2010. An antibody against the colony-stimulating factor 1 receptor depletes the resident subset of monocytes and tissue- and tumor-associated macrophages but does not inhibit inflammation. *Blood* 116: 3955–3963.
88. Mass, E., I. Ballesteros, M. Farlik, F. Halbritter, P. Günther, L. Crozet, C. E. Jacome-Galarza, K. Händler, J. Klughammer, Y. Kobayashi, et al. 2016. Specification of tissue-resident macrophages during organogenesis. *Science* 353: aaf4238.
89. Lavin, Y., D. Winter, R. Blecher-Gonen, E. David, H. Keren-Shaul, M. Merad, S. Jung, and I. Amit. 2014. Tissue-resident macrophage enhancer landscapes are shaped by the local microenvironment. *Cell* 159: 1312–1326.
90. Gosselin, D., V. M. Link, C. E. Romanoski, G. J. Fonseca, D. Z. Eichenfield, N. J. Spann, J. D. Stender, H. B. Chun, H. Garner, F. Geissmann, and

C. K. Glass. 2014. Environment drives selection and function of enhancers controlling tissue-specific macrophage identities. *Cell* 159: 1327–1340.
91. Verreck, F. A., T. de Boer, D. M. Langenberg, M. A. Hoeve, M. Kramer, E. Vaisberg, R. Kastelein, A. Kolk, R. de Waal-Malefyt, and T. H. Ottenhoff. 2004. Human IL-23-producing type 1 macrophages promote but IL-10-producing type 2 macrophages subvert immunity to (myco)bacteria. *Proc. Natl. Acad. Sci. USA* 101: 4560–4565.
92. Pillarisetty, V. G., A. B. Shah, G. Miller, J. I. Bleier, and R. P. DeMatteo. 2004. Liver dendritic cells are less immunogenic than spleen dendritic cells because of differences in subtype composition. *J. Immunol.* 172: 1009–1017.
93. Ju, C., and F. Tacke. 2016. Hepatic macrophages in homeostasis and liver diseases: from pathogenesis to novel therapeutic strategies. *Cell. Mol. Immunol.* 13: 316–327.
94. Dal-Secco, D., J. Wang, Z. Zeng, E. Kolaczkowska, C. H. Wong, B. Petri, R. M. Ransohoff, I. F. Charo, C. N. Jenne, and P. Kubes. 2015. A dynamic spectrum of monocytes arising from the in situ reprogramming of CCR2+ monocytes at a site of sterile injury. *J. Exp. Med.* 212: 447–456.
95. Wang, Y., K. J. Szretter, W. Vermi, S. Gilfillan, C. Rossini, M. Cella, A. D. Barrow, M. S. Diamond, and M. Colonna. 2012. IL-34 is a tissue-restricted ligand of CSF1R required for the development of Langerhans cells and microglia. *Nat. Immunol.* 13: 753–760.

4.2 Discussion

In this collaborative study, a new transgenic fluorescent reporter mouse line, the *Csf1r*-mApple mouse, was generated. Using this line, I compared mApple expression across multiple tissues, revealing mature macrophages to express the highest levels of the transgene. A combination of mApple expression, expression of additional markers and bone marrow- and CCR2-dependence in chimeras allowed clear definition of myeloid cell subsets present in the liver, revealing the mixed identity of the F4/80^{lo}CD11b^{hi} population. Analysis of CSF1-Fc^{AF647} uptake revealed that monocytes, KC and cDC2 bind CSF1 in the liver, with KC binding the most on a per cell basis than any other cell across all tissues analysed.

As has been shown previously with *Csf1r*-EGFP (MacGreen) mice (Sasmono et al. 2003), the *Csf1r*-mApple transgene was expressed across macrophages and monocytes, but also in neutrophils, eosinophils and a proportion of B cells. However, in the latter 3 cell types, mApple expression did not equate to functional uptake of CSF1-Fc^{AF647}. Thus either the CSF1R protein is not functional in these cell types, or it is not expressed altogether; indeed neutrophils have been shown previously to produce CFS1R mRNA but not protein (Sasmono et al. 2007). In the blood and peritoneal cavity, where it is possible in our hands to detect CSF1R (CD115) expression by flow cytometry using an α-CD115 antibody, CSF1R staining was detectable on monocytes and macrophages, but not neutrophils, eosinophils or B cells. mApple expression in these cell type may thus be a relic of expression of the CSF1R in upstream precursor cells, since granulocyte-monocyte progenitors (GMPs) constitutively express the CFS1R (Endele et al. 2017).

Monocytes, dendritic cells and macrophages could broadly be distinguished across tissues by their level of mApple expression. In particular, the level of mApple expression correlated to macrophage maturation status in the peritoneal cavity, with long-lived F4/80^{hi} resMϕ expressing higher levels than the more short-lived F4/80^{lo} macrophages (Bain et al. 2016) and Ly6C^{hi} monocytes expressing lower levels still. Characterisation of the populations in the liver was particularly pertinent to the rest of my project, and to the wider field, since the F4/80^{lo}CD11b^{hi} population in the liver had been labelled a macrophage population by several other groups (Schulz et al. 2012; Yona et al. 2013). In the study by Yona and colleagues, immunofluorescent imaging of CX3CR1^{gfp} mice revealed the perivascular location of these cells (Yona et al. 2013), although this did not prove their macrophage identity since monocytes (Auffray et al. 2007) and DCs (David et al. 2016) also express CX3CR1, nor did GFP

expression account for the entire F4/80^{lo}CD11b^{hi} population. Whilst KC were uniformly very bright for mApple transgene expression, there was no evidence for a secondary macrophage population with intensity greater than monocytes as observed in the peritoneal cavity. Dissection of the F4/80^{lo}CD11b^{hi} gate revealed a heterogeneous population which could be split into at least 3 populations of the basis of Ly6C and MHCII expression. Further analysis of expression of the macrophage marker CD64 (Tamoutounour et al. 2012; Gautier et al. 2012), CD11c, and the dendritic cell marker CD26 (Guilliams et al. 2016), along with bone marrow- and CCR2-depedence allowed us to define Ly6C^{hi} monocytes and cDC2s within the F4/80^{lo} population. The F4/80^{lo}CD11b^{hi} gate also contained a Ly6C^{-}MHCII^{-} population which were likely Ly6C^{lo} monocytes, although additional positive markers for this population would be required to ensure that this was not a mixed population. Ly6C^{hi} monocytes in the liver displayed a different CD26 and CD11c expression profile to blood monocytes suggesting these had been actively recruited to the liver and were not simply blood monocyte contaminates present due to inefficient perfusion of the livers. This was in keeping with the suggestion that CCR2^{+}Ly6C^{hi} monocytes patrol the liver sinusoids (Dal-Secco et al. 2015), rather than Ly6C^{lo} monocytes which are reported to patrol the vasculature in other anatomical sites (Auffray et al. 2007). Interestingly, cDC2, cDC1 and pDC (defined by their PDCA1 expression) also expressed mApple to almost equivalent levels as Ly6C^{hi} monocytes, in contrast to the much more limited expression of transgene found in cDC2 and cDC1 in the peritoneal cavity and lung.

While conventional flow cytometric analysis of CSF1R (CD115) protein expression using α-CD115 antibodies was possible on blood and peritoneal cavity cells, we were not able to get any satisfactory CSF1R staining in the liver (data not shown). A combination of CSF1 bioavailability along with the number of CSF1R-expressing cells in a tissue, and the number of CSF1R molecules on the surface of each cell affects the level of signalling achieved by each cell. Thus the total uptake of CSF1 is likely a better measure of CSF1R activity than CSF1R expression alone. Signalling through the CSF1R generally results in internalisation of the CSF1R-CSF1 complex, followed by its incorporation into lysosomes and degradation of both ligand and receptor (Stanley and Chitu 2014). Using radioactive Iodine-labelled CSF1 (^{125}I-CSF1) it was shown that 6 out of 7 binding events of CSF1 to CSF1R result in internalisation of the complex rather than dissociation and release of the ligand back into the media by bone marrow derived macrophages (Guilberts and Stanley 1986). Furthermore, degradation of ligand was found not to begin until after 10 minutes after uptake. Thus, the intensity of AF647

detected in my assays likely reflects close to total CSF1-Fc uptake over 10 minutes *in vivo*. Transgene expression by cDC2 was reflected in their ability to capture CSF1-Fc^{AF647}, but this did not hold true for cDC1 or pDC, indicating that of the DCs, only cDC2 actively compete for CSF1 in the liver. In keeping with their ability to efficiently clear CSF1 (Bartocci et al. 1987), KC bound the most CSF1-Fc^{AF647} on a per cell basis than any other cell in the liver or lung, and 10 times as much CSF1-Fc^{AF647} as either Ly6C^{hi} or Ly6C^{lo} macrophages in the liver. Hence it is possible that monocytes arriving and patrolling in the liver under homeostatic conditions may simply not receive sufficient signalling through the CSF1R to facilitate differentiation, survival or proliferation. Indeed, a lack of monocyte differentiation due to CSF1 'starvation' might provide an explanation for why no second population of macrophages could be identified in the liver. In contrast, direct injection of CSF1^{AF647} into the peritoneal cavity revealed that F4/80^{lo} monocyte-derived peritoneal macrophages (also known as small peritoneal macrophages) seemed to rapidly increase in their ability to capture CSF1 above that of the mature resident F4/80^{hi} macrophages, potentially explaining why they survive in this site. Therefore in the next chapter I will explore whether CSF1 availability is a limiting factor in the differentiation and survival of recruited monocytes into long-lived, mature resident KC, and whether exogenous administration of CSF1-Fc can therefore affect the origin of the resident KC population, and compare this with peritoneal cavity macrophages.

Chapter 5: Role of CSF1 in maintenance of KC population and conversion of monocytes to KC

5.1 Introduction

The development of a robust method to isolate and study macrophages in the liver, along with a more detailed understanding of their CSF1R expression, and CSF1 uptake enabled me to begin investigating the role of CSF1 in maintaining KC population size and origin, and whether CSF1 is a limiting factor in the conversion of monocytes in to KC. At the start of the project, recent studies had shown that primitive macrophages from the yolk sac, together with varying contributions from foetal monocyte-derived macrophages from the foetal liver went on to seed resident macrophage populations in all embryonic tissues (Schulz et al. 2012b; Hoeffel et al. 2012; Ginhoux et al. 2010; Hoeffel et al. 2015; Gomez Perdiguero et al. 2015; Epelman et al. 2014a; Bain et al. 2014). The survival of resident macrophages of embryonic origin in adult mice is highly tissue-dependent. For example, macrophages in the intestine are continually replaced by adult monocyte-derived cells (Bain et al. 2014), whilst the murine brain is colonized almost exclusively by yolk-sac derived macrophages during the earliest stage of foetal development, and this lineage is maintained independently of adult monocytes post-birth through local self-renewal (Ginhoux et al. 2010; Ajami et al. 2007, 2011; Schulz et al. 2012b). The survival and maintenance of the embryonic lineage of KC had been less well studied. A key initial study using parabiosis and genetic labelling of progenitor cells found that resident macrophages across multiple tissues including the lung, peritoneum and spleen did not require significant adult monocyte contribution, but unfortunately the liver was not included in this work (Hashimoto et al. 2013). Other groups had shown only minimal contribution of YFP-labelled CX3CR1^{+} monocytes to the KC population in adult mice using a tamoxifen inducible system (Yona et al. 2013). Consistent with this, it had been reported that there was no deficit in the number of KC in *Ccr2*$^{-/-}$ mice, which due to defective egress from the bone marrow have a 10-fold reduction in circulating monocytes (Bain et al. 2014; Serbina and Pamer 2006). These studies provided some initial evidence that KC do not require any major contribution from adult monocytes in mice, though they were limited in that they only looked in young adult mice. I therefore set out initially to further establish

whether there is any requirement for monocyte replenishment of liver KC, taking age into account.

I then turned to explore what factors might control the KC niche, and thus what regulates the size and origin of the KC population. CSF1 availability has been postulated previously as a possible limiting factor in the control of the tissue macrophage niche (Jenkins and Hume 2014), and CSF1 has long been studied as a key regulator of macrophage differentiation and survival. The *op/op* mouse, which has a natural mutation in the coding region of the CSF1 gene, has provided an invaluable tool for the study of CSF1 biology (Yoshida et al. 1990). Using this system, it has been formally demonstrated that whilst KC are initially independent of CSF1, they become highly dependent from 2 weeks of age (Cecchini et al. 1994), and there is a clear deficit in resident macrophage numbers in many tissues in *op/op* mice, including liver KC and F4/80^{hi} resMϕ in the peritoneal cavity (Wiktor-Jedrzejczak et al. 1982).

CSF1 can be expressed in multiple forms, either presented on the surface of cells which synthesize it, or it can be secreted and transported through the circulation as a proteoglycan (Price et al. 1992; Cecchini et al. 1994), and different tissue macrophage populations appear to differ in their dependence for the excreted versus the cell surface form. Through exogenous administration of murine CSF1 (Cecchini et al. 1994; Yamamoto et al. 2008), or transgenic expression of CSF1 (Ryan et al. 2001) in *op/op* mice it has been shown that some tissue macrophage populations, including liver Kupffer Cells, can be fully restored, indicating that their survival is dependent on the circulating form of CSF1, whilst the density of tissue macrophages in other tissues including the peritoneal cavity was not restored, implicating local presentation of CSF1 for their survival. More recently, a study in which the cell surface form, but not the circulating form of CSF1 was restored in 3 month old *op/op* mice led to only incomplete recovery of liver Kupffer Cell density, again implicating circulating CSF1 as crucial for maintaining population size (Dai et al. 2004).

A study in which trace amounts of radiolabelled CSF1 was injected into mice showed that the majority of the circulating CSF1 is cleared in the liver, specifically by Kupffer Cells (Bartocci et al. 1987). Furthermore, both peritoneal macrophages *ex vivo* and more importantly, Kupffer Cells *in vivo* have both been shown to degrade radiolabelled CSF1 through CSF1R-mediated internalization and lysosomal degradation (Stanley et al. 1983; Bartocci et al. 1987), thus directly breaking down their own growth factor, in a negative feedback loop which may be critical for the control of overall population size.

CSF1 signals to macrophages through the CSF1 receptor (CSF1R) and mice in which the *csf1r* gene has been knocked out also displayed reduced macrophage numbers in multiple tissues including the peritoneal cavity and the liver (Dai et al. 2002). Equally, antibody blockade of the CSF1R led to depletion of resident macrophages in many tissues including in the liver (MacDonald et al. 2010), whilst administration of an anti-CSF1 antibody confirmed that CSF1 is key for the regulation of peritoneal resMϕ proliferation in both inflammation and steady state (Davies et al. 2013). Our own study using *cfs1r*-mApple transgenic mice (chapter 4; Hawley et al. 2018) demonstrated that KC express much higher levels of the CSF1R than circulating monocytes in the blood, and exogenous administration of a fluorescently labelled CSF1-Fc conjugate showed that this translated into a significant difference in uptake of circulating CSF1, with KC able to bind more CSF1 than monocytes. Although a direct role for CSF1 in monocyte differentiation and maturation is less clear, I hypothesized that monocytes may not mature into KC in the steady state due to the limited availability of CSF1 that results from the efficient clearance of this growth factor by KC. I therefore set out to explore whether administration of exogenous CSF1-Fc (Gow et al. 2014), which has a longer half-life (between 12 and 24 hours) (Gow et al. 2014) than CSF1 (around 1.6 hours) due to its recycling via the neonatal Fc receptor (FcRn) (Roopenian and Akilesh 2007; Sockolosky et al. 2012), would drive monocyte survival and differentiation into mature macrophages, thereby allowing them to engraft and replace the endogenous KC.

Proliferation is thought to contribute to the maintenance of the KC population in steady state, as low but detectable basal levels of cells in S-Phase can be detected in naïve adult mice (Jenkins et al. 2011; Crofton et al. 1978). Furthermore, exogenous administration of CSF1-Fc has been shown previously to increase proliferation and numbers of liver macrophages (Gow et al. 2014). Basal proliferation can be detected in many resident macrophage populations. In the heart, however, progressive influx of blood monocyte-derived macrophages post birth parallels the loss of proliferation and the subsequent loss of the embryonic-derived macrophage population (Molawi et al. 2014). These observations led the authors to hypothesise that replenishment from the BM may occur due to exhaustion of the embryonic cells. Thus, I also set out to determine whether the autonomy of the KC population could be broken by driving exhaustion of the incumbent cells, and whether this might ultimately lead to replenishment through monocyte recruitment.

Finally, it also remains unclear whether all KC have an equal ability to proliferate. In the skin, it has been suggested using multicolour fate mapping and imaging techniques that

Langerhans cells do not proliferate equally (Ghigo et al. 2013), implying the presence of local tissue progenitors and hence a hierarchy. In contrast, proliferation of alveolar macrophages is reported to occur stochastically following infection (Hashimoto et al. 2013). Hierarchical proliferation of haematopoietic stem cells has been formally demonstrated in the bone marrow by looking at rate of loss of fluorescence in genetically labelled, histone 2B-GFP^{+} cells (Foudi et al. 2009). In this model, slowly dividing stem cells retained the fluorescent label for over a year whilst the label was more quickly diluted in their rapidly dividing daughter cells, in a process hypothesized to protect the genomic integrity of the stem cell.

In this chapter I aimed to investigate parameters that control KC autonomy under steady state conditions. Specifically, does the mechanism for maintenance of KC change over time with respect to proliferation versus monocyte recruitment? How does bioavailability of CSF1 affect KC population size, proliferative capacity and monocyte to macrophage conversion? And finally can all KC proliferate equally or is there any evidence of quiescent KC progenitor cells present in the liver?

5.2 KC maintain autonomy in aged *Ccr2*$^{-/-}$ mice despite decline in proliferation with age

Kupffer Cells have been shown to proliferate in the steady state (Edwards and Klein 1961; Wisse 1974; Jenkins et al. 2011), and self-renewal is thought to be an important mechanism through which they maintain population size independently of monocyte recruitment. However, studies assessing proliferation have focused only on young adult mice or rats. We therefore assessed KC proliferation in C57BL/6 mice aged up to 33 weeks. Mice were injected with the thymidine analogue BrdU 2 hours before necropsy in order to assess the proportion of the population in S phase. Leukocytes in the liver were identified following the gating strategy established in chapter 3, with the exception of CD31, as these experiments were conducted before its utility in removing contaminating endothelial cells had been established. There was a 50% decrease in the proportion of the KC population that was BrdU^{+} between 11 and 33 weeks of age, which appeared to plateau between 25 and 33 weeks (fig. 5.1A), suggesting that KC proliferation in the steady state may wane over time. This plateau coincided with a plateau in liver weight gain, measured in a separate experiment with similarly aged mice (fig. 5.1B). A decline in proliferation of the F4/80^{hi} resMϕ in the peritoneal cavity was also observed, suggesting this may be a more wide-spread phenomenon (fig. 5.1C;

see chapter 4 for peritoneal cavity gating strategy). It must be noted that the overall levels of proliferation recorded in the liver were particularly low compared to steady state observations in the rest of this study, and may be because it was carried out before the liver protocol was fully optimized.

Although limited studies in young mice had suggested relative autonomy of KC from circulating adult monocytes, we hypothesized that the possible decline in proliferative potential with age might represent exhaustion of the incumbent population, leading to increased requirement for monocyte input into the population. To examine this possibility, I first looked at the effect of prolonged monocytopenia by aging *Ccr2*$^{-/-}$ mice to one year. There was around a 10-fold reduction in the frequency of circulating Ly6C^{hi} monocytes (see chapter 4 for blood gating strategy) compared to C57BL/6 WT controls (fig. 5.2A). Equally, there was a large and significant reduction in the total number of Ly6C^{hi} monocytes that could be recovered from the liver (fig. 5.2B). However, there was no difference in KC number between WT and *Ccr2*$^{-/-}$ mice (fig. 5.2C), in keeping with the notion that the KC population can self-renew independently of monocytes derived from circulation. I also looked at maintenance of the F4/80^{hi} resMϕ population in the peritoneal cavity which showed around 5% non-host chimerism after 5 months of parabiosis (Hashimoto et al. 2013). Interestingly, here there was a slight deficit in the size of the total F4/80^{hi} resMϕ in *Ccr2*$^{-/-}$ mice compared to WT at one year of age (fig. 5.2D). Alongside the aged *Ccr2*$^{-/-}$ experiments, and as part of a wider study within the lab, tissue-protected bone marrow chimeras were used to fate map the contribution of circulating adult monocytes to resident macrophage populations in multiple tissues over time. CD45.1^{+}CD45.2^{+} host mice were irradiated from the hips down and were reconstituted with CD45.2^{+} bone marrow giving around 20-30% chimerism in Ly6C^{hi} monocytes in blood. This showed that F4/80^{hi} resMϕ in the peritoneal cavity were gradually replaced by monocyte-derived macrophages over time, whilst liver KC were relatively autonomous with only a small and non-significant increase in chimerism from 7% to 10% between 8 and 33 weeks of age (Bain et al. 2016). Thus, despite the reduction in the proliferation rate in the KC population with age, our *Ccr2*$^{-/-}$ and aged chimera experiments supported the idea that KC retain autonomy from monocytes, even with age.

5.3 CSF1-Fc causes conversion of circulating bone marrow cells into highly proliferative F4/80^{hi} KC-like cells.

Given this relative autonomy of KC in the steady state, I explored whether CSF1 bioavailability could be a potential limiting factor in the conversion of monocytes to resident KC. It was shown previously that exogenous CSF1-Fc administration led to the recruitment of Ly6C^{hi} monocytes in the peritoneal cavity (Jenkins et al. 2013), and CSF1R blockade led to reduced recruitment and conversion of Ly6C^{hi} monocytes into macrophages in the myometrium of pregnant mice (Tagliani et al. 2011). Thus elevated bioavailability of CSF1 can cause increased monocyte recruitment, and we hypothesized that surplus CSF1 might allow these recruited monocytes to mature and contribute to the resident KC population. In an initial pilot experiment, female, tissue-protected bone marrow chimeric mice were given 2 doses of CSF1-Fc at day -2 and day 0 (fig. 5.3A). The livers were harvested at day 2 and weighed. This showed that CSF1-Fc treatment led to increased liver weight (fig. 5.3B) and increased liver:body weight ratio (fig. 5.3C), as previously described (Gow et al. 2014). CSF1-Fc treatment did not overtly affect the phenotype of immune cells in the liver by any of the markers we had measured (fig. 5.4A), but it led to a general increase in the total number of KC, monocytes, neutrophils, eosinophils and lymphocytes per gram of liver compared with PBS control injections (fig. 5.4B). Hence, CSF1-Fc appeared to affect not only monocytes and macrophages, but leukocytes of multiple lineages, through either direct or indirect mechanisms.

Consistent with previous observations (Gow et al. 2014), treatment with CSF1-Fc stimulated elevated proliferation of F4/80^{hi}CD11b^{lo} KC cells in the liver, as determined by a 2 hour BrdU pulse before necropsy. Approximately 13% of KC were double positive for BrdU along with the cell cycle marker Ki67 with CSF1-Fc treatment, compared to just 1% of the population in the PBS treated control group (fig. 5.5A). Proliferation of the F4/80^{lo}CD11b^{hi} bulk population has been reported previously in response to CSF1-Fc treatment (Stutchfield et al. 2015). However, in contrast we found that CSF1-Fc did not increase proliferation of the Ly6C^{hi} monocytes that comprise the majority of these cells (fig. 5.5B) indicating that CSF1-Fc did not stimulate proliferation in all cells of myeloid origin at least with the dose and delivery regime used here.

To examine whether this increased rate of proliferation in the F4/80^{hi}CD11b^{lo} KC population fully accounted for the expansion in the size of the population following CSF1-Fc treatment

or whether generation of new BM-derived KC had occurred, donor bone marrow chimerism was assessed. In the blood, the overall level of chimerism was comparable between groups prior to treatment (fig. 5.6A) with around 20-30% of circulating Ly6C^{hi} monocytes of donor origin. The chimerism of the Ly6C^{hi} monocytes in the liver normalized to the total chimerism of Ly6C^{hi} monocytes in the blood was 100% in both groups (fig. 5.6B). This was as expected given that monocytes in tissues are considered recently derived from the blood, and should therefore show maximal levels of chimerism. In PBS treated control mice, KC were predominantly of tissue origin revealed by <2% normalized chimerism (fig. 5.6C). In contrast, CSF1-Fc treatment led to around 15% of the KC population having originated from the bone marrow (fig. 5.6C). Intriguingly, a greater proportion of the donor KC population were proliferating following CSF1-Fc treatment (fig. 5.6D). Hence, treatment with CSF1-Fc stimulated both proliferation and accumulation of endogenous tissue-derived KC and conversion of bone-marrow derived cells into a highly proliferative population that bore the crude F4/80^{hi}CD11b^{lo} hallmarks of KC.

5.4 Tim4 expression differentiates donor and host F4/80^{hi}CD11b^{lo} KC

Until this point, KC were defined solely on their CD45^{+}F4/80^{hi}CD11b^{lo} expression profile. Tim4 is a phosphatidyl serine receptor which is highly expressed by resident KC according to microarray data available from the Immunological Genome Project (Heng et al. 2008; www.immgen.org). We therefore looked at Tim4 expression in order to gauge how faithfully the donor bone marrow-derived KC acquired other phenotypic markers typical of resident KC. Whilst the majority of the host KC expressed very high levels of Tim4, the donor cells uniformly expressed only low levels of Tim4 in both PBS and CSF1-FC-treated mice, although they still appeared dimly positive for this marker when compared to the FMO control (fig. 5.6E). Given that these donor cells did not fully recapitulate the expression pattern of the host KC, they will be referred to as KC-like cells for the rest of the chapter.

5.5 The emergence of recruited KC-like cells is transient

The appearance of donor-derived F4/80^{hi}CD11b^{lo} KC-like cells following treatment with CSF1-Fc prompted me to assess the long-term survival of these newly arrived cells. To do so, tissue protected BM chimeric mice were treated with PBS or CSF1-Fc twice as before, and a group

of mice was left for 2, 8 or 14 days after the final treatment respectively (fig. 5.7A). CSF1-Fc treatment again drove increased numbers of leukocytes without affecting their basic phenotype (fig. 5.7B). The increased number of KC seen at day 2 post treatment with CSF1-Fc remained elevated by 8 days, but returned to normal by 14 days (fig. 5.7C), suggesting a period of substantial contraction of the population between 8 and 14 days. Consistent with this, the enhanced levels of proliferation of KC detected at 2 days post final treatment was followed by a complete cessation of proliferation at 8 days before restoration of the basal rate at 14 days (fig. 5.7D). The total number of Ly6C^{hi} monocytes in the liver was significantly increased at day 2, but returned to normal by day 8 (fig. 5.7E). The elevated frequency of bone marrow-derived KC-like cells evident at day 2, again revealed by ~20% normalized non-host chimerism, was transient, as the chimerism returned to the basal levels seen in PBS-treated control mice by day 14 (fig. 5.7F). This indicated that the enhanced rate of proliferation of the donor KC compared to host KC (fig. 5.6D), did not convey a survival advantage, and the autonomy of the embryonic-derived KC population was maintained, with the transient KC-like cells being lost, presumably through death or migration from the liver.

To determine if recruitment of bone marrow derived KC-like cells was a feature unique to CSF1 or shared by other macrophage mitogens, an additional group of mice was given two doses of IL-4 in the form of IL-4 complex (IL-4c). IL-4c treatment drove reduced CD11b expression in KC as has been seen previously (Jenkins et al. 2011), but the population was still clearly identifiable (fig. 5.7B). IL-4c has been shown previously to induce accumulation of resident peritoneal macrophages through proliferation with an absence of recruitment of inflammatory monocytes (Jenkins et al. 2011), and in this same study KC were also shown to proliferate in response to IL-4c treatment. In my IL-4c treated group, I was able to replicate this elevated proliferation and accumulation of KC (fig. 5.7C & 5.7D). In keeping with the published results in the peritoneal cavity, there was no elevated recruitment of Ly6C^{hi} monocytes (fig. 5.7E), and no contribution of recruited cells to the liver KC population with IL-4c treatment, as there was no significant change in the level of chimerism compared to the PBS vehicle control group at day 2 (fig 5.7F). This demonstrated that although IL-4c and CSF1-Fc both caused an increase in the total number of KC, the kinetics through which this was achieved was different.

5.6 CSF1-Fc does not induce differentiation of BM-derived cells to resident macrophages in the peritoneal cavity

To determine if CSF1-Fc administration could also drive transient recruitment of resident-like macrophages in other tissues, cells were washed from the peritoneal cavity in the time course experiments. There was no change in the level of chimerism of the F4/80^{hi} resMϕ population with either IL-4c or CSF1-Fc treatment (fig. 5.8A), despite induction of proliferation and accumulation of macrophages at day 2 in both sexes (fig. 5.8B & 5.8C) Thus, it appears that exogenous CSF1-Fc is not sufficient to drive conversion of bone-marrow cells to a resident macrophage phenotype in the peritoneal cavity.

5.7 Repetitive CSF1-Fc treatment recruits BM-derived KC-like cells without causing exhaustion of endogenous KC

My data indicated that liver KC persist autonomously from circulating Ly6C^{hi} monocytes in steady state and remained autonomous following an acute high dose of exogenous CSF1-Fc despite recruitment of KC-like monocyte-derived macrophages to the liver. However, in light of our data which suggested that KC proliferation may wane with age, I hypothesized that multiple rounds of expansion of the population through proliferation followed by contraction might exhaust the endogenous KC and cause replenishment by monocyte-derived macrophages recruited from circulation.

Given that CSF1-Fc is a porcine fusion protein, it was possible that its repeated administration may provoke a neutralising antibody immune response in mice. Therefore, I first trialled the delivery schedule in which CSF1-Fc was given twice two days apart, then mice were allowed to recover for 12 days before the process was repeated a further 2 times with two mice per group. The efficacy of CSF1-Fc was assessed two days after each round of administration (1x, 2x and 3x on fig. 5.9A). The fold-change in liver:body weight ratio over each animal's starting weight increased with each subsequent treatment (fig. 5.9B) and the number of KC was elevated after each round of treatment (fig. 5.9C). The level of proliferation in KC was also elevated after each round of CSF1-Fc (fig. 5.9D), and when this was expressed as fold change over the PBS control at each time point it appeared that there was no decline in the level of proliferation induced (fig. 5.9E). Together, these results demonstrated that CSF1-Fc retained its efficacy even after the third round of administration.

I then gave partial chimeric mice 3 rounds of CSF1-Fc treatment and assessed livers at day 2 and day 14 after the final injection (fig. 5.10A). Again, CSF1-Fc caused an increase in liver weight at day 2 compared with PBS controls, which returned to the level of the control group at day 14 (fig. 5.10B). The CSF1-Fc caused a robust increase in proliferation within the KC compartment at day 2 (fig. 5.10C), correlating with the large increase in the total number of KC (fig. 5.10D) of a similar magnitude to the increase seen after only one round of treatment previously (fig. 5.4B & 5.7C) and which returned to baseline by day 14 (fig. 5.10D). Finally, I assessed the chimerism in the KC compartment. Two days after the third and final round of CSF1-Fc, the chimerism was just over 30% when normalized to the chimerism in the blood (fig. 5.10E), which was higher than the total chimerism seen with only a single round of CSF1-Fc treatment before (fig. 5.6C & 5.7F). After 14 days, unlike with a single round of treatment, chimerism had not returned to baseline levels (fig. 5.10E), and approximately 20% of the donor cells had acquired the KC marker Tim4 (data not shown) suggesting that at least some recruited cells had fully matured into KC at this time point. However, given that the level of chimerism underwent a significant reduction between day 2 and 14 after the final treatment, it was not possible to say whether the recruited KC would engraft permanently.

Unfortunately, the length of these experiments, the time constraints of my PhD, and the need to focus on other aspects of my PhD project, meant it was not possible to repeat this experiment with a longer chase period to address this issue. However, analysis of proliferation of donor and host-derived KC revealed that although the newly recruited donor KC-like cells proliferated more than their host-derived counterparts both at day 2 and day 14, the host-derived cells still exhibited significant levels of proliferation (fig. 5.10F). After accounting for the levels of chimerism in the total KC population, the proliferation rate that could be attributed to the endogenous KC 2 days following the final dose of CSF1-Fc was 5.9% in the acute and 6.5% in the chronic experimental systems. Thus, even when the frequency of monocyte-derived cells within the host population is accounted for, it would appear that the incumbent tissue-derived KC exhibit similar levels of proliferation in response to repeated delivery of exogenous CSF1-Fc as observed after a single dose. Hence it would appear that recruitment of BM-derived KC does not occur as a consequence of exhaustion of the endogenous cells.

5.8 Search for progenitor cells in liver using CSF1-Fc and IL-4c with H2B-GFP mice

My data suggested that resident, embryonic-derived host KC were able to self-maintain, despite the transient appearance of monocyte-derived F4/80^{hi}CD11b^{lo} KC-like cells. Even after multiple doses of CSF1-Fc over several weeks, the endogenous KC were able to continue to proliferate, and were largely not replaced by monocyte-derived donor cells. To determine whether proliferation of KC was random or hierarchical, possibly including a quiescent progenitor-like KC population, I used mice which express a doxycycline-inducible histone 2B – GFP fusion protein (Foudi et al. 2009) that becomes stably incorporated into chromatin during the labelling period, but which is lost after removal of doxycycline as cells proliferate during a subsequent chase period (fig. 5.11A). Two weeks on doxycycline chow gave uniform, bright labelling of Ly6C^{hi} monocytes in the blood (fig. 5.11B). I therefore put mice on doxycycline chow for two weeks before giving two doses of CSF1-Fc, IL-4c or PBS and assessing loss of GFP within the KC population two days later (fig. 5.11C).

As a surrogate method to identify cells in S phase, I arbitrarily gated only on those with very high levels of Ki67 expression. Both CSF1-Fc and IL-4c gave robust increases in proliferation rate in this system (fig. 5.12A), confirming that neither mouse strain nor doxycycline treatment affected the normal response to these macrophage mitogens. The geometric mean fluorescence intensity of GFP expressed by Ly6C^{hi} monocytes in the blood was lower with both IL-4c and CSF1-Fc than the PBS-injected vehicle control mice (fig. 5.12B). There was also an enhanced rate of loss of GFP in the KC treated with either IL-4c or CSF1-Fc (fig. 5.12B & 5.12C) in accordance with the elevated level of proliferation induced. However, the flow plots and histograms showed that there was no evidence of a 'peak' of label retaining cells with any treatment (fig. 5.12C). Thus I found no evidence for any quiescent sub-population of KC, rather most KC appeared to proliferate in response to mitogens.

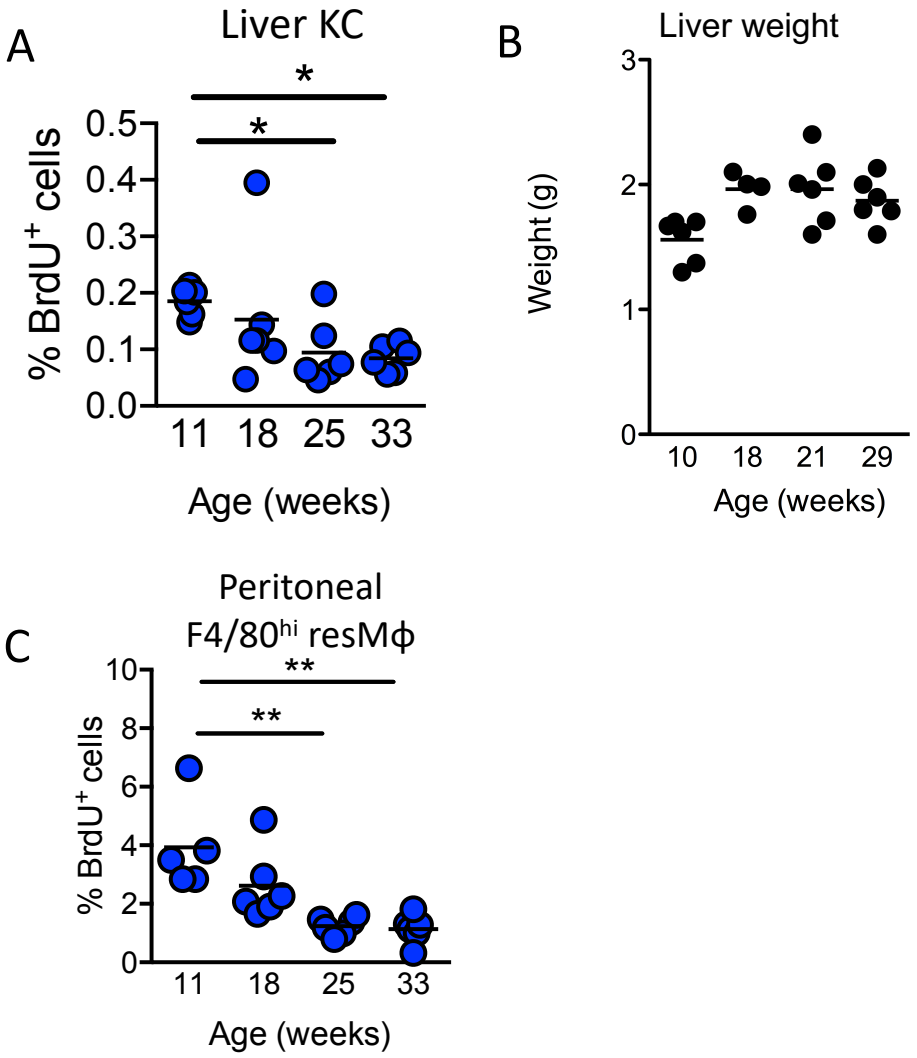

Figure 5.1 Proliferation of KC wanes with age. (A) Proportion of KC and **(C)** F4/80^{hi} resident peritoneal cavity macrophages which were BrdU^{+} after a 2-hour pulse in 11, 18, 25 and 33 week old C57BL/6 mice. n=6 per group pooled from two experiments. **(B)** Liver weights of 10, 18, 21 and 29 week old mice where n=4-6 per group pooled from two separate experiments. Significance determined by one-way ANOVA where *p<0.05, **p<0.01. Data acquired in collaboration with C. Bain and analysed by C. Bain.

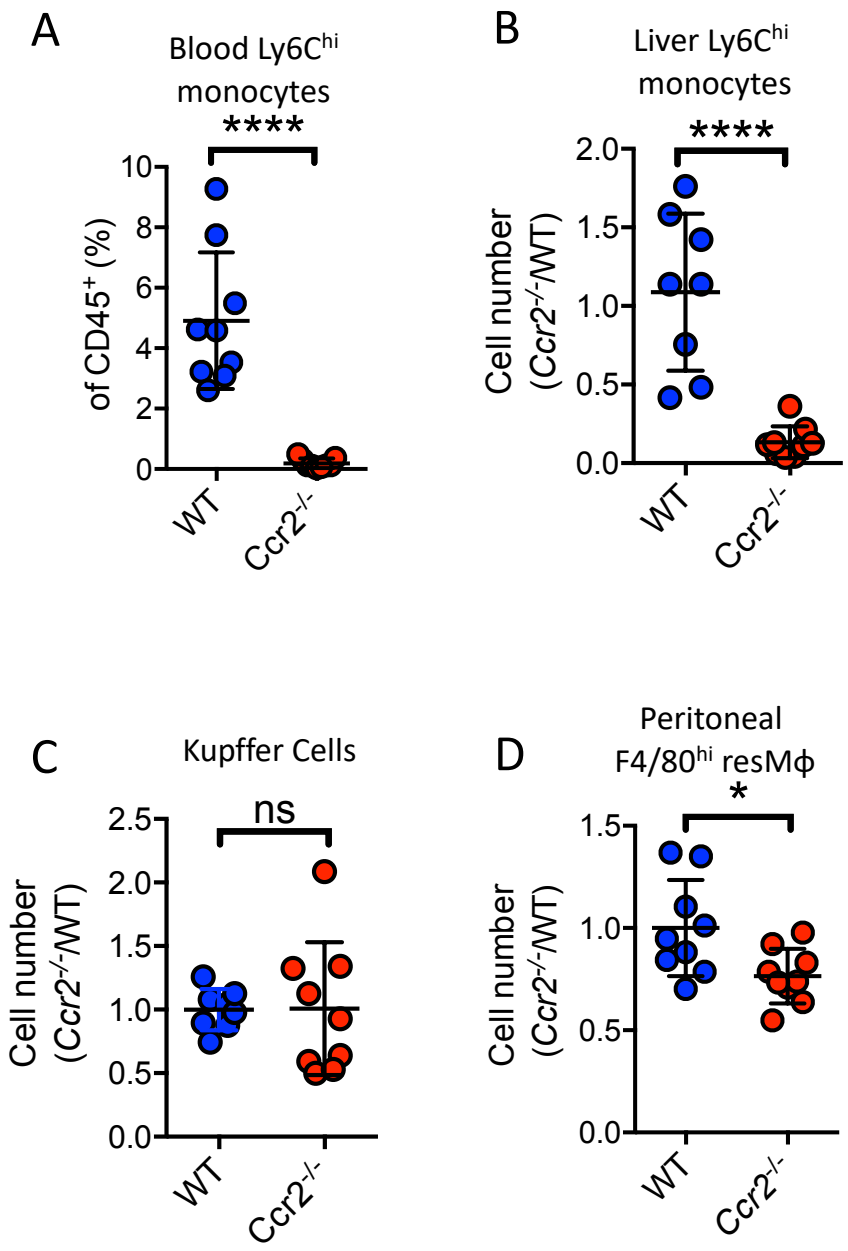

Figure 5.2 Maintenance of resident macrophage populations in year old *Ccr2*$^{-/-}$ mice. (A) Frequency of Ly6C^{hi} monocytes in blood as a proportion of total CD45^{+} population in year old male C57BL/6 (WT) and *Ccr2*$^{-/-}$ mice. **(B)** Total number of Ly6C^{hi} monocytes, **(C)** total number of KC in the in liver and **(D)** total number of F4/80^{hi} resident peritoneal macrophages in male WT and *Ccr2*$^{-/-}$ mice expressed as a ratio to the mean value in WT mice (*Ccr2*$^{-/-}$/WT). n=9 pooled from 3 independent experiments. Significance determined by determined by t-test where * p<0.05, **** p<0.0001.

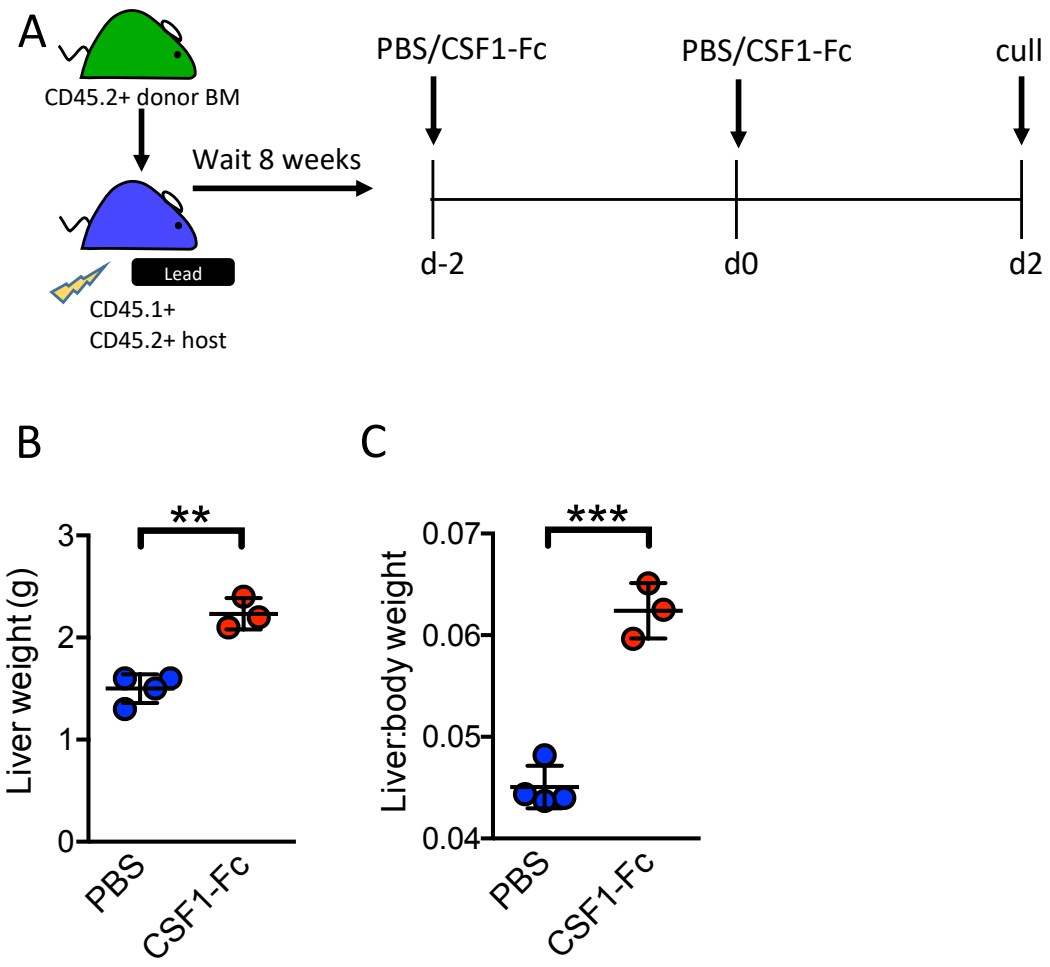

Figure 5.3 Exogenous CSF1-Fc administration causes increased liver weight. (A) Male CD45.1^{+} CD45.2^{+} host mice were irradiated with the upper body shielded by lead then reconstituted with bone marrow from CD45.2^{+} donor mice. Mice were left for 8 weeks before s.c. injection with CSF1-Fc or PBS vehicle control at day -2 and day 0, and mice were culled on day 2. **(B)** Total liver weight and **(C)** Liver:body weight ratio n=4 (PBS) or 3 (CSF1-Fc) from 1 experiment. Significance determined by t-test where ** p<0.01 ***p<0.001.

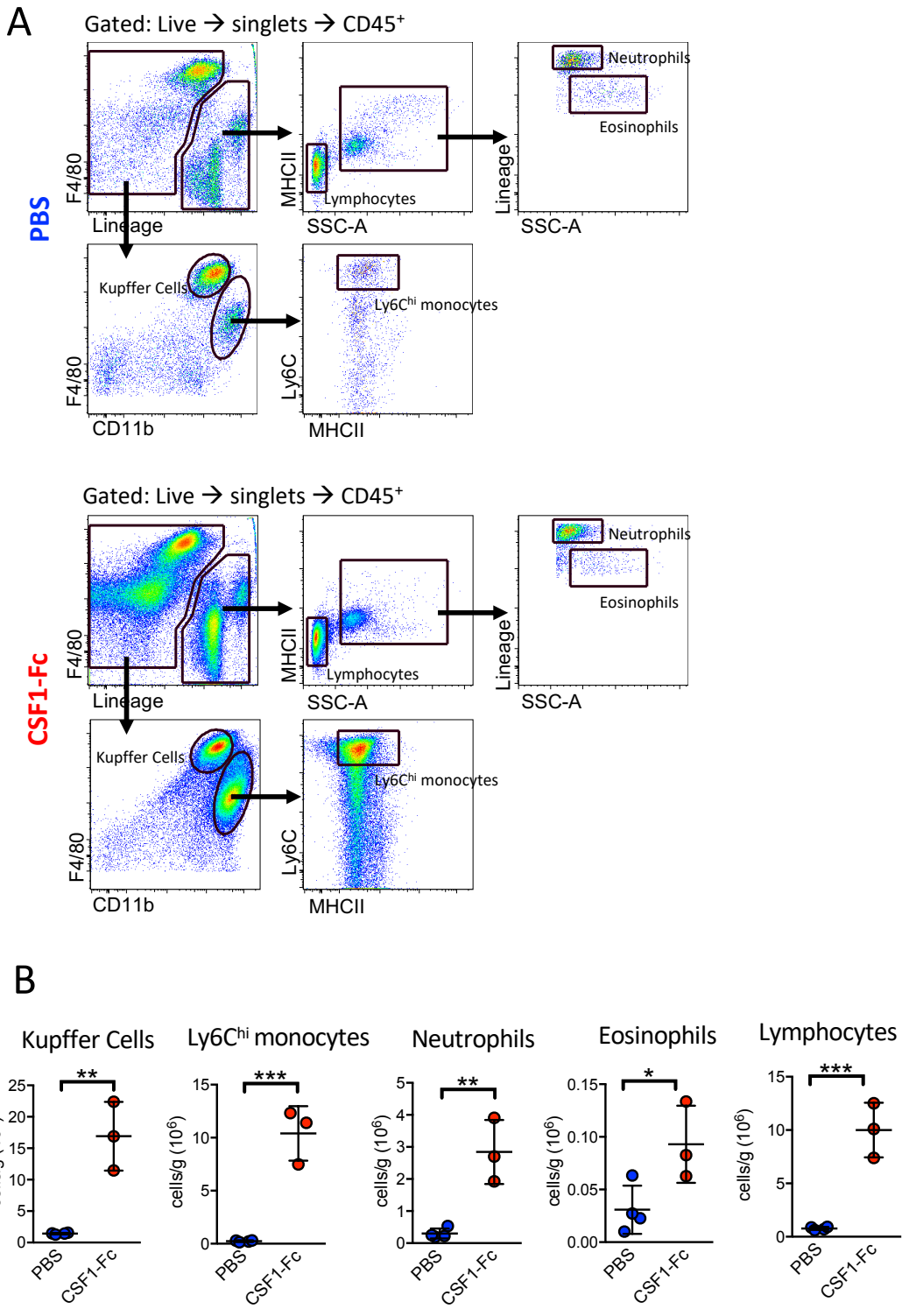

Figure 5.4 Increase in liver leukocyte numbers following exogenous CSF1-Fc administration. (A) Gating strategy to identify leukocyte populations in the liver with representative plots from PBS and CSF1-Fc treated animals. **(B)** Total number of Kupffer Cells, Ly6C^{hi} monocytes, neutrophils, eosinophils and lymphocytes per gram of liver tissue with PBS and CSF1-Fc treatment. Significance determined by t-test where *p<0.05, **p<0.01, ***p<0.001, ***p<0.0001. From same experiment as figure 5.3

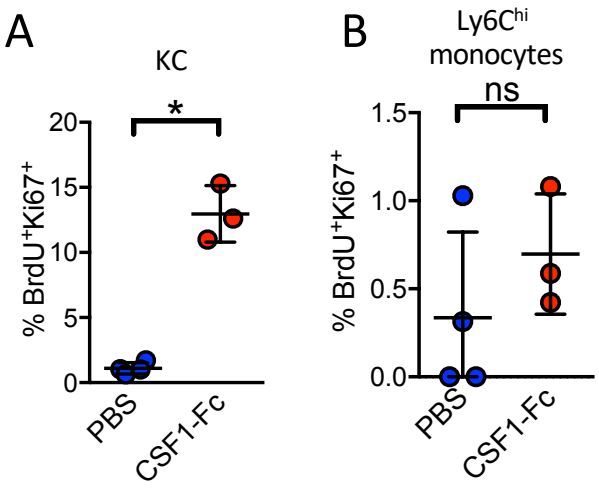

Figure 5.5 Enhanced proliferation of KC following exogenous CSF1-Fc administration. (A) Proportion of Kupffer Cells and **(B)** Ly6C^{hi} liver monocytes which were BrdU^{+}Ki67^{+} double positive 2 hours following BrdU pulse (1mg). Significance determined by t-test where ***p<0.01, ***p<0.001. From same experiment as figure 5.3.

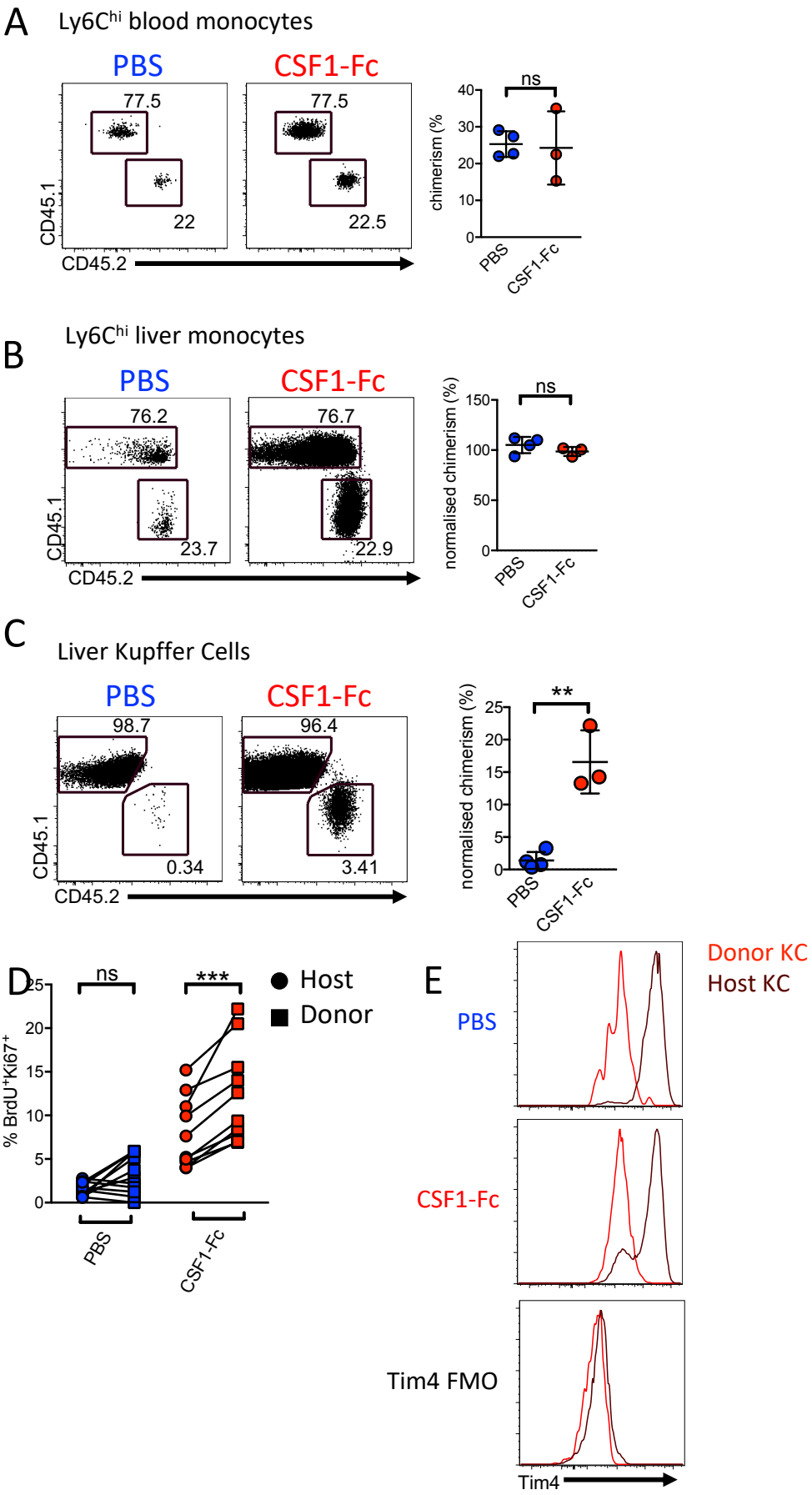
A
Ly6C^hi blood monocytes
PBS
CSF1-Fc
77.5
77.5
22
22.5
CD45.1
CD45.2
ns
chimerism (%
PBS
CSF1-Fc
B
Ly6C^hi liver monocytes
PBS
CSF1-Fc
76.2
76.7
23.7
22.9
CD45.1
CD45.2
ns
normalised chimerism (%)
PBS
CSF1-Fc
C
Liver Kupffer Cells
PBS
CSF1-Fc
98.7
96.4
0.34
3.41
CD45.1
CD45.2
**
normalised chimerism (%)
PBS
CSF1-Fc
D
ns
***
Host
Donor
% BrdU+Ki67+
PBS
CSF1-Fc
E
Donor KC
Host KC
PBS
CSF1-Fc
Tim4 FMO
Tim4

Figure 5.6 Exogenous CSF1-Fc administration leads to chimerism in KC population with donor cells with a high proliferation rate. (A) Representative flow plots of non-host chimerism and replicate data of absolute chimerism (% $CD45.2^{+}$) in $Ly6C^{hi}$ monocytes circulating in blood with PBS and CSF1-Fc treatment. **(B)** Representative flow plots of non-host chimerism and replicate data of chimerism in $Ly6C^{hi}$ monocytes in liver normalized to $Ly6C^{hi}$ monocytes in blood and **(C)** as in (B) but for Kupffer Cells. **(D)** Proportion of donor (squares) versus host (circles) derived KC which were $BrdU^{+}Ki67^{+}$ double positive after PBS or CSF1-Fc treatment. **(E)** Representative histograms for Tim4 expression by donor KC (red) and host KC (brown) and Tim4 FMO control. Significance determined by t-tests either unpaired (A-C) or paired (D) where **P<0.01, ***p<0.001. (A-C, E from same experiment as figure 5.3). (D) n=10 per group pooled from 3 independent experiments.

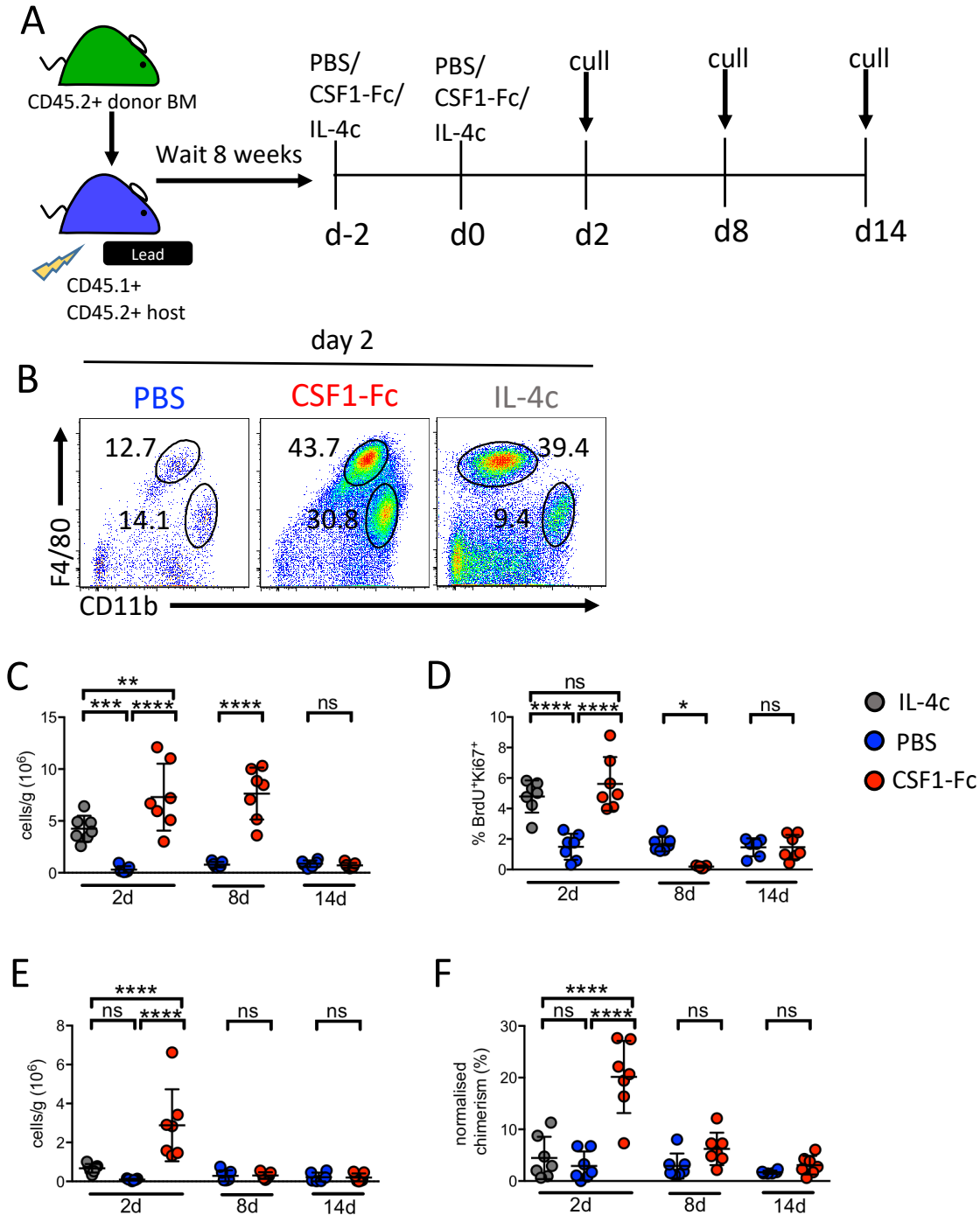

Figure 5.7 Chimerism in KC population is transient following exogenous CSF1-Fc administration. (A) CD45.1^{+}CD45.2^{+} host mice (male and female) were irradiated with the upper body shielded by lead then reconstituted with bone marrow from CD45.2^{+} donor mice. Mice were left for 8 weeks before being injected s.c. twice with PBS, CSF1-Fc or IL-4c and were culled on day 2, 8 or 14 following the second dose. **(B)** Representative flow plots of F4/80 versus CD11b for each treatment at day 2. **(C)** Number of KC per gram of liver tissue, **(D)** proportion of KC which were BrdU^{+}Ki67^{+} double positive, **(E)** number of Ly6C^{hi} monocytes per gram of liver and **(F)** normalized non-host chimerism in the KC population at each time point. One repeat of the day 2 timepoint of (F) has been published in Stutchfield *et al.* 2015. Significance determined by one-way ANOVA compared to the PBS control for each time point where *p<0.05, ***p<0.001, ***p<0.0001. n=7 per group pooled from 2 experiments.

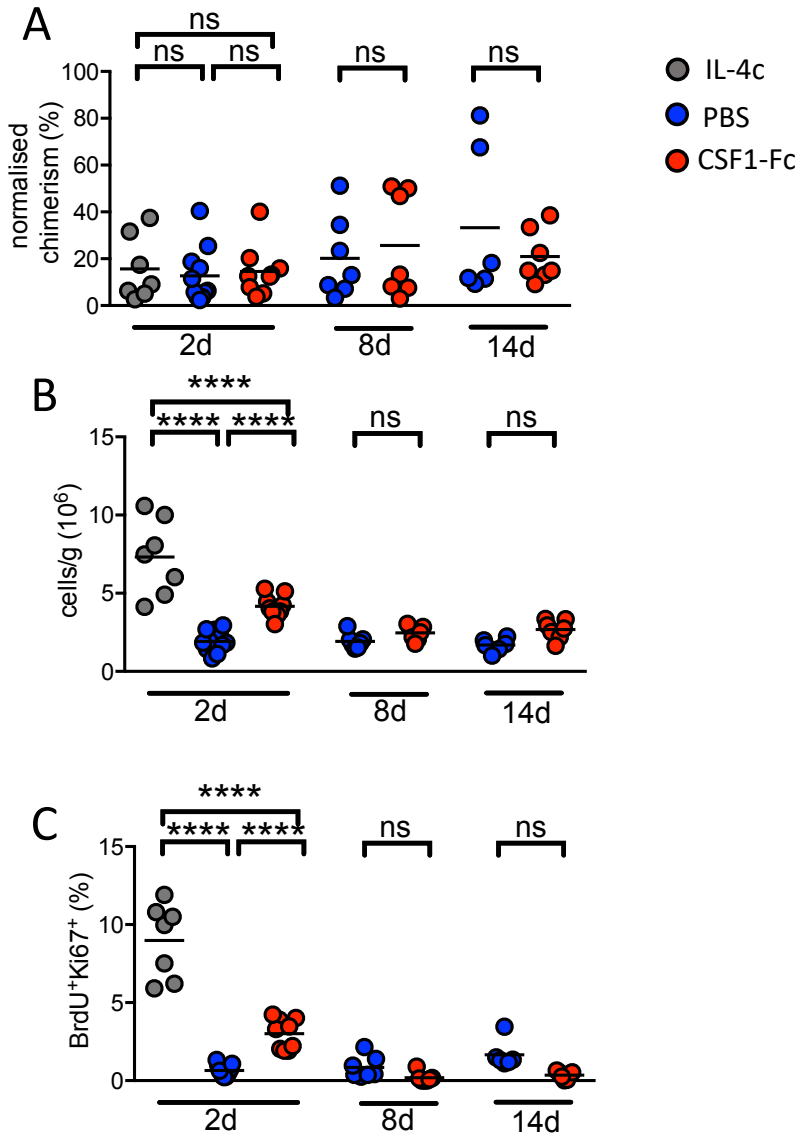

Figure 5.8 Effect of sub-cutaneous CSF1-Fc administration on peritoneal F4/80^{hi} resMϕ. (A) Total number, **(B)** proliferation and **(C)** normalized non-host chimerism in the peritoneal F4/80^{hi} resMϕ population at each time point. n=6-11 per group pooled from 3 experiments. Significance determined by one-way ANOVA compared to the PBS control for each time point where *p<0.05, ***p<0.001, ****P<0.0001.

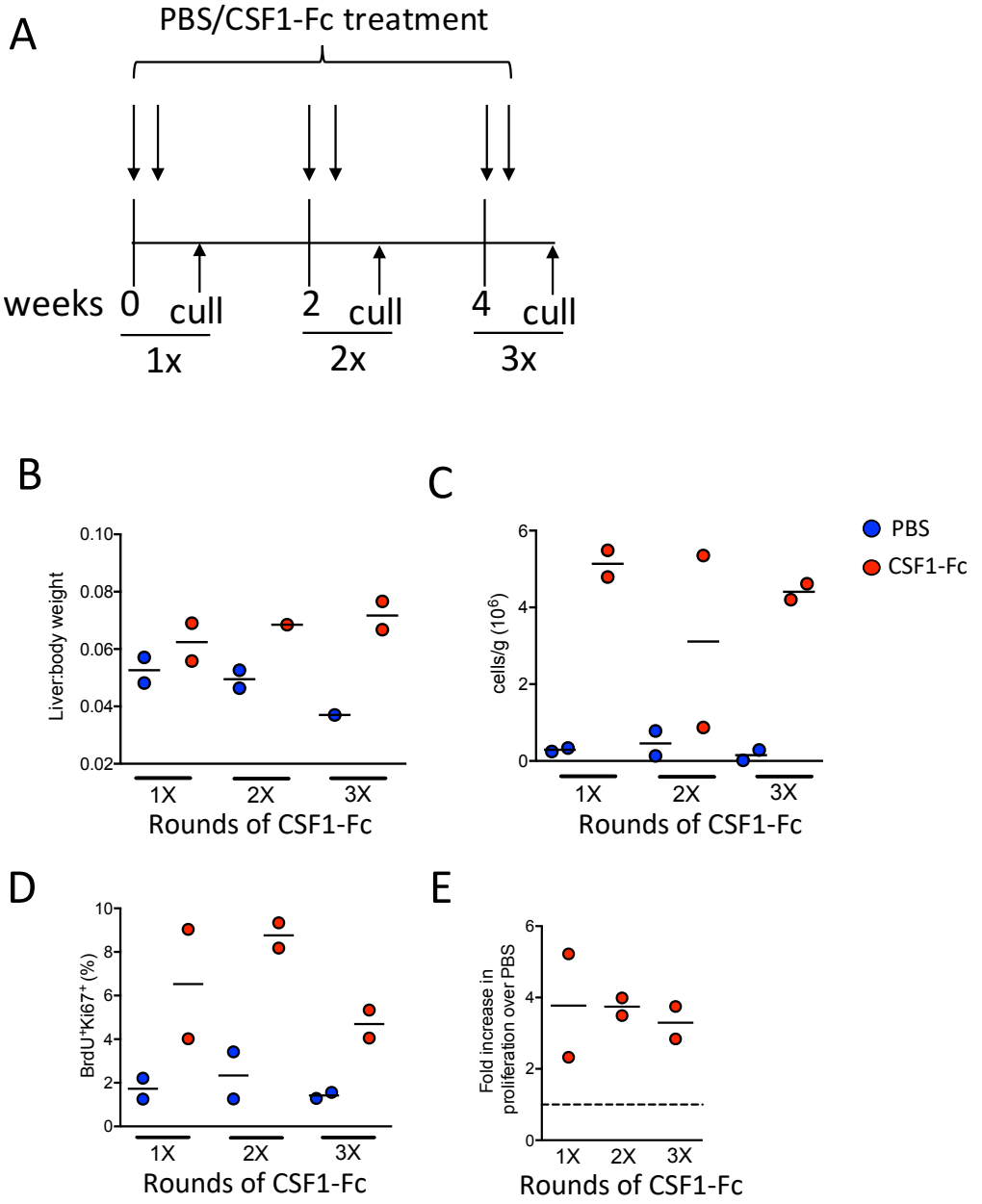

Figure 5.9 CSF1-Fc retains efficacy after multiple doses. (A) Female C57BL/6 mice were given 3 rounds of two doses of CSF1-Fc or PBS vehicle control at the indicated time points. Mice were culled at day 2 after each round of two injections, indicated by 1x (one round of injections), 2x (two rounds) and 3x (three rounds). **(B)** Fold change in liver:body weight ratio for each treatment after each round of injections. **(C)** Total number of KC per gram of liver. **(D)** Proportion of KC population which was $BrdU^{+}Ki67^{+}$ double positive and **(E)** fold increase in $BrdU^{+}Ki67^{+}$ double positive cells in the CFS1-Fc treated mice over PBS control (where PBS = 1 for each time point). n=2 per group from a single, pilot experiment. N.B. two liver:body weight ratio measurements missing due to human error.

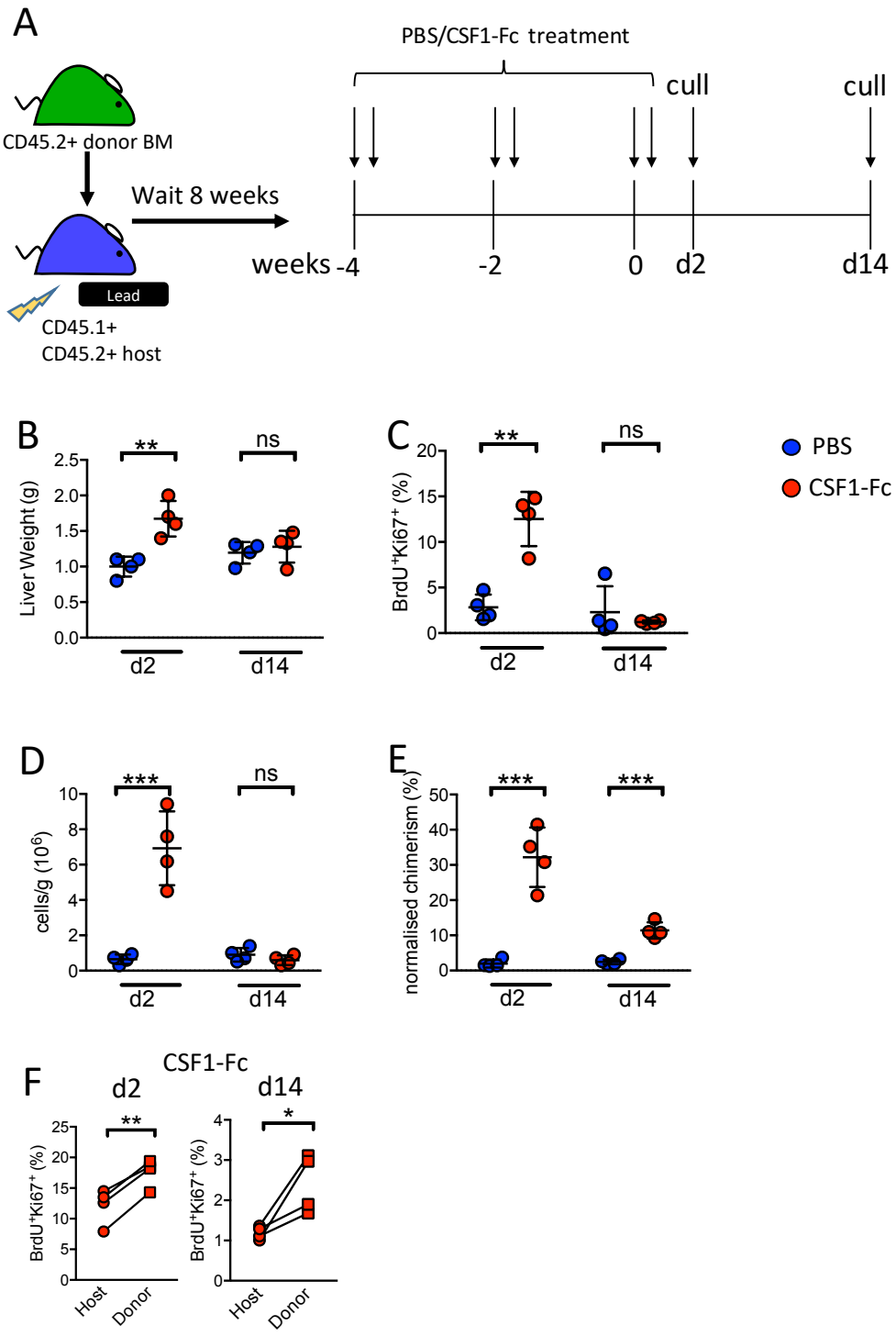
A
PBS/CSF1-Fc treatment
cull
cull
CD45.2+ donor BM
Wait 8 weeks
Lead
CD45.1+
CD45.2+ host
weeks -4
-2
0
d2
d14
B
Liver Weight (g)
**
ns
d2
d14
C
BrdU+Ki67+ (%)
**
ns
d2
d14
PBS
CSF1-Fc
D
cells/g (10^6)
***
ns
d2
d14
E
normalised chimerism (%)
***
***
d2
d14
F
CSF1-Fc
d2
d14
BrdU+Ki67+ (%)
**
*
Host
Donor
Host
Donor

Figure 5.10 Multiple round of CSF1-Fc administration leads to non-host chimerism of KC and donor cells with high proliferative capacity. (A) Female $CD45.1^+CD45.2^+$ host mice were irradiated with the upper body shielded by lead then reconstituted with bone marrow from $CD45.2^+$ donor mice. Mice were injected s.c. with PBS of CSF1-Fc at the indicated timepoints and culled 2 and 14 days after the final injection. **(B)** Total liver weight. **(C)** Proportion of KC which were $BrdU^+Ki67^+$ double positive. **(D)** Total number of KC per gram of liver. **(E)** Normalized non-host chimerism in KC population at each time point after final injection. **(F)** Proportion of donor (squares) versus host (circles) derived KC which were $BrdU^+Ki67^+$ double positive after CSF1-Fc treatment at day 2 or day 14 following the final dose of CSF1-Fc. n=4 per group from one experiment. (B-E) *p<0.05, **p<0.01, ***p<0.001, ***p<0.0001 determined by one-way ANOVA and (F) *p<0.05, **p<0.01 determined by paired t-test.

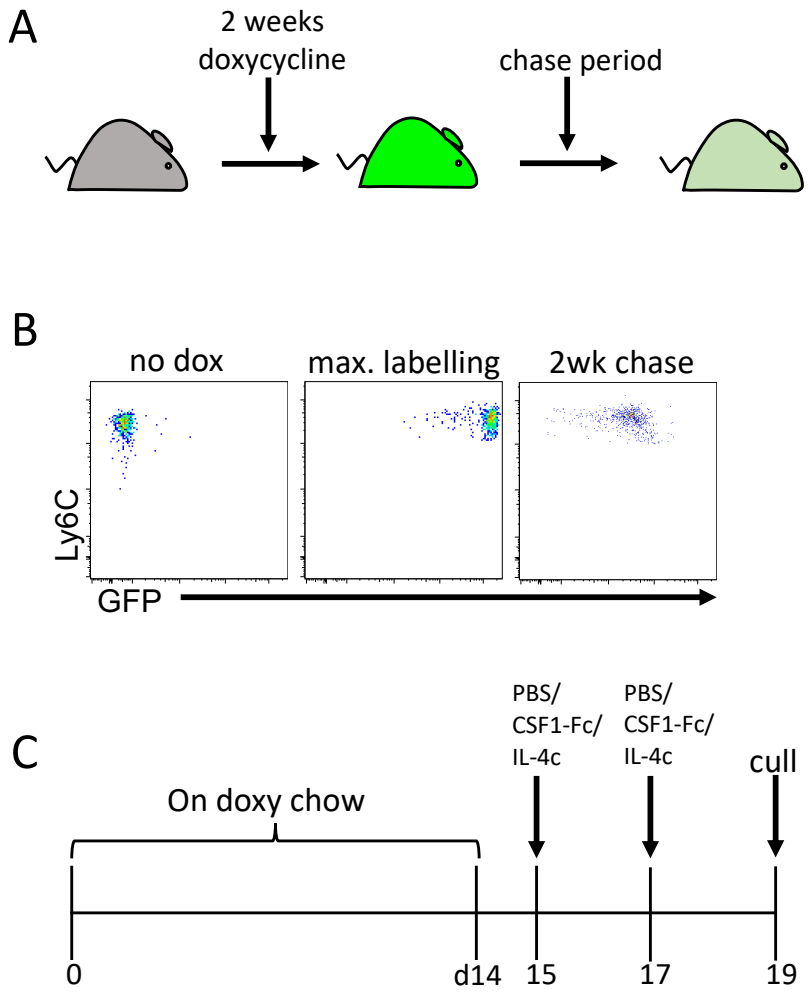

Figure 5.11 System to assess proliferative heterogeneity of KC. (A) H2B-GFP mice were given doxycycline in their chow resulting in expression of histone 2B –GFP fusion protein, which dilutes over the chase period. **(B)** Representative flow plots of GFP versus Ly6C showing GFP intensity in mice given no doxycycline, maximal labelling of Ly6C^{hi} monocytes in blood after 2 weeks on doxy chow and intensity after a 2-week chase period. **(C)** After 2 weeks on doxy chow, mice were injected twice with CSF1-Fc, IL-4c or PBS vehicle control and culled two days later.

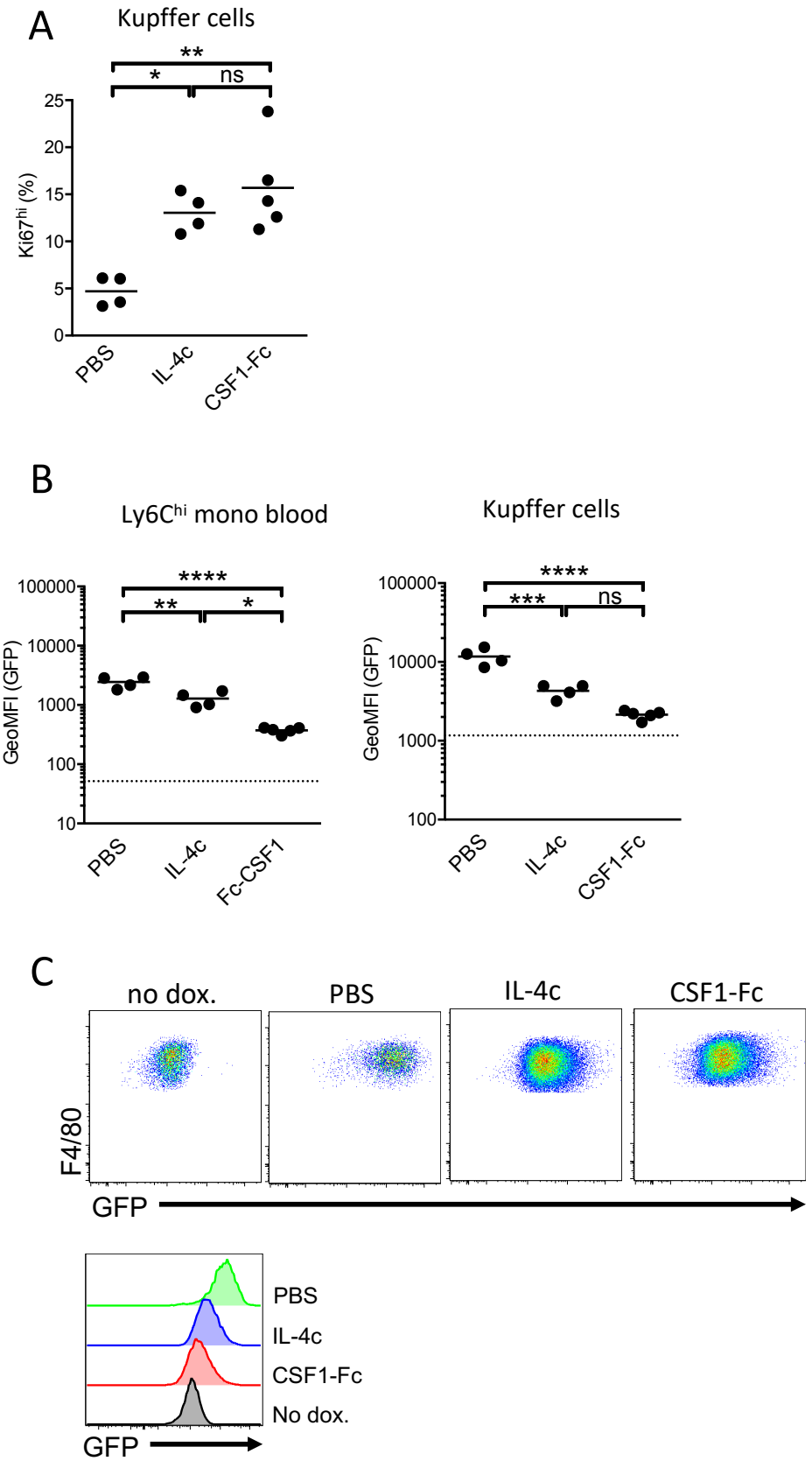
A
Kupffer cells
**
*
ns
Ki67hi (%)
25
20
15
10
5
0
PBS
IL-4c
CSF1-Fc
B
Ly6Chi mono blood
Kupffer cells
****
**
*
***
ns
GeoMFI (GFP)
100000
10000
1000
100
10
PBS
IL-4c
Fc-CSF1
CSF1-Fc
C
no dox.
PBS
IL-4c
CSF1-Fc
F4/80
GFP
PBS
IL-4c
CSF1-Fc
No dox.
GFP

Figure 5.12 No evidence of slowly cycling or quiescent KC sub-population (A) % of KC which were $Ki67^{hi}$ with each treatment. **(B)** The geometric mean fluorescence intensity (geoMFI) of GFP with each treatment in $Ly6C^{hi}$ monocytes in blood (left) and Kupffer cells in the liver (right). **(C)** Representative flow plots of GFP versus F4/80 and histogram of GFP fluorescence of KC after each treatment. Representative of 2 independent experiments with n=6-7 per group. Significance determined by one-way Anova where *p<0.05 **p<0.01 ***p<0.001 ****p<0.0001.

5.9 Discussion

In this chapter I found that in contrast to F4/80^{hi} resMϕ of the peritoneal cavity, KC appeared capable of self-maintenance even in year old mice, despite a reduction in rate of proliferation with time. Administration of exogenous CSF1-Fc caused the appearance of transient KC-like macrophages to be recruited from circulation, but withdrawal of the CSF1-Fc led to their loss from the liver. Repeated treatments with CSF1-Fc did not appear to cause exhaustion of the incumbent KC population, which raised the question of whether there was a slowly cycling KC progenitor cell in the liver. However, experiments using a genetic label dilution system did not reveal a population of quiescent KC and suggested that proliferation in the liver may not be hierarchical.

5.9.1 Maintenance and origin of KC in steady state

To understand further whether KC were able to self-maintain even in aged I we used *Ccr2*$^{-/-}$ mice. There was no deficit in KC number in year old *Ccr2*$^{-/-}$ mice, suggesting that the KC population established during embryogenesis can be maintained independently of contribution from circulating adult monocytes, even with age. Although *Ccr2*$^{-/-}$ mice displayed significant monocytopenia, with approximately 10-fold reduction in the frequency of circulating monocytes, this is not a definitive lineage tracing system, and it remained possible that the few monocytes which are able to egress from the bone marrow into the blood may be sufficient to replenish the resident KC population. However, we also took a chimeric fate-mapping approach to assess monocyte contribution to resident macrophage populations with age (Bain et al. 2016), and found no significant increase in chimerism to the KC population between 8 and 36 weeks post-irradiation. Around the time of these experiments, another study was published in which Flt3^{Cre}-YFP mice were used to label all foetal and adult HSCs and their progeny, which demonstrated only a small initial contribution of these cells to KC up to 8 days of age, after which there was no further increase in the proportion of YFP^{+} cells up to one year of age (Gomez Perdiguero et al. 2015). Thus, our results are supported by this study and strongly indicate that resident KC in the liver do not require any major contribution from recruited monocytes to maintain their numbers in the steady state. As a comparison, we also assessed F4/80^{hi} resMϕ in the peritoneal cavity in both the chimeric and *Ccr2*$^{-/-}$ studies, which showed a reduction in resident macrophage numbers in the *Ccr2*$^{-/-}$ system, and an increased level of chimerism with age (Bain et al. 2016), indicating that, at least in males, this population does rely on monocytes as mice age.

5.9.2 Role of CSF1 in maintaining the embryonic KC population and conversion of monocytes to KC

The tight self-maintenance of KC in the steady state raised the question of what constitutes the KC niche, and in particular what controls the niche size. A hypothesis of 'niche availability' has recently been put forward which predicts that resident macrophage niche space is restricted, and can be full (Guilliams and Scott 2017), and CSF1 has previously been put forward as a possible limiting factor in macrophage niche size (Jenkins and Hume 2014). The delivery of exogenous CSF1 in the form of CSF1-Fc and the resultant increased availability of CSF1 led to a general expansion of all leukocyte populations assessed. The expansion of cell populations which do not express the CSF1R (eosinophils, neutrophils and lymphocytes) is likely a knock on effect of direct signalling to KC and monocytes (chapter 4; Hawley et al. 2018). The expansion of the KC population was concurrent with an initial increase in proliferation. Withdrawal of further CSF1-Fc then resulted in a complete shut off of proliferation and a contraction of the artificially expanded KC population which then returned to its steady state size within 2 weeks following treatment, at which point proliferation returned to steady state levels. Low, but detectable levels of proliferation could been seen in the Ly6C^{hi} monocyte subset, indicating that they had begun the process of differentiation having arrived in the liver (Swirski *et al.,* 2014). However, CSF1-Fc did not induce further proliferation of Ly6C^{hi} monocytes, in contrast with another recently published study (Stutchfield et al. 2015). However, in this study, the livers were analysed at day 2 following a single CSF1-Fc dose rather than at day 4 following 2 doses in our model, so it is conceivable that we missed any early spike in proliferation of recruited Ly6C^{hi} monocytes in our study. Differences in dose of CSF1-Fc may also provide an explanation. Overall, our data are consistent with the model in which local CSF1 levels tightly regulate KC numbers through local proliferation (Jenkins and Hume 2014).

Alongside the increase in KC numbers and proliferation, the partial bone marrow chimera system confirmed the emergence of donor KC-like macrophages which expressed the classical F4/80^{hi}CD11b^{lo} KC profile. Hence CSF1 would appear to be a limiting factor in the differentiation of bone marrow derived cells – likely classical Ly6C^{hi} monocytes – into a mature KC phenotype. However, the mechanism through which CSF1 achieves this remains unanswered. It is possible that CSF1 directly instructs monocytes to mature into macrophages, or that the increased availability of CSF1 through exogenous administration

may simply allow monocytes, which express lower levels of the CSF1R than KC (chapter 4; Hawley et al. 2018) to survive for longer in the tissue, allowing local tissue-specific signals to direct their acquisition of a mature macrophage phenotype. Either way, these monocyte-derived macrophages largely did not express Tim4, indicating that they had not fully differentiated into resident KC, although others have shown that monocyte-derived cells recruited after depletion of KC take between 7 days to over a month to express Tim4 (Scott et al. 2016a). It would have therefore been beneficial to include additional markers such as the KC-specific marker Clec4f (Yang et al. 2013; Lavin et al. 2014), which has more recently been shown to be switched on by newly recruited monocytes within 4 days following depletion of the endogenous KC population (Scott et al. 2016). Regardless, my data suggest that exogenous CSF1 is a limiting factor in monocyte differentiation in the liver.

5.9.3 Why is the emergence of recruited BM-derived KC-like cells only transient?

Intriguingly, the BM-derived KC-like cells were only found transiently in the liver, and appeared to be lost by 14 days post treatment, as chimerism in the KC population had returned to PBS control levels. This suggested that 4 days of elevated CSF1-Fc levels alone was insufficient to support full conversion of monocytes to a resident KC phenotype, or that there was simply not enough time for donor cells to switch on the full KC gene expression program. A further experiment in which mice are given a prolonged CSF1-Fc treatment would be required to determine if this is the case, although the length of time chosen for treatment to be given may be somewhat arbitrary. The transient donor KC-like cells did proliferate, however, indicating that they had acquired a key feature of mature resident KC. It is particularly interesting to note that the donor KC-like cells proliferated at a higher level than their host KC counterparts, and yet were still unable to outcompete the endogenous KC, which is perhaps surprising given that changes in the balance between embryonic-derived and monocyte-derived resident macrophages in the heart over time coincides with dynamic changes in rates of proliferation due to both a general reduction in proliferation of macrophages of embryonic origin and replacement with non-renewing bone-marrow derived macrophages (Molawi et al. 2014). However, our data also demonstrated a general decline in proliferation of resident macrophages with age in the liver and peritoneal cavity, suggesting that loss of proliferative capacity over time may be a general effect across tissues. Thus, the transient nature of the donor KC-like cells was unexpected, and suggests that additional parameters limit the conversion of monocytes into long-lived liver KC.

In addition to dependence on CSF1, KC sit in close association with liver sinusoidal endothelial cells (LSECs) (chapter 3; Lynch et al. 2018) and mice with a deficiency in the endothelial molecule PLVAP can barely support adult KC (Rantakari et al. 2016). Blood continually passes through the sinusoids which are formed by LSECs, and it might therefore be expected that monocytes should not have a problem in accessing this physical KC niche. Indeed, this lack of physical barrier may be a reason why bone marrow-derived F4/80^{hi} cells accumulated in the liver but not the peritoneal cavity in response to CSF1-Fc treatment. So why then do these bone marrow-derived cells not appear to engraft? It is possible that only specific LSECs have the capacity to support KC, and these LSECs were already in contact with host KC when we delivered CSF1-Fc, preventing the long-term survival of the donor KC-like cells. Consistent with this hypothesis, KC have been shown to be immotile cells in the steady state over short time frames (Egen et al. 2008; McDonald and Kubes 2016), further supporting the fact that they inhabit a very specific, spatially restricted niche. Alternatively, the donor BM-derived cells could have an altogether different identity, perhaps in the form of recently described liver capsular macrophages (LCM) (Sierro et al. 2017). These cells were found to be dependent on CSF1R signalling, and parabiosis experiments suggest they had a faster turnover from monocytes than KC over an 8 week period (Sierro et al. 2017). Although LCM were described as Tim4^{-}CX3CR1^{+} cells, there is no specific marker which truly distinguishes them from monocytes. However, a future approach in which the location of the BM-derived donor cells in our model could be identified by imaging of the liver would be highly informative in terms of whether they are found in the capsule or the sinusoids of the liver. A different spatial location of these BM-derived cells could also provide an explanation for why they proliferate more than endogenous KC in response to CSF1-Fc. This is in contrast to the observation that both embryonic and bone-marrow derived F4/80^{hi} resMϕ in the peritoneal cavity responded equally to CSF1-Fc treatment (Bain et al. 2016). However, this could be because there was no additional recruitment of bone-marrow derived cells to the peritoneal cavity with CSF1-Fc treatment, so most donor cells would have been in the cavity for longer than 4 days, giving time to mature into a true resident phenotype. Alternatively, the lack of physical restricted niches in the peritoneal cavity would allow equal access of donor and host cells to CSF1-Fc resulting in equivalent proliferation.

5.9.4 Do KC become exhausted with age?

The plateau in proliferation of KC in the steady state between 25 and 33 weeks of age was intriguing, and one explanation for this was that prior to the 25-week time point, the liver was still growing, requiring a higher rate of KC proliferation to fill the expanding physical niche. An alternative explanation was that KC became exhausted over time, and given that CSF1-Fc appeared to tightly regulate proliferation of KC, I used CSF1-Fc as a tool to induce multiple rounds of enhanced proliferation to try to accelerate any possible exhaustion of KC. Although the donor KC-like cells displayed higher levels of proliferation than the host cells 2 days following the final dose of CSF1-Fc, host KC still proliferated at the basal rate of 1% two weeks following the final dose of CSF1-Fc, suggesting that they had not become exhausted. The maximum non-host chimerism in the blood of the partial chimeras was around 30% 2 days following this treatment regime, meaning that it was possible that these proliferating host 'KC' were those of host monocyte origin. However, even accounting for the recently recruited fraction of the host KC population there was still robust and equivalent proliferation of the endogenous resident KC after both acute and chronic CSF1-Fc treatment. This strongly argues that the endogenous KC population did not become exhausted. Although there was a significant reduction in chimerism in the KC population two weeks after the final dose of CSF1-Fc, it did not return to PBS control levels, so I was unable to conclude as to whether there was a low level of permanent engraftment of donor cells, and a longer recovery period would be necessary to determine this.

5.9.5 Search for liver resident KC progenitor cell

To examine heterogeneity of proliferation within the KC population I used the H2B-GFP mice which have been used previously used by the Jenkins group to determine heterogeneity in the proliferative capacity of cells in the peritoneal cavity (Bain et al. 2016). In this system the fluorescent GFP tag is progressively diluted as cells proliferate. However, in experiments carried out in the Jenkins lab, the rate of loss of the label in the liver KC over 14 weeks under steady state conditions was faster than the loss in F4/80^{hi} resMϕ in the peritoneal cavity, despite the basal rate of proliferation of KC being much lower than cavity macrophages in our hands (data not shown). These data suggest that proliferation alone could not account for the rate of GFP loss in KC over long time frames. However, when I gave CSF1-Fc or IL-4c, the rate of loss appeared to roughly mirror the rate of proliferation induced over the short time course, providing greater confidence that over short time frames GFP-loss does

measure proliferative history of KC. However, no 'label-retaining' cells could be identified in the F4/80^{hi}CD11b^{lo} KC population, nor within any other CD45^{+} population with either mitogen treatment, suggesting that this approach could not reveal any possible cells with progenitor potential in the liver. Furthermore, the entire KC population lost GFP uniformly, suggesting the population had proliferated equally in response to the mitogen stimuli. However, I cannot conclusively say that all KC have an equal ability to proliferate as I could only detect a shift in GFP intensity at the population level following induction of proliferation.

5.9.6 Concluding remarks

In summary, the data presented in this chapter reveal that the KC niche appears to be well protected from replenishment by monocyte-derived macrophages under steady state conditions, and that CSF1 availability may be a contributing factor for the maturation of monocytes in the liver, but is likely not the only limiting factor preventing their full conversion and persistence as resident KC. Furthermore I found no evidence for a quiescent KC progenitor in the liver, and although further investigation would be required to confirm this my data is entirely consistent with a model whereby rather than the presence of a specific tissue progenitor of macrophages, it is the niche that controls the regenerative capacity of the KC suggested by recent depletion and repopulation studies (Scott et al. 2016). However, the question of how tissue damage and inflammation affect control of the KC niche autonomy remains to be determined and will be explored in the next chapter.

Chapter 6: Maintenance of Kupffer Cells and recruitment of monocyte-derived macrophages in acute and chronic liver injury

6.1 Introduction

In the previous chapter I explored the role for CSF1 in maintenance of the KC niche and found that addition of exogenous CSF1 was not sufficient to cause permanent engraftment of recruited monocyte-derived cells in long-lived, self-renewing KC, indicating that KC ontogeny is tightly regulated even with monocyte influx to the liver. It had been shown, however, that experimentally-induced depletion of the KC population using whole body irradiation led to repopulation through both proliferation of the remaining few radioresistant KC, but also significant recruitment of adult monocytes which were able to differentiate into new KC (Klein et al. 2007). However, the fate of KC and monocyte-derived macrophages in the more clinically relevant context of liver injury had not yet been explored. Liver injury represents a serious global health and economic burden (Asrani et al. 2019), and both resident KC and monocyte-derived recruited hepatic macrophages are highly implicated in both the injury and repair phases of liver disease and damage. In many liver injury and infection models, there is a reported 'macrophage disappearance reaction' and a loss of KC following injury has been reported previously after chronic CCl_4-induced injury expressed as relative loss in frequency (Ramachandran et al. 2012) or absolute number (Heymann et al. 2015). Similarly, a reduction in both the frequency (Zigmond et al. 2014) and total number (David et al. 2016) of KC has been demonstrated after acute paracetamol (APAP) overdose in mice. However, none of these studies have clearly detailed when or whether the KC population returns back to its original absolute size, and none have looked following CCl_4-driven acute injury. Following injury there is also vast recruitment of monocytes to the liver which mature into macrophages. Although initially inflammatory, these macrophages have been shown to down-regulate inflammatory genes and acquire a 'pro-restorative' phenotype (Ramachandran et al. 2012; Dal-Secco et al. 2015). However the dynamics of whether recruited macrophages ultimately convert into KC following recovery from injury is poorly understood. Following acute paracetamol overdose there was proliferation of the remaining endogenous KC, and concurrent recruitment of $CX3CR1^+$ monocyte-derived macrophages at

day 3 after injury (Zigmond et al. 2014). Adoptive transfer of GFP^+ bone marrow from $CX3CR1^{+/GFP}$ mice into wild type mice prior to liver injury indicated that there were no GFP^+ KC at any time point examined and the authors concluded that monocytes recruited to the liver therefore do not contribute to the resident KC population (Zigmond et al. 2014). However, CX3CR1 is not expressed by KC to any high degree, so this was not a robust method to track the fate of monocytes to KC. After chronic CCl_4-induced fibrotic damage, again the depleted KC population was found to replenish through local proliferation, and there was some evidence that latex bead-labelled $Ly6C^{lo}$ monocytes in the circulation went on to mature into KC 7 days following the cessation of injury (Ramachandran et al. 2012). However, bead-labelled monocytes may simply be cleared by KC due to their high phagocytic capacity and again is not a robust fate-mapping method. Additionally, the long-term fate of monocyte-derived macrophages was not assessed in either study.

Thus the premise for this chapter was to answer the outstanding question of whether Kupffer Cells are replaced long-term by BM-derived macrophages following disturbance due to injury and if so, whether the resultant change in KC ontogeny would have long-term implications on the function of the population after injury had fully resolved. I used the CCl_4-driven model of injury as this same hepatotoxic agent can lead to both an acute centrilobular necrosis (Shi et al. 1998; Weber et al. 2003), or reversible periportal fibrosis following prolonged exposure to low doses (Ramachandran et al. 2012). This had the added advantage of allowing me to compare the dynamics of KC maintenance after single versus iterative injury using the same injurious toxin. I also combined flow cytometry and immunofluorescent imaging to quantify the absolute changes in the number of KC following injury, as this was pertinent to the idea of niche availability, which is discussed further at the end of this chapter.

6.2 Analysis of hepatic KC and recruited macrophage populations during injury and repair following CCl_4-driven acute liver injury

6.2.1 CCl_4-driven acute liver injury drives dynamic changes in the liver myeloid compartment

To assess the effect of acute liver injury on monocyte and macrophage dynamics in the liver, CCl_4 or olive oil alone was given intra-peritoneally to 8 week old, male C57BL/6 mice and livers harvested 24 hours, 3, or 6 days later (fig 6.1A). Liver sections were stained using

Periodic Acid Schiff (PAS), a reagent which binds glycogen and stains hepatocytes a deep magenta, revealing clear areas representing necrotic damage around the central veins at 24 hours post injury that largely persisted at day 3 but were resolved by day 6 (fig. 6.1B). This confirmed that CCl_4 induced acute hepatocyte damage that rapidly resolved within a week, consistent with published data using CCl_4 at a variety of concentrations (Kovalovich et al. 2000; Nakamura et al. 2004; Yu et al. 2002).

To assess the effect of injury on the hepatic myeloid compartment, flow cytometric analysis following the gating strategy established in chapter 3 was used. Live, single cells of myeloid lineage were identified as $CD45^{+}CD31^{-}Dump^{-}$. At 24 hours and 3 days after injury there was a clear increase in relative abundance of the $F4/80^{lo}CD11b^{hi}$ population compared with those in olive oil control mice (fig. 6.2A) that corresponded to greater than a 10-fold increase in total number (fig. 6.2B). However, this increase was transient, with numbers returning to normal by day 6 (fig. 6.2A and 6.2B). I then sub-divided this population further using Ly6C and MHCII expression, and identified $Ly6C^{hi}$ monocytes, $MHCII^{+}Ly6C^{-}$ cells which had been identified as cDC2s previously in the steady state (chapter 4; Hawley et al. 2018), and an emergent population with a $Ly6C^{mid}MHCII^{mid}$ phenotype, which was most apparent at day 3 (fig 6.2C). Based on these gates, it was clear that the majority of the increase in $F4/80^{lo}CD11b^{hi}$ cells at 24 hours and 3 days was due to the vast increase in $Ly6C^{hi}$ monocytes recruited to the tissue (fig 6.2D), while the cDC2s increased in frequency following recovery from the injury (fig. 6.2E). In contrast, the $Ly6C^{mid}MHCII^{mid}$ cells were only elevated at day 3, returning to normal at day 6 (fig. 6.2F). Further characterization of these populations revealed the transient $Ly6C^{mid}MHCII^{mid}$ cells appeared to express higher levels of F4/80 (fig. 6.2G, left, blue population) than $Ly6C^{hi}$ or $Ly6C^{lo}$ monocytes or cDC2s. Although these cells also appeared to express Tim4 (fig. 6.2G, middle), a Tim4 FMO control sample (data not shown) indicated that this was not genuine staining, and could possibly be attributable to increased autofluorescence due to increased forward scatter (fig. 6.2G, right) (Tzur et al. 2011). However, they did appear to express CD64 when compared to an FMO control in a pilot experiment (data not shown), which together with their greater size would suggest the $Ly6C^{mid}MHCII^{mid}$ cells represent mature $CD11b^{hi}$ macrophages transiently present in the injured liver.

I next turned my attention to the dynamics of the resident KC population. Although a reduction in both the frequency and number of KC has been reported after iterative CCl_4-induced injury, this has not been formally demonstrated after only a single dose of CCl_4, and

neither has any study directly combined both flow cytometry with imaging to directly enumerate KC following CCl_4-induced acute liver injury. By flow cytometry, there was a reduction in frequency of KC at 24 hours and 3 days after acute injury (fig. 6.2A & 6.3A), that translated to a reduction in the total number of KC per gram of liver by around 50% at 24 hours (fig. 6.3B). The loss of KC persisted for at least 3 days post-injury, although this did not reach statistical significance likely due to high variance in the data, but numbers had returned to pre-injury levels by day 6 (fig 6.3B). To complement the flow cytometry analysis, and to ensure that the differences in KC number between olive oil and CCl_4-treated mice at 24 hours and 3 days were not an artefact of the digestion and staining process, immunofluorescence staining for the macrophage marker F4/80 was performed on fixed frozen sections of liver. Enumeration of the number of $F4/80^+$ events per field of view at each time point (fig 6.3C) indicated ~40% reduction in KC number at both 24h and 3 days following CCl_4, which returned to olive oil control levels by 6 days after injury (fig 6.3D). Unfortunately this did not reach statistical significance likely due to low sample number, but the data clearly mirrors that seen with the flow cytometric analysis. KC appeared to be lost specifically from the areas around blood vessels which was assumed to be regions of necrotic damage with a dense inflammatory infiltrate indicated by dense DAPI staining (Cummings et al. 2004) (fig 6.3C, dotted region). By day 6 the necrotic regions appeared to have been largely repopulated, but clusters of $F4/80^+$ cells not normally found in uninjured liver were also apparent (fig. 6.3C, white arrows). Thus, both flow cytometry and immunofluorescent staining of liver sections indicated that approximately half the KC population is lost from the liver by 24 hours after injection of CCl_4 and numbers do not recover until sometime between day 3 and day 6.

6.2.2 Transient elevated proliferation of KC 3 days post injury

Murine KC proliferate following acetaminophen overdose (Zigmond et al. 2014) and elevated Ki67 expression suggests this also occurs after chronic exposure to CCl_4 (Ramachandran et al. 2012). Thus I assessed proliferation of KC following acute CCl_4. As previously, mice were pulsed with BrdU prior to necropsy, and proliferating KC defined at each time point as BrdU and Ki67 double positive (fig 6.4A). From this point on I have shown only a single olive oil control which was taken from the 24 hour time point to represent all olive oil controls. Gates were determined using a Ki67 isotype control antibody, and a sample given no DNase treatment, preventing access of the anti-BrdU antibody to the BrdU incorporated into the

nucleus (fig. 6.4B and 6.4C). Ki67 isotype staining and the no DNase control were carried out on both a pool of samples given olive oil and a separate pool given CCl_4 to ensure that treatment did not affect the baseline of where to set gates. Only the pooled olive oil staining controls are shown as there was no difference between olive oil and CCl_4. Dynamic changes in the rates of KC proliferation across the time course were apparent. There was a peak in proliferation at 3 days post-injury (fig 6.4D), in keeping with the notion that proliferation may contribute to maintenance of the population following injury. There was also notable a reduction in proliferation at the 24h time point compared its to olive oil control group. This suggested that switching off of proliferation may also be a mechanism for controlling the KC population size during the acute injury phase. Notably there was fluctuation in the olive oil control level of proliferation, indicating that olive oil itself may have an effect on KC proliferation rate, though this idea was not explored further within the scope of this project.

6.2.3 The F4/80^{hi}CD11b^{lo} KC gate contains a population of bone-marrow derived, recruited cells 6 days after injury

Although elevated proliferation of KC was evident following injury, I hypothesised that monocyte-derived macrophages recruited from bone marrow could also contribute to the restoration of KC number by 6 days. Hence, tissue-protected BM chimeras constructed from CD45.1$^+$CD45.2$^+$ host mice given CD45.2$^+$ bone marrow were again used to definitively fate map cells recruited to the liver from bone marrow following administration of CCl_4. Eight weeks after irradiation mice were given a single dose of CCl_4 or olive oil control (fig 6.5A). To confirm injury, serum was analysed for the presence of two acute hepatocyte damage markers, alanine aminotransferase (ALT) and aspartate transaminase (AST). Both markers were elevated in the serum at 24 hours after injury, indicative of hepatocyte necrosis, but had returned to normal by 6 days (fig. 6.5B). I also confirmed that changes in macrophage numbers in these mice were consistent with those seen in non-irradiated C57BL/6 mice. By flow cytometry, a vast recruitment of F4/80^{lo}CD11b^{hi} cells (fig. 6.5C) was again apparent at 24hrs, as was the reduction in KC number, albeit with high variation within the control group, that resolved between 3 and 6 days after injury (fig. 6.5D). F4/80 staining of fresh frozen sections was also consistent with that seen in non-irradiated mice, with loss of F4/80$^+$ cells in the areas of necrotic damage (fig. 6.6A), that again equated to a 50% reduction in number when enumerated in ImageJ (fig. 6.6B). The F4/80 staining, acquisition of images and

enumeration in figure 6.6 was carried out by Alíz Owolabi, an honours project student whom I co-supervised. The editing of images and statistical analysis of counts was performed by me.

Chimerism was first assessed in all F4/80^{lo}CD11b^{hi} cells, with donor cells identified as CD45.1^{-} CD45.2^{+} (fig. 6.7A). Consistent with them being of bone marrow origin, these cells exhibited the same degree of chimerism as blood monocytes, translating to ~100% chimerism when normalized to the maximum chimerism of Ly6C^{hi} monocytes in blood for each mouse (fig 6.7B), and this remained consistent across all treatment groups. When donor cells were identified in the KC population (fig. 6.7C), a low basal level of chimerism of around 2% was evident in the olive oil control group (fig. 6.7C & 6.7D), in keeping with the low levels of bone marrow contribution to the KC population in the absence of injury found using this technique (Bain et al. 2016). However, with CCl_4 treatment, there was a clear contribution from cells recruited from bone marrow, which gradually increased over time after injury (fig 6.7C & 6.7D). The complete time course was performed only once in chimeric mice, but the significant contribution of donor cells to the KC population at day 6 post-injury was validated a further two times. Mice in these experiments displayed even higher levels of chimerism at day 6, with around 25% of the KC population of bone marrow origin (fig 6.7E). These results indicated that although acute damage markers, necrosis, and numbers of inflammatory cells and KC had returned to baseline by 6 days, the origin of the KC population was a mix of endogenous, host cells which are likely largely of embryonic origin, and recently recruited cells of adult bone marrow origin, which constituted approximately one fifth to one quarter of the population. Thus the ontogeny of the KC population was altered by CCl_4-driven acute liver injury.

6.2.4 Bone-marrow derived F4/80^{hi}CD11b^{lo} cells do not express KC markers Tim4 or Clec4f, but do express the macrophage marker CSF1R

To determine if newly recruited F4/80^{hi}CD11b^{lo} cells expressed markers of mature KC I first stained cells for additional known markers of mature KC. Assessment of Tim4 expression within the F4/80^{hi}CD11b^{lo} population in non-chimeric mice revealed an emergent Tim4$^{lo/-}$ population that was most pronounced at day 6 (fig. 6.8A). Further investigation at the day 6 time point in chimeras revealed that almost all donor cells were Tim4$^{lo/-}$, whilst approximately 80% host cells were Tim4^{hi} (fig. 6.8 B & 6.8C). The remaining 20% of host cells were Tim4^{lo} (fig. 6.8B) and represent the recently recruited BM-derived macrophages of host origin, since

these animals only have partial chimerism due to the protected irradiation. Thus resident KC could be defined by their F4/80^{hi}CD11b^{lo}Tim4^{hi} expression profile whilst recruited cells were F4/80^{hi}CD11b^{lo}Tim4^{lo}. Staining for the KC-specific marker Clec4f (Yang et al. 2013; Lavin et al. 2014) was also assessed, as its expression can be detected as early as 4 days by monocyte-derived macrophages recruited to the liver following experimental depletion of KC (Scott et al. 2016). Although detection of Clec4f was limited in this experiment, there was there was an apparent shift in Clec4f staining within the F4/80^{hi}CD11b^{lo}Tim4^{hi} KC compared with to the FMO control, whilst the F4/80^{hi}CD11b^{lo}Tim4^{lo} recruited cells remained largely negative (fig. 6.8D). Consistent with this, host cells in chimeric mice expressed higher levels of Clec4f at day 6 than donor cells (fig. 6.8E). Equally, gating on KC and assessing Tim4 expression in non-chimeric mice revealed an emergent Tim4$^{lo/-}$ population that was most pronounced at day 6 (fig. 6.8C). To confirm that the recruited cells were indeed macrophages, CSF1R expression at the day 6 time point following acute injury was assessed in a separate experiment using *csf1r*-mApple reporter mice. The F4/80^{hi}CD11b^{lo}Tim4^{lo} recruited cells expressed high levels of the *Csf1r*, though expression was a half-log lower than in F4/80^{hi}CD11b^{lo}Tim4^{hi} KC (fig. 6.8F). Thus the recruited fraction of the F4/80^{hi}CD11b^{lo} population represents a mature macrophage population which is phenotypically distinct from F4/80^{hi}CD11b^{lo}Tim4^{hi} KC, and will be referred to as F4/80^{hi}CD11b^{lo}Tim4^{lo} recruited mϕ from this point on. In light of the knowledge that the F4/80^{hi}CD11b^{lo} was a mixed population at the day 6 time point, I re-evaluated changes in the number of these cells over the time course. Enumeration of the F4/80^{hi}CD11b^{lo}Tim4^{lo} recruited mϕ by flow cytometry revealed that there were approximately 400,000 recruited cells at the day 6 time point (fig. 6.9A). Deducting the number of these cells from the total of F4/80^{hi}CD11b^{lo} population allowed me to re-evaluate whether the endogenous F4/80^{hi}CD11b^{lo}Tim4^{hi} KC population had returned to normal size, as indicated previously (fig. 6.3). Even with the contribution of the F4/80^{hi}CD11b^{lo}Tim4^{lo} recruited mϕ removed, there was no significant difference in F4/80^{hi}CD11b^{lo}Tim4^{hi} KC number between CCl_4-treated and olive oil controls at day 6 (fig. 6.9B).

6.2.5 Use of Tim4 as a marker of recently recruited F4/80^{hi}CD11b^{lo} mϕ

Once it became clear that the F4/80^{hi}CD11b^{lo} cells of donor origin were Tim4^{lo}, I considered the possibility that Tim4 expression could be used as an alternative way to bone marrow chimeras of distinguishing resident KC which are largely of embryonic origin from newly

recruited F4/80^{hi}CD11b^{lo} macrophages of bone marrow origin. When data from control olive oil- (chapter 6) or PBS-treated (chapter 5) control mice were pooled, no linear relationship was found between the normalised chimerism in the F4/80^{hi}CD11b^{lo} population and the proportion that were low or negative for Tim4 (r^2=0.0824; p=0.2801) (fig. 6.10A). The lack of correlation between bone marrow origin and lack of Tim4 expression in control mice may be because cells of bone marrow origin recruited to the KC compartment gradually acquire Tim4 expression over a time period of around a month (Scott et al. 2016), and there is no sudden influx of recruited cells in these control mice since they are intended to be close to steady state conditions. However, when the same comparison was performed on cells from CCl_4 or CSF1-Fc treated mice, there was a highly significant positive correlation between normalised chimerism and frequency of Tim4^{lo} cells in the population (r^2=0.8007; p<0.0001) (fig. 6.10B), suggesting that lack of Tim4 expression is a good surrogate marker for identifying cells of recent BM (<1 month) origin in the liver.

6.2.6 BM-derived Tim4^{lo} mϕ are largely spatially distinct from Tim4^{hi} KC

The finding that Tim4 expression distinguishes endogenous KC from F4/80^{hi}CD11b^{lo} macrophages recruited to the liver upon injury led me to examine whether Tim4 and F4/80 co-staining could allow visualization of the location of each population, thereby providing insight into possible differences in the function and regulation of these cells. A standard dual immunofluorescence staining protocol was trialled in which the staining was carried out in a sequential manner. The order of addition of antibodies was α-F4/80 1°, AF594-conjugated 2°, α-Tim4 1°, AF488-conjugated 2° (fig. 6.11A). Washing steps were included after incubation with each antibody, as was an additional blocking step between staining for F4/80 and Tim4. An initial problem was that both the α-F4/80 and α-Tim4 1° antibodies were raised in rat, meaning that the AF488-conjugated 2° bound to both the α-F4/80 1° and α-Tim4 1° antibodies resulting in false Tim4 staining even when the α-Tim4 1° antibody was not added to the tissue on a control slide (fig. 6.11A & 6.11B). Unfortunately, there was a lack of antibodies available which had been raised in an alternative species and use of directly conjugated 1° antibodies resulted in no visible staining (data not shown). Development of a suitable protocol to circumvent this issue of cross reactivity became the focus of undergraduate student's honours project that I co-supervised. We identified that a goat anti-rat F(ab) fragment bound to FITC may be a suitable secondary for the Tim4 antibody. The

F(ab) fragment is polyclonal and when used at saturating concentrations ensures that no available binding sites remain on the α-Tim4 1° antibody. It is also monovalent meaning there are no potential exposed binding sites left which can cross react with the goat-α-rat 2° antibody intended to detect the F4/80 staining (fig. 6.11C). Note that the order of staining was reversed at this point as the Tim4 and F(ab) fragment staining was required to be carried out first in order to prevent the cross reactivity. This protocol was successful, and there was no staining for F4/80 on the staining control slide where the α-F4/80 1° antibody was not added (fig. 6.11D).

Staining of livers at day 6 post olive oil injection revealed cells within the normal liver parenchyma to be both F4/80 and Tim4 double positive, identifying them as KC. Following CCl_4-driven acute liver injury, double positive cells were still found in the parenchyma, but there were clear clusters of F4/80 single positive cells focused around blood vessels (fig. 6.12, indicated by white arrows). Whilst there also appeared to be some F4/80^{+}Tim4^{hi} KC within the clusters, F4/80^{+}Tim4^{lo} recruited mϕ were found exclusively within clusters. Images shown are from chimeric mice, and are representative of images taken of both chimeric and non-chimeric livers. Thus, F4/80^{+}Tim4^{hi} KC and F4/80^{+}Tim4^{lo} recruited mϕ are largely spatially distinct following CCl_4-driven acute liver injury.

6.2.7 Transcriptional differences between F4/80^{hi}CD11b^{lo}Tim4^{hi} KC and F4/80^{hi}CD11b^{lo}Tim4^{lo} mϕ

Given the fact that the F4/80^{hi}CD11b^{lo}Tim4^{lo} cells were a transient macrophage population that were largely present in the liver during the tissue repair phase, I focused my attention on the possible functions of these cells. The ability to use Tim4 as a discriminator between true KC and recruited macrophages was an important finding as it allowed me to FACS-sort the entire recruited mϕ population from C57BL/6 mice. This saved time and money in comparison to using chimeras, and was superior in that I would only have been able to identify a subset of recruited macrophages since the nature of the protected chimera system means that recruited macrophages are a mix of donor and host phenotype. The transcriptional profiles of F4/80^{hi}CD11b^{lo}Tim4^{hi} KC and the F4/80^{hi}CD11b^{lo}Tim4^{lo} recruited mϕ populations were compared using NanoString, a technology akin to microarray but which utilises a smaller pre-determined panel of genes. For this purpose, I chose the 'nCounter myeloid innate immunity panel' (nanostring.com), a panel of 734 macrophage-related genes.

F4/80^{hi}CD11b^{lo}Tim4^{hi} KC and F4/80^{hi}CD11b^{lo}Tim4^{lo} recruited mϕ at day 6 post acute CCl_4 injury, and F4/80^{hi}CD11b^{lo}Tim4^{hi} KC from control mice receiving olive oil injection were FACS purified and post-purity checks confirmed that each population was >95% pure (fig. 6.13A). In total between 3.6-6.9ng/µl of RNA was recovered per sample, all of which achieved high RNA quality scores (fig. 6.13B), except for sample 'Tim4^{hi} 4', which appeared to have very low RNA content when assessed by size fractionation. Limited sample volume prevented repeat analysis by size fraction, but since this sample appeared to have RNA present when quantified by Nanodrop, it was sent for analysis. The raw data was then normalized to the 20 house keeping control genes included in the NanoString chip, and fold change and significance were determined. Genes with a greater than 2-fold change in gene expression in either direction, along with a p-value of greater than 0.05 were considered significant. Unadjusted p-values were used as corrections for multiple tests are not recommended by NanoString as the assumption of independence between genes does not hold true when analysing a pre-selected panel of functionally related genes.

Comparison of Tim4^{hi} KC in control (olive oil) and CCl_4-treated mice revealed very high similarity with only 17 genes significantly differentially expressed (fig. 6.14A). In Tim4^{hi} KC post injury only a handful of genes were upregulated including *Mmp12*, *Itgax* and *Anxa1,* while *Nr4a2*, an orphan nuclear receptor was strongly enriched in the control KC group (fig. 6.14A). In contrast, many more and much larger differences in gene expression were apparent between Tim4^{hi} KC and Tim4^{lo} recruited mϕ after injury. In particular Tim4^{lo} recruited mϕ showed very high expression of *CX3CR1*, *CCR2*, *CCR1*, *Lat2* and *Emp1* compared to Tim4^{hi} KC whilst Tim4^{hi} KC expressed very high levels of the scavenger receptor Marco compared to the recruited Tim4^{lo} population (fig. 6.14B). Comparison of the top 50 differentially regulated genes between Tim4^{hi} KC and Tim4^{lo} recruited mϕ after injury revealed a clear gene signature between Tim4^{hi} KC and Tim4^{lo} recruited mϕ post injury whilst Tim4^{hi} KC post injury closely aligned with the Tim4^{hi} control KC group (fig. 6.14C).

6.2.8 F4/80^{hi}CD11b^{lo}Tim4^{lo} recruited mϕ are recruited independently of CCR2

As high levels of *Ccr2* expression were identified in the recruited Tim4^{-} macrophage population by the NanoString gene analysis, and given the availability of *Ccr2*$^{-/-}$ mice in the lab, I took advantage of these animals to try to knock down recruitment of these cells following injury, in the hope of learning more about their role in injury and resolution. *Ccr2*$^{-}$

$^{/-}$ or C57BL/6 control mice were given a single acute dose of CCl_4 or olive oil, and assessed 24 hours or 6 days later to look at both the acute damage and repair phases (fig. 6.15A). Comparison of serum ALT levels showed no significant difference between C57BL/6 and *Ccr2*$^{-/-}$ mice (fig. 6.15B). As expected, compared with the large number of Ly6C^{hi} monocytes recruited to the livers of C57BL/6 mice at 24 hours, more than 4-fold fewer were observed in the liver of *Ccr2*$^{-/-}$ mice (fig. 6.15C), confirming that there was not a significant recruitment of monocytes to the liver via a CCR2-independent mechanism in the context of the injury model. In contrast, the disappearance and reappearance of F4/80^{hi}CD11b^{lo} cells at 24hr and 6 days respectively was equivalent between genotypes (fig. 6.15D), and no difference in the levels of proliferation of these cells was detected at either time point between C57BL/6 and *Ccr2*$^{-/-}$ mice (fig. 6.15E). Most surprisingly, it appeared that the Tim4^{lo} macrophages still emerged in the liver of *Ccr2*$^{-/-}$ mice by day 6 post-injury, at an equivalent frequency to that seen in control mice (fig. 6.15F). This prevented further use of the *Ccr2*$^{-/-}$ mice to investigate the function of the F4/80^{hi}CD11b^{lo}Tim4^{lo} recruited mϕ since they were still present, however it suggested, albeit not conclusively, that these recruited macrophages may not arise from classical Ly6C^{hi}, CCR2-dependent monocytes.

6.3 Long-term maintenance of KC following acute and chronic CCl_4-driven liver damage

6.3.1 Recruited F4/80^{hi}CD11b^{lo}Tim4^{lo} mϕ do not persist long-term in the liver following acute injury

Although in the lung alveolar macrophages repopulate through local proliferation following influenza infection (Yona et al. 2013), it has been shown in the liver that when KC are experimentally depleted, monocytes can replace them, converting into self-renewing KC which closely phenocopy the embryonic KC population (Scott et al. 2016). Thus, although F4/80^{hi}CD11b^{lo}Tim4^{lo} recruited mϕ were spatially distinct from endogenous F4/80^{hi}CD11b^{lo}Tim4^{hi} KC at day 6 following injury, I hypothesised that these newly recruited macrophages would become permanently engrafted into the KC population following total resolution of injury. I again used the partial chimera system to identify recruited cells within the liver at 6 days following acute injury, but this time included an 8 week recovery group (fig. 6.16A). As seen previously, there was no difference in the total number of F4/80^{h}CD11b^{lo}Tim4^{hi} KC 6 days following injury, but unexpectedly, there was a small

reduction after 8 weeks (fig. 6.16B). This experiment was only performed once as these are very long experiments, and I focussed on the long-term recovery from chronic injury detailed below. Thus I cannot be sure that there is a biologically significant reduction in KC number 8 weeks after injury. Chimerism of Ly6C^{hi} monocytes in the blood remained stable in both olive oil control and CCl_4 treatment groups across the time course (fig. 6.16C). As previously, there was a clear population of F4/80^{hi}CD11b^{lo} cells of donor origin at the 6 day time-point, but there was no evidence that these cells survived long-term, and chimerism within the total F4/80^{hi}CD11b^{lo} population was reduced back to basal levels 8 weeks after injury (fig. 6.16D).

6.3.2 Recruited F4/80^{hi}CD11b^{lo}Tim4^{lo} mϕ do not persist long-term in the liver following chronic CCl_4 injury and endogenous KC numbers are permanently reduced

My data supported the conclusion that the endogenous resident KC self-maintained independently of recruited mϕ following an acute injury. I next investigated whether the same was true following a chronic liver injury. For this purpose I again used CCl_4 to induce injury. Similar to my observations following acute injury, it has been shown previously that a marked loss of KC is evident in the liver immediately following cessation of CCl4-mediated iterative injury followed by a period proliferation and reconstitution over the following 6 days (Ramachandran et al. 2012). Hence, tissue-protected bone marrow chimeras were given the same dose of CCl_4 used in the acute model, but animals received two doses a week for 4 weeks. Following the final injection, mice were left for either 6 days at which point the resulting fibrosis is largely resolved (Ramachandran et al. 2012), or 8 weeks to examine long term survival potential of any recruited macrophages (fig. 6.17A). In contrast to the acute injury model, the number of F4/80^{hi}CD11b^{lo} cells identified by flow-cytometry was reduced at the 6 day time point compared to olive oil control, and the numbers did not return to normal even after 8 weeks of recovery (fig. 6.17B). The level of chimerism in the F4/80^{hi}CD11b^{lo} population at 6 days after chronic injury was remarkably similar to that after only an acute injury, with approximately 15% of the total F4/80^{hi}CD11b^{lo} population of bone marrow origin (fig. 6.17C). Despite the chronic nature of the injury, these donor macrophages were still unable to engraft permanently into the liver, and chimerism returned back to a level which was not significantly different to the olive oil control group at 8 weeks following injury (fig. 6.17C). Although it was not statistically significant, the chimerism at 8 weeks did

appear slightly elevated compared to olive oil control. However, when the total number of F4/80^{hi}CD11b^{lo}Tim4^{lo} recruited mϕ was calculated there was a clear increase in number at 6 days which returned to normal 8 weeks after chronic injury (fig. 6.17D). For completeness, the total number of F4/80^{hi}CD11b^{lo}Tim4^{hi} KC was also calculated, and numbers were indeed reduced at day 6, and did not return to normal even by 8 weeks following injury (fig. 6.17E).

6.3.3 Attempted use of *csf1r*-EGFP 'MacGreen' donor bone marrow chimeric mice to provide a positive marker for recruited macrophages on immunofluorescent liver sections

To provide a positive marker for recruited mϕ on immunofluorescent sections, MacGreen donor bone marrow was used for the acute experiment in section 6.3.1 and for one of the repeat chronic experiments included in section 6.3.2. In particular this would have allowed me to visualise the location of any recruited mϕ at the 8 week time point had they been permanently engrafted. The use of a positive marker for the recruited mϕ would have been superior to the F4/80 and Tim4 dual staining protocol since Tim4 was upregulated within one month of arrival of donor macrophages into the liver following experimental depletion of the embryonic KC population (Scott et al. 2016), and would therefore no longer be a useful discriminator between embryonic and recruited KC at 8 weeks following injury. With both the acute and the chronic injury models, the same pattern of GFP fluorescence could be observed surrounding vessels at the 6 day time point following CCl_4 treatment (fig. 6.18A & 6.18B). However, a chimeric mouse which had received control C57BL/6 donor bone marrow followed by chronic CCl_4 treatment showed the same pattern of green fluorescence (fig. 6.18B), indicating autofluorescence rather than genuine detection of EGFP expression. Use of a staining protocol in which a tyramide amplification step was added to boost EGFP detection did not reveal any additional EGFP staining in these livers, despite the fact that this protocol produced clear EGFP staining in a naïve whole MacGreen liver (data not shown). The autofluorescence pattern detected in these experiments is highly reminiscent of the autofluorescence seen by another group following an 8 week CCl_4 treatment (Rantakari et al. 2016). The authors identified these autofluorescent bodies as 'ceroid-laden macrophages'. Thus this protocol required further optimisation to be able to visualise the EGFP recruited cells but unfortunately there was not time for this within my doctoral studies.

6.3.4 Identification of recruited mϕ location following chronic liver injury using Tim4 and F4/80 double immunofluorescence

To visualise the spatial location of the F4/80^{hi}CD11b^{lo}Tim4^{lo} recruited mϕ following chronic injury, I resorted back to the F4/80 and Tim4 double immunofluorescence protocol, where recruited mϕ could be identified as F4/80^{+} but Tim4^{-} cells. A staining control sample revealed autofluorescence in the GFP channel even when the primary Tim4 antibody which is detected by the Fab-FITC secondary antibody was not added (fig. 6.19A, yellow arrows), confirming what was seen in with the MacGreen donor bone marrow chimeric images above. Thus with the fully stained sections, these autofluorescent cells could be identified by their location around vessels and because they were extremely bright in the GFP imaging channel (fig. 6.19B, yellow arrows). However, there were also very clear single positive F4/80^{+}Tim4^{-} recruited mϕ (red), which had typical KC morphology and were scattered within the parenchyma (fig. 6.19B, white arrows), in high contrast to the clusters of recruited mϕ seen around vessels following acute injury. This indicated that following chronic injury, the F4/80^{hi}CD11b^{lo}Tim4^{lo} recruited mϕ may be occupying the same niche as the F4/80^{hi}CD11b^{lo}Tim4^{hi} KC of embryonic origin, yet despite this they did not permanently engraft into the KC population (fig. 6.17C).

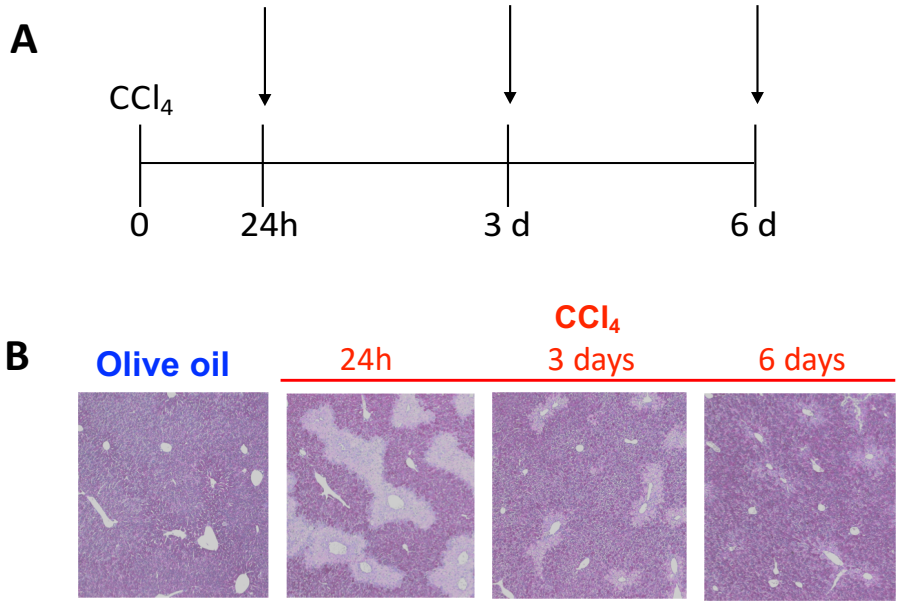

Figure 6.1 CCl_4 drives an acute necrotic liver injury. (A) Male C57Bl/6 mice were given a single dose of CCl_4 and livers were assessed at 24 hours, 3 days and 6 days after injury. **(B)** Representative images of PAS staining of livers from each time point.

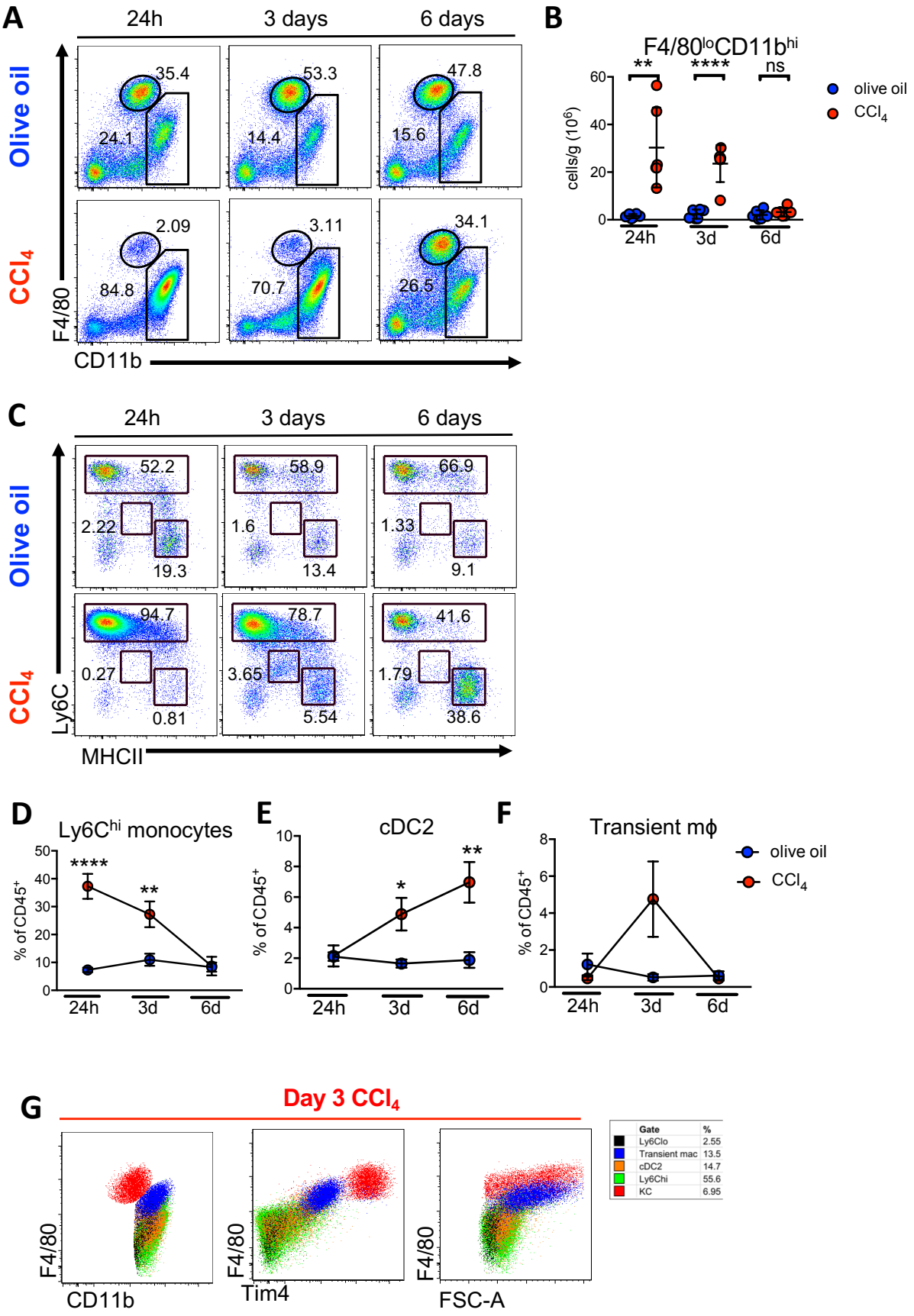
A
24h
3 days
6 days
Olive oil
CCl4
35.4
24.1
53.3
14.4
47.8
15.6
2.09
84.8
3.11
70.7
34.1
26.5
F4/80
CD11b
B
F4/80loCD11bhi
**
****
ns
cells/g (10^6)
olive oil
CCl4
24h
3d
6d
C
52.2
2.22
19.3
58.9
1.6
13.4
66.9
1.33
9.1
94.7
0.27
0.81
78.7
3.65
5.54
41.6
1.79
38.6
Ly6C
MHCII
D
Ly6Chi monocytes
% of CD45+
E
cDC2
F
Transient mϕ
G
Day 3 CCl4
Gate
%
Ly6Clo 2.55
Transient mac 13.5
cDC2 14.7
Ly6Chi 55.6
KC 6.95
Tim4
FSC-A

Figure 6.2 Changes in myeloid cell populations over time following acute CCl_4. (A) Representative flow plots of CD11b versus F4/80 at 24 hours, 3 days and 6 days after acute olive oil control or CCl_4. Gated live, singlets, $CD45^+CD31^-Lineage^-$. Gates show $F4/80^{hi}CD11b^{lo}$ KC and $F4/80^{lo}CD11b^{hi}$ mixed myeloid population. **(B)** Replicate data of total number of $F4/80^{lo}CD11b^{hi}$ cells per gram of liver. **(C)** Representative flow plots of Ly6C versus MHCII with gates for $Ly6C^{hi}$ monocytes, cDC2 and a recruited macrophage population that emerges at day 3 after injury, gated on live, $CD45^+CD31^-Lineage^-$ $F4/80^{lo}CD11b^{hi}$ cells. **(D)** Proportion of the total $CD45^+$ leukocyte population represented by $Ly6C^{hi}$ monocytes, **(E)** cDC2 and **(F)** recruited macrophages at each time point following CCl_4 or olive oil control. **(G)** Overlays of $Ly6C^{hi}$ monocytes (green), cDC2 (orange), recruited macrophages (blue) $Ly6C^{lo}$ (black) and KC (red) and their expression of CD11b, Tim4 or FSC-A versus F4/80. n=6 per group pooled from two independent experiments. Graphs show mean ± SD. *p<0.05 **p<0.01 ***p<0.001 ****p<0.0001 (multiple *t* tests with Holm-Sidak correction).

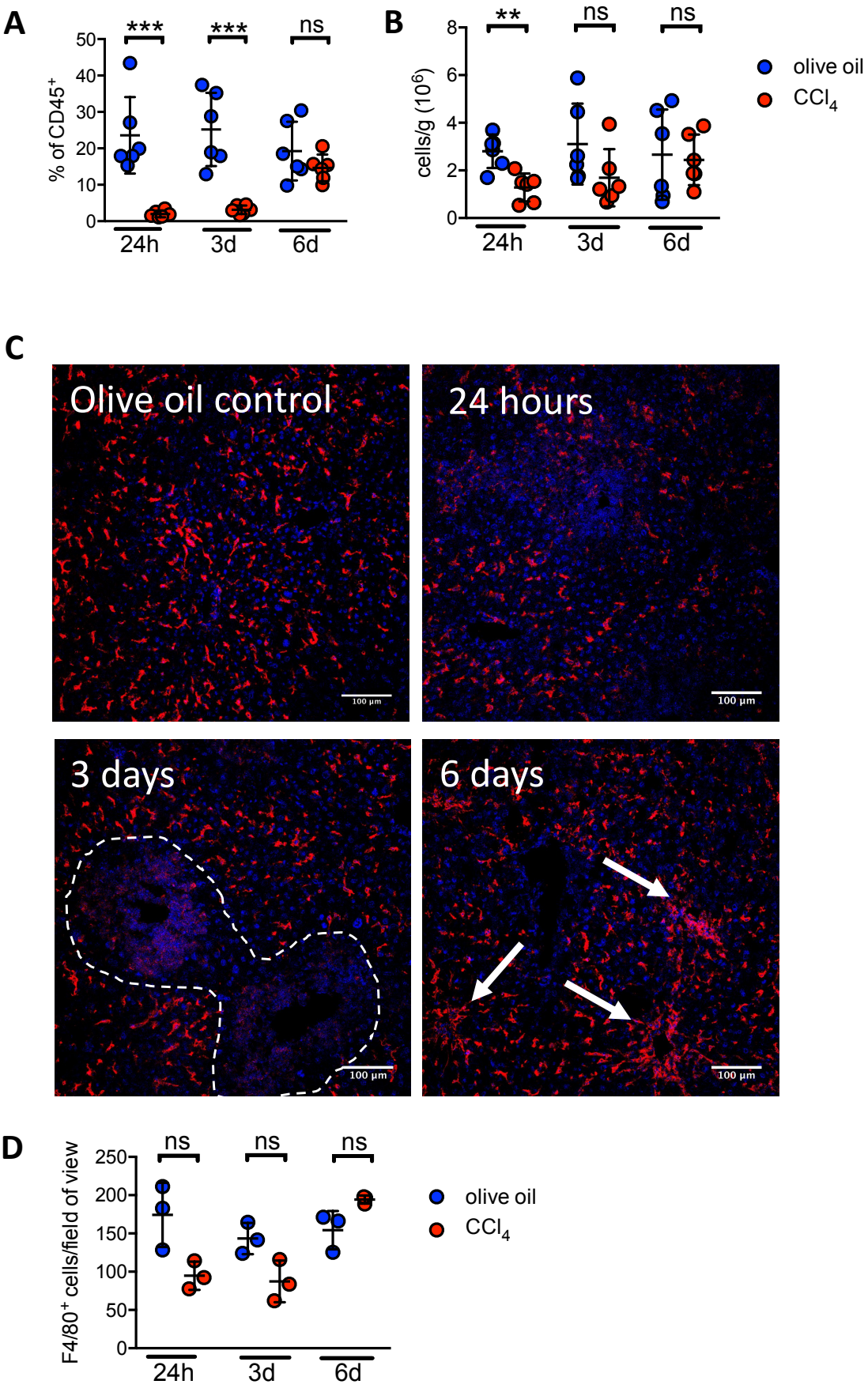
A
***
***
ns
% of CD45+
50
40
30
20
10
0
24h
3d
6d
B
**
ns
ns
cells/g (10^6)
8
6
4
2
0
24h
3d
6d
olive oil
CCl4
C
Olive oil control
24 hours
3 days
6 days
100 µm
D
ns
ns
ns
F4/80+ cells/field of view
250
200
150
100
50
0
24h
3d
6d
olive oil
CCl4

Figure 6.3 Acute loss and recovery of KC following acute CCl_4. (A) Frequency of total F4/80^{hi}CD11b^{lo} KC population expressed as a % of the total CD45^{+}CD31^{-} leukocyte population and **(B)** total number of F4/80^{hi}CD11b^{lo} KC per gram of liver at each time point following acute CCl_4 or olive oil determined by flow cytometry. n=6 per group from 2 experiments, mean ± SD. **(C)** Representative confocal images of cryosectioned livers at each time point following CCl_4 and a representative olive oil control stained with F4/80 (red) and DAPI (blue). White arrows indicate vessel-associated clusters and dotted region indicates area of loss of F4/80^{bright} cells. **(D)** Quantification of total number of F4/80^{bright} cells per field of view (FoV). 10 FoV counted per liver, each point represents the mean for each liver. Graph shows mean ± SD for each group. n=3 per group from one of the two experiments shown in A and B. **p<0.01 ***p<0.001 (multiple *t* tests with Holm-Sidak correction).

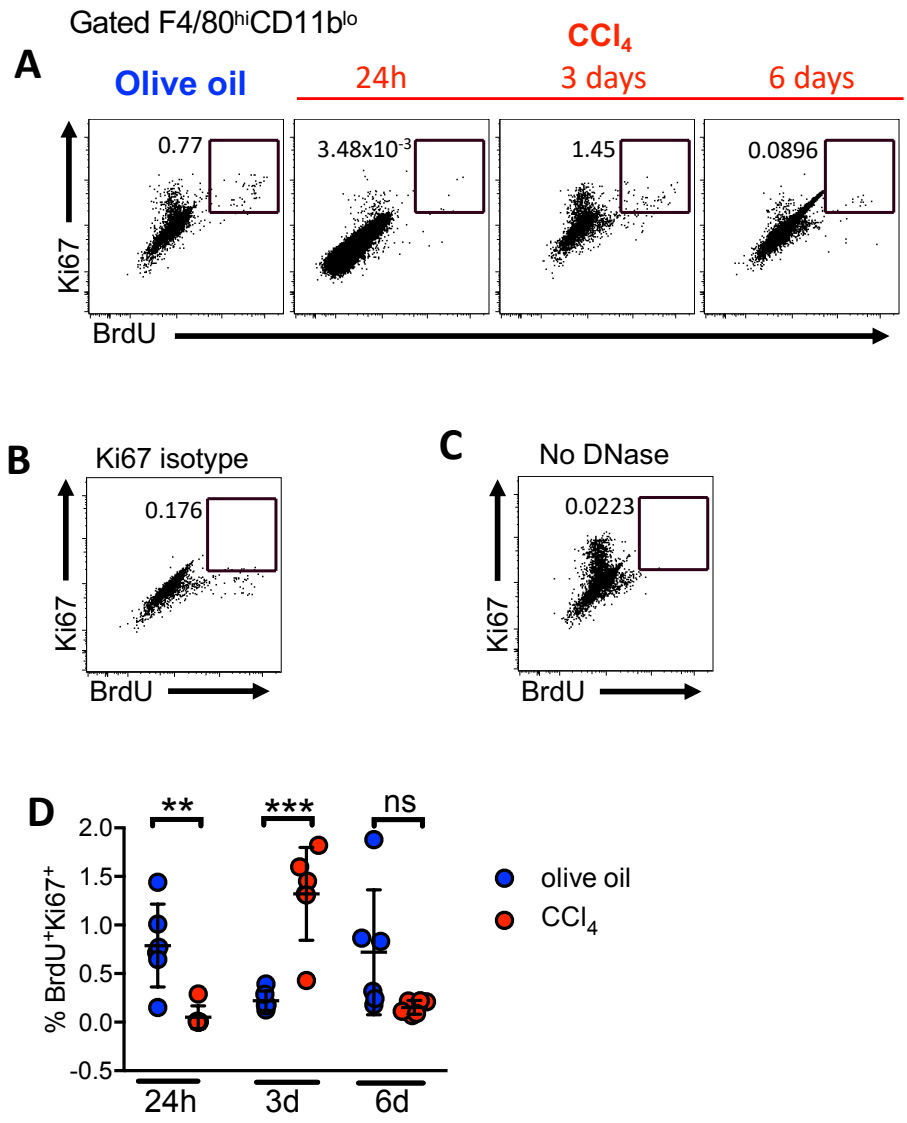

Figure 6.4 Proliferation of KC following acute CCl_4. (A) Representative flow plots showing $BrdU^+Ki67^+$ double positive cells on gated $F4/80^{hi}CD11b^{lo}$ KC and **(D)** replicate data at each time point after CCl_4 injury and a representative olive oil control. **(B)** Ki67 antibody isotype control sample and **(C)** a 'no DNase' sample as a negative control for BrdU incorporation. n=6 per group from 2 experiments, mean ± SD. **p<0.01 ***p<0.001 (multiple *t* tests with Holm-Sidak correction).

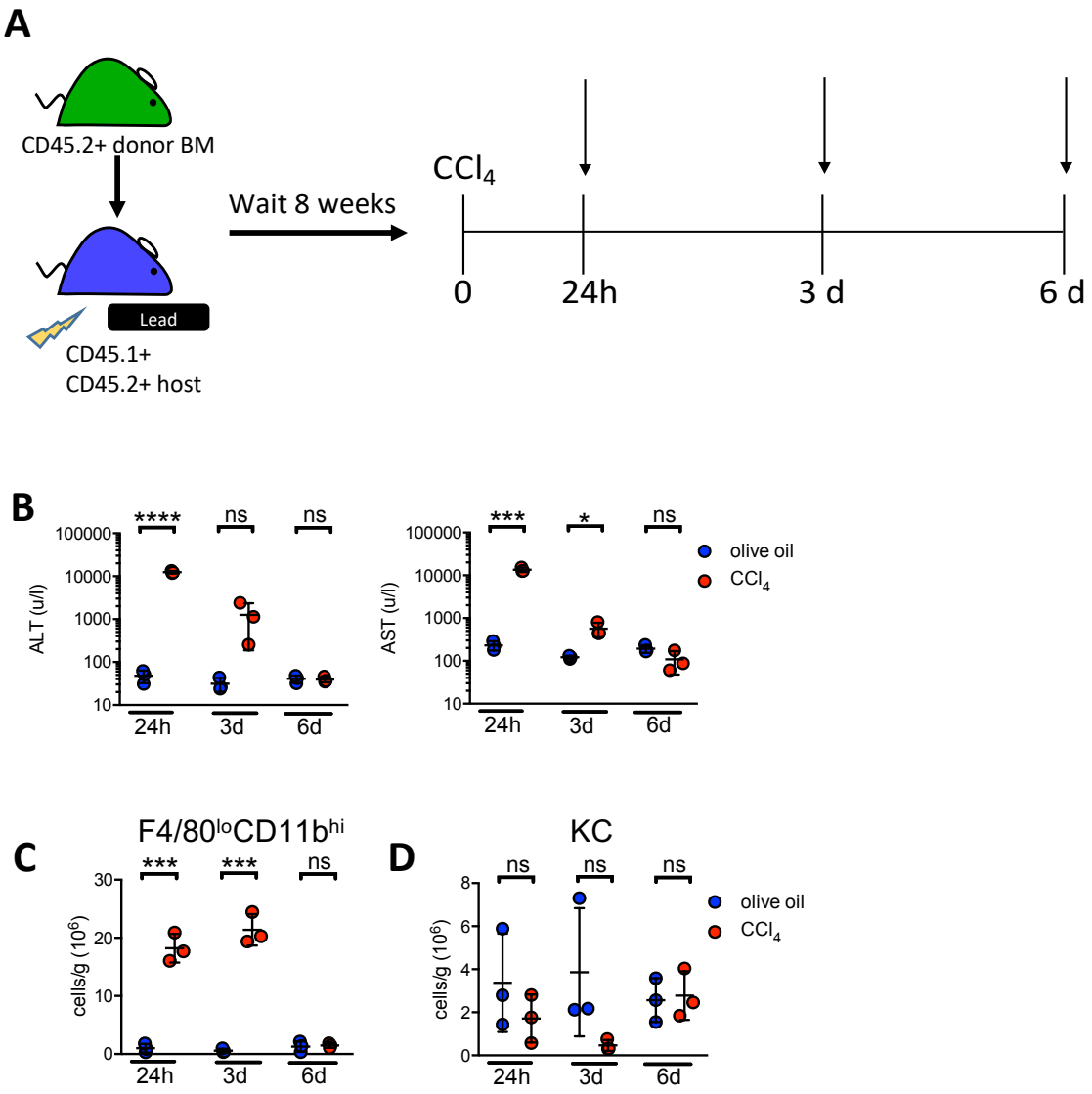

Figure 6.5 Liver injury and myeloid cell numbers in protected BM chimeric mice. (A) CD45.1$^+$ CD45.2$^+$ host mice were irradiated with the upper body shielded by lead then reconstituted with bone marrow from CD45.2$^+$ donor mice. Mice were left for 8 weeks before being given a single dose of CCl_4 or olive oil control, and livers were assessed 24 hours, 3 and 6 days after injection. **(B)** serum ALT (left) and AST (right) levels. **(C)** Total number of F4/80^{lo}CD11b^{hi} myeloid cells and **(D)** KC per gram of liver. n=3 per group from a single experiment, mean ± SD. *p<0.05 ***p<0.001 ****p<0.0001 (multiple *t* tests with Holm-Sidak correction).

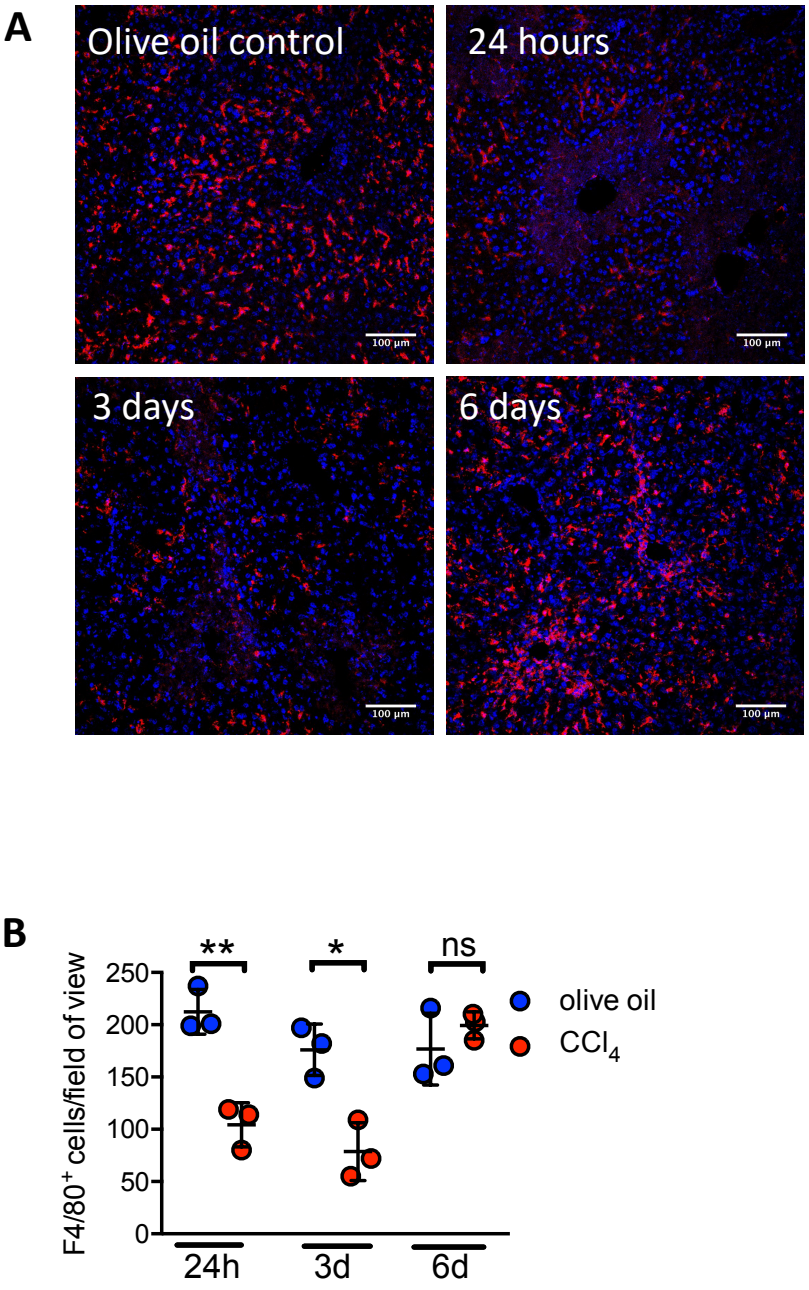

Figure 6.6 Changes in KC number in chimeric mice by immunofluorescence. (A) Representative confocal images of cryosectioned livers at each time point following CCl_4 and an olive oil control stained with F4/80 (red) and DAPI (blue). **(B)** Quantification of total number of F4/80^{bright} cells per field of view (FoV). 10 FoV counted per liver, each point represents the mean for each liver. Graph shows mean ± SD for each group. n=3 per group. *p<0.05 **p<0.01 (multiple *t* tests with Holm-Sidak correction).

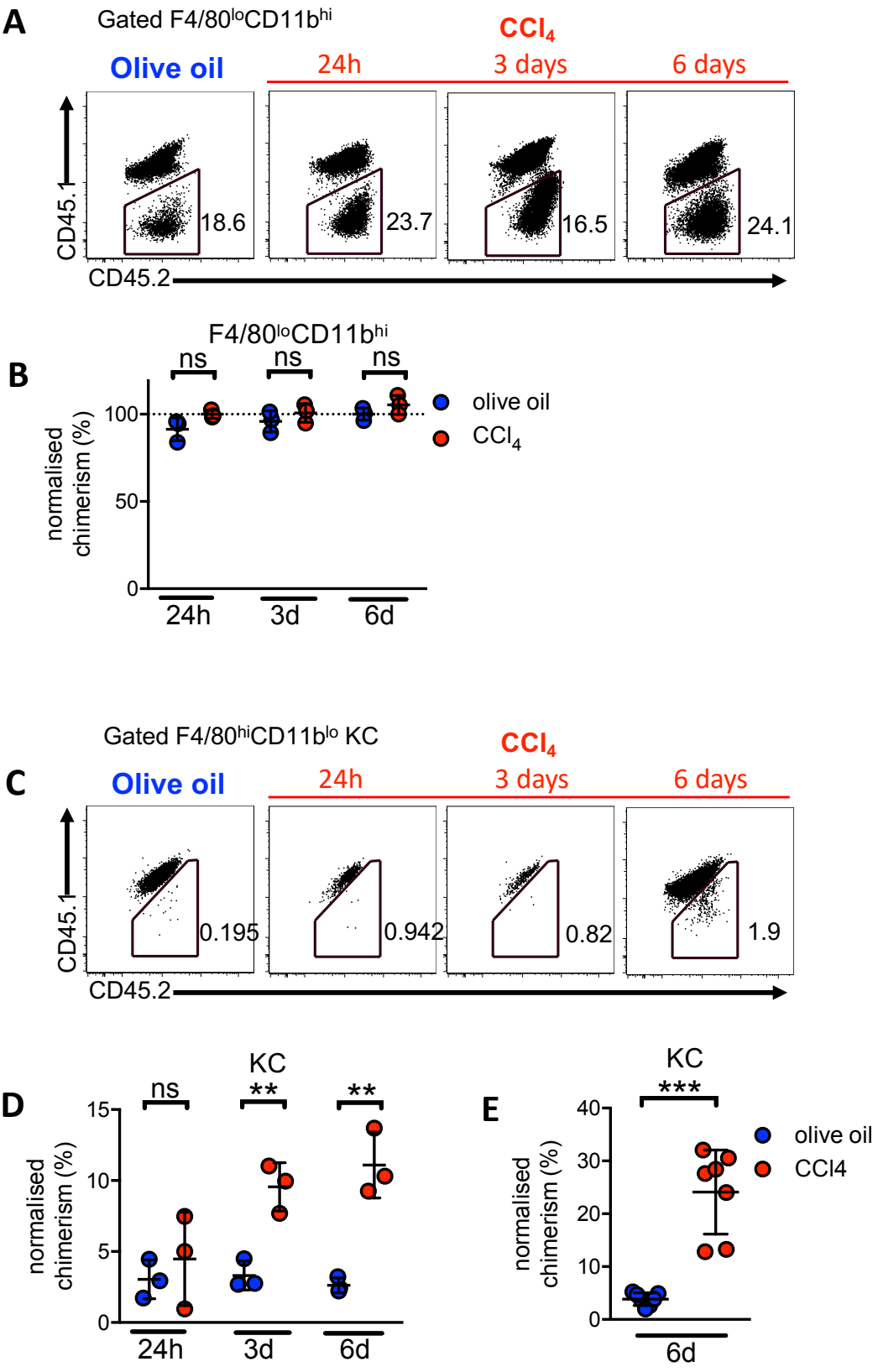
A
Gated F4/80loCD11bhi
CCl4
Olive oil
24h
3 days
6 days
CD45.1
CD45.2
18.6
23.7
16.5
24.1
B
F4/80loCD11bhi
ns
ns
ns
normalised chimerism (%)
100
50
0
24h
3d
6d
olive oil
CCl4
C
Gated F4/80hiCD11blo KC
CCl4
Olive oil
24h
3 days
6 days
CD45.1
CD45.2
0.195
0.942
0.82
1.9
D
KC
ns
**
**
normalised chimerism (%)
15
10
5
0
24h
3d
6d
E
KC
***
normalised chimerism (%)
40
30
20
10
0
6d
olive oil
CCl4

Figure 6.7 Emergence of donor BM recruited cells in the KC population. (A) Representative plots of CD45.2 vs CD45.1 pre-gated on F4/80^{lo}CD11b^{hi} myeloid cells or **(C)** F4/80^{hi}CD11b^{lo} KC at each time point after CCl_4 injury and a representative olive oil control. Gates show donor cells. **(B)** Chimerism in the F4/80^{lo}CD11b^{hi} population or **(D)** F4/80^{hi}CD11b^{lo} KC population normalized to Ly6C^{hi} monocytes in blood. n=3 per group from one experiment, mean $\pm$ SD. **p<0.01 (multiple *t* tests with Holm-Sidak correction). **(E)** Repeat data from subsequent experiments showing KC chimerism at the day 6 time point only. n=7 per group pooled from two independent experiments. ***p<0.001 (unpaired *t* test with Welch's correction).

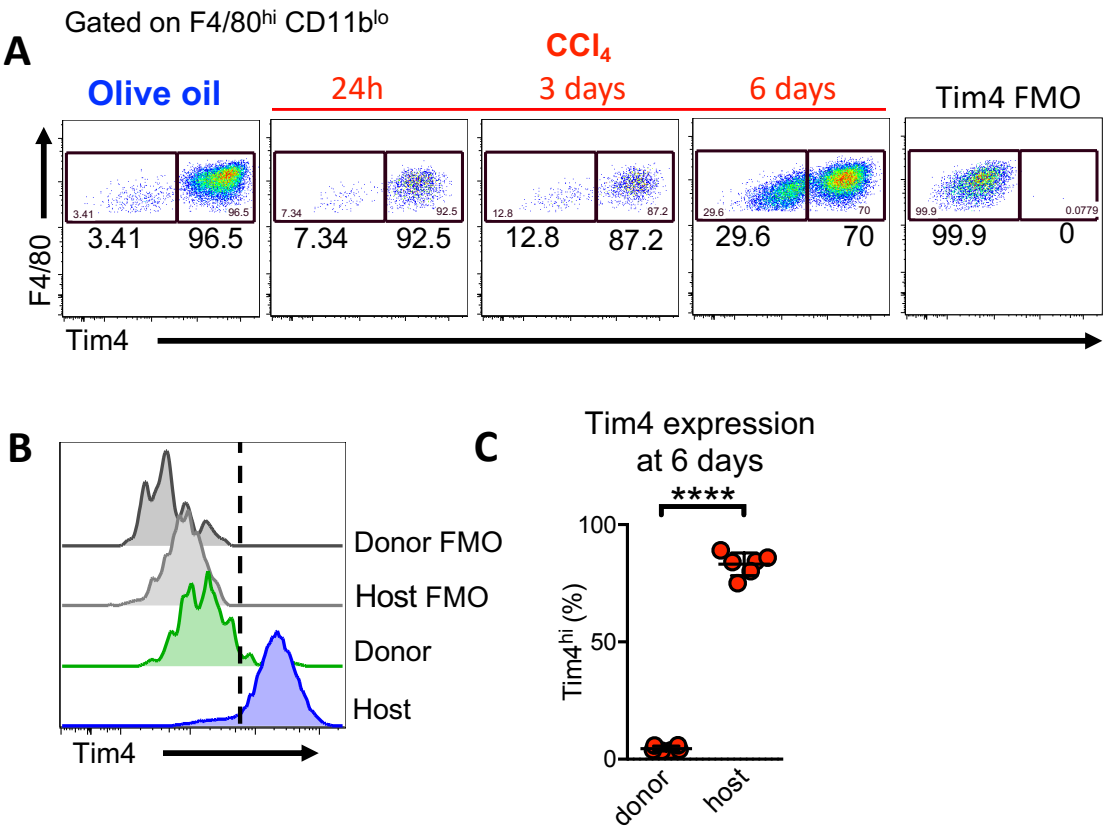
A
Gated on F4/80hi CD11blo
CCl4
Olive oil
24h
3 days
6 days
Tim4 FMO
F4/80
Tim4
3.41
96.5
7.34
92.5
12.8
87.2
29.6
70
99.9
0
B
Donor FMO
Host FMO
Donor
Host
Tim4
C
Tim4 expression at 6 days
****
Tim4hi (%)
100
50
0
donor
host
D
Gated on F4/80hiCD11blo
CCl4
Olive oil
24h
3 days
6 days
Clec4f FMO
Tim4
Clec4f
22.8
25.4
27.8
26.4
0.235
E
Donor FMO
Host FMO
Donor
Host
Clec4f
F
mApple-ve
Tim4lo
Tim4hi
Csf1r-mApple

Figure 6.8 Analysis of Tim4, Clec4f and CSF1R expression in recruited mϕ. (A) Representative flow plots of Tim4 and **(D)** Clec4f expression pre gated on F4/80^{hi}CD11b^{lo} KC. Gates show proportions of Tim4^{+} and Tim4^{-} KC at each time point and a representative olive oil control in non-chimeric C57BL/6 WT mice. Representative of n=6 per group from 2 experiments. **(B)** Representative Tim4 expression in donor and host KC and respective FMO controls in livers of partial BM chimeric mice at day 6 following injury when donor KC are present. **(C)** % of donor and host KC that were Tim4^{hi} at day 6. Representative of n=10 from 3 experiments. **(E)** Representative Clec4f expression in donor and host KC and respective FMO controls in livers of partial BM chimeric mice at day 6 following injury. Representative of n=6 from 2 experiments. **(F)** Representative mApple expression by Tim4^{hi} (KC) and Tim4^{lo} (recruited mϕ) F4/80^{hi}CD11b^{lo} cells in *csf1r*-mApple mice and mApple^{-} littermate control at day 6 following injury. Representative of n=5 (mApple^{+}) and n=2 (mApple^{-} control) from 2 experiments.

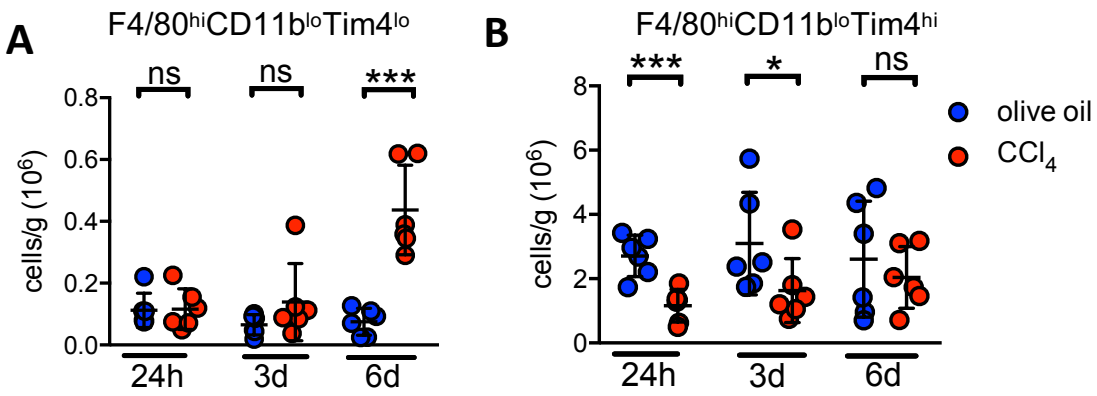

Figure 6.9 Changes in numbers of Tim4^{hi} KC and Tim4^{lo} recruited mϕ following acute CCl_4. (A) Total number of F4/80^{hi}CD11b^{lo}Tim4^{lo} recruited mϕ and **(B)** F4/80^{hi}CD11b^{lo}Tim4^{lo} KC per gram of liver following acute CCl_4 or olive oil control. NB these are more detailed analysis of cell number from the same experiments shown in fig. 6.6 in light of the finding that a proportion of the presumed 'KC' was a recruited mϕ with a distinct phenotype from KC. n=6 per group from two experiments, mean ± SD. *p<0.05 ***p<0.001 (multiple *t* tests with Holm-Sidak correction).

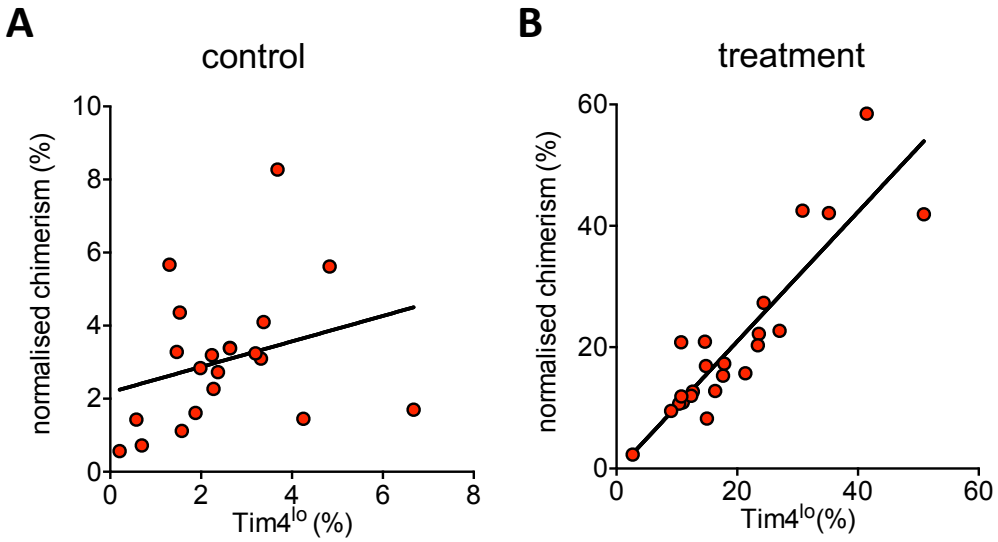

Figure 6.10 Tim4 as a marker of recent bone marrow origin. (A) Linear regression plot of % Tim4^{lo} of F4/80^{hi}CD11b^{lo} cells versus normalized chimerism of F4/80^{hi}CD11b^{lo} cells in partial BM chimeras used as controls across multiple experiments (ie given PBS s.c. or olive oil i.p.) R^2=0.08204, p=0.2801. n=19 pooled from 6 experiments. **(B)** Linear regression plot as in A but for partial BM chimeras given 'treatment' (ie CSF1-Fc s.c. or CCl_4 i.p.). R^2=0.8007, p<0.0001. n=23 from 6 experiments.

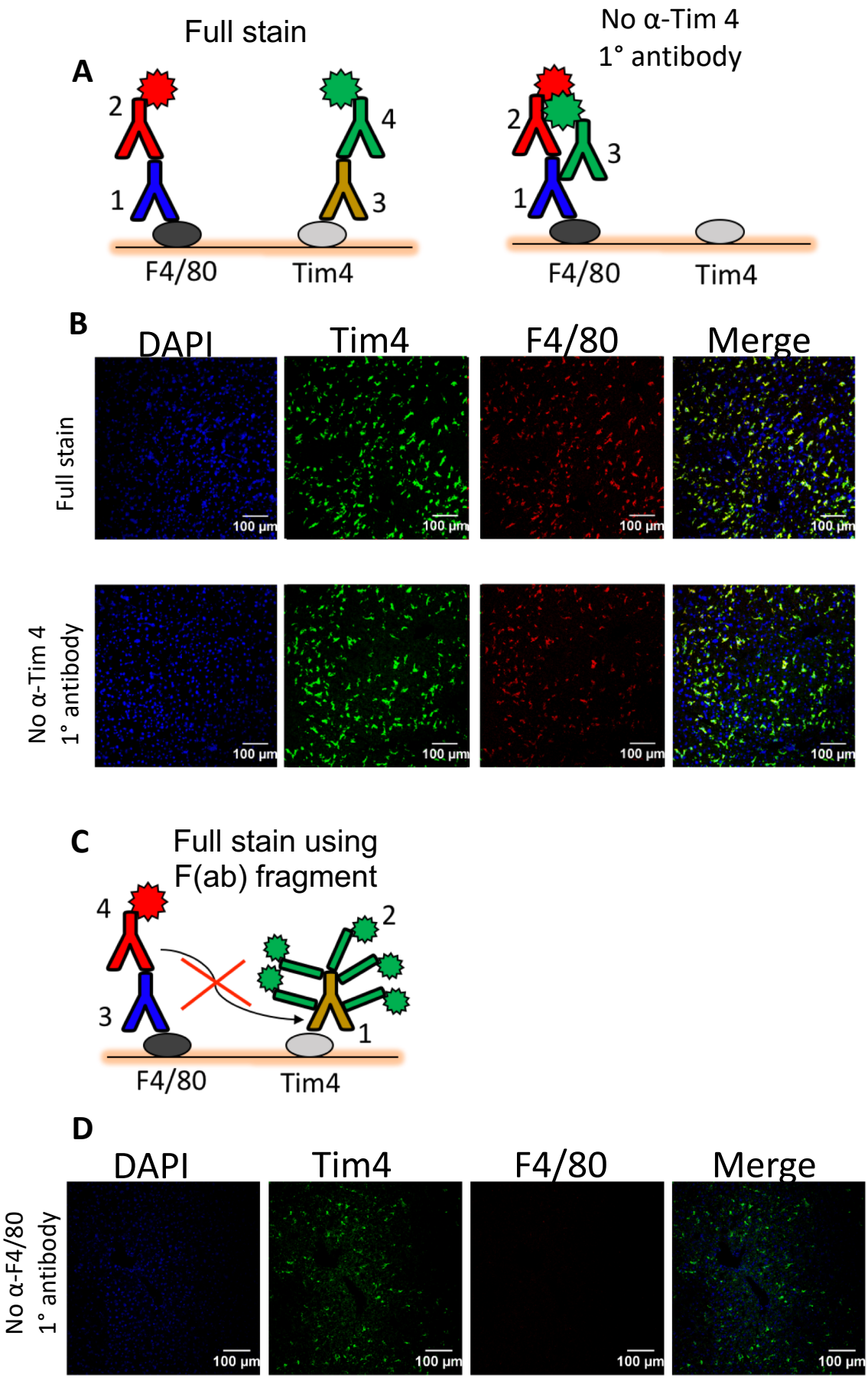
A
Full stain
2
1
4
3
F4/80
Tim4
No α-Tim 4
1° antibody
2
3
1
F4/80
Tim4
B
DAPI
Tim4
F4/80
Merge
Full stain
No α-Tim 4
1° antibody
100 µm
C
Full stain using
F(ab) fragment
4
3
2
1
F4/80
Tim4
D
DAPI
Tim4
F4/80
Merge
No α-F4/80
1° antibody
100 µm

Figure 6.11 Development of F4/80 and Tim4 dual immunofluorescence staining protocol. (A) Schematic for primary and secondary antibodies used in pilot staining protocol and order of addition of antibodies. Cross reactivity can occur when the anti-Tim4 primary antibody is omitted between the fluorophore-conjugated secondary and the anti-F4/80 primary antibody **(B)** No Tim4 primary antibody staining control slide which indicates non-specific cross reactivity between the secondary antibody intended to detect Tim4 with the F4/80 primary antibody. **(C)** Schematic for revised protocol using Fab fragment secondary to saturate all possible binding sites on the primary antibody, to prevent cross reactivity. In this case note that the order of staining has been reversed from A, ie staining for Tim4 was carried out before staining for F4/80. **(D)** No F4/80 primary antibody staining control indicating that the Fab fragment successfully prevented any binding of the secondary intended to detect F4/80 with the Tim4 primary antibody. The staining and acquisition of images was performed by Aliz Owolabi and these images were presented within her undergraduate dissertation. However, the figure shown here has been created by me.

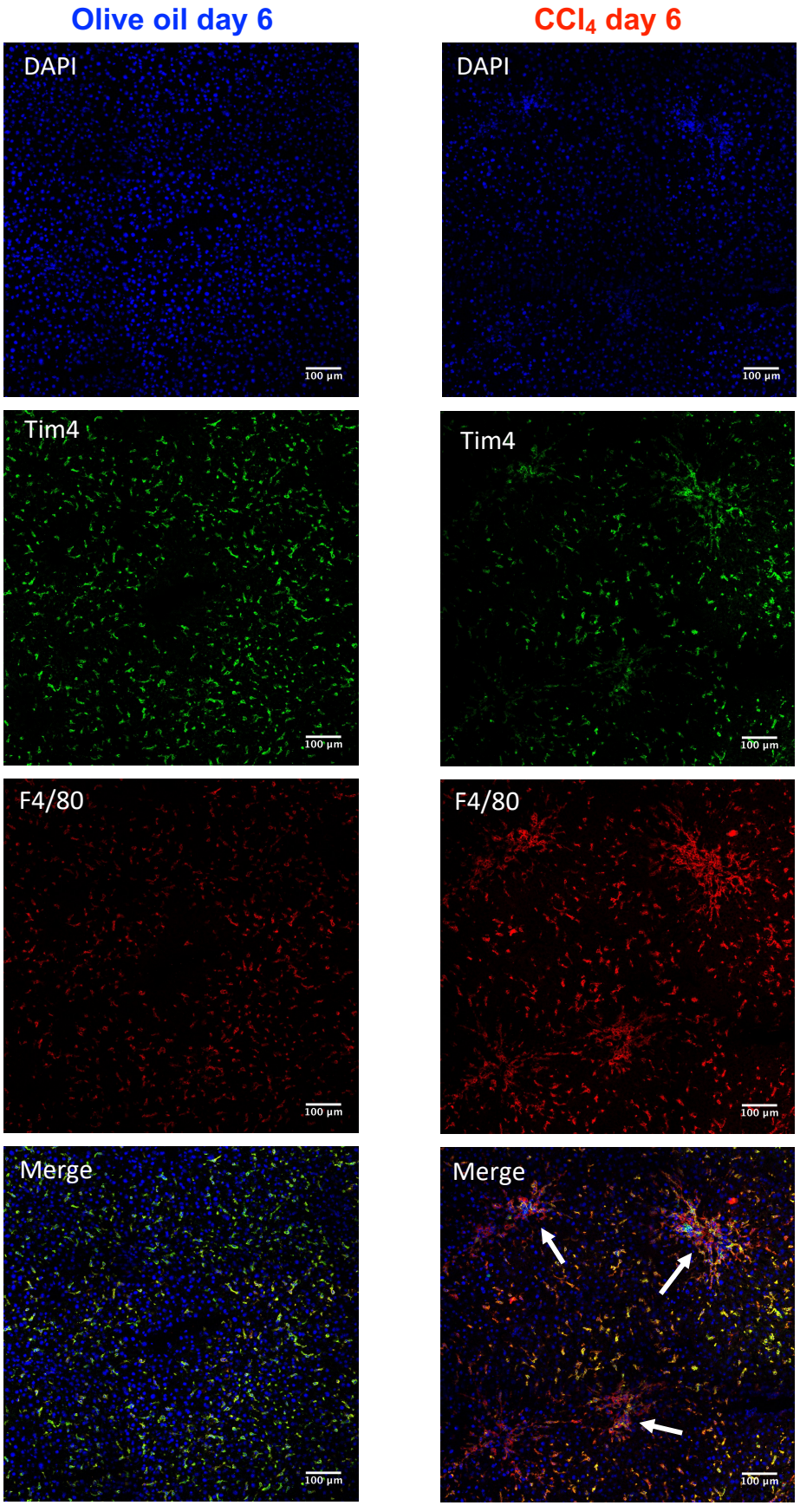
Olive oil day 6
CCl4 day 6
DAPI
DAPI
Tim4
Tim4
F4/80
F4/80
Merge
Merge
100 µm

Figure 6.12 Tim4 and F4/80 staining of acute CCl_4 injured livers. Representative confocal images of livers stained with DAPI (blue), Tim4 (green) and F4/80 (red) in an olive oil and CCl_4 treated mouse 6 days post acute injury. Arrows indicate clusters of $F4/80^{+}Tim4^{-}$ recruited mϕ. Images representative of n=9 per group (a mix of C57BL/6 and chimeric mice) from 3 independent experiments.

A

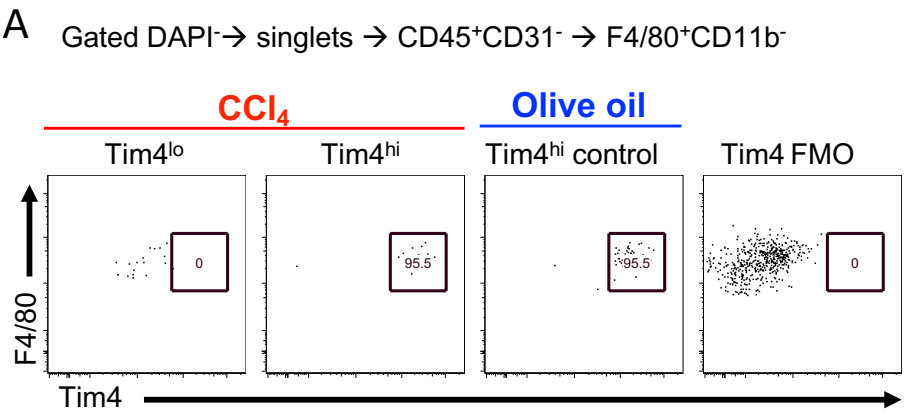

B

Sample	RNA conc. (ng/µl)	Total RNA (ng)	RNA quality score
Tim4^{lo} 1	3.883	46.596	9.9
Tim4^{lo} 2	3.662	43.944	9.5
Tim4^{lo} 3	6.708	80.496	9.6
Tim4^{lo} 4	6.470	77.640	9.0
Tim4^{hi} 1	5.928	71.136	7.2
Tim4^{hi} 2	6.060	72.720	8.1
Tim4^{hi} 3	5.648	67.776	8.3
Tim4^{hi} 4	0.087	1.044	NA
Tim4^{hi} control 1	6.815	81.780	9.1
Tim4^{hi} control 2	6.630	79.560	8.8
Tim4^{hi} control 3	5.388	64.656	8.8
Tim4^{hi} control 4	6.589	79.068	8.8

Figure 6.13 FACS sort and RNA extraction for NanoString gene comparison analysis. (A) Representative post-sort purity flow plots of F4/80^{hi}CD11b^{lo}Tim4^{lo} recruited mϕ and Tim4^{hi} KC after acute CCl_4 injury and Tim4^{hi} control KC after olive oil injection, and Tim4 FMO control sample. **(B)** Concentration, total amount and quality scores of RNA extracted from 50,000 sorted cells from each sample.

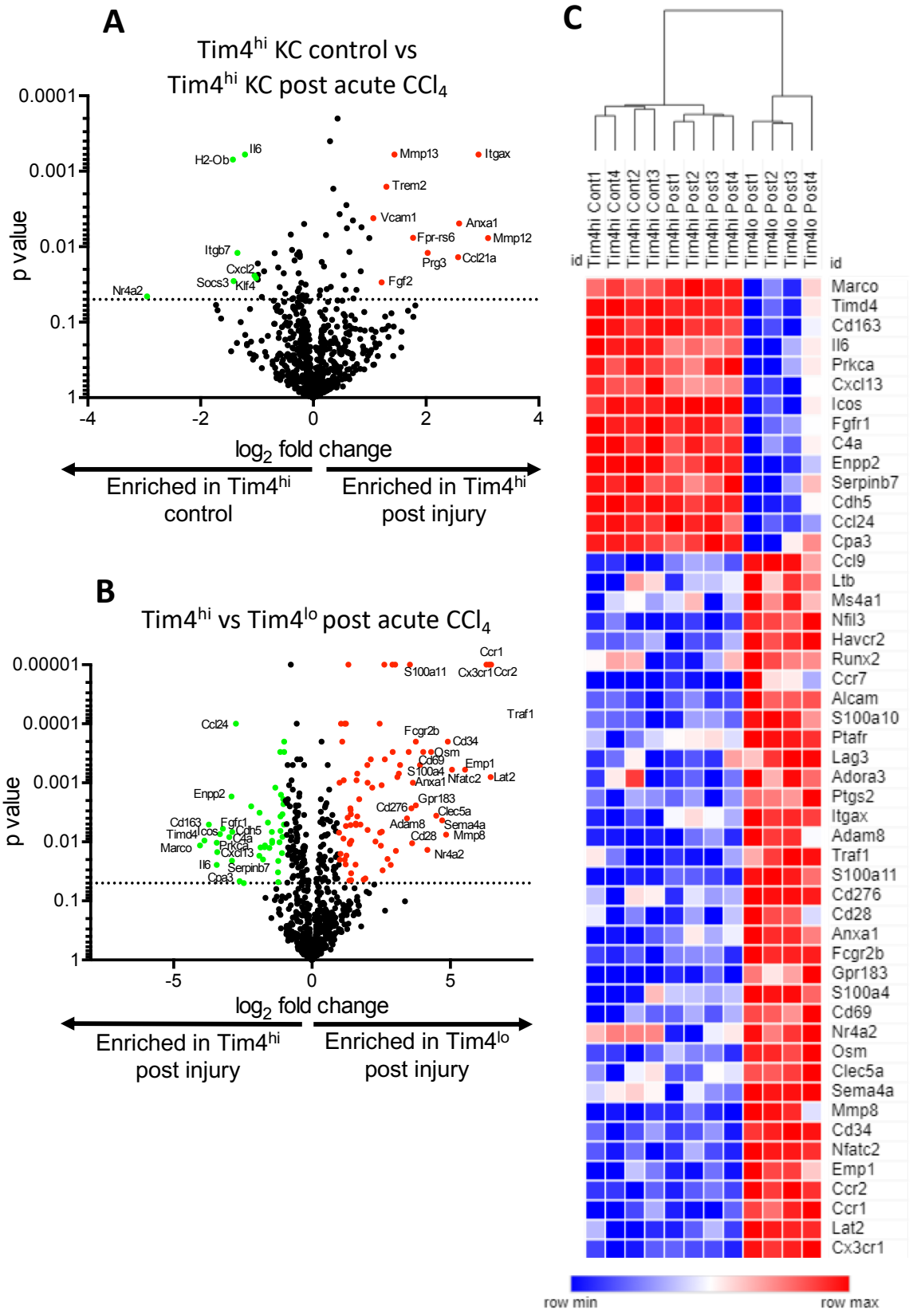
A
Tim4hi KC control vs
Tim4hi KC post acute CCl4
p value
0.0001
0.001
0.01
0.1
1
-4
-2
0
2
4
log2 fold change
Enriched in Tim4hi control
Enriched in Tim4hi post injury
H2-Ob
Il6
Mmp13
Itgax
Trem2
Vcam1
Anxa1
Fpr-rs6
Mmp12
Itgb7
Cxcl2
Prg3
Ccl21a
Socs3
Klf4
Fgf2
Nr4a2
B
Tim4hi vs Tim4lo post acute CCl4
p value
0.00001
0.0001
0.001
0.01
0.1
1
-5
0
5
log2 fold change
Enriched in Tim4hi post injury
Enriched in Tim4lo post injury
Ccr1
S100a11
Cx3cr1
Ccr2
Traf1
Ccl24
Fcgr2b
Cd34
Osm
Cd69
Emp1
S100a4
Anxa1
Nfatc2
Lat2
Enpp2
Gpr183
Cd276
Clec5a
Cd163
Fgfr1
Adam8
Sema4a
Timd4
Icos
Cdh5
Cd28
Mmp8
Cpa4
Marco
Prkca
Nr4a2
Cxcl13
Il6
Serpinb7
Cpa3
C
id
Tim4hi Cont1
Tim4hi Cont4
Tim4hi Cont2
Tim4hi Cont3
Tim4hi Post1
Tim4hi Post2
Tim4hi Post3
Tim4hi Post4
Tim4lo Post1
Tim4lo Post2
Tim4lo Post3
Tim4lo Post4
id
Marco
Timd4
Cd163
Il6
Prkca
Cxcl13
Icos
Fgfr1
C4a
Enpp2
Serpinb7
Cdh5
Ccl24
Cpa3
Ccl9
Ltb
Ms4a1
Nfil3
Havcr2
Runx2
Ccr7
Alcam
S100a10
Ptafr
Lag3
Adora3
Ptgs2
Itgax
Adam8
Traf1
S100a11
Cd276
Cd28
Anxa1
Fcgr2b
Gpr183
S100a4
Cd69
Nr4a2
Osm
Clec5a
Sema4a
Mmp8
Cd34
Nfatc2
Emp1
Ccr2
Ccr1
Lat2
Cx3cr1
row min
row max

Figure 6.14 NanoString gene comparison analysis 6 days after acute CCl_4. (A) Volcano plot of log_2 fold change versus p-value for expression of all 754 genes in control $Tim4^{hi}$ KC and $Tim4^{hi}$ KC and **(B)** in $Tim4^{hi}$ KC and $Tim4^{lo}$ recruited mϕ after injury. **(C)** Heat map of 50 most differentially expressed genes with fold change >2 and $p<0.05$ determined by *t* tests between $Tim4^{hi}$ KC and $Tim4^{lo}$ recruited mϕ, and expression in $Tim4^{hi}$ control samples for comparison. n=4 per group from a single experiment. Bioinformatic analysis was conducted by Dr Andrew Mason.

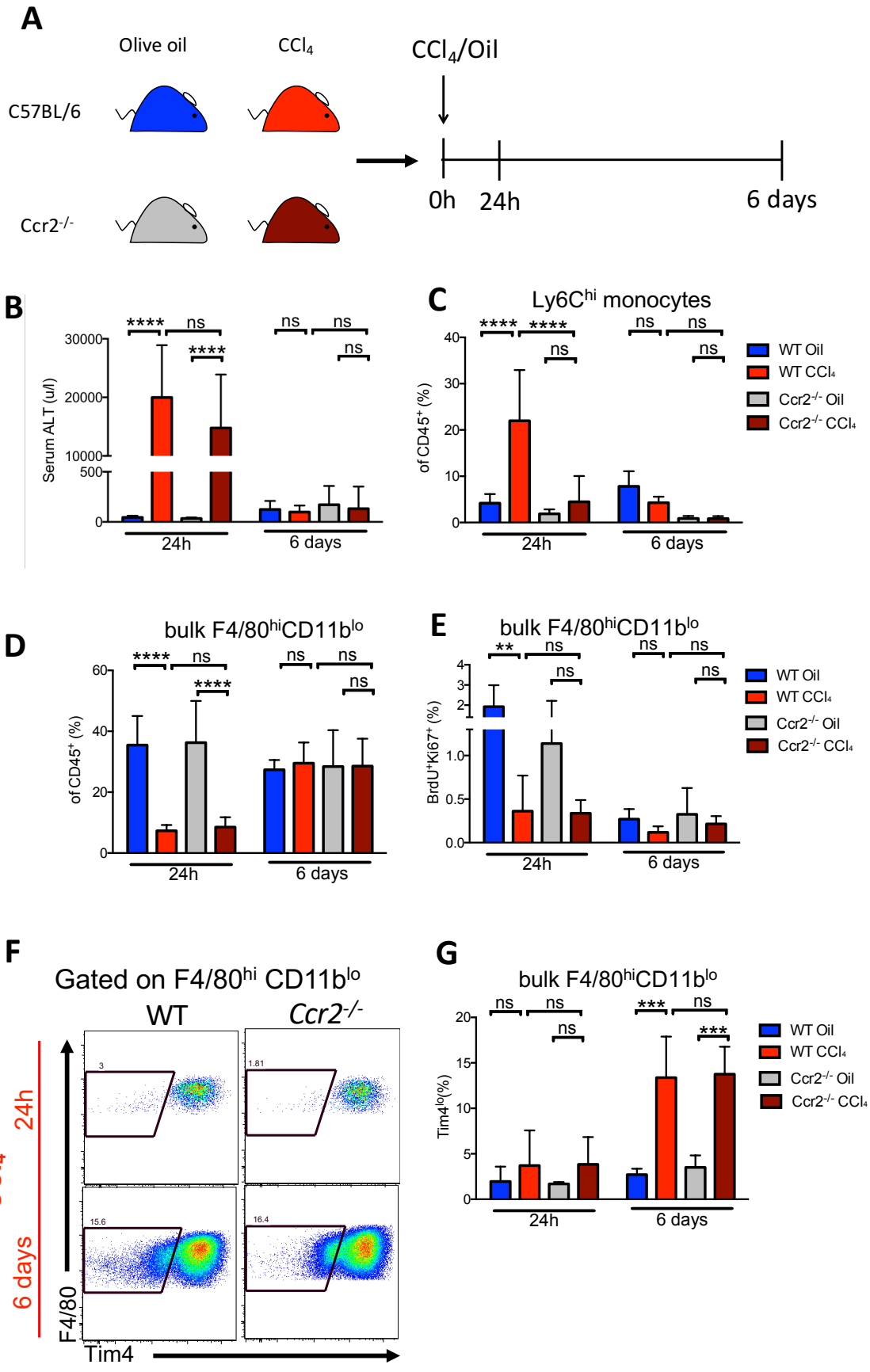
A
Olive oil
CCl4
CCl4/Oil
C57BL/6
Ccr2-/-
0h
24h
6 days
B
Serum ALT (u/l)
24h
6 days
C
Ly6Chi monocytes
of CD45+ (%)
WT Oil
WT CCl4
Ccr2-/- Oil
Ccr2-/- CCl4
D
bulk F4/80hiCD11blo
of CD45+ (%)
E
bulk F4/80hiCD11blo
BrdU+Ki67+ (%)
F
Gated on F4/80hi CD11blo
WT
Ccr2-/-
CCl4
24h
6 days
F4/80
Tim4
G
bulk F4/80hiCD11blo
Tim4lo(%)

Figure 6.15 Acute CCl_4 injury in *Ccr2*$^{-/-}$ mice. (A) Age and sex-matched C57BL/6J Crl and *Ccr2*$^{-/-}$ mice were given olive oil or CCl_4 and were analysed 24h and 6 days later. **(B)** Serum ALT. **(C)** Frequency of Ly6C^{hi} monocytes and **(D)** bulk F4/80^{hi}CD11b^{lo} as a proportion of CD45^{+} leukocytes. n=4-10 pooled from 3 independent experiments. **(E)** Percentage of bulk F4/80^{hi}CD11b^{lo} which were BrdU^{+}Ki67^{+} double positive. **(F)** Representative flow plots of Tim4 versus F4/80 in each group after CCl_4 treatment at day 6 post injury and **(G)** replicate data of percentage of KC which were Tim4^{lo}. n=3-6 pooled from 2 of the 3 experiments, as in repeat 3 BrdU and Ki67 staining was performed but samples were spilled prior to acquisition, and in repeat 2 Tim4 staining was performed but frequency that were Tim4^{lo} was extremely low across all groups at day 6 compared to all other experiments performed in this chapter and were therefore excluded from analysis. Graphs show mean ± SD. **p<0.01 ***p<0.001 ****p<0.0001 (Ordinary two way ANOVA with Tukey's multiple comparisons).

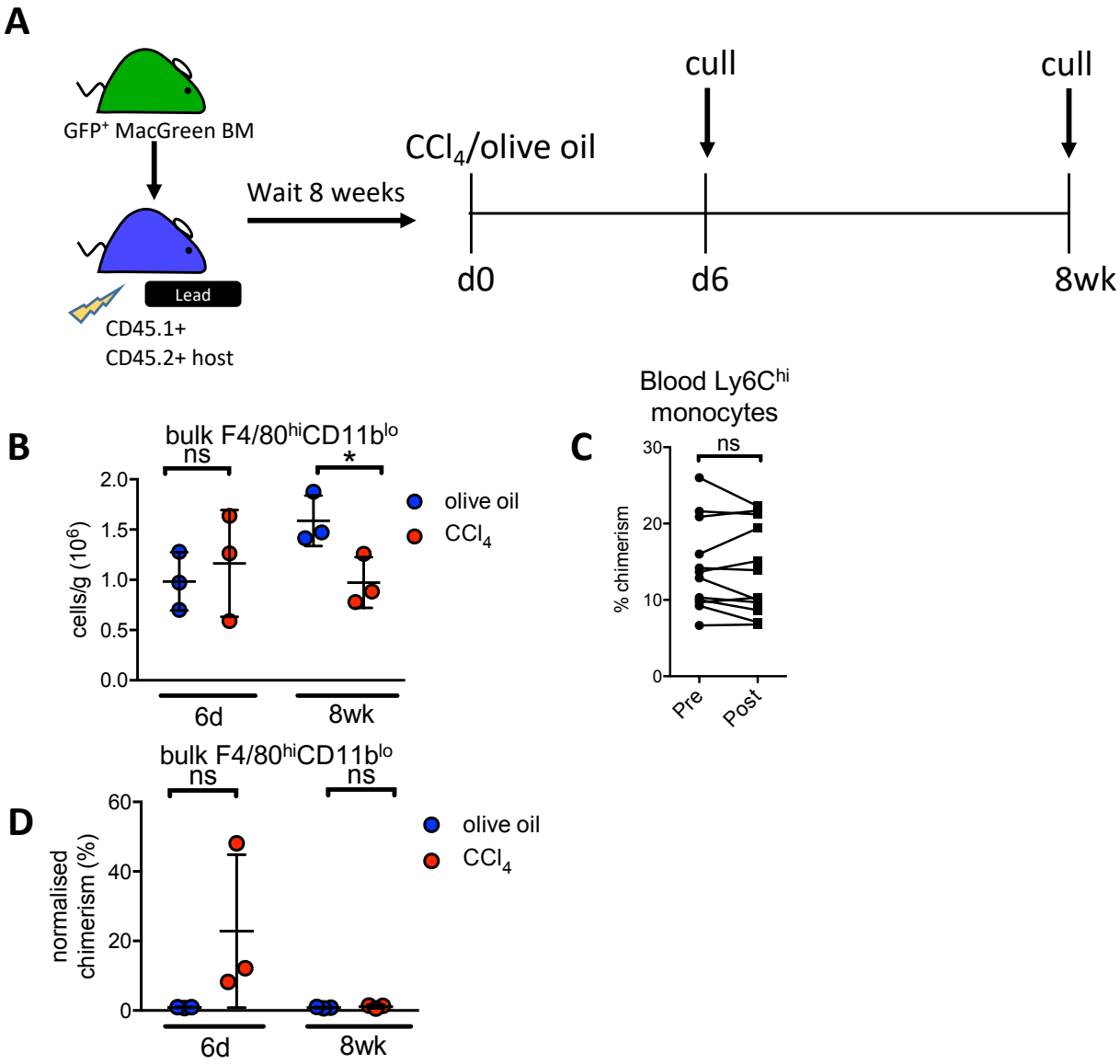

Figure 6.16 Effect of acute CCl_4 on long term maintenance of KC. (A) $CD45.1^+CD45.2^+$ host mice were irradiated with the upper body shielded by lead then reconstituted with $EGFP^+$ bone marrow from MacGreen donor mice. Mice were left for 8 weeks before being given a single dose of CCl_4 or olive oil control, and livers were assessed 6 days or 8 weeks later. **(B)** Total number of $F4/80^{hi}CD11b^{lo}$ cells per gram of liver. **(C)** $Ly6C^{hi}$ blood monocyte chimerism in all mice before and after olive oil and CCl_4. **(D)** Chimerism in the $F4/80^{hi}CD11b^{lo}$ population normalized to chimerism in $Ly6C^{hi}$ blood monocytes. n=3 per group from a single experiment, mean ± SD. **p<0.01 (multiple *t* test with Holm-Sidak correction), except (C) (paired *t* test).

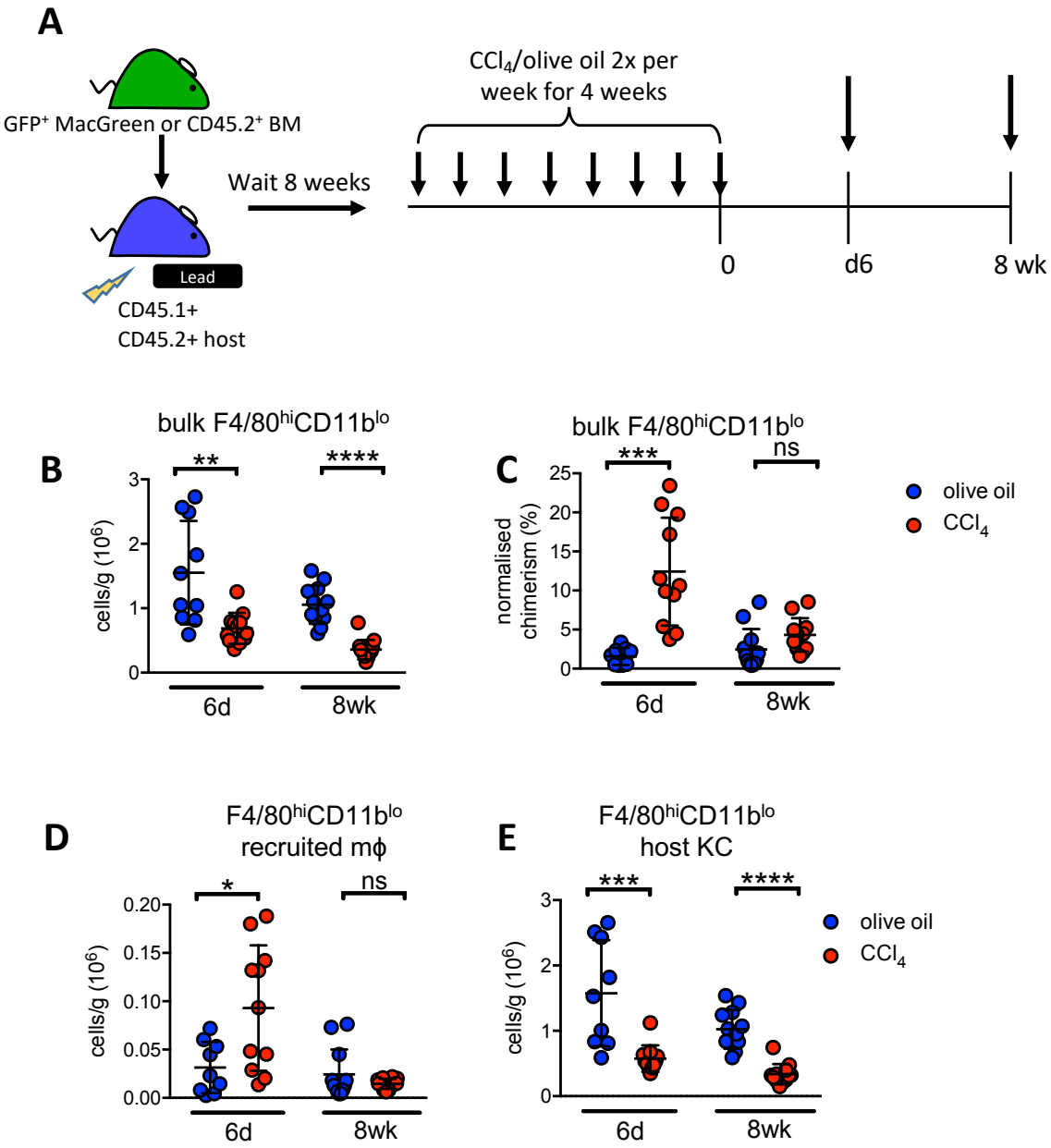

Figure 6.17 Effect of chronic CCl_4 on long term maintenance of KC. (A) CD45.1$^+$CD45.2$^+$ host mice were irradiated with the upper body shielded by lead then reconstituted with EGFP$^+$ bone marrow from MacGreen or CD45.2$^+$ donor mice. Mice were left for 8 weeks before being given CCl_4 or olive oil control twice a week for 4 weeks, and livers were assessed 6 days or 8 weeks following the final dose. **(B)** Total number of F4/80^{hi}CD11b^{lo} cells per gram of liver. **(C)** Chimerism in the F4/80^{hi}CD11b^{lo} population normalized to chimerism in blood Ly6C^{hi} monocytes. **(D)** Total number of F4/80^{hi}CD11b^{lo} recruited mϕ calculated by normalising the number of donor cells in the F4/80^{hi}CD11b^{lo} to the maximum chimerism in Ly6C^{hi} monocytes in blood. **(E)** Total number of F4/80^{hi}CD11b^{lo} host macrophages calculated by subtracting the number of recruited mϕ shown in D from the total number shown in A . n= 9-12 per group pooled from 3 independent experiments, mean± SD *p<0.05 **p<0.01 ***p<0.001 ****p<0.0001 (multiple *t* test with Holm-Sidak correction).

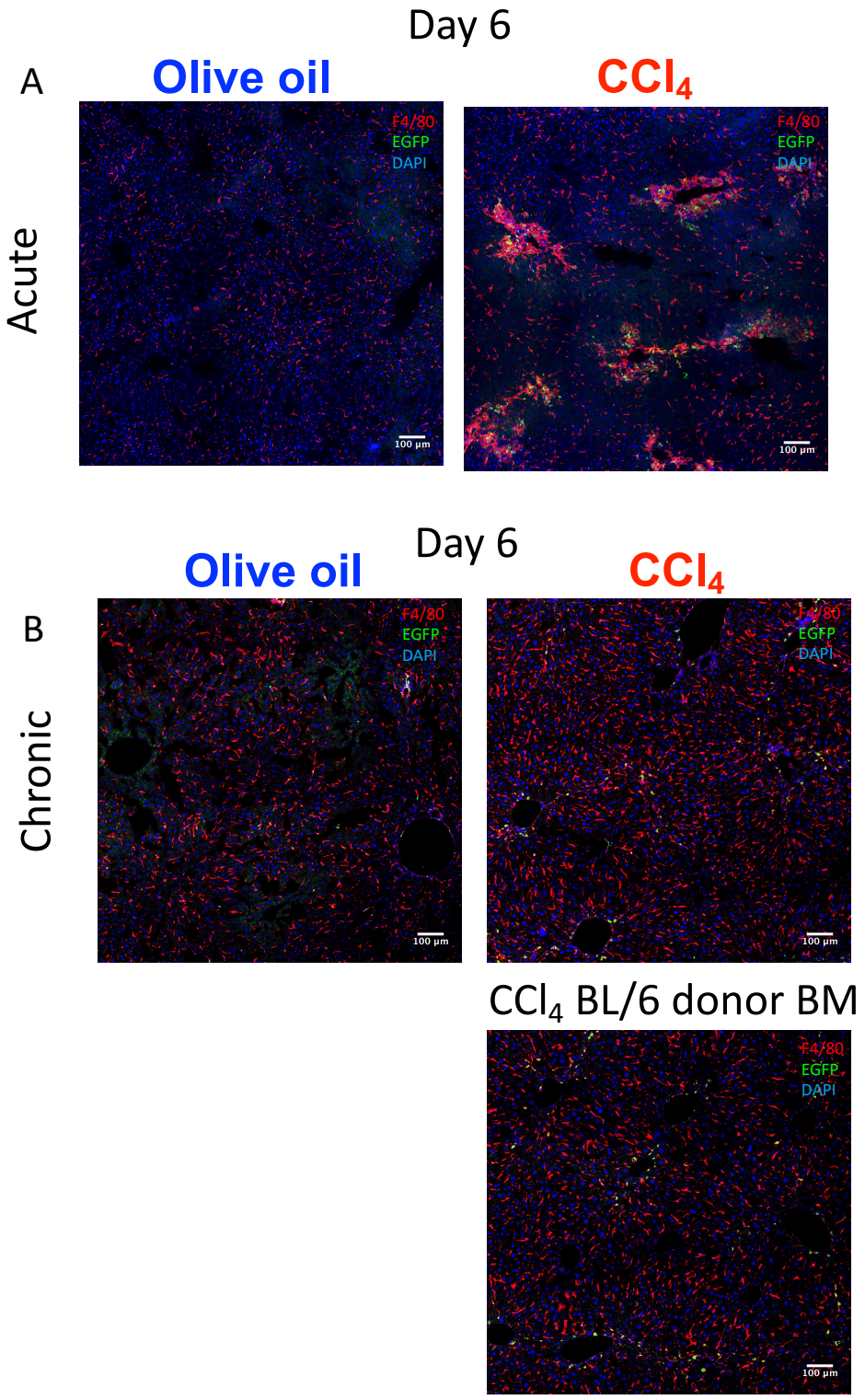

Figure 6.18 Unsuccessful imaging of GFP fluorescence in MacGreen donor BM chimeras. (A) Representative confocal images of liver stained with DAPI (blue), F4/80 (red) and endogenous EGFP fluorescence (green) in olive oil and CCl_4 treated mice 6 days post acute and **(B)** chronic injury. Representative of n=3 per group. Also **(B)**, fluorescence in the GFP imaging channel in a control mouse which received C57BL/6 CD45.2$^+$ donor bone marrow and CCl_4, n=1.

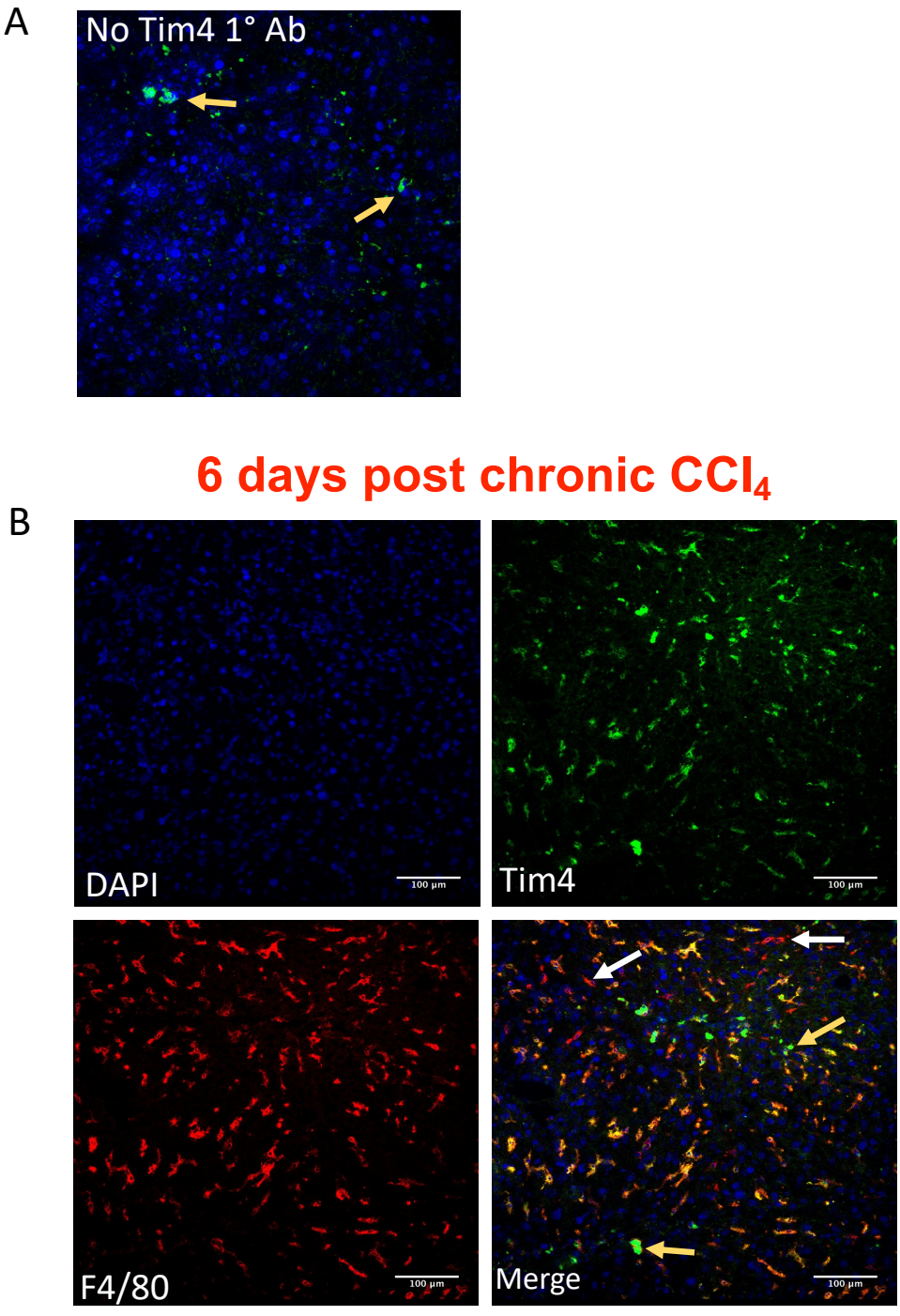

Figure 6.19 Tim4 and F4/80 staining of chronic CCl_4 injured livers. (A) No Tim4 primary antibody staining control slide. **(B)** Representative confocal images of liver stained with DAPI (blue), Tim4 (green) and F4/80 (red) and a merged image 6 days post chronic CCl_4-driven injury. Yellow arrows indicate autofluorescence in the GFP imaging channel and white arrows indicate genuine $F4/80^+$ $Tim4^-$ recruited mϕ. Representative of n=4 from a single experiment.

6.4 Discussion

In this chapter I have shown that a reduction in the number of KC in the liver following both acute and chronic injury does not lead to their replenishment by monocyte-derived macrophages. Proliferation, at least in the acute setting may account for their return to normal numbers, but following chronic injury, KC number was permanently reduced. I have identified a population of recruited cells present at 6 days after acute and chronic injury which acquired an F4/80^{hi}CD11b^{lo} phenotype but did not express the KC markers Tim4 or Clec4f. These cells were short-lived in the liver, and did not convert into self-renewing KC. These recruited macrophages were spatially distinct from F4/80^{hi}CD11b^{lo}Tim4^{hi} KC following acute injury, but this was less obvious following chronic injury. The recruited macrophages clustered around vessels during the repair phase following acute injury, and expressed genes associated with cell adhesion, cytokine, chemokine and growth factor signalling and ECM remodelling, suggestive of a role in tissue repair and resolution of injury.

6.4.1 Reduction in KC number following acute injury

Through a combination of flow cytometric and imaging techniques I was able to show that there was a ~50% reduction in total KC numbers by 24 hours after a single dose of CCl_4. The loss of F4/80^{+} cells on immunofluorescent liver sections mirrors the loss seen previously following APAP-driven injury (Dambach et al. 2002). In their study, Dambach *et al.* argue that activated KC down-regulate F4/80 which may explain why they appeared to be reduced in number on liver sections (Dambach et al. 2002). However, in my study I also stained liver sections for Tim4 and although I did not quantify the loss of Tim4^{+} cells on sections, there also appeared to be loss of Tim4 staining in the necrotic areas. By flow cytometry, the total number of KC defined as F4/80^{hi}CD11b^{lo}Tim4^{hi} was also reduced by around 50%, and in chimeras there was no 'appearance' of an F4/80^{lo} macrophage population of largely host origin which would account for the embryonic KC population having simply down regulated F4/80. Thus it appears most likely that following CCl_4-driven acute liver injury KC are lost from the liver, which is in agreement with data from other studies which demonstrated a loss in frequency of KC following APAP-driven acute liver injury (Holt et al. 2008; Zigmond et al. 2014; Mossanen et al. 2016). It is unclear where these 'disappearing' cells go. One possibility is that those are in the vicinity of the liver damage simply die *in situ* through necrosis as collateral damage. In support of this idea, staining of liver sections using PAS revealed areas

of necrosis surrounding blood vessels, and there was also loss of F4/80^{+} cells surrounding vessels at 24 hours post injury, which appeared to be the necrotic areas as there was a dense cloud of DAPI staining in these regions. Additional staining with propidium iodide would confirm definitively that loss of F4/80^{+} cells was in the necrotic area. Additionally, KC may die through apoptosis, and I cannot rule out the possibility that F4/80^{+} cells were not also lost in areas where there was no necrotic damage without more sophisticated analysis, for example using caspase 3 staining to assess apoptosis (Porter et al. 1998). Alternatively, loss of F4/80^{+} cells could be due to their migration out of the liver, rather than cell death. Indeed, alveolar macrophages have been shown to migrate from the lung to the draining lymph node following bacterial infection (Kirby et al. 2009). Thus rather than being simply collateral damage, the 'disappearance' of KC through apoptosis or migration might serve to trigger the initial immune response, either through local release of immune factors in the liver or by carrying antigen to lymph nodes.

It was evident that the KC population returned to steady state size by 6 days after an acute CCl_4 injury. A small spike in proliferation of KC at day 3 that occurred before emergence of the F4/80^{hi}CD11b^{lo}Tim4^{lo} recruited mϕ, suggests the remaining 50% of KC of embryonic lineage underwent self-renewal to restore the population. However, the level of proliferation detected in KC at day 3 following injury appeared relatively minor. It is possible that I missed the peak of elevated proliferation with the chosen time points. It is also notable that the level of KC proliferation also fluctuated in the olive oil control mice across the time course, despite the fact that all mice were given BrdU on the same day, and livers were harvested, stained and run through the flow cytometer on the same end point day. Low endotoxin olive oil was used for injections, but there may have been some low level of inflammation induced by the olive oil or the intra peritoneal injection itself, and a completely naïve group of mice would have been a useful additional control for these experiments. Unfortunately constraints on the number of livers that it was possible to process for flow cytometry in a single day whilst ensuring high quality data meant this was not possible. Overall, I would still conclude that it is likely that elevated proliferation of KC contributes to their return to normal population size as this is in keeping with findings that KC underwent elevated proliferation following APAP-driven acute liver injury (Zigmond et al. 2014), and following KC loss using a diphtheria toxin depletion model (Scott et al. 2016).

6.4.2 Emergence of F4/80^{hi}CD11b^{lo}Tim4^{lo} recruited mϕ following acute liver injury

In addition to evidence of elevated local proliferation, chimeras revealed that 10-30% of the F4/80^{hi}CD11b^{lo} population was of recruited, bone marrow origin at day 6. There was a high level of variance within the CCl_4 treatment group which may be a reflection of level of injury achieved in each individual mouse, despite the fact that CCl_4 was weight dosed and mice were age and sex matched. However, in each separate experiment there was an increase in chimerism in the CCl_4 treated group compared to the olive oil control group. Unlike host KC, the donor F4/80^{hi}CD11b^{lo} mϕ were not positive for either Tim4, or the KC-specific marker Clec4f, although overall, detection of Clec4f was admittedly poor. One possibility was that that 6 days was insufficient time for expression of these KC markers to occur in these cells. In a recent study, monocytes were shown to be recruited to the liver and replenish the KC population following depletion via diphtheria toxin, and in this scenario, there was a delay of at least one month in the expression of Tim4 by the recruited cells (Scott et al. 2016). However, there was no such delay in expression of Clec4f, which is not in keeping with our finding that at 6 days the donor cells did not express this marker. Furthermore, when a group of mice were left for 8 weeks to recover from acute injury, the donor population was no longer apparent within the F4/80^{hi}CD11b^{lo} cells, showing that it was not simply a matter of allowing the recruited cells observed at day 6 more time to differentiate and acquire full KC phenotype. Thus the monocyte-derived recruited mϕ present at day 6 did not appear to be macrophages in the process of maturing into self-renewing KC. This suggested that the monocytes being recruited into the inflammatory environment of the injured liver were following an alternative pathway of differentiation to that observed in more steady state conditions by Scott *et al.*, and indicated that the recruited mϕ served a specific purpose within the injury or repair process. Although the presence of recruited macrophages which are phenotypically distinct from resident KC has been demonstrated previously following acute or chronic liver injury (Ramachandran et al. 2012; Zigmond et al. 2014; Dal-Secco et al. 2015), these have been assumed to be very transient and were not observed in the liver by 7 or 5 days following injury respectively (Ramachandran et al. 2012; Zigmond et al. 2014). Since the recruited mϕ identified in my study - using the definitive fate mapping system of chimeric mice - express the classic F4/80^{hi}CD11b^{lo} profile typically used to define KC, they would have been missed in these previous studies or assumed to be bona fide KC.

6.4.3 Spatial location of recruited mϕ following acute injury

As discussed in chapter 5, an additional population of macrophages has recently been described in the liver. Termed 'capsular macrophages', these cells have been identified as CX3CR1^{+} cells which are more rapidly turned over from CCR2^{+} monocytes than resident KC (Sierro et al. 2017). Thus, using flow cytometry data alone, I could not rule out the possibility that the F4/80^{hi}CD11b^{lo}Tim4^{lo} recruited mϕ were not capsular macrophages, which had increased in number through additional recruitment of monocytes or through local proliferation, since capsular macrophages are replenished from bone marrow even in steady state and would therefore be of donor origin prior to injury (Sierro et al. 2017). The most robust way to identify the recruited mϕ in liver sections would have been with a positive marker to uniquely distinguish them from embryonic KC. To provide this, I used MacGreen donor bone marrow in some chimera experiments for both acute and chronic liver damage experiments. Unfortunately I was unable to successfully detect true EGFP signal, and instead saw very autofluorescent cells in the GFP imaging channel, the pattern of which was akin to the autofluorescent 'ceroid-laden macrophages' described elsewhere (Rantakari et al. 2016). This autofluorescence was present in BL/6 donor bone marrow staining control mice, and adjusting of acquisition settings on the confocal microscope was unable to remove the autofluorescent signal from detection. Trial staining of sections with a tyramide step to enhance EGFP signal did not reveal any additional EGFP staining compared to naïve EGFP fluorescence, though further optimisation of the protocol may have been necessary to detect EGFP. Although using a lack of marker to identify the recruited mϕ is arguably less robust, staining of liver sections for Tim4 and F4/80, allowed the clear identification of F4/80^{+}Tim4^{-} recruited mϕ at day 6 following injury. This revealed a peri-vascular location of at least a significant number of these recruited cells, arguing that they are intra-hepatic macrophages and not capsular macrophages. However, new markers may be required in future to adequately distinguish capsular macrophages from intrahepatic bone marrow-derived macrophages recruited during injury.

The F4/80^{+}Tim4^{-} mϕ were seen in clusters surrounding blood vessels after acute injury which was in stark contrast to the sinusoidal location of F4/80^{+}Tim4^{+} KC revealed through immunofluorescence. The presence of macrophages in a ring-like structure around the area of injury is not a novel finding (Mori et al. 2009; Dal-Secco et al. 2015; Triantafyllou et al. 2018). Thus it is likely in the acute CCl_4 model the F4/80^{+}Tim4^{-} mϕ are clustered around the

central vein, which would indicate that they may play a role in repair and remodelling of the necrotic damage that occurs in this area. PanCK staining could be used to identify the portal tract since it stains hepatic progenitor cells found in this region (Lu et al. 2015), and thus its absence would reveal central veins, and would be a useful stain to add to future analysis.

6.4.4 NanoString gene expression analysis

To further elucidate possible roles for the F4/80^{hi}CD11b^{lo}Tim4^{lo} mϕ I used Tim4 as a discriminator to allow me to FACS sort the embryonic F4/80^{hi}CD11b^{lo}Tim4^{hi} KC and F4/80^{hi}CD11b^{lo}Tim4^{lo} recruited mϕ. I was then able to use NanoString technology to compare gene expression between the two populations. F4/80^{hi}CD11b^{lo}Tim4^{hi} KC in olive oil control mice and following CCl_4-driven acute liver injury closely aligned, suggesting that the role of KC in injury is not differ dramatically from their role in steady state. Admittedly, only 732 genes were studied, and assessment of the whole genome using RNAseq may reveal more differences. However, KC were also shown to be highly similar pre and post APAP-driven acute liver injury (Zigmond et al. 2014). There were many differences between the Tim4^{hi} KC population and the Tim4^{lo} recruited mϕ population following injury. Of note, KC expressed higher levels of scavenger receptors including MARCO, which is important for clearance of bacteria in the liver (van der Laan et al. 1999). However, most of the significant differences were genes enriched in the Tim4^{lo} mϕ population. They expressed high levels of the chemokine receptors *Cx3cr1*, *Ccr2* and *Ccr1*, in line with being migratory cells recently derived from blood monocytes. Co-expression of CCR2 and CX3CR1 was shown on wound associated macrophages in a sterile sponge wound model (Crane et al. 2014), and in a liver burn injury model (Dal-Secco et al. 2015). This suggested that the Tim4^{lo} recruited mϕ were indeed associated with the wound site, as the Tim4 and F4/80 immunofluorescence imaging had indicated. The Tim4^{lo} recruited mϕ present at day 6 following CCl_4 were closely aligned to the CX3CR1^{+} recruited mϕ present at day 3 following APAP overdose which the authors described as having a 'prorestorative genetic signature' (Zigmond et al. 2014). In the study by Zigmond *et al.,* the recruited cells expressed high levels of metallomatrix proteinases, a group of zinc-dependent enzymes with the ability to degrade extra cellular matrix (Nagase et al. 2006). Likewise, the Tim4^{lo} recruited mϕ in my study expressed high levels of MMP8 which preferentially degrades type 1 collagen (Siller-Lopez et al. 2004). In a rat model of CCl_4-induced liver fibrosis, its over-expression was shown to reduce fibrosis, and the authors

suggest that it is critical for degradation of ECM in the necrotic area to allow efficient tissue remodelling and hepatocyte expansion (Siller-Lopez et al. 2004). The Tim4^{lo} recruited mϕ also expressed *Osm* and OSMR$^{-/-}$ mice displayed impaired liver regeneration following high dose acute CCl_4, in part through reduced hepatocyte proliferation (Nakamura et al. 2004). OSM was found to act down stream of IL-6 signalling (Nakamura et al. 2004), and *Il6* was highly enriched in Tim4^{hi} KC in my study, indicating that KC may contribute to activating the tissue repair phenotype of the Tim4^{lo} mϕ. The Tim4^{lo} mϕ were also enriched for *Anxa1* and *Havcr2* which encodes TIM3, both of which reduced production of ROS and dampened inflammation in a mouse model of non-alcoholic steatohepatitis, a chronic liver disease (Du et al. 2018; Locatelli et al. 2014). Thus the Tim4^{lo} mϕ appear to have a pro-restorative phenotype and likely contribute to tissue repair in the area of necrosis. Liver regeneration is associated with proliferation of hepatocytes, and peak hepatocyte proliferation was seen at only 36 hours after partial hepatectomy (Goh et al. 2013). Thus it is perhaps unexpected that the Tim4^{lo} mϕ, which arrived between day 3 and day 6 expressed genes associated with hepatocyte proliferation such as *Osm*. However, they may have been recruited to the tissue earlier than day 3, and the transient macrophage population identified at day 3 likely represent the intermediate phenotype between Ly6C^{hi} monocytes recruited to the liver and the Tim4^{lo} mϕ. Indeed, there is experimental evidence to suggest that pro-wound healing mϕ which promote tissue formation through secretion of growth factors later differentiate into pro-resolving mϕ which help to remodel ECM (Crane et al. 2014; Hesketh et al. 2017). Thus the phenotype of the recruited mϕ likely changes throughout the course of the injury and repair phases in response to local signals. Inclusion of the Ly6C^{hi} monocytes at an early time point, along with the transient macrophages at day 3 into the Nanostring analysis may have revealed their developmental relationship, and could explain expression of genes associated with the earlier wound healing phase.

6.4.5 *Ccr2*$^{-/-}$ experiment

The emergence of monocyte-derived macrophages in this study provoked the question of whether they were derived from classical Ly6C^{hi}CCR2^{+} monocytes, non-classical Ly6C^{lo}CCR2^{-} or possibly an intermediate phenotype. During liver injury classical, inflammatory monocytes are recruited to the liver and express high levels of pro-inflammatory cytokines including TNF-α and IL-6 (Triantafyllou et al., 2018). In APAP-induced acute liver injury this recruitment

was shown to be CCR2-dependent, upon which they were found to contribute to resolution of injury (Holt et al., 2009). Similarly, in chronic CCl_4-induced liver injury, classical monocytes were found to downregulate Ly6C and become pro-restorative (Ramachandran et al., 2012). This phenotypic switch of inflammatory monocytes to an anti-inflammatory, pro-restorative phenotype was elegantly demonstrated by directly visualising their conversion from $CCR2^+CX3CR1^+$ cells labelled with RFP to $CCR2^-CX3CR1^+$ GFP^+ cells, along with intermediate orange and yellow cells which were dual positive for both CCR2 and CX3CR1 (Dal Secco et al., 2015). IL-10, IL-4 and clearance of necrotic material all contributed to triggering this phenotypic switch. The CX3CL1-CX3CR1 axis appears to be crucial for this phenotypic switch, as recruited monocytes in $CX3CR1^{-/-}$ mice do not effectively convert and remain inappropriately pro-inflammatory resulting in prolonged liver inflammation (Karlmark et al., 2009). Thus, rather than sequential recruitment of inflammatory- followed by reparatory-monocytes from blood, differentiation of classical monocytes *in situ* appears to be necessary for the process of injury followed by repair. A similar differentiation process appears to be necessary in humans. $CD14^+CD16^-$ classical monocytes have been demonstrated to switch towards the intermediate $CD14^+CD16^+$ phenotype in response to TGF-β and IL-10 (Liaskon et al., 2012). These intermediate cells were pro-inflammatory and may contribute to ongoing hepatic fibrosis in humans with chronic liver injury (Liaskon et al., 2012). Interestingly, CX3CR1 is downregulated in patients with cirrhosis, compared to healthy volunteers, indicating that for resolution of liver disease the phenotypic switch to a $CX3CR1^+$ non-classical, pro-restorative monocyte may be dis-regulated (Karlmark et al., 2009).

Given the high levels of expression of *Ccr2* on the $F4/80^{hi}CD11b^{lo}Tim4^{lo}$ recruited mϕ compared to the $F4/80^{hi}CD11b^{lo}Tim4^{hi}$ KC, and the dependence of monocyte-derived macrophages on Ccr2 for recruitment following acetaminophen overdose (Zigmond et al. 2014), $Ccr2^{-/-}$ mice were used to try to prevent their recruitment to the liver following injury, to give insight into their function. $Ccr2^{-/-}$ mice showed no difference in injury compared to WT controls as serum ALT levels were equivalent. The extent of loss of $F4/80^{hi}CD11b^{lo}$ cells was also equivalent between $Ccr2^{-/-}$ and WT, and most surprisingly, the $F4/80^{hi}CD11b^{lo}Tim4^{lo}$ population was recruited to the liver in the same abundance as in WT control mice. It is therefore possible that despite the high levels of *Ccr2* expression in the NanoString data, $Ly6C^{hi}$ monocytes are not the precursor of the $F4/80^{hi}CD11b^{lo}Tim4^{lo}$ recruited mϕ population. An alternative precursor might be $Ly6C^{lo}$ monocytes, and this hypothesis would be in keeping with previously published data in which latex bead-labelled $Ly6C^{lo}$ monocytes in circulation

were later found in the F4/80^{hi}CD11b^{lo} KC population 7 days into the resolution phase following chronic CCl4-induced injury (Ramachandran et al. 2012). It has been shown that deletion of a specific enhancer region in the Nr4a1 gene, which is specific and critical to Ly6C^{lo} monocyte survival (Hanna et al. 2011), can be used to deplete Ly6C^{lo} monocytes whilst leaving the rest of the mononuclear phagocyte system intact (Thomas et al. 2016). Delivery of CCl_4 to these mice would allow me to test whether Ly6C^{lo} monocytes are the precursor to the F4/80^{hi}Tim4^{lo} population that arises in our model. However, given the high degree of *Ccr2* expression in F4/80^{hi}CD11b^{lo}Tim4^{lo} recruited mϕ, the fact that *Ccr2* is a gene which is switched off in Ly6C^{lo} monocytes (Yamasaki et al. 2012), and the fact that monocytes were only reduced 4-fold in the blood of the *Ccr2*$^{-/-}$ mice used in this experiment, it seems more likely that some recruited Ly6C^{hi} monocytes remain able to enter the injured liver in *Ccr2*$^{-/-}$ mice and become F4/80^{hi}CD11b^{lo}Tim4^{lo} cells. Perhaps the small number of monocytes which do make it into the liver are able to proliferate to increase numbers, and a time point between 24 hours and 6 days would have been required to determine this. If Ly6C^{hi} monocytes are indeed the precursor of F4/80^{hi}CD11b^{lo}Tim4^{lo} recruited mϕ, their transient depletion at day 6 when the liver has regenerated could be possible using anti-CCR2 strategies to further explore their function. Such experiments would have the added benefit of allowing initial recruitment of monocytes to occur unimpaired, thereby revealing what functions may be specific to the mature population of F4/80^{hi}CD11b^{lo}Tim4^{lo} recruited mϕ.

6.4.6 Long-term fate of KC following acute or chronic injury

Whether resident macrophages rely on monocyte replenishment is highly tissue specific, leading to much interest into the factors that determine whether monocytes can convert to long-lived resident macrophages, or whether resident macrophages survive independently of monocytes through proliferation or longevity. Thus in this chapter I ultimately set out to determine whether KC, which are relatively autonomous from monocytes in the steady state required monocyte replenishment in the context of liver injury. However, the F4/80^{hi}CD11b^{lo}Tim4^{lo} recruited mϕ did not permanently contribute to the KC population, following either acute or chronic injury, which is consistent with another study published towards the end of this study in which monocyte-derived macrophages recruited to the liver were tracked using robust fate mapping approaches following non-alcoholic fatty liver disease (NAFLD), and found to be only short lived (Devisscher et al. 2017). Ablation of the KC

population by irradiation or by Clec4f-specific deletion using diphtheria toxin has provided proof of principle that when there is an experimentally empty niche space in the liver, monocyte-derived cells can differentiate into KC, permanently engraft in the liver, and go on to proliferate in the steady state, with no further requirement for monocyte recruitment (Klein et al. 2007; Scott et al. 2016; Beattie et al. 2016). These studies are in keeping with the idea that an empty niche is required for monocyte conversion to KC (Guilliams and Scott 2017). Accordingly, Devisscher *et al.* did not observe a loss of KC during NASH, and did not see monocyte contribution to KC (Devisscher et al. 2017). In contrast, my data suggest that despite a 50% loss in KC following injury, the KC niche remains highly regulated and protected from monocytes in the context of CCl_4-driven liver injury and repair. It is possible that the recruited macrophages may not have sufficient access to survival factors such as CSF1, although experiments detailed in chapter 5 argue against CSF1 availability being the sole limiting factor in monocyte to KC conversion. Alternatively, one hypothesis is that the recruited macrophages do not receive the correct local, possibly even physical, signals to become KC. In the acute model, the fact that F4/80^{hi}CD11b^{lo}Tim4^{lo} recruited mϕ are spatially distinct from F4/80^{hi}CD11b^{lo}Tim4^{hi} KC seems to support this hypothesis. In a sterile wound model, pro-inflammatory Ly6C^{hi} monocytes were shown to be recruited to the wound site where they became Ly6C^{lo} macrophages and matured into pro-restorative macrophages (Crane et al. 2014). This switch to a wound healing macrophage was driven by IL-10 and IL-4 within the local environment in a small, sterile burn wound to the liver, and the macrophages were found to encircle and then enter the wound upon maturation (Dal-Secco et al. 2015). Thus monocytes recruited to the liver in the context of tissue injury and repair following acute CCl_4-driven damage may be diverted down a pathway towards a pro-restorative phenotype due to the local signals they receive, and are physically diverted from the KC niche. In the mean-time, it would appear that the remaining KC are able to proliferate to restore numbers. Once tissue repair is complete and KC numbers have been restored, the recruited macrophages may die out simply because the KC niche space has been filled.

In the chronic model, it is less clear that there is any spatial distinction between recruited mϕ and KC. However, following chronic CCl_4 delivery, the total number of KC did not fully recover, even 8 weeks after cessation of injury. Perhaps the niche space vacated by KC becomes somehow uninhabitable long-term following injury, such that monocytes cannot permanently engraft into self-renewing KC, and nor can remaining KC self-renew and the total population size is diminished. It would be important to leave mice for a much longer

recovery time than 8 weeks to confirm that KC population is permanently reduced in size, however. Long-term loss of KC may have serious clinical relevance since it would be expected to impact on the homeostatic function of the liver, and may have wide-spread implications in terms of inappropriate immune responses since KC are thought to maintain peripheral tolerance (Heymann et al. 2015).

6.4.7 Concluding remarks

My data indicate that in both acute and chronic injury settings, the embryonic origin of liver KC is highly 'protected' and monocyte-derived macrophages which are recruited to the liver following injury do not convert into long-lived KC, and are instead diverted to mature into short-lived macrophages which in the acute setting may be involved in tissue repair. KC were transiently reduced in number following acute injury and appeared permanently (over 8 weeks) depleted following chronic injury. Thus although KC appeared to have vacated their niche, the fact that monocytes were unable to replenish them in the context of injury and repair raises further questions about whether injury renders the niche unavailable, and/or drives monocytes down an alternative path of differentiation from which they are unable to later convert into long-lived KC.

Chapter 7: Final discussion

7.1 Summary

This thesis had two major aims: to investigate the role of CSF1 in KC maintenance and conversion of monocyte to KC, and to determine whether the KC population is replenished by monocytes following acute and/or chronic liver injury, and if so, what effect this may have on subsequent KC function.

Before exploring these aims, in chapter 3 I established the most suitable protocol for the isolation and identification of KC from digested livers for flow cytometry, as this was to be the major mode of analysis in this project. A more comprehensive breakdown of myeloid cell populations using *Csf1r* transgene expression and additional cell surface markers in combination with reliance on CCR2 was used to identify KC, monocytes and DCs in the liver. A second population of liver macrophages, in addition to subcapsular macrophages identified by another group (Sierro et al. 2017), could not be identified.

Chapters 4 and 5 addressed the first major aim. In chapter 4, KC were found to uptake the most circulating labelled CSF1-Fc^{AF647} on a per cell basis, in keeping with their role in CSF1 clearance (Bartocci et al. 1987). Monocytes in the blood and liver were also able to capture CSF1-Fc^{AF647}, but not as efficiently as KC. In chapter 5, exogenous administration of CSF1-Fc to chimeric mice identified the recruitment from bone marrow of a population of $F4/80^{hi}CD11b^{lo}$ macrophages, in addition to proliferation of both host resident KC and the donor recruited macrophages. However, monocyte-derived macrophages failed to express the KC marker Tim4, and persisted only transiently. Overall I found that CSF1 availability may be a limiting factor in the recruitment and conversion of monocytes to KC in the liver, but that autonomy of KC from monocytes is highly maintained in the steady state, suggesting that factors in addition to CSF1 availability may be responsible for maintaining the autonomy of the KC population.

Chapter 6 addressed the second major aim. A KC 'disappearance reaction' was noted following both acute and chronic CCl_4-driven liver injury, along with recruitment of monocyte-derived macrophages which acquired an $F4/80^{hi}CD11b^{lo}$ phenotype. Despite this, KC were not replenished by these recruited macrophages following either acute or chronic injury. Following acute injury the recruited macrophages did not express the KC markers

Clec4f or Tim4, and comparison of gene expression revealed the recruited macrophages to have a genotype consistent with a role in wound repair. Following chronic injury the recruited macrophages were not found in obvious clusters, as seen in acute injury, but were seemingly integrated alongside KC. KC were permanently reduced in number (for over 8 weeks) suggestive of possible damage to a component of their niche.

7.2 Caveats with the chimera system and use of inbred mice

This study relied heavily on the tissue-protected chimera system to fate map bone marrow-derived cells, a method used extensively to determine the rate of monocyte contribution to tissue macrophages in a variety of settings and tissues (Jenkins et al. 2011; Bain et al. 2016; Scott et al. 2016; Devisscher et al. 2017). In our hands this protocol results in partial chimerism of around 20-30% in circulating Ly6C^{hi} monocytes, but crucially protects tissue macrophages in organs shielded by the lead from the potentially toxic effects of total body irradiation, such as enhanced rate of turnover (Murphy et al. 2008). A downside of this technique is that we cannot determine the origin of the KC prior to irradiation, however, there is data to suggest they are largely of embryonic origin, with some contribution from BM-derived cells that engraft post birth (Perdiguero et al. 2014; Scott et al. 2016). However, the exact nature of origin of the KC population at the point of irradiation does not impact the conclusions of this study on how the population is maintained over the course of CSF1-Fc or CCl_4 treatment.

A more serious possible caveat of using BM chimeras is that there is potential for there to be a competitive effect between cells of host and donor lineage. An inherent advantage of CD45.2$^+$ HSCs over CD45.1$^+$ HSCs has been demonstrated in mixed competitive chimeras, including in terms of their myeloid differentiation potential (Mercier et al. 2016). However, I used heterozygous host mice which expressed both CD45.1 and CD45.2 alleles, to attenuate any competitive advantage of transplanted CD45.2$^+$ homozygous bone marrow cells. Additionally, if CD45.2$^+$ cells do exhibit a competitive advantage over CD45.1$^+$ cells, this might be expected to over predict the contribution of monocytes to the KC pool, since donor cells were exclusively CD45.2$^+$ in my study. Since monocytes did not contribute long-term to KC in any scenario tested this is not likely of concern and does not affect the conclusions of this study.

The routine extrapolation of findings using C57BL/6 mice as a model for macrophage origins has been challenged recently (Hume et al. 2019), in particular citing a study in which C57BL/6 and Balb/c mice displayed differing responses to filarial nematode infection in terms of resident macrophage proliferation versus monocyte recruitment (Campbell et al. 2018). However, the level of KC chimerism I observed in PBS-treated Balb/c chimeras was just over 2% (taken from the above-mentioned Campbell study), which was the level also seen in PBS-treated control C57BL/6 chimeras (from my study in chapter 5) (data not shown). Whilst reassuring, I cannot say definitively that my observations that KC remain autonomous of monocytes following liver injury would hold true in other mouse strains, or indeed other species. However, the wealth of data fate-mapping steady state origins of macrophages in the C57BL/6 mouse is backed up by results from human transplant cases, as detailed in the introduction (chapter 1), giving further confidence that my results may be relevant to human health.

7.3 Maintenance and origin of KC in steady state

As introduced in chapter 1, resident macrophages vary in reliance on self-renewal versus replenishment from monocytes, in a tissue-specific manner. Additional factors including age, sex (Bain et al. 2016) and inflammation also critically effect this balance. The microglia of the brain are highly autonomous of infiltrating monocytes, and an inability of circulating monocytes to cross the blood brain barrier in the steady state may play a role in this (Ajami et al. 2007; Mildner et al. 2011). Resident macrophages in the intestine are continually replaced by monocyte-derived macrophages which appears to be driven by the presence of microbiota (Bain et al. 2014). KC in the liver are located in the sinusoids through which monocytes are continually circulating and although KC are unlikely to be exposed to live commensals in healthy animals, they are continually exposed to gut bacterial products (Balmer et al. 2014). Thus it is perhaps surprising that KC do not appear to have any major contribution of adult monocytes in homeostatic conditions, apart from a possible window of recruitment during the immediate post-natal phase (Bain et al. 2014; Gomez Perdiguero et al. 2014; Hoeffel et al. 2015; Scott et al. 2016). Even as mice age there does not appear to be increased monocyte incorporation, reflected by only a small but insignificant increase in chimerism in tissue-protected chimeras over a 24 week period (Bain et al. 2016) and the results of my own study revealing equivalent population sizes in year-old *Ccr2*$^{-/-}$ and WT mice.

Notably, total body irradiation of mice leads to replenishment of KC through a combination of proliferation of surviving KC and recruitment of monocytes (Klein et al. 2007; Beattie et al. 2016). Partial depletion of KC in a Clec4f-DTR mouse also resulted in both proliferation of surviving resident KC and recruitment of monocyte-derived macrophages which matured into long-lived self-renewing KC, after which there was no further input of monocytes (Scott et al. 2016). Together these studies, along with my own, have shown that whilst monocytes are capable in principle of becoming KC and recapitulating their genotype and phenotype, in steady state conditions, they do not.

7.4 Contribution of cellular origin versus local environmental factors on macrophage function

7.4.1 Importance of origin on macrophage function

I found that KC were not replenished by monocytes following CSF1-Fc treatment, or acute and chronic CCl_4 liver injury, which is supported by the findings of another study which observed only a transient increase in chimerism in the KC population following MCD-induced NAFLD in mice (Devisscher et al. 2017). However, monocyte-derived KC do arise following *Listeria monocytogenes* infection (Blériot et al. 2015), indicating that the mode of KC replenishment is specific to the infection or injury model. Beattie *et al.* demonstrated that whilst monocyte-derived and embryonic KC were comparable in their ability to clear old red blood cells, respond to LPS and to *Leishmania* infection, there were some differences in scavenging ability and phagocytosis of bacterial products (Beattie et al. 2016). Furthermore, mice with a population of monocyte-derived KC recruited following chlodronate liposome (CLP) depletion of the endogenous KC displayed enhanced injury to APAP overdose, and delayed return of liver function (David et al. 2016). The monocyte-derived KC displayed reduced phagocytic ability demonstrated by poor internalisation of *E. coli* (David et al. 2016). Thus there appears to be a functional consequence of replacing embryonic KC with monocyte-derived KC, which may explain why it is favourable for KC to be replenished through self-renewal, as has been observed in all tested scenarios apart from the *Listeria* infection model. To test this idea, KC could be knocked down during the recovery phase following acute CCl_4, at the time when the monocyte-derived macrophages are being recruited to the liver, between 3 and 6 days post injury, for example using the Clec4f-DTR

mouse (Scott et al. 2016). Differences in function, for example phagocytosis between monocyte-derived KC and embryonic KC could then be tested.

7.4.2 Importance of environment on macrophage function

The differences in phagocytic ability observed in the study by David and colleagues were absent 60 days following CLP treatment (David et al. 2016), however, suggesting that time-of-residence in the tissue, and thus local environmental factors are ultimately more important in conveying function than cellular origin. In support of this, yolk sac macrophages, foetal liver monocytes and bone marrow monocytes were all shown to be capable of giving rise to alveolar macrophages when transferred to AM-deficient *Csf2r*$^{-/-}$ mice, acquiring near identical gene expression patterns and preventing pulmonary alveolar proteinosis (PAP) that normally occurs in *Csf2r*$^{-/-}$ mice (van de Laar et al. 2016). Transferred peritoneal macrophages in the lung acquire 70% of AM genes (Lavin et al. 2014), indicating that even a highly differentiated tissue macrophage can largely alter its gene expression in response to changes in local environment. However, whilst AMs from a WT mouse transferred to a mouse with no AM were also able to prevent PAP, transferred peritoneal macrophages, KC, or colonic macrophages into the lung were unable to prevent PAP (van de Laar et al. 2016). One possible interpretation for this is that the tissue environment in which the macrophage first differentiated may have imprinted long-term or irreversible effects on its genome. Indeed, differences in epigenetic programming have been observed in macrophages differentiated from monocytes in differing conditions (Saeed et al. 2014). This resulted in 'long-lasting' (up to 5 days) effects in terms of their subsequent response – either tolerogenic or trained immunity leading to a decreased or increased pro-inflammatory response respectively (Saeed et al. 2014). Immune training and tolerance can also be induced in resident macrophages, as has been demonstrated in microglia. Wendeln and colleagues gave either 1 or 4 injection(s) of LPS to mice intra-peritoneally, resulting in immune training or immune tolerance respectively in microglia. Immune training led to reduced IL-10 production and increased neuropathology in a mouse model of Alzheimer's disease or in focal brain ischaemia, whilst immune tolerance resulted in decreased production of IL-1β, IL-6 and IL-12 and alleviated brain injury (Wendeln et al. 2018). Given that KC self-renew under non-homeostatic conditions following acute CCl_4-driven liver injury, it may be important to examine whether there are epigenetic changes driven by the inflammatory or indeed repair-

associated environmental factors, and whether these confer long-lasting effects on their function, particularly in response to subsequent liver injury, but also in terms of their homeostatic functions. Although origin may have some effect on tissue macrophage function, environment appears to be the major contributing factor, and it is therefore important to understand what constitutes the macrophage niche, as discussed below.

7.5 A model for the KC niche

In a recent review, Guilliams and Scott hypothesize that tissue macrophage populations are regulated by a theoretical niche, which likely comprises biochemical and/or signalling molecules, along with physical factors such as the presence of specific structural cells (Guilliams and Scott 2017). They propose that there is limited niche space available in every tissue which defines the size of the resident macrophage population, and whether they are replenished through self-renewal or monocyte recruitment. Here I propose that two of the niche factors for KC are the availability of CSF1 and a requirement for physical contact with a specific cell type, likely liver sinusoidal endothelial cells (LSECs). A summary of how niche availability following CSF1-Fc and acute and chronic CCl_4 affects KC maintenance is shown below (fig. 7.1).

7.5.1 CSF1 and CSF1-producing cells as a niche factor

CSF1 availability has been proposed previously as a way in which tissue macrophage numbers are regulated and restored following apoptosis in steady state or the macrophage disappearance reaction following inflammation (Jenkins and Hume 2014). Elevated levels of CSF1 alone were sufficient to cause recruitment and maturation of monocyte-derived macrophages in the liver. Despite this, monocyte-derived macrophages were lost preferentially over resident KC upon withdrawal of exogenous CSF1 (see fig. 7A). If the monocyte-derived KC had full access to all factors controlling the KC niche, then loss of host and donor KC would be expected to be stochastic. It is possible that the monocyte-derived KC are not as efficient at capturing CSF1 as the resident KC, and the CSF1-Fc^{AF647} assay developed in chapter 4 could be used to determine this. Staining of livers using the Tim4 and F4/80 immunofluorescence protocol developed in chapter 6 would determine where the monocyte-derived KC are. If the $Tim4^{lo}$ recruited KC were found within the parenchyma

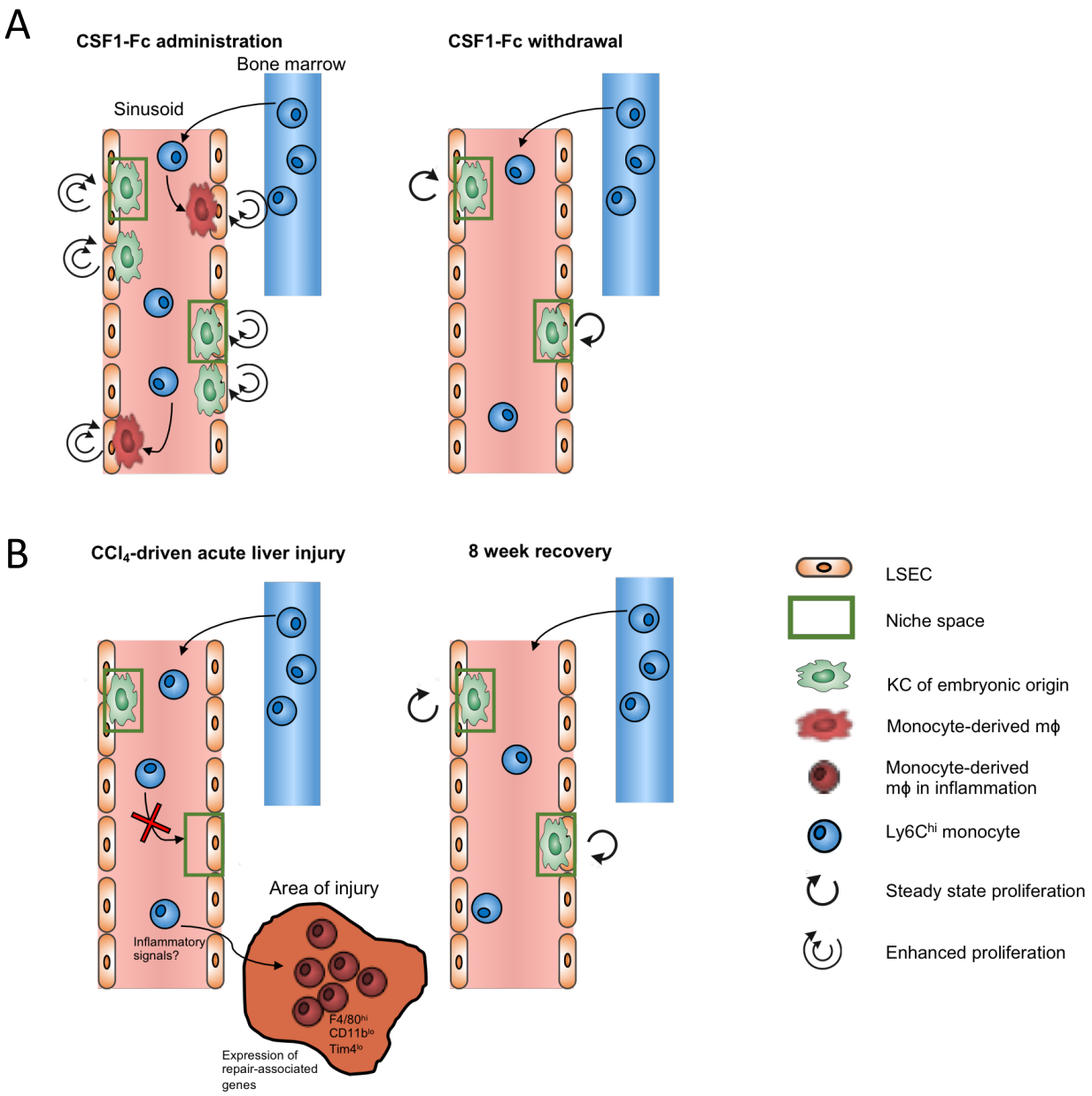
A
CSF1-Fc administration
Bone marrow
Sinusoid
CSF1-Fc withdrawal
B
CCl4-driven acute liver injury
8 week recovery
Area of injury
Inflammatory signals?
F4/80hi CD11blo Tim4lo
Expression of repair-associated genes
LSEC
Niche space
KC of embryonic origin
Monocyte-derived mϕ
Monocyte-derived mϕ in inflammation
Ly6Chi monocyte
Steady state proliferation
Enhanced proliferation
C
CCl4-driven chronic liver injury
8 week recovery
or?
Damaged niche?

Figure 7.1 Graphical summary of findings in chapters 5 and 6. (A) Monocyte-derived macrophages are recruited to the liver during CSF1-Fc treatment, and both donor and host macrophages proliferate at an enhanced rate. Upon CSF1-Fc withdrawal, donor macrophages are selectively lost over host macrophages. **(B)** 50% of KC are lost with acute CCl_4, but monocyte-derived macrophages are diverted to the area of injury instead of replenishing the lost KC, which proliferate to restore normal numbers. **(C)** KC are lost with chronic CCl_4 and do not return to normal numbers after 8 weeks of recovery. Monocyte-derived macrophages are recruited and may or may not come into contact with the KC niche supporting cells, but they do not replenish the KC population long-term, nor do monocytes recruited to the tissue once homeostasis is restored, indicating damage to the niche.

alongside the Tim4^{hi} KC this would further support the idea that there are spatially defined niche cells which are required to support long-lived KC. It was recently shown that macrophages and fibroblasts form a stable two-cell circuit *in vitro*, with macrophages producing the fibroblast growth factor PDGFβ whilst fibroblasts produce CSF1 (Zhou et al. 2018). Proliferation of fibroblasts was related to the amount of space available, whilst macrophage proliferation was largely independent of space, indicating that fibroblasts and not macrophages were at 'carrying capacity' (Zhou et al. 2018). In other words, the size of the macrophage population appears to be limited by the maximum size of the fibroblast population in this two cell circuit. Thus *in vivo*, KC population size may be limited by population size of another cell type with which it forms a stable circuit. There are no fibroblasts in the liver, but there are hepatic stellate cells which become myofibroblasts when activated, and produce CSF1 (Baum and Duffy 2011) making them a possible niche cell candidate. Cell contacts were shown to be critical for the stability of the two cell circuit *in* vitro, thus perhaps when the CSF1-Fc is removed in my model, embryonic KC may still be attached to the CSF1-producing cell, conveying a survival advantage over the recently recruited KC.

7.5.2 LSECs as a possible niche factor

Macrophages are extremely sensitive to physical factors in their microenvironment, for example rigidity, interstitial flow and substrate softness (Jain et al. 2019), further suggesting there could be a specific cell type which constitutes the KC niche. Whilst physical contacts between macrophages and fibroblasts were shown to be critical for establishment of a stable circuit, LSECs have also been proposed to be a likely candidate 'niche cell' for supporting KC (Guilliams and Scott 2017). KC have been shown to put their filopodia through the fenestrations of LSECs (Lough et al. 1987), which may be to anchor themselves and prevent

them being carried away by the blood flow through the sinusoid. The central zone of the liver is largely devoid of KC and there is good evidence that endothelial cells also change in different regions of the liver, and it has been shown in rats that the endothelial cells of the central zone are not fenestrated (Burkel and Low 1966). Furthermore, KC numbers were reduced in cirrhotic livers in rats during CCl_4-driven injury specifically in the regions of capillarisation (Lough et al. 1987). Additionally, we have identified that the 'endothelial contamination' discovered in the KC gate following a conventional $CD45^+Lineage^-F4/80^{hi}CD11b^{lo}$ gating strategy included some LSECs which were in tight association with KC or KC membranes (Lynch et al. 2018). These associations were not separated even with enzymatic digestion, mechanic and manual shaking and the presence of EDTA which diminishes cell-cell contacts through chelation of Ca_2^+ (Le et al. 1999). Thus these associations identified by flow cytometry may actually represent a functionally significant conjugate, as was demonstrated between T follicular helper cells and B cells (Reinhardt et al. 2009). The isolation of $CD31^+$ LSECs which are still in association with $F4/80^{hi}CD11b^{lo}$ KC in our study (Lynch et al. 2018) provides a tool to further examine these cells, and compare differences between these LSECs and the rest of the LSEC population to determine whether there are specific transcriptional or morphological differences which confer ability to support a KC.

Following chronic injury, flow cytometry indicated that KC did not recover in number even 8 weeks after the final dose of CCl_4. This finding needs to be further backed up with imaging, but it appears that neither incumbent KC nor monocyte-derived macrophages were able to replenish the population, indicating that a component of the niche had been damaged. This may be due to loss of KC-supporting LSECs through capillarization. Very recently, it was shown that defenestration does not occur in the chronic condition NAFLD that results from high fat diet over 20 weeks (Kus et al. 2019), and this could explain why KC were not reduced in number in the Devisscher study of NAFLD, discussed in chapter 6 (Devisscher et al. 2017). Proving that fenestrated LSECs are absolutely required for maintaining KC will be difficult, but one way to do this might be by using 2D and 3D co-culture systems. For example, contact with endothelial cells has already been shown to be able to support differentiation of $F4/80^+$ cells from a mixed haematopoietic cell population using a 2D co-culture system (He et al. 2012). Using macrophages and neurones derived from induced pluripotent stem cells, it has been shown that the soluble components in neuron-conditioned media were sufficient for induced macrophage survival, but that direct contact with neurons was required for their full differentiation into microglia-like macrophages (Takata et al. 2017). Thus this technique

could be adapted to show that full development of KC requires contacts with fenestrated endothelium. If treatments which cause defenestration, for example, knock down of Cav-1 (Luo et al. 2018), also result in loss of KC, or disruption of their morphology or phenotype this would further support a role of fenestrated LSEC in maintaining KC. A drug called Plumbagin has recently been shown to ameliorate capillarization of LSECs *in vitro* (Li et al. 2017), and it would be interesting to know whether treatment with Plumbagin or similar drugs could reverse or prevent defenestration *in vivo*, and if this would also lead to recovery of normal KC numbers in chronic CCl_4 injury. Thus the next major next step will be proving the exact identity of the KC niche cell, as this may be critical for manipulating KC and monocyte-derived macrophage fate, function and number during liver injury and repair.

7.6 Why does injury lead to a macrophage disappearance reaction?

The loss of macrophages following injury or infection is not unique to the liver: alveolar macrophages are reduced in number following influenza A infection, F4/80^{hi} peritoneal macrophages are lost following zymosan-induced inflammation and Langerhans cells are lost following exposure to UV light (Merad et al. 2002; Davies et al. 2011; Lauder et al. 2011). The loss of KC following liver injury observed in my study following both acute and chronic CCl_4-driven injury may serve to activate the subsequent immune response. Indeed, chlodronate liposome depletion of KC resulted in enhanced recruitment of Ly6C^{hi} monocytes and more rapid clearance of hepatitis B virus in mice (Wu et al. 2019). But how does the loss of KC result in enhanced recruitment of monocytes? Activated macrophages are known to increase in size, but resident macrophages may be prevented from fully spreading due to the fact that they are tightly packed by surrounding cells. Confinement of macrophages resulted in a reduced pro-inflammatory response to LPS *in vitro*, including reduced expression of IL-6, IL-1β and iNOS (Jain and Vogel 2018), and Hume *et al.* theorize that loss of a proportion of the resident macrophage population allows the remaining cells to spread fully, resulting in an inflammatory immune response. (Hume et al. 2019). This doesn't appear to be the case in the CCl_4 model as immunofluorescence imaging indicates that KC were lost in the area of injury. However, more sophisticated analysis of images would be required to confirm that there is not also a reduction in density of KC in the healthy parenchyma. With CCl_4, KC may be lost through apoptosis or more likely necrosis or necroptosis, which in itself results in release of DAMPs and immune cell activation (Sachet et al. 2017). Given the high

consumption of CSF1 by KC demonstrated in chapter 4 (Hawley et al. 2018), it is also possible that loss of KC may be required to 'free up' CSF1 availability to allow sufficient recruitment of monocytes to the injured liver. Certainly recruitment of inflammatory macrophages to the peritoneal cavity is CSF1-dependent in a variety of inflammation models, as neutralisation of CSF1 using an anti-CSF1 antibody resulted in reduced numbers of recruited macrophages (Louis et al. 2015). CSF1 expression in the liver increased 4-fold 24 hours following APAP-induced acute liver injury, and delivery of rCSF1 in this model resulted in increased numbers of monocyte-derived macrophages (Zigmond et al. 2014). Thus loss of KC may result in monocyte recruitment through a combination of expression or release of inflammatory cytokines and DAMPs, and by allowing CSF1 levels which are sufficient to result in enhanced monocyte recruitment. Death of KC may also serve an additional purpose which could be to aid tissue regeneration – necroptosis of microglia has been shown to be critical for remyelination following injury to the CNS, as the death of the proinflammatory microglia allows repopulation to a pro-regenerative phenotype (Lloyd et al. 2019). The authors demonstrated the role of necroptosis through its inhibition using necrostatin-1, and a similar approach could be employed following CCl_4 injury to reveal whether KC death plays a similar role in this model.

7.7 Role of monocyte subsets in liver injury

The emergence of monocyte-derived macrophages in this study provoked the question of whether they were derived from classical Ly6C^{hi}CCR2^{+} monocytes, non-classical Ly6C^{lo}CCR2^{-} or possibly an intermediate phenotype. During liver injury classical, inflammatory monocytes are recruited to the liver and express high levels of pro-inflammatory cytokines including TNF-α and IL-6 (Triantafyllou et al., 2018). In APAP-induced acute liver injury this recruitment was shown to be CCR2-dependent, upon which they were found to contribute to resolution of injury (Holt et al., 2009). Similarly, in chronic CCl_4-induced liver injury, classical monocytes were found to downregulate Ly6C and become pro-restorative (Ramachandran et al., 2012). This phenotypic switch of inflammatory monocytes to an anti-inflammatory, pro-restorative phenotype was elegantly demonstrated by directly visualising their conversion from CCR2^{+}CX3CR1^{+} cells labelled with RFP to CCR2^{-}CX3CR1^{+} GFP^{+} cells, along with intermediate orange and yellow cells which were dual positive for both CCR2 and CX3CR1 (Dal Secco et al., 2015). IL-10, IL-4 and clearance of necrotic material all contributed to triggering this

phenotypic switch. The CX3CL1-CX3CR1 axis appears to be crucial for this phenotypic switch, as recruited monocytes in CX3CR1$^{-/-}$ mice do not effectively convert and remain inappropriately pro-inflammatory resulting in prolonged liver inflammation (Karlmark et al., 2009). Thus, rather than sequential recruitment of inflammatory- followed by reparatory-monocytes from blood, differentiation of classical monocytes *in situ* appears to be necessary for the process of injury followed by repair. A similar differentiation process appears to be necessary in humans. CD14^{+}CD16^{-} classical monocytes have been demonstrated to switch towards the intermediate CD14^{+}CD16^{+} phenotype in response to TGF-β and IL-10 (Liaskou et al., 2012). These intermediate cells were pro-inflammatory and may contribute to ongoing hepatic fibrosis in humans with chronic liver injury (Liaskou et al., 2013). Interestingly, CX3CR1 is downregulated in patients with cirrhosis, compared to healthy volunteers, indicating that for resolution of liver disease the phenotypic switch to a CX3CR1^{+} non-classical, pro-restorative monocyte may be dis-regulated (Karlmark et al., 2009). Thus, Ly6C^{hi}CCR2^{+} classical monocytes remain the most likely candidate for the precursor of the recruited macrophages identified in this study.

7.8 Concluding remarks

Overall I believe that this body of work contributes significantly to our understanding of how KC are maintained in both homeostasis and liver injury, and provides answers to questions which were pertinent in the field when I embarked on this research. The clear outstanding questions are whether manipulation of niche factors provides a promising way to affect macrophage population size and function and prevent the pathological consequences that accompany loss or change KC function during chronic liver injury (Balmer et al. 2014; Heymann et al. 2015), and what are the specific niche factors that govern resident macrophages in other tissues? My finding that KC persist via self-renewal through the course of acute and chronic injury also raises the question of whether inflammation imprints long term effects on KC function, akin to so called 'trained immunity' that occurs in monocytes and other tissue macrophages with activation, and if so, what these effects may be? This question maybe particularly pertinent to pathological processes that occur with intermittent liver injury, for example with binge drinking. If we can begin to answer these questions, this could help with understanding how KC can be targeted in human health, particularly with regard to improving homeostatic liver function in the setting of chronic liver diseases.

References

Ajami, Bahareh, Jami L Bennett, Charles Krieger, Kelly M McNagny, and Fabio M V Rossi. 2011. Infiltrating Monocytes Trigger EAE Progression, but Do Not Contribute to the Resident Microglia Pool. *Nature Neuroscience* **14 (9)**: 1142–1149

Ajami, Bahareh, Jami L Bennett, Charles Krieger, Wolfram Tetzlaff, and Fabio M V Rossi. 2007. Local Self-Renewal Can Sustain CNS Microglia Maintenance and Function throughout Adult Life. *Nature Neuroscience* **10 (12):** 1538–1543

Aschoff, L. 1924. "Das Reticulo-Endotheliale System." In *Ergebnisse Der Inneren Medizin Und Kinderheilkunde*, 1–118. Berlin, Heidelberg: Springer Berlin Heidelberg

Asrani, Sumeet K., Harshad Devarbhavi, John Eaton, and Patrick S. Kamath. 2019. Burden of Liver Diseases in the World. *Journal of Hepatology* **70 (1)**: 151–171

Auffray, Cedric, Darin Fogg, Meriem Garfa, Gaelle Elain, Olivier Join-Lambert, Samer Kayal, Sabine Sarnacki, Ana Cumano, Gregoire Lauvau, and Frederic Geissmann. 2007. Monitoring of Blood Vessels and Tissues by a Population of Monocytes with Patrolling Behavior. *Science* **317 (5838)**: 666–670

Austyn, Jonathan M, Siamon Gordon, and Sir William Dunn. 1981. Monoclonal Anti-Macrophage Antibody F4/80, a Monoclonal Antibody Directed Specifically against the Mouse Macrophage. *Eur. J. Immunol* **11**: 805–815

Bain, Calum C, Alberto Bravo-Blas, Charlotte L Scott, Elisa Gomez Perdiguero, Frederic Geissmann, Sandrine Henri, Bernard Malissen, Lisa C Osborne, David Artis, and Allan McI Mowat. 2014. Constant replenishment from circulating monocytes maintains the macrophage pool in the intestine of adult mice. *Nature Immunology* **15 (10)**: 929–937

Bain, Calum C, Catherine A Hawley, Hannah Garner, Charlotte L Scott, Anika Schridde, Nicholas J Steers, Matthias Mack, Anagha Joshi, Martin Guilliams, Allan Mc I. Mowat, Frederic Geissmann, Stephen J Jenkins. 2016. Long-Lived Self-Renewing Bone Marrow-Derived Macrophages Displace Embryo-Derived Cells to Inhabit Adult Serous Cavities. *Nat. Commun.* **7**: ncomms11852

Balmer, Maria L, Emma Slack, Andrea de Gottardi, Melissa A E Lawson, Siegfried Hapfelmeier, Luca Miele, Antonio Grieco, et al. 2014. The Liver May Act as a Firewall Mediating Mutualism between the Host and Its Gut Commensal Microbiota. *Science Translational Medicine* **6 (237)**: 237ra66

Bartocci, A, D S Mastrogiannis, G Migliorati, R J Stockert, A W Wolkoff, and E R Stanley. 1987. Macrophages Specifically Regulate the Concentration of Their Own Growth Factor in the Circulation. *PNAS* **84 (17)**: 6179–6183

Bauer, Michael, and Inge Bauer. 2002. Heme Oxygenase-1: Redox Regulation and Role in the Hepatic Response to Oxidative Stress. *Antioxidants & Redox Signaling* **4 (5)**: 749–758

Baum, Jennifer, and Heather S Duffy. 2011. Fibroblasts and Myofibroblasts: What Are We Talking About? *Journal of Cardiovascular Pharmacology* **57 (4)**: 376–379

Beattie, Lynette, Amy Sawtell, Jason Mann, Teija C.M. Frame, Bianca Teal, Fabian de Labastida Rivera, Najmeeyah Brown, et al. 2016. Bone Marrow-Derived and Resident Liver Macrophages Display Unique Transcriptomic Signatures but Similar Biological Functions. *Journal of Hepatology* **65 (4)**: 758–768

Bernal, William, and Julia Wendon. 2013. Acute Liver Failure. *N Engl j Med* **369**: 2525–2534

Bertrand, Julien Y, Abdelali Jalil, Michèle Klaine, Steffen Jung, Ana Cumano, and Isabelle Godin. 2005.

Three Pathways to Mature Macrophages in the Early Mouse Yolk Sac. *Blood* **106 (9)**: 3004–3011

Blériot, Camille, Théo Dupuis, Grégory Jouvion, Gérard Eberl, Olivier Disson, and Marc Lecuit. 2015. Liver-Resident Macrophage Necroptosis Orchestrates Type 1 Microbicidal Inflammation and Type-2-Mediated Tissue Repair during Bacterial Infection. *Immunity* **42 (1)**: 145–158

Bonifer, Constanze, and David A Hume. 2008. The Transcriptional Regulation of the Colony-Stimulating Factor 1 Receptor (Csf1r) Gene during Hematopoiesis. *Frontiers in Bioscience*. **13**: 549-560

Bryan, Andrea K, Alexi Goranov, Angelika Amon, and Scott R Manalis. 2010. Measurement of Mass, Density, and Volume during the Cell Cycle of Yeast. *PNAS* **107 (3)**: 999–1004

Buchmann, Kurt. 2014. Evolution of Innate Immunity: Clues from Invertebrates via Fish to Mammals. *Frontiers in Immunology* **5**: 459

Bunchorntavakul C, N Chamroonkul, and D Chavalitdhamrong. 2016. Bacterial infection in cirrhosis: A critical review and practical guidance. *World Journal of Hepatology* **8 (6):** 307-321

Burkel, William E, and Frank N Low. 1966. The Fine Structure of Rat Liver Sinusoids, Space of Disse and Associated Tissue Space. *Am. J. Anat.* **118**: 769–84

Bykov, I., P. Ylipaasto, L. Eerola, and K. O. Lindros. 2003. Phagocytosis and LPS-stimulated Production of Cytokines and Prostaglandin E2 Is Different in Kupffer Cells Isolated from the Periportal or Perivenous Liver Region. *Scandinavian Journal of Gastroenterology* **38 (12)**: 1256–61

Campbell, Sharon M, Johanna A Knipper, Dominik Ruckerl, Conor M Finlay, Nicola Logan, Carlos M Minutti, Matthias Mack, Stephen J Jenkins, Matthew D Taylor, and Judith E Allen. 2018. Myeloid Cell Recruitment versus Local Proliferation Differentiates Susceptibility from Resistance to Filarial Infection. *ELife* **7**: e30947

Carlin, Leo M, Efstathios G Stamatiades, Cedric Auffray, Richard N Hanna, Leanne Glover, Gema Vizcay-Barrena, Catherine C Hedrick, H Terence Cook, Sandra Diebold, and Frederic Geissmann. 2013. Nr4a1-Dependent Ly6C(Low) Monocytes Monitor Endothelial Cells and Orchestrate Their Disposal. *Cell* **153 (2)**: 362–75

Cecchini, MG, Melissa G. Dominguez, S Mocci, A Wetterwald, R Felix, H Fleisch, O Chrisholm, W Hofstetter, Jeffrey W. Pollard, and Richard E. Stanley. 1994. Role of Colony Stimulating Factor-1 in the Establishment and Regulation of Tissue Macrophages during Postnatal Development of the Mouse. *Development* **120**: 1357–72

Chorro, Laurent, Aurélien Sarde, Mei Li, Kevin J Woollard, Pierre Chambon, Bernard Malissen, Adrien Kissenpfennig, Jean-Baptiste Barbaroux, Richard Groves, and Frédéric Geissmann. 2009. Langerhans Cell (LC) Proliferation Mediates Neonatal Development, Homeostasis, and Inflammation-Associated Expansion of the Epidermal LC Network. *The Journal of Experimental Medicine* **206 (13)**: 3089–3100

Cline, M J, and M A S Moore. 1972. Embryonic Origin of the Mouse Macrophage. *Blood* **39 (6)**: 842-849

Crane, Meredith J., Jean M. Daley, Olivier van Houtte, Samielle K. Brancato, William L. Henry, and Jorge E. Albina. 2014. The Monocyte to Macrophage Transition in the Murine Sterile Wound.. *PLoS ONE* **9 (1)**: e86660

Crofton, R W, M M Diesselhoff-den Dulk, and R van Furth. 1978. The Origin, Kinetics, and Characteristics of the Kupffer Cells in the Normal Steady State. *The Journal of Experimental Medicine* **148 (1)**: 1–17

Cummings, Brian S, Rick G Schnellmann, and Rick G. Schnellmann. 2004. Measurement of Cell Death in Mammalian Cells. *Current Protocols in Pharmacology* Chapter 12: Unit 12.8

Czernielewsk I, Janusz, Pierre Vaigot, and Michel Prunieras. 1985. Epidermal Langer Hans Cells-A Cycling Cell Population. *Journal of Investigative Dermatology* **84(5)**: 424-426

Dai, Xu-Ming, Gregory R Ryan, Andrew J Hapel, Melissa G Dominguez, Robert G Russell, Sara Kapp, Vonetta Sylvestre, and E Richard Stanley. 2002. Targeted Disruption of the Mouse Colony-Stimulating Factor 1 Receptor Gene Results in Osteopetrosis, Mononuclear Phagocyte Deficiency, Increased Primitive Progenitor Cell Frequencies, and Reproductive Defects. *Blood* **99 (1)**: 111–120

Dai, Xu-ming, Xiao-hua Zong, Vonetta Sylvestre, and E Richard Stanley. 2004. Incomplete Restoration of Colony-Stimulating Factor 1 (CSF-1) Function in CSF-1–Deficient Csf1. *Cell* **103 (3)**: 1114–1123

Dal-Secco, Daniela, Jing Wang, Zhutian Zeng, Elzbieta Kolaczkowska, Connie H Y Wong, Björn Petri, Richard M Ransohoff, Israel F Charo, Craig N Jenne, and Paul Kubes. 2015. A Dynamic Spectrum of Monocytes Arising from the in Situ Reprogramming of CCR2+ Monocytes at a Site of Sterile Injury. *The Journal of Experimental Medicine* **212 (4)**: 447-456

Dambach, D, Linda M. Watson, Kevin R. Gray, Stephen K. Durham, and Debra L. Laskin. 2002. Role of CCR2 in Macrophage Migration into the Liver during Acetaminophen-Induced Hepatotoxicity in the Mouse. *Hepatology* **35 (5)**: 1093–1103

David, Bruna Araujo, Rafael Machado Rezende, Maísa Mota Antunes, Mônica Morais Santos, Maria Alice Freitas Lopes, Ariane Barros Diniz, Rafaela Vaz Sousa Pereira, et al. 2016. Combination of Mass Cytometry and Imaging Analysis Reveals Origin, Location, and Functional Repopulation of Liver Myeloid Cells in Mice. *Gastroenterology* **151 (6)**: 1176–91

Davies, Luke C, Marcela Rosas, Stephen J Jenkins, Chia-Te Liao, Martin J Scurr, Frank Brombacher, Donald J Fraser, Judith E Allen, Simon a Jones, and Philip R Taylor. 2013. Distinct Bone Marrow-Derived and Tissue-Resident Macrophage Lineages Proliferate at Key Stages during Inflammation. *Nature Communications* **4**: 1886

Davies, Luke C, Marcela Rosas, Paul J Smith, Donald J Fraser, Simon a Jones, and Philip R Taylor. 2011. "A Quantifiable Proliferative Burst of Tissue Macrophages Restores Homeostatic Macrophage Populations after Acute Inflammation." *European Journal of Immunology* **41 (8)**: 2155–2164

Devey, Luke, David Ferenbach, Elodie Mohr, Kathryn Sangster, Christopher O Bellamy, Jeremy Hughes, and Stephen J Wigmore. 2009. Tissue-Resident Macrophages Protect the Liver From Ischemia Reperfusion Injury via a Heme Oxygenase-1-Dependent Mechanism. *Molecular Therapy* **17 (1)**: 65–72

Devisscher, Lindsey, Charlotte L. Scott, Sander Lefere, Sarah Raevens, Eliene Bogaerts, Annelies Paridaens, Xavier Verhelst, Anja Geerts, Martin Guilliams, and Hans Van Vlierberghe. 2017. Non-Alcoholic Steatohepatitis Induces Transient Changes within the Liver Macrophage Pool. *Cellular Immunology* **322**: 74–83

Dini, Luciana, Patrizia Pagliara, and Emanuela C Carla. 2002. Phagocytosis of Apoptotic Cells by Liver: A Morphological Study. *Microsc. Res. Tech* **57**: 530–540

Dixon, Laura J, Mark Barnes, Hui Tang, Michele T Pritchard, and Laura E Nagy. 2013. Kupffer Cells in the Liver. *Comprehensive Physiology* **3 (2)**: 785–797

Dranoff, Glenn, Alexander D Crawford, Michel Sadelain, Beverly Ream, Asif Rashid, Roderick T Bronson, G Richard Dickersin, et al. 1994. Involvement of Granulocyte-Macrophage Colony-Stimulating Factor in Pulmonary Homeostasis. *Science* **264 (5159)**:713-716

Du, Xianhong, Zhuanchang Wu, Yong Xu, Yuan Liu, Wen Liu, Tixiao Wang, Chunyang Li, et al. 2018. Increased Tim-3 Expression Alleviates Liver Injury by Regulating Macrophage Activation in MCD-Induced NASH Mice. *Cellular & Molecular Immunology* doi: 10.1038/s41423-018-0032-0

Edwards, Joshua L, and Robert E Klein. 1961. Cell Renewal in Adult Mouse Tissues. *American Journal of Pathology* **38 (4)**: 437–453

Egen, Jackson G, Antonio Gigliotti Rothfuchs, Carl G Feng, Nathalie Winter, Alan Sher, and Ronald N Germain. 2008. Macrophage and T Cell Dynamics during the Development and Disintegration of Mycobacterial Granulomas. *Immunity* **28 (2)**: 271–284

Elliott, Michael R., Faraaz B. Chekeni, Paul C. Trampont, Eduardo R. Lazarowski, Alexandra Kadl, Scott F. Walk, Daeho Park, et al. 2009. Nucleotides Released by Apoptotic Cells Act as a Find-Me Signal to Promote Phagocytic Clearance. *Nature* **461 (7261)**: 282–286

Endele, Max, Dirk Loeffler, Konstantinos D Kokkaliaris, Oliver Hilsenbeck, Stavroula Skylaki, Philipp S Hoppe, Axel Schambach, E Richard Stanley, and Timm Schroeder. 2017. CSF-1-Induced Src Signaling Can Instruct Monocytic Lineage Choice. *Blood* **129 (12)**: 1691–1701

Epelman, Slava, Kory J. Lavine, Anna E. Beaudin, Dorothy K. Sojka, Javier A. Carrero, Boris Calderon, Thaddeus Brija, et al. 2014. Embryonic and Adult-Derived Resident Cardiac Macrophages Are Maintained through Distinct Mechanisms at Steady State and during Inflammation. *Immunity* **40 (1)**: 91–104

Epelman, Slava, Kory J Lavine, and Gwendalyn J Randolph. 2014. Origin and Functions of Tissue Macrophages. *Immunity* **41 (1)**: 21–35

Fallowfield, Jonathan A, Masashi Mizuno, Timothy J Kendall, Christothea M Constandinou, R Christopher Benyon, Jeremy S Duffield, and John P Iredale. 2007. Scar-Associated Macrophages Are a Major Source of Hepatic Matrix Metalloproteinase-13 and Facilitate the Resolution of Murine Hepatic Fibrosis. *Journal of Immunology* **178 (8)**: 5288–5295

Ferrero, Giuliano, Christopher B Mahony, David Traver, Julien Y Bertrand, and Valé Rie Wittamer. 2018. Embryonic Microglia Derive from Primitive Macrophages and Are Replaced by Cmyb-Dependent Definitive Microglia in Zebrafish. *Cell rep.* **24 (1)**: 130-141

Forbes, Amy, Mike Pickell, Mehry Foroughian, Li-Juan Yao, James Lewis, and Ruud Veldhuizen. 2007. Alveolar Macrophage Depletion Is Associated with Increased Surfactant Pool Sizes in Adult Rats. *Journal of Applied Physiology* **103 (2)**: 637–645

Forbes, Stuart J., and Philip N. Newsome. 2016. Liver Regeneration — Mechanisms and Models to Clinical Application. *Nature Reviews Gastroenterology & Hepatology* **13 (8)**: 473–485

Foudi, Adlen, Konrad Hochedlinger, Denille Van Buren, Jeffrey W Schindler, Rudolf Jaenisch, Vincent Carey, and Hanno Hock. 2009. Analysis of Histone 2B-GFP Retention Reveals Slowly Cycling Hematopoietic Stem Cells. *Nature Biotechnology* **27 (1)**: 84–90

Frame, Jenna M, Kathleen E McGrath, and James Palis. 2013. Erythro-Myeloid Progenitors: "Definitive" Hematopoiesis in the Conceptus Prior to the Emergence of Hematopoietic Stem Cells. *Blood Cells, Molecules & Diseases* **51 (4)**: 220–325

Furth, R Van, Z A Cohn, J G Hirsch, J H Humphrey, W G Specior, and H L Langevoort5. 1972. The Mononuclear Phagocyte System: A New Classification of Macrophages, Monocytes, and Their Precursor Cells. *Bulletin of the World Helath Organization* **46 (6)**: 845–852

Furth, Ralph van, and Zanvil A. Cohn. 1968. The Origin and Kinetic of Mononuclear Phagocytes. *Journal*

of Experimental Medicine **128 (3)**: 415-435

Ganesan, Latha P., Jonghan Kim, Yun Wu, Sudhasri Mohanty, Gary S. Phillips, Daniel J. Birmingham, John M. Robinson, and Clark L. Anderson. 2012. FcγRIIb on Liver Sinusoidal Endothelium Clears Small Immune Complexes. *The Journal of Immunology* **189 (10)**:4981-4988

Gautier, Emmanuel L, Tal Shay, Jennifer Miller, Melanie Greter, Claudia Jakubzick, Stoyan Ivanov, Julie Helft, et al. 2012. Gene-Expression Profiles and Transcriptional Regulatory Pathways That Underlie the Identity and Diversity of Mouse Tissue Macrophages. *Nature Immunology* **13 (11)**: 1118–1128

Geissmann, Frederic, Steffen Jung, and Dan R Littman. 2003. Blood Monocytes Consist of Two Principal Subsets with Distinct Migratory Properties. *Immunity* **19 (1)**: 71–82

Ghigo, Clément, Isabelle Mondor, Audrey Jorquera, Jonathan Nowak, Stephan Wienert, Sonja P Zahner, Björn E Clausen, et al. 2013. Multicolor Fate Mapping of Langerhans Cell Homeostasis. *The Journal of Experimental Medicine* **210 (9)**: 1657–1664

Ginhoux, Florent, Melanie Greter, Marylene Leboeuf, Sayan Nandi, Peter See, Solen Gokhan, Mark F. Mehler, et al. 2010. Fate Mapping Analysis Reveals That Adult Microglia Derive from Primitive Macrophages. *Science* **330 (6005)**: 841-845

Ginhoux, Florent, and Steffen Jung. 2014. Monocytes and Macrophages: Developmental Pathways and Tissue Homeostasis. *Nature Reviews Immunology* **14 (6)**: 392-404

Ginhoux, Florent, Frank Tacke, Veronique Angeli, Milena Bogunovic, Martine Loubeau, Xu-Ming Dai, E Richard Stanley, Gwendalyn J Randolph, and Miriam Merad. 2006. Langerhans Cells Arise from Monocytes in Vivo. *Nature Immunology* **7 (3)**: 265–273

Goh, Y P Sharon, Neil C Henderson, Jose E Heredia, Alex Red Eagle, Justin I Odegaard, Nadja Lehwald, Khoa D Nguyen, et al. 2013. Eosinophils Secrete IL-4 to Facilitate Liver Regeneration. *PNAS* 110 (24): 9914–9919

Gomez Perdiguero, Elisa, Kay Klapproth, Christian Schulz, Katrin Busch, Emanuele Azzoni, Lucile Crozet, Hannah Garner, et al. 2015. Tissue-Resident Macrophages Originate from Yolk-Sac-Derived Erythro-Myeloid Progenitors. *Nature* **518 (7540)**: 547-551

Goodman, Joan Wright. 1964. On the Origin of Peritoneal Fluid Cells. *Blood* **32 (1)**: 18–26

van der Laan, LJ, Ed A Döpp, Richard Haworth, Timo Pikkarainen, Maarit Kangas, Outi Elomaa, CD Dijkstra, Siamon Gordon, Karl Tryggvason, and Georg D Kraal. 1999. Regulation and Functional Involvement Of Macrophage Scavenger Receptor MARCO in Clearance of Bacteria In Vivo. *J. Immunol.* **162 (2)**: 939-947

Gow, Deborah J, Kristin A Sauter, Clare Pridans, Lindsey Moffat, Anuj Sehgal, Ben M Stutchfield, Sobia Raza, et al. 2014. Characterisation of a Novel Fc Conjugate of Macrophage Colony-Stimulating Factor. *Molecular Therapy : The Journal of the American Society of Gene Therapy* **22 (9)**: 1580–1592

Graubardt, Nadine, Milena Vugman, Odelia Mouhadeb, Gabriele Caliari, Metsada Pasmanik-Chor, Debby Reuveni, Ehud Zigmond, et al. 2017. Ly6Chi Monocytes and Their Macrophage Descendants Regulate Neutrophil Function and Clearance in Acetaminophen-Induced Liver Injury. *Frontiers in Immunology* **8**: 626.

Greenhill, C J, S Rose-John, R Lissilaa, W Ferlin, M Ernst, P J Hertzog, A Mansell, and B J Jenkins. 2011. Via STAT3 TLR4-Dependent Inflammatory Responses-Signaling Modulates Trans IL-6. *J Immunol* **186**: 1199–1208

Guilberts, Larry J, and E Richard Stanley. 1986. The Interaction of 125I-Colony-Stimulating Factor-1 with Bone Marrow-Derived Macrophages. *The Journal of Biological Chemistry* **261 (9)**: 4024–4032

Guilliams, Martin, Charles-Antoine Dutertre, Charlotte L Scott, Naomi McGovern, Dorine Sichien, Svetoslav Chakarov, Sofie Van Gassen, et al. 2016. Unsupervised High-Dimensional Analysis Aligns Dendritic Cells across Tissues and Species. *Immunity* **45 (3)**: 669–684

Guilliams, Martin, Ismé De Kleer, Sandrine Henri, Sijranke Post, Leen Vanhoutte, Sofie De Prijck, Kim Deswarte, Bernard Malissen, Hamida Hammad, and Bart N Lambrecht. 2013. Alveolar Macrophages Develop from Fetal Monocytes That Differentiate into Long-Lived Cells in the First Week of Life via GM-CSF. *The Journal of Experimental Medicine* **210 (10)**: 1977–1992

Guilliams, Martin, Alexander Mildner, and Simon Yona. 2018. Developmental and Functional Heterogeneity of Monocytes. *Immunity* **49 (4)**: 595–613

Guilliams, Martin, and Charlotte L. Scott. 2017. Does Niche Competition Determine the Origin of Tissue-Resident Macrophages? *Nature Reviews Immunology* **17 (7)**: 451–460

Haarl, Jack L, and GA Ackerman. 1971. A Phase and Electron Microscopic Study of Vasculogenesis and Erythropoiesis in the Yolk Sac of the Mouse. *Anat. Rec.* **170 (2)**: 199-223

Hafenrichter, D G, C R Roland, M J Mangino, and M W Flye. 1994. The Kupffer Cell in Endotoxin Tolerance: Mechanisms of Protection against Lethal Endotoxemia. *Shock* **2 (4)**: 251–256

Haniffa, Muzlifah, Florent Ginhoux, Xiao-Nong Wang, Venetia Bigley, Michal Abel, Ian Dimmick, Sarah Bullock, et al. 2009. Differential Rates of Replacement of Human Dermal Dendritic Cells and Macrophages during Hematopoietic Stem Cell Transplantation. *The Journal of Experimental Medicine* **206 (2)**: 371–385

Hanna, Richard N, Leo M Carlin, Harper G Hubbeling, Dominika Nackiewicz, Angela M Green, Jennifer A Punt, Frederic Geissmann, and Catherine C Hedrick. 2011. The Transcription Factor NR4A1 (Nur77) Controls Bone Marrow Differentiation and the Survival of Ly6C− Monocytes. *Nature Immunology* **12 (8)**: 778–785

Hashimoto, Daigo, Andrew Chow, Clara Noizat, Pearline Teo, Mary Beth Beasley, Marylene Leboeuf, Christian D Becker, et al. 2013. Tissue-Resident Macrophages Self-Maintain Locally throughout Adult Life with Minimal Contribution from Circulating Monocytes. *Immunity* **38 (4)**: 792–804

Haskill, Stephen, and Susanne Becker. 1985. Disappearance and Reappearance of Resident Macrophages: Importance in C. Parvum-Induced Tumoricidal Activity. *Cellular Immunology* **90 (1)**: 179–189

Hawley, Catherine A, Rocio Rojo, Anna Raper, Kristin A Sauter, Zofia M Lisowski, Kathleen Grabert, Calum C Bain, et al. 2018. Csf1r-MApple Transgene Expression and Ligand Binding In Vivo Reveal Dynamics of CSF1R Expression within the Mononuclear Phagocyte System. *Journal of Immunology* **200 (6)**: 2209–2223

He, Huanhuan, Jingying Xu, Carmen M Warren, Dan Duan, Xinmin Li, Lily Wu, and M Luisa Iruela-Arispe. 2012. Endothelial Cells Provide an Instructive Niche for the Differentiation and Functional Polarization of M2-like Macrophages. *Blood* **120 (15)**: 3152–3162

Heng, Tracy S P, Michio W Painter, Kutlu Elpek, Veronika Lukacs-Kornek, Nora Mauermann, Shannon J Turley, Daphne Koller, et al. 2008. The Immunological Genome Project: Networks of Gene Expression in Immune Cells. *Nature Immunology* **9 (10)**: 1091–1094

Hesketh, Mark, Katherine B Sahin, Zoe E West, and Rachael Z Murray. 2017. Macrophage Phenotypes

Regulate Scar Formation and Chronic Wound Healing. *International Journal of Molecular Sciences* **18 (7)**: pii:E1545

Hess, David C., Takanori Abe, William D. Hill, Angeline Martin Studdard, Jo Carothers, Masahiro Masuya, Paul A. Fleming, Christopher J. Drake, and Makio Ogawa. 2004. Hematopoietic Origin of Microglial and Perivascular Cells in Brain. *Experimental Neurology* **186 (2)**: 134–144

Hettinger, Jan, David M Richards, Jenny Hansson, Melanie M Barra, Ann-Cathrin Joschko, Jeroen Krijgsveld, and Markus Feuerer. 2013. Origin of Monocytes and Macrophages in a Committed Progenitor. *Nature Immunology* **14 (8)**: 821–830

Heymann, Felix, Julia Peusquens, Isis Ludwig-Portugall, Marlene Kohlhepp, Can Ergen, Patricia Niemietz, Christian Martin, et al. 2015. Liver Inflammation Abrogates Immunological Tolerance Induced by Kupffer Cells. *Hepatology* **62 (1)**: 279–291

Heymann, Felix, and Frank Tacke. 2016. Immunology in the Liver--from Homeostasis to Disease. *Nature Reviews. Gastroenterology & Hepatology* **13 (2)**: 88–110

Hoeffel, Guillaume, Jinmiao Chen, Yonit Lavin, Donovan Low, Francisca F. Almeida, Peter See, Anna E. Beaudin, et al. 2015. C-Myb^{+} Erythro-Myeloid Progenitor-Derived Fetal Monocytes Give Rise to Adult Tissue-Resident Macrophages. *Immunity* **21 (424)**: 665-678

Hoeffel, Guillaume and Florent Ginhoux. 2015. Ontogeny of Tissue-Resident Macrophages. *Frontiers in Immunology* **6**: 486

Hoeffel, Guillaume and Florent Ginhoux. 2018. Fetal Monocytes and the Origins of Tissue-Resident Macrophages *Cellular Immunology* **330**: 5–15

Hoeffel, Guillaume, Yilin Wang, Melanie Greter, Peter See, Pearline Teo, Benoit Malleret, Marylène Leboeuf, et al. 2012. Adult Langerhans Cells Derive Predominantly from Embryonic Fetal Liver Monocytes with a Minor Contribution of Yolk Sac–Derived Macrophages. *Journal of Experimental Medicine* **209 (6)**: 1167-1181

Holt, Michael P, LinLing Cheng, and Cynthia Ju. 2008. Identification and Characterization of Infiltrating Macrophages in Acetaminophen-Induced Liver Injury. *Journal of Leukocyte Biology* **84 (6)**: 1410–1421

Hughes, D A, I P Fraser, and W S Gordon. 1995. Murine Macrophage Scavenger Receptor: In Vivo Expression and Function as Receptor for Macrophage Adhesion in Lymphoid and Non-Lymphoid Organs. *Journal of Immunology* **25**: 466–473.

Hume, David A. 2008. Macrophages as APC and the Dendritic Cell Myth. *The Journal of Immunology* **181 (9)**: 5829–5835

Hume, David A, Katharine M Irvine, and Clare Pridans. 2019. The Mononuclear Phagocyte System: The Relationship between Monocytes and Macrophages. *Trends in Immunology* **40 (2)**: 98–112

Imaeda, Avlin B, Azuma Watanabe, Muhammad A Sohail, Shamail Mahmood, Mehdi Mohamadnejad, Fayyaz S Sutterwala, Richard A Flavell, and Wajahat Z Mehal. 2009. Acetaminophen-Induced Hepatotoxicity in Mice Is Dependent on Tlr9 and the Nalp3 Inflammasome. *The Journal of Clinical Investigation* **119 (2)**: 305–314

Iredale, J P, C Hovell, M J Arthur, R C Benyon, J Pickering, M Mccullen, M Northrop, S Pawley, and M J P Arthur. 1998. Mechanisms of Spontaneous Resolution of Rat Liver Fibrosis. Hepatic Stellate Cell Apoptosis and Reduced Hepatic Expression of Metalloproteinase Inhibitors. Mechanisms of Spontaneous Resolution of Rat Liver Fibrosis Hepatic Stellate Cell Apoptosis and Reduced Hepatic Expression of Metalloproteinase Inhibitors. *J. Clin. Invest* **102 (3)**: 538–549

Jain, Nikhil, Jens Moeller, and Viola Vogel. 2019. Mechanobiology of Macrophages: How Physical Factors Coregulate Macrophage Plasticity and Phagocytosis. *Annual Review of Biomedical Engineering* **21 (1)**: 267–297

Jain, Nikhil, and Viola Vogel. 2018. Spatial Confinement Downsizes the Inflammatory Response of Macrophages. *Nature Materials* **17 (12)**: 1134–1144

Jenkins, Stephen J, and David a Hume. 2014. Homeostasis in the Mononuclear Phagocyte System. *Trends in Immunology* **35 (8)**: 358–367

Jenkins, Stephen J, Dominik Ruckerl, Peter C Cook, Lucy H Jones, Fred D Finkelman, Nico van Rooijen, Andrew S MacDonald, and Judith E Allen. 2011. Local Macrophage Proliferation, Rather than Recruitment from the Blood, Is a Signature of TH2 Inflammation. *Science* **332 (6035)**: 1284–1288

Jenkins, Stephen J, Dominik Ruckerl, Graham D Thomas, James P Hewitson, Sheelagh Duncan, Frank Brombacher, Rick M Maizels, David a Hume, and Judith E Allen. 2013. IL-4 Directly Signals Tissue-Resident Macrophages to Proliferate beyond Homeostatic Levels Controlled by CSF-1. *The Journal of Experimental Medicine* **210 (11)**: 2477–2491

Kanayama, Masashi, Makoto Inoue, Keiko Danzaki, Gianna Hammer, You-Wen He, and Mari L. Shinohara. 2015. Autophagy Enhances NFκB Activity in Specific Tissue Macrophages by Sequestering A20 to Boost Antifungal Immunity. *Nature Communications* **6 (1)**: 5779

Karlmark, Karlin Raja, Ralf Weiskirchen, Henning W. Zimmermann, Nikolaus Gassler, Florent Ginhoux, Christian Weber, Miriam Merad, Tom Luedde, Christian Trautwein, and Frank Tacke. 2009. Hepatic Recruitment of the Inflammatory Gr1 $^{+}$ Monocyte Subset upon Liver Injury Promotes Hepatic Fibrosis. *Hepatology* 50 (1): 261–274

Kau, C L, and J B Turpen. 1983. Dual Contribution of Embryonic Ventral Blood Island and Dorsal Lateral Plate Mesoderm during Ontogeny of Hemopoietic Cells in Xenopus Laevis. *Journal of Immunology* **131 (5)**: 2262–2266

Kegel, Victoria, Daniela Deharde, Elisa Pfeiffer, Katrin Zeilinger, Daniel Seehofer, and Georg Damm. 2016. Protocol for Isolation of Primary Human Hepatocytes and Corresponding Major Populations of Non-Parenchymal Liver Cells. *Journal of Visualized Experiments* **109**: e53069

Kieusseian, Aurelie, Philippe Brunet de la Grange, Odile Burlen-Defranoux, Isabelle Godin, and Ana Cumano. 2012. Immature Hematopoietic Stem Cells Undergo Maturation in the Fetal Liver. *Development* **139 (19)**: 3521–3530

Kirby, Alun C, Mark C Coles, and Paul M Kaye. 2009. Alveolar Macrophages Transport Pathogens to Lung Draining Lymph Nodes. *J. Immunol.* **183 (3)**: 1983–1989

Klein, Ingo, Judith C. Cornejo, Noelle K. Polakos, Beena John, Sherry A. Wuensch, David J. Topham, Robert H. Pierce, and Ian Nicholas Crispe. 2007. Kupffer Cell Heterogeneity: Functional Properties of Bone Marrow–Derived and Sessile Hepatic Macrophages. *Blood* **110 (12)**:4077-4085

Kohyama, Masako, Wataru Ise, Brian T. Edelson, Peter R. Wilker, Kai Hildner, Carlo Mejia, William A. Frazier, Theresa L. Murphy, and Kenneth M. Murphy. 2009. Role for Spi-C in the Development of Red Pulp Macrophages and Splenic Iron Homeostasis. *Nature* **457 (7227)**: 318–321

Kovalovich, Kellen, Robert A Deangelis, Wei Li, Emma E Furth, Gennaro Ciliberto, and Rebecca Taub. 2000. Increased Toxin-Induced Liver Injury and Fibrosis in Interleukin-6–Deficient Mice. *Hepatology* **31 (1)**: 149–159

Krall, Jordan A., Elsa M. Beyer, and Gavin MacBeath. 2011. High- and Low-Affinity Epidermal Growth

Factor Receptor-Ligand Interactions Activate Distinct Signaling Pathways. *PLoS ONE* **6 (1)**: e15945

Kus, Edyta, Patrycja Kaczara, Izabela Czyzynska-Cichon, Karolina Szafranska, Bartlomiej Zapotoczny, Agnieszka Kij, Agnieszka Sowinska, et al. 2019. LSEC Fenestrae Are Preserved Despite Pro-Inflammatory Phenotype of Liver Sinusoidal Endothelial Cells in Mice on High Fat Diet. *Frontiers in Physiology* **10**: 6

Laan, L J van der, E A Döpp, R Haworth, T Pikkarainen, M Kangas, O Elomaa, C D Dijkstra, S Gordon, K Tryggvason, and G Kraal. 1999. Regulation and Functional Involvement of Macrophage Scavenger Receptor MARCO in Clearance of Bacteria in Vivo. *Journal of Immunology* **162 (2)**: 939–947

Laar, Lianne van de, Wouter Saelens, Sofie De Prijck, Liesbet Martens, Charlotte L Scott, Gert Van Isterdael, Eik Hoffmann, et al. 2016. Yolk Sac Macrophages, Fetal Liver, and Adult Monocytes Can Colonize an Empty Niche and Develop into Functional Tissue-Resident Macrophages. *Immunity* **44 (4)**: 755–768

Lassila, Olli, Jussi Eskola, Paavo Toivanen, Calude Martin and Francoise Dieterlen-Lievre. 1978. The Origin of Lymphoid Stem Cells Studied in Chick Yolk Sac–Embryo Chimaeras. *Nature* **272 (5651)**: 353–354

Lauder, Sarah N, Philip R Taylor, Stephen R Clark, Rhys L Evans, James P Hindley, Kathryn Smart, Heather Leach, et al. 2011. Paracetamol Reduces Influenza-Induced Immunopathology in a Mouse Model of Infection without Compromising Virus Clearance or the Generation of Protective Immunity. *Thorax* **66 (5)**: 368–374

Lavin, Yonit, Deborah Winter, Ronnie Blecher-Gonen, Eyal David, Hadas Keren-Shaul, Miriam Merad, Steffen Jung, et al. 2014. Tissue-Resident Macrophage Enhancer Landscapes Are Shaped by the Local Microenvironment. *Cell* **159 (6)**: 1312–1326

Le, T L, A S Yap, and J L Stow. 1999. Recycling of E-Cadherin: A Potential Mechanism for Regulating Cadherin Dynamics. *The Journal of Cell Biology* **146 (1)**: 219–232

Lee, W and P. Kubes. 2008. Leukocyte adhesion in the liver: distinct adhesion paradigm from other organs. *Journal of Hepatology* **48 (3):** 504-512

Li, Guiyu, Yue Peng, Tiejian Zhao, Jiyong Lin, Xuelin Duan, Yanfei Wei, and Jing Ma. 2017. Plumbagin Alleviates Capillarization of Hepatic Sinusoids In Vitro by Downregulating ET-1, VEGF, LN, and Type IV Collagen. *BioMed Research International* **2017**: 5603216

Liaskou, E., H. W. Zimmermann, K. K. Li, Y. H. Oo, S. Suresh, Z. Stamataki, O. Qureshi, P. F. Lalor, J. Shaw, W. K. Syn, S. M. Curbishley, D. H. Adams. 2013. Monocyte subsets in human liver disease show distinct phenotypic and functional characteristics. *Hepatology* **57 (1):** 385-398

Lin, Hsi-Hsien, Douglas E. Faunce, Martin Stacey, Ania Terajewicz, Takahiko Nakamura, Jie Zhang-Hoover, Marilyn Kerley, Michael L. Mucenski, Siamon Gordon, and Joan Stein-Streilein. 2005. The Macrophage F4/80 Receptor Is Required for the Induction of Antigen-Specific Efferent Regulatory T Cells in Peripheral Tolerance. *Journal of Experimental Medicine* **201 (10)**: 1615-1625

Liu, Yan, Christoph Meyer, Chengfu Xu, Honglei Weng, Claus Hellerbrand, Peter ten Dijke, and Steven Dooley. 2013. Animal Models of Chronic Liver Diseases. *American Journal of Physiology-Gastrointestinal and Liver Physiology* **304 (5)**: G449–468

Liu, Zuo-Jin, Lu-Nan Yan, Xu-Hong Li, Fa-Liang Xu, Xian-Feng Chen, Hai-Bo You, and Jian-Ping Gong. 2008. Up-Regulation of IRAK-M Is Essential for Endotoxin Tolerance Induced by a Low Dose of Lipopolysaccharide in Kupffer Cells. *Journal of Surgical Research* **150 (1)**: 34–39

Lloyd, Amy F., Claire L. Davies, Rebecca K. Holloway, Yasmine Labrak, Graeme Ireland, Dario Carradori, Alessandra Dillenburg, et al. 2019. Central Nervous System Regeneration Is Driven by Microglia Necroptosis and Repopulation. *Nature Neuroscience* **22 (7)**: 1046–1052

Locatelli, Irene, Salvatore Sutti, Aastha Jindal, Marco Vacchiano, Cristina Bozzola, Chris Reutelingsperger, Dennis Kusters, et al. 2014. Endogenous Annexin A1 Is a Novel Protective Determinant in Nonalcoholic Steatohepatitis in Mice. *Hepatology* **60 (2)**: 531–544

Lopez, Bryan G, Monica S Tsai, Janie L Baratta, Kenneth J Longmuir, and Richard T Robertson. 2011. Characterization of Kupffer Cells in Livers of Developing Mice. *Comparative Hepatology* **10 (1)**: 2

Lough, John, Leonard Rosenthall, Artin Arzoumanian, and Carl A. Goresky. 1987. Kupffer Cell Depletion Associated with Capillarization of Liver Sinusoids in Carbon Tetrachloride-Induced Rat Liver Cirrhosis. *Journal of Hepatology* **5 (2)**: 190–198

Louis, Cynthia, Andrew D. Cook, Derek Lacey, Andrew J. Fleetwood, Ross Vlahos, Gary P. Anderson, and John A. Hamilton. 2015. Specific Contributions of CSF-1 and GM-CSF to the Dynamics of the Mononuclear Phagocyte System. *The Journal of Immunology* **195 (1)**: 134–144

Lu, Wei-Yu, Thomas G Bird, Luke Boulter, Atsunori Tsuchiya, Alicia M Cole, Trevor Hay, Rachel V Guest, et al. 2015. Hepatic Progenitor Cells of Biliary Origin with Liver Repopulation Capacity. *Nature Cell Biology* **17 (8)**: 971–983

Lucas, Tina, Ari Waisman, Rajeev Ranjan, Jürgen Roes, Thomas Krieg, Werner Müller, Axel Roers, and Sabine A. Eming. 2010. Differential Roles of Macrophages in Diverse Phases of Skin Repair. *The Journal of Immunology* **184 (7)**: 3964–3977

Luo, Xiaoying, Dan Wang, Xintao Zhu, Guozhen Wang, Yuehua You, Zuowei Ning, Yang Li, et al. 2018. Autophagic Degradation of Caveolin-1 Promotes Liver Sinusoidal Endothelial Cells Defenestration. *Cell Death & Disease* **9 (5)**: 576

Lynch, Ruairi W., Catherine A. Hawley, Antonella Pellicoro, Calum C. Bain, John P. Iredale, and Stephen J. Jenkins. 2018. An Efficient Method to Isolate Kupffer Cells Eliminating Endothelial Cell Contamination and Selective Bias. *Journal of Leukocyte Biology* **104 (3)**: 579-586

MacDonald, Kelli P A, James S Palmer, Stephen Cronau, Elke Seppanen, Stuart Olver, Neil C Raffelt, Rachel Kuns, et al. 2010. An Antibody against the Colony-Stimulating Factor 1 Receptor Depletes the Resident Subset of Monocytes and Tissue- and Tumor-Associated Macrophages but Does Not Inhibit Inflammation. *Blood* **116 (19)**: 3955–3963

Marcellin, Patrick, and Blaise K Kutala. 2018. Liver Diseases: A Major, Neglected Global Public Health Problem Requiring Urgent Actions and Large-Scale Screening. *Liver Int.* **38 (1)**: 2-6

Markose, D., P. Kirkland, P. Ramachandran, and N.C. Henderson. 2018. Immune Cell Regulation of Liver Regeneration and Repair. *Journal of Immunology and Regenerative Medicine* **2**: 1–10

Martin-Murphy, Brittany V, Michael P Holt, and Cynthia Ju. 2010. The Role of Damage Associated Molecular Pattern Molecules in Acetaminophen-Induced Liver Injury in Mice. *Toxicology Letters* **1 (3)**: 387–394

McCuskey, Robert S and Patricia A Mccuskey. 1990. Fine Structure and Function of Kupffer Cells. *J. Electron Microsc. Tech.* **14 (3)**: 237-246

McDonald, Braedon, and Paul Kubes. 2016. Innate Immune Cell Trafficking and Function During Sterile Inflammation of the Liver. *Gastroenterology* **151 (6)**: 1087–1095

McGrath, K. E., Anne D Koniski, Jeffrey Malik, and James Palis. 2003. Circulation Is Established in a

Stepwise Pattern in the Mammalian Embryo. *Blood* **101 (5)**: 1669–1675

McGrath, Kathleen E, Jenna M Frame, Katherine H Fegan, James R Bowen, Simon J Conway, Seana C Catherman, Paul D Kingsley, Anne D Koniski, and James Palis. 2015. Distinct Sources of Hematopoietic Progenitors Emerge before HSCs and Provide Functional Blood Cells in the Mammalian Embryo. *Cell Reports* **11 (12)**: 1892–1904

Medvinsky, A, and E Dzierzak. 1996. Definitive Hematopoiesis Is Autonomously Initiated by the AGM Region. *Cell* **86 (6)**: 897–906

Merad, Miriam, Markus G. Manz, Holger Karsunky, Amy Wagers, Wendy Peters, Israel Charo, Irving L. Weissman, Jason G. Cyster, and Edgar G. Engleman. 2002. Langerhans Cells Renew in the Skin throughout Life under Steady-State Conditions. *Nature Immunology* **3 (12)**: 1135–1141

Mercier, Francois E, David B Sykes, and David T Scadden. 2016. Single Targeted Exon Mutation Creates a True Congenic Mouse for Competitive Hematopoietic Stem Cell Transplantation: The C57BL/6-CD45.1 (STEM) Mouse. *Stem Cell Reports* **6 (6)**: 985–992

Mildner, Alexander, Bernhard Schlevogt, Katrin Kierdorf, Chotima Böttcher, Daniel Erny, Markus P Kummer, Michael Quinn, et al. 2011. Distinct and Non-Redundant Roles of Microglia and Myeloid Subsets in Mouse Models of Alzheimer's Disease. *Journal of Neuroscience* **31 (31)**: 11159–11171

Mildner, Alexander, Jörg Schönheit, Amir Giladi, Eyal David, David Lara-Astiaso, Erika Lorenzo-Vivas, Franziska Paul, et al. 2017. Genomic Characterization of Murine Monocytes Reveals C/EBPβ Transcription Factor Dependence of Ly6C− Cells. *Immunity* **46 (5)**: 849-862

Minutti, Carlos M., Johanna A. Knipper, Judith E. Allen, and Dietmar M.W. Zaiss. 2017. Tissue-Specific Contribution of Macrophages to Wound Healing. *Seminars in Cell & Developmental Biology* **61**: 3–11

Misharin, Alexander V, Luisa Morales-Nebreda, Paul A Reyfman, Carla M Cuda, James M Walter, Alexandra C McQuattie-Pimentel, Ching-I Chen, et al. 2017. Monocyte-Derived Alveolar Macrophages Drive Lung Fibrosis and Persist in the Lung over the Life Span. *The Journal of Experimental Medicine* **214 (8)**: 2387–2404

Mitchell, Claudia, Dominique Couton, Jean-Pierre Couty, Marie Anson, Anne-Marie Crain, Vinciane Bizet, Laurent Rénia, Stanislas Pol, Vincent Mallet, and Hélène Gilgenkrantz. 2009. Dual Role of CCR2 in the Constitution and the Resolution of Liver Fibrosis in Mice. *The American Journal of Pathology* **174 (5)**: 1766–1775

Miyanishi, Masanori, Kazutoshi Tada, Masato Koike, Yasuo Uchiyama, Toshio Kitamura, and Shigekazu Nagata. 2007. Identification of Tim4 as a Phosphatidylserine Receptor. *Nature* **450 (7168)**: 435–439

Molawi, Kaaweh, Yochai Wolf, Prashanth K Kandalla, Jeremy Favret, Nora Hagemeyer, Kathrin Frenzel, Alexander R Pinto, et al. 2014. Progressive Replacement of Embryo-Derived Cardiac Macrophages with Age. *The Journal of Experimental Medicine* **211 (11)**: 2151–2158

Mori, Yoko, Takeshi Izawa, Shigeo Takenaka, Mitsuru Kuwamura, and Jyoji Yamate. 2009. Participation of Functionally Different Macrophage Populations and Monocyte Chemoattractant Protein-1 in Early Stages of Thioacetamide-Induced Rat Hepatic Injury. *Toxicologic Pathology* **37 (4)**: 463–473

Mosher, B, R Dean, J Harkema, D Remick, J Palma, and E Crockett. 2001. Inhibition of Kupffer Cells Reduced CXC Chemokine Production and Liver Injury. *The Journal of Surgical Research* **99 (2)**: 201–210

Mossanen, Jana C., Oliver Krenkel, Can Ergen, Olivier Govaere, Anke Liepelt, Tobias Puengel, Felix Heymann, et al. 2016. Chemokine (C-C Motif) Receptor 2-Positive Monocytes Aggravate the Early Phase of Acetaminophen-Induced Acute Liver Injury. *Hepatology* **64 (5)**: 1667–1682

Movita, Dowty, Kim Kreefft, Paula Biesta, Adri Van Oudenaren, Pieter J M Leenen, Harry L A Janssen, and Andre Boonstra. 2012. Kupffer Cells Express a Unique Combination of Phenotypic and Functional Characteristics Compared with Splenic and Peritoneal Macrophages. *Journal of Leukocyte Biology* **92**: 723–733

Munn, D H, J Pressey, A C Beall, R Hudes, and M R Alderson. 1996. Selective Activation-Induced Apoptosis of Peripheral T Cells Imposed by Macrophages. A Potential Mechanism of Antigen-Specific Peripheral Lymphocyte Deletion. *Journal of Immunology* **156 (2)**: 523–532

Murphy, Jaime, Ross Summer, Andrew A. Wilson, Darrell N. Kotton, and Alan Fine. 2008. The Prolonged Life-Span of Alveolar Macrophages. *American Journal of Respiratory Cell and Molecular Biology* **38 (4)**: 380

Nagase, H, R Visse, and G Murphy. 2006. Structure and Function of Matrix Metalloproteinases and TIMPs. *Cardiovascular Research* **69 (3)**: 562–573

Naito, Makoto, Kiyoshi Takahashi, and Shin-Lchi Nishikawa. 1990. Development, Differentiation, and Maturation of Macrophages in the Fetal Mouse Liver. *Journal of Leukocyte Biology* **48**: 27–37

Nakamura, Koji, Hidenori Nonaka, Hiroki Saito, Minoru Tanaka, and Atsushi Miyajima. 2004. Hepatocyte Proliferation and Tissue Remodeling Is Impaired After Liver Injury in Oncostatin M Receptor Knockout Mice. *Hepatology* **39 (3)**: 635–644

Nayak, D. K., F. Zhou, M. Xu, J. Huang, M. Tsuji, R. Hachem, and T. Mohanakumar. 2016. Long-Term Persistence of Donor Alveolar Macrophages in Human Lung Transplant Recipients That Influences Donor-Specific Immune Responses. *American Journal of Transplantation* **16 (8)**: 2300–2311

Nelson, D S, and S V Boyden. 1963. The Loss of Macrophages from Peritoneal Exudates Following the Injection of Antigens into Guinea-Pigs with Delayed-Type Hypersensitivity. *Immunology* **6 (3)**: 264–275

Ohashi, Koji, Volker Burkart, Stefanie Flohé, and Hubert Kolb. 2000. Heat Shock Protein 60 is a Putative Endogneous Ligand of the Toll-Like Receptor-4 Complex. *J. Immunol.* **163 (5)**: 2382–2386

Okabe, Yasutaka, and Ruslan Medzhitov. 2014. Tissue-Specific Signals Control Reversible Program of Localization and Functional Polarization of Macrophages. *Cell* **157 (4)**: 832–844

Orthgiess, Johannes, Martin Gericke, Kerstin Immig, Angela Schulz, Johannes Hirrlinger, Ingo Bechmann, and Jens Eilers. 2016. Neurons Exhibit *Lyz2* Promoter Activity in Vivo: Implications for Using LysM-Cre Mice in Myeloid Cell Research. *European Journal of Immunology* **46 (6)**: 1529–1532

Palis, J, S Robertson, M Kennedy, C Wall, and G Keller. 1999. Development of Erythroid and Myeloid Progenitors in the Yolk Sac and Embryo Proper of the Mouse. *Development* **126**: 5073–5084

Palis, James, Rebecca J Chan, Anne D. Koniski, Reena S. Patel, Mark G Starr, and Mervin C. Yoder. 2001. Spatial and Temporal Emergence of High Proliferative Potential Hematopoietic Precursors during Murine Embryogenesis. *PNAS* **98 (8)**: 4528-4533

Paolicelli, Rosa C, Giulia Bolasco, Francesca Pagani, Laura Maggi, Maria Scianni, Patrizia Panzanelli, Maurizio Giustetto, et al. 2011. Synaptic Pruning by Microglia Is Necessary for Normal Brain Development. *Science* **333**: 1456–1458

Phythian-Adams, Alexander T, Peter C Cook, Rachel J Lundie, Lucy H Jones, Katherine A Smith, Tom A Barr, Kristin Hochweller, et al. 2010. CD11c Depletion Severely Disrupts Th2 Induction and Development in Vivo. *The Journal of Experimental Medicine* **207 (10)**: 2089–2096

Porter, Alan G, Reiner U Ja, and È Nicke. 1998. Emerging Roles of Caspase-3 in Apoptosis. *Cell Death and Differentiation* **6**: 99–104

Price, L K, H U Choi, L Rosenberg, and E R Stanley. 1992. The Predominant Form of Secreted Colony Stimulating Factor-1 Is a Proteoglycan. *The Journal of Biological Chemistry* **267 (4)**: 2190–2199

Ramachandran, Prakash, Antonella Pellicoro, Madeleine A Vernon, Luke Boulter, Rebecca L Aucott, Aysha Ali, Stephen N Hartland, et al. 2012. Differential Ly-6C Expression Identifies the Recruited Macrophage Phenotype, Which Orchestrates the Regression of Murine Liver Fibrosis. *PNAS* **109 (46)**: E3186-3195

Rantakari, Pia, Norma Jäppinen, Emmi Lokka, Elias Mokkala, Heidi Gerke, Emilia Peuhu, Johanna Ivaska, Kati Elima, Kaisa Auvinen, and Marko Salmi. 2016. Fetal Liver Endothelium Regulates the Seeding of Tissue-Resident Macrophages. *Nature* **538 (7625)**: 392–396

Rantakari, Pia, Daniel A. Patten, Joona Valtonen, Marika Karikoski, Heidi Gerke, Harriet Dawes, Juha Laurila, et al. 2016. Stabilin-1 Expression Defines a Subset of Macrophages That Mediate Tissue Homeostasis and Prevent Fibrosis in Chronic Liver Injury. *Proceedings of the National Academy of Sciences* **113 (33)**: 9298–9303

Reinhardt, R Lee, Hong-Erh Liang, and Richard M Locksley. 2009. Cytokine-Secreting Follicular T Cells Shape the Antibody Repertoire. *Nature Immunology* **10 (4)**: 385–393

Roopenian, Derry C., and Shreeram Akilesh. 2007. FcRn: The Neonatal Fc Receptor Comes of Age. *Nature Reviews Immunology* **7 (9)**: 715–725

Ryan, Gregory R., Xu Ming Dai, Melissa G. Dominguez, Wei Tong, Fenchi Chuan, Orin Chisholm, Robert G. Russell, Jeffrey W. Pollard, and E. Richard Stanley. 2001. Rescue of the Colony-Stimulating Factor 1 (CSF-1)-Nullizygous Mouse (Csf1op/Csf1op) Phenotype with a CSF-1 Transgene and Identification of Sites of Local CSF-1 Synthesis. *Blood* **98 (1)**: 74–84

Sachet, Monika, Ying Yu Liang, and Rudolf Oehler. 2017. The Immune Response to Secondary Necrotic Cells. *Apoptosis : An International Journal on Programmed Cell Death* **22 (10)**: 1189–1204

Saeed, Sadia, Jessica Qunitin, H D H Kerstens, N A Rao, A Aghajanirefah, F Matarese, S Cheng, et al. 2014. Epigenetic Programming of Monocyte to Macrophage Differentiation and Trained Innate Immunity. *Science* **345 (6204)**: 1251086

Samokhvalov, Igor M, Natalia I Samokhvalova, and Shin-Ichi Nishikawa. 2007. Cell Tracing Shows the Contribution of the Yolk Sac to Adult Haematopoiesis. *Nature* **446 (26)**: 1056–1061

Sasmono, R. T., A. Ehrnsperger, S. L. Cronau, T. Ravasi, R. Kandane, M. J. Hickey, A. D. Cook, S. R. Himes, J. A. Hamilton, and D. A. Hume. 2007. Mouse Neutrophilic Granulocytes Express MRNA Encoding the Macrophage Colony-Stimulating Factor Receptor (CSF-1R) as Well as Many Other Macrophage-Specific Transcripts and Can Transdifferentiate into Macrophages in Vitro in Response to CSF-1. *Journal of Leukocyte Biology* **82 (1)**: 111–123

Sasmono, R. T., D. Oceandy, Jeffrey W. Pollard, Wei Tong, P Pavli, Brandon J. Wainwright, Michael C Ostrowski, S. R. Himes, and D. A. Hume. 2003. A Macrophage Colony-Stimulating Factor Receptor-Green Fluorescent Protein Transgene Is Expressed throughout the Mononuclear Phagocyte System of the Mouse. *Blood* **101 (3)**: 1155–1163

Schulz, Christian, Elisa Gomez Perdiguero, Laurent Chorro, Heather Szabo-Rogers, Nicolas Cagnard,

Katrin Kierdorf, Marco Prinz, et al. 2012. A Lineage of Myeloid Cells Independent of Myb and Hematopoietic Stem Cells. *Science* **336 (6077)**: 86–90

Schuppan, Detlef, and Nezam H Afdhal. 2008. Liver Cirrhosis. *Lancet* **371 (9615)**: 838–851

Scott, Charlotte L., Fang Zheng, Patrick De Baetselier, Liesbet Martens, Yvan Saeys, Sofie De Prijck, Saskia Lippens, et al. 2016. Bone Marrow-Derived Monocytes Give Rise to Self-Renewing and Fully Differentiated Kupffer Cells." *Nature Communications* **7**: 10321

Serbina, Natalya V, and Eric G Pamer. 2006. Monocyte Emigration from Bone Marrow during Bacterial Infection Requires Signals Mediated by Chemokine Receptor CCR2. *Nature Immunology* **7 (3)**: 311–317

Shi, J, K Aisaki, Y Ikawa, and K Wake. 1998. Evidence of Hepatocyte Apoptosis in Rat Liver after the Administration of Carbon Tetrachloride. *The American Journal of Pathology* **153 (2)**: 515–525

Sierro, Frederic, Maximilien Evrard, Simone Rizzetto, Michelle Melino, Andrew J Mitchell, Manuela Florido, Lynette Beattie, et al. 2017. A Liver Capsular Network of Monocyte-Derived Macrophages Restricts Hepatic Dissemination of Intraperitoneal Bacteria by Neutrophil Recruitment. *Immunity* **47 (2)**: 374-388

Sieweke, Michael H, and Judith E Allen. 2013. Beyond Stem Cells: Self-Renewal of Differentiated Macrophages. *Science* **342 (6161)**: 1242974

Siller-Lopez, F, A Sandoval, S Salgado, A Salazar, M Bueno, J Garcia, J Vera, et al. 2004. Treatment with Human Metalloproteinase-8 Gene Delivery Ameliorates Experimental Rat Liver Cirrhosis. *Gastroenterology* **126**: 1122–1133.

Silver, L, and J Palis. 1997. Initiation of Murine Embryonic Erythropoiesis: A Spatial Analysis. *Blood* **89 (4)**: 1154–1164

Sitia, Giovanni, Matteo Iannacone, Roberto Aiolfi, Masanori Isogawa, Nico van Rooijen, Cristina Scozzesi, Marco E. Bianchi, Ulrich H. von Andrian, Francis V. Chisari, and Luca G. Guidotti. 2011. Kupffer Cells Hasten Resolution of Liver Immunopathology in Mouse Models of Viral Hepatitis. *PLoS Pathogens* **7 (6)**: e1002061

Sitia, Giovanni, Matteo Iannacone, Susanne Müller, Marco E. Bianchi, and Luca G. Guidotti. 2007. Treatment with HMGB1 Inhibitors Diminishes CTL-Induced Liver Disease in HBV Transgenic Mice. *Journal of Leukocyte Biology* **81 (1**): 100–107

Sockolosky, Jonathan T, Matthew R Tiffany, and Francis C Szoka. 2012. Engineering Neonatal Fc Receptor-Mediated Recycling and Transcytosis in Recombinant Proteins by Short Terminal Peptide Extensions. *PNAS* **109 (40)**: 16095–16100

Sorensen, Karen K, Jaione Simon-Santamaria, Robert S. McCuskey and Bard Smedsrod. 2015. Liver sinusoidal endothelial cells. *Comprehensive Physiology* **5:** 1751-1774

Stanley, E R, L J Guilbert, R J Tushinski, and S H Bartelmez. 1983. CSF-1 - A Monoculear Phagocyte Lineage-Specific Hemopoietic Growth Factor. *Journal of Cellular Biochemistry* **21**: 151–159.

Stanley, E Richard, and Violeta Chitu. 2014. CSF-1 Receptor Signaling in Myeloid Cells. *Cold Spring Harbor Perspectives in Biology* **6 (6)**: pii: a021857

Stijlemans, Benoit, Amanda Sparkes, Chloe Abels, Jiri Keirsse, Lea Brys, Yvon Elkrim, Patrick Baetselier, Alain Beschin, and Jo Ginderachter. 2015. Murine Liver Myeloid Cell Isolation Protocol. *Bio. Protocol* **5 (10)**: 10.21769/BioProtoc.1471

Stutchfield, Benjamin M., Daniel J. Antoine, Alison C. Mackinnon, Deborah J. Gow, Calum C. Bain, Catherine A. Hawley, Michael J. Hughes, et al. 2015. CSF1 Restores Innate Immunity After Liver Injury in Mice and Serum Levels Indicate Outcomes of Patients With Acute Liver Failure. *Gastroenterology* **149 (7)**: 1896-1909

Swirski, F., I. Hilgendorf, C. Robbins. 2014. From proliferation to proliferation: monocyte lineage comes full circle. *Seminars in Immunopathology* **36 (2):** 137-148

Tagliani, Elisa, Chao Shi, Patrice Nancy, Chin-Siean Tay, Eric G Pamer, and Adrian Erlebacher. 2011. Coordinate Regulation of Tissue Macrophage and Dendritic Cell Population Dynamics by CSF-1. *The Journal of Experimental Medicine* **208 (9)**: 1901–1916

Takahashi, Kazuya, Yumiko Kakuda, Saori Munemoto, Hirohito Yamazaki, Ichiro Nozaki, and Masahito Yamada. 2016. Long-Lived Human Tissue-Resident Macrophages in the Central Nervous System. *Clinical and Experimental Neuroimmunology* **7 (3)**: 286–287

Takahashi, Kiyoshi, Fumie Yamamura, and Makoto Naito. 1989. Differentiation, Maturation, and Proliferation of Macrophages in the Mouse Yolk Sac: A Light-Microscopic, Enzyme-Cytochemical, Immunohistochemical, and Ultrastructural Study. *Journal of Leukocyte Biotogy* **45**: 87–96

Takata, Kazuyuki, Tatsuya Kozaki, Christopher Zhe Wei Lee, Morgane Sonia Thion, Masayuki Otsuka, Shawn Lim, Kagistia Hana Utami, et al. 2017. Induced-Pluripotent-Stem-Cell-Derived Primitive Macrophages Provide a Platform for Modeling Tissue-Resident Macrophage Differentiation and Function. *Immunity* **47 (1)**: 183-198

Tamoutounour, Samira, Sandrine Henri, Hugues Lelouard, Béatrice de Bovis, Colin de Haar, C Janneke van der Woude, Andrea M Woltman, et al. 2012. CD64 Distinguishes Macrophages from Dendritic Cells in the Gut and Reveals the Th1-Inducing Role of Mesenteric Lymph Node Macrophages during Colitis. *European Journal of Immunology* **42 (12)**: 3150–3166

Terpstra, Valeska, and Theo J. C. van Berkel. 2000. Scavenger Receptors on Liver Kupffer Cells Mediate the in Vivo Uptake of Oxidatively Damaged Red Blood Cells in Mice. *Blood* **95 (6)**: 2157-2163

Thomas, Graham D, Richard N Hanna, Neelakatan T Vasudevan, Anouk A Hamers, Casey E Romanoski, Sara McArdle, Kevin D Ross, et al. 2016. Deleting an Nr4a1 Super-Enhancer Subdomain Ablates Ly6Clow Monocytes While Preserving Macrophage Gene Function. *Immunity* **45 (5)**: 975–987

Thomas, Graham, Robert Tacke, Catherine C Hedrick, and Richard N Hanna. 2015. Nonclassical Patrolling Monocyte Function in the Vasculature. *Arteriosclerosis, Thrombosis, and Vascular Biology* **35 (6)**: 1306–1316

Trapnell, Bruce C, Brenna C Carey, Kanji Uchida, and Takuji Suzuki. 2009. Pulmonary Alveolar Proteinosis, a Primary Immunodeficiency of Impaired GM-CSF Stimulation of Macrophages. *Current Opinion in Immunology* **21 (5)**: 514–521

Triantafyllou, Evangelos, Kevin J. Woollard. Mark J. W. McPhail, Charalambos G. Antoniades and Lucia A. Possamai. 2018. The role of monocytes and macrophages in acute and acute-on-acute chronic liver failure. *Frontiers in Immunology* **9:** 2948

Triantafyllou, Evangelos, Oltin T Pop, Lucia A Possamai, Annika Wilhelm, Evaggelia Liaskou, Arjuna Singanayagam, Christine Bernsmeier, et al. 2018. MerTK Expressing Hepatic Macrophages Promote the Resolution of Inflammation in Acute Liver Failure. *Gut* **67 (2)**: 333–347

Tsung, Allan, John R. Klune, Xianghong Zhang, Geetha Jeyabalan, Zongxian Cao, Ximei Peng, Donna B. Stolz, David A. Geller, Matthew R. Rosengart, and Timothy R. Billiar. 2007. HMGB1 Release Induced by Liver Ischemia Involves Toll-like Receptor 4–Dependent Reactive Oxygen Species Production and Calcium-Mediated Signaling. *The Journal of Experimental Medicine* **204 (12)**:

2913–2923

Tushinski, Robert J., Ivan T. Oliver, Larry J. Guilbert, P. Wendy Tynan, Jonathan R. Warner, and E. Richard Stanley. 1982. Survival of Mononuclear Phagocytes Depends on a Lineage-Specific Growth Factor That the Differentiated Cells Selectively Destroy. *Cell* **28 (1)**: 71–81

Tzur, Amit, Jodene K Moore, Paul Jorgensen, Howard M Shapiro, and Marc W Kirschner. 2011. Optimizing Optical Flow Cytometry for Cell Volume-Based Sorting and Analysis" *PloS One* **6 (1)**: e16053

Varol, C, A Mildner, and S Jung. 2015. Macrophages: Development and Tissue Specialization. *Annu Rev Immunol*. **33**: 643-675

Varol, Chen, Limor Landsman, Darin K. Fogg, Liat Greenshtein, Boaz Gildor, Raanan Margalit, Vyacheslav Kalchenko, Frederic Geissmann, and Steffen Jung. 2007. Monocytes Give Rise to Mucosal, but Not Splenic, Conventional Dendritic Cells. *Journal of Experimental Medicine* **204 (1)**: 171–180

Virolainen, M. 1968. Hematopoietic Origin of Macrophages As Studied By Chromosome Markers in Mice. *Journal of Experimental Medicine* **127 (5)**: 943–952

Weber, Lutz W. D., Meinrad Boll, and Andreas Stampfl. 2003. Hepatotoxicity and Mechanism of Action of Haloalkanes: Carbon Tetrachloride as a Toxicological Model. *Critical Reviews in Toxicology* **33 (2)**: 105–136

Wen, Zongmei, Yan Liu, Feng Li, Feng Ren, Dexi Chen, Xiuhui Li, and Tao Wen. 2013. Circulating Histones Exacerbate Inflammation in Mice With Acute Liver Failure. *Journal of Cellular Biochemistry* **114**: 2384–2391

Wendeln, Ann-Christin, Karoline Degenhardt, Lalit Kaurani, Michael Gertig, Thomas Ulas, Gaurav Jain, Jessica Wagner, et al. 2018. Innate Immune Memory in the Brain Shapes Neurological Disease Hallmarks. *Nature* **556 (7701)**: 332–338

Wick, Georg, Aleksandar Backovic, Evelyn Rabensteiner, Nadine Plank, Christian Schwentner, and Roswitha Sgonc. 2010. The Immunology of Fibrosis: Innate and Adaptive Responses. *Trends in Immunology* **31 (3)**: 110–119

Wiktor-Jedrzejczak, Wieslaw, Aftab Ahmed, Cezary Szczylik, and Regina R Skelly. 1982. Hematological Characterization of Congenital Osteopetrosis in Op/Op Mouse. *Journal of Experimental Medicine* **156**: 1516–1527

Wisse, E. 1974. Kupffer Cell Reactions in Rat Liver under Various Conditions as Observed in the Electron Microscope. *Journal of Ultrastructure Research* **46 (3)**: 499–520

Wisse, E, R B De Zanger, R Jacobs, and R S McCuskey. 1983. Scanning Electron Microscope Observations on the Structure of Portal Veins, Sinusoids and Central Veins in Rat Liver. *Scanning Electron Microscopy*,**3**: 1441–1452

Wu, Li-Ling, Wei-Hao Peng, Hui-Lin Wu, Shi-Chuen Miaw, Shiou-Hwei Yeh, Hung-Chih Yang, Pei-Hsuan Liao, et al. 2019. Lymphocyte Antigen 6 Complex, Locus C $^{+}$ Monocytes and Kupffer Cells Orchestrate Liver Immune Responses Against Hepatitis B Virus in Mice. *Hepatology* **69 (6)**: hep.30510

Wynn, Thomas A, and Luke Barron. 2010. Macrophages: Master Regulators of Inflammation and Fibrosis. *Seminars in Liver Disease* **30 (3)**: 245–257

Yamamoto, Takashi, Chikako Kaizu, Takashi Kawasaki, Go Hasegawa, Hajime Umezu, Riuko Ohashi,

Junko Sakurada, Shuying Jiang, Leonard Shultz, and Makoto Naito. 2008. Macrophage Colony-Stimulating Factor Is Indispensable for Repopulation and Differentiation of Kupffer Cells but Not for Splenic Red Pulp Macrophages in Osteopetrotic (Op/Op) Mice after Macrophage Depletion. *Cell and Tissue Research* **332 (2)**: 245–256

Yamasaki, Ryo, Liping Liu, Jessica Lin, and Richard M Ransohoff. 2012. Role of CCR2 in Immunobiology and Neurobiology. *Clinical and Experimental Neuroimmunology* **3**: 16–29

Yang, Chih-Ya, Jiun-Bo Chen, Ting-Fen Tsai, Yi-Chen Tsai, Ching-Yen Tsai, Pi-Hui Liang, Tsui-Ling Hsu, et al. 2013. CLEC4F Is an Inducible C-Type Lectin in F4/80-Positive Cells and Is Involved in Alpha-Galactosylceramide Presentation in Liver. Edited by Christian Schulz. *PLoS ONE* **8 (6)**: e65070

Yona, Simon, Ki-Wook Kim, Yochai Wolf, Alexander Mildner, Diana Varol, Michal Breker, Dalit Strauss-Ayali, et al. 2013. Fate Mapping Reveals Origins and Dynamics of Monocytes and Tissue Macrophages under Homeostasis. *Immunity* **38 (1)**: 79–91

Yoshida, Hisahiro, Shin-Ichi Hayashi, Takahiro Kunisada, Minetaro Ogawa, Satomi Nishikawa, Hitoshi Okamura, Tetsuo Sudo, Leonard D. Shultz, and Shin-Ichi Nishikawa. 1990. The Murine Mutation Osteopetrosis Is in the Coding Region of the Macrophage Colony Stimulating Factor Gene. *Nature* **345 (6274)**: 442–444.

Yu, Chundong, Fen Wang, Chengliu Jin, Xiaochong Wu, Wai-kin Chan, and Wallace L McKeehan. 2002. Increased Carbon Tetrachloride-Induced Liver Injury and Fibrosis in FGFR4-Deficient Mice. *The American Journal of Pathology* **161 (6)**: 2003–2010

Yu, Wenfeng, Jian Chen, Ying Xiong, Fiona J Pixley, Yee-Guide Yeung, and E Richard Stanley. 2012. Macrophage Proliferation Is Regulated through CSF-1 Receptor Tyrosines 544, 559, and 807. *The Journal of Biological Chemistry* **287 (17)**: 13694–13704.

Zhang, Hui, Wenjuan Pu, Xueying Tian, Xiuzhen Huang, Lingjuan He, Qiaozhen Liu, Yan Li, et al. 2016. Genetic Lineage Tracing Identifies Endocardial Origin of Liver Vasculature. *Nature Genetics* **48 (5)**: 537–543

Zhou, Xu, Ruth A Franklin, Miri Adler, Avi Mayo, Uri Alon, and Ruslan Medzhitov. 2018. Circuit Design Features of a Stable Two-Cell System. *Cell* **172**: 744-747

Ziegler-Heitbrock, Loems, Petronela Ancuta, Suzanne Crowe, Marc Dalod, Veronika Grau, Derek N Hart, Pieter J M Leenen, et al. 2010. Nomenclature of Monocytes and Dendritic Cells in Blood. *Blood* **116 (16)**: e74-80

Zigmond, Ehud, Shany Samia-Grinberg, Metsada Pasmanik-Chor, Eli Brazowski, Oren Shibolet, Zamir Halpern, and Chen Varol. 2014. Infiltrating Monocyte-Derived Macrophages and Resident Kupffer Cells Display Different Ontogeny and Functions in Acute Liver Injury. *The Journal of Immunology* **193 (1)**: 344-353

Appendix

DOI: 10.1002/JLB.1TA0517-169R

JLB JOURNAL OF LEUKOCYTE BIOLOGY

TECHNICAL ADVANCE

An efficient method to isolate Kupffer cells eliminating endothelial cell contamination and selective bias

Ruairi W. Lynch | **Catherine A. Hawley** | **Antonella Pellicoro** | **Calum C. Bain** | **John P. Iredale*** | **Stephen J. Jenkins**

MRC Centre for Inflammation Research, University of Edinburgh, Edinburgh, United Kingdom

Correspondence
Stephen J. Jenkins, MRC Centre for Inflammation Research, University of Edinburgh, Edinburgh, United Kingdom.
Email: stephen.jenkins@ed.ac.uk

*Current address: Senate House, University of Bristol, Bristol, United Kingdom

Abstract

Multicolor flow cytometry and cell sorting are powerful immunologic tools for the study of hepatic mϕ, yet there is no consensus on the optimal method to prepare liver homogenates for these analyses. Using a combination of mϕ and endothelial cell reporter mice, flow cytometry, and confocal imaging, we have shown that conventional flow-cytometric strategies for identification of Kupffer cells (KCs) leads to inclusion of a significant proportion of CD31^{hi} endothelial cells. These cells were present regardless of the method used to prepare cells for flow cytometry and represented endothelium tightly adhered to remnants of KC membrane. Antibodies to endothelial markers, such as CD31, were vital for their exclusion. This result brings into focus recently published microarray datasets that identify high expression of endothelial cell-associated genes by KCs compared with other tissue-resident mϕ. Our studies also revealed significant and specific loss of KCs among leukocytes with commonly used isolation methods that led to enrichment of proliferating and monocyte-derived mϕ. Hence, we present an optimal method to generate high yields of liver myeloid cells without bias for cell type or contamination with endothelial cells.

KEYWORDS

endothelial cell, flow cytometry, Kupffer cell

1 | INTRODUCTION

Liver Kupffer cells (KCs) are one of the largest populations of resident mϕ in the body. KCs are located in the sinusoids of the liver where they scavenge and phagocytose apoptotic cells and damaged erythrocytes,[1] contribute to maintenance of immunologic tolerance by priming Foxp3^{+} T-regulatory cells,[2] and capture gut commensal bacteria that enter the circulation.[3] Under homeostatic conditions, KCs proliferate in situ and persist with relatively little input from conventional hematopoiesis in adult mice.[4–6] However, during liver inflammation, stress, or injury, Ly6C^{hi} monocytes are recruited to the liver and subsequently mature into monocyte-derived hepatic mϕ. Both KCs and monocyte-derived mϕ have been attributed prorestorative or proinflammatory roles in models of acute and chronic liver damage.[7–9] To better understand the function of KCs and monocyte derived mϕ, it is important not only to accurately identify these cells but also to ensure a comprehensive portrait of the in vivo population is generated.

Multiparameter flow cytometry is a powerful tool for evaluating changes in number, frequency, and phenotype of diverse monocyte and mϕ populations and is the basis by which these cells are purified for subsequent functional and genomic analyses. Many protocols have been used to isolate leukocytes from the liver, but there is no consensus on which method is most valid, particularly for KCs. Furthermore, although the definition of KCs by flow cytometry is widely accepted as F4/80^{hi}CD11b^{lo} cells, the reliability of this approach has not been fully investigated. For example, several microarray and RNA-seq datasets identified *Cdh5*, a gene typically associated with endothelial cells,[10] as differentially expressed by KCs compared with other tissue-resident mϕ.[11–13]

Abbreviations: *Cdh5*, Cadherin 5; CLEC4F, C-type lectin domain family 4 member F; KCs, Kupffer cells; LSEC, liver sinusoidal endothelial cells

Received: 3 May 2017 | Revised: 14 February 2018 | Accepted: 27 February 2018

Here, we demonstrate that the population of KCs conventionally defined by their F4/80^{hi}CD11b^{lo} phenotype contains a significant proportion of contaminating CD45^{+}CD31^{hi} endothelial cells, and that this contamination was present regardless of the method used for isolating leukocytes from the liver. Inclusion of endothelial markers rather than additional surface markers of mϕ was critical for excluding these cells from analysis. Furthermore, quantity and quality of isolated KCs varied significantly dependent on the purification method used. We therefore present a comprehensive protocol for faithfully isolating leukocytes from the liver and a modified gating strategy to effectively eliminate contaminating endothelial cells.

2 | METHODS

2.1 | Mice

Wild-type (WT) C57BL/6OlaHsd CD45.2^{+}, congenic C57BL/6 CD45.1^{+}CD45.2^{+}, C57BL/6OlaHsd *Csf1r*-mApple^{+} mice,[14] and *Cdh5*-Cre-ERT2 mice[15] crossed with the mTmG (*Rosa26*Sor$^{tm4(ACTB-tdTomato, EGFP)Lou}$/J) line,[16] were bred and maintained in specific pathogen-free facilities at the University of Edinburgh, UK. Mice were sex and age matched, 6–12 weeks for WT studies and 11–12 weeks for *Cdh5* mice. Bone marrow chimeric mice were generated as previously described.[17] Briefly, C57BL/6 CD45.1^{+}CD45.2^{+} mice were anesthetized and hind legs irradiated with 950 rad while remaining tissues were protected by lead. Mice were reconstituted the next day with 2–5 $\times$ 10^{6} donor bone marrow cells from congenic CD45.2^{+} animals and rested for 8 weeks prior to analysis. All experiments were approved by the University of Edinburgh Animal Welfare and Ethical Review Body under license granted by the UK Home Office.

2.2 | Tamoxifen administration

To induce Cre expression in *Cdh5*-Cre-ERT2:mTmG mice, sterile filtered tamoxifen (Sigma, Irvine, UK; 100 mg/kg) dissolved in corn oil (Sigma; 20 mg/ml) was administered i.p. for 5 consecutive days and mice left for 2 weeks.

2.3 | CSF1-Fc and BrdU administration

An Fc conjugate of porcine CSF1 (CSF1-Fc) was prepared as described.[18] Analysis of KC and endothelial cell proliferation in response to administration of CSF1-Fc was performed on cells from a larger unpublished study aimed at assessing the effect of chronic CSF1 delivery on KCs origin in tissue-protected bone marrow chimeric mice made as described previously.[17] Tissue protected chimeric mice were given 1 μg/g CSF1-Fc delivered in PBS s.c. or PBS control on day 1, 3, 17, 19, 33, and 35 before analysis on day 37. Mice were pulsed with 1 mg BrdU s.c. 2 h before necropsy.

2.4 | Isolation of leukocytes from liver

Following perfusion of PBS through the inferior vena cava, livers were placed into RPMI, finely chopped using a razor blade and digested in 5 ml of enzyme mix (RPMI with 0.625 mg/ml collagenase D, 30 U/ml DNase [Roche, Burgess Hill, UK], 0.85 mg/ml collagenase V [Sigma], and 1 mg/ml dispase [Invitrogen, Paisley, UK] for 25 min at 37°C, in an orbital shaker with additional manual shaking every 5 min. Digests were poured through a 100 μm strainer and then prepared according to the protocols below. Unless otherwise stated, all wash buffers were kept at 4°C. At the end of all protocols, cell pellets were resuspended, passed through a 40 μm strainer, and live cells counted using a Casey TT counter (Roche).

2.5 | 300 *g* centrifugation

Cells were washed in 50 ml, then 30 ml RPMI, and centrifuged at 300 *g* for 5 min, maximum break and accelerator. RBC lysis buffer (Sigma; 2 ml) was added for 2 min, followed by 2 ml FACS buffer (PBS supplemented with 0.5% BSA and 2 mM EDTA). Cells were pelleted (300 *g*, 5 min) and the supernatant discarded.

2.6 | 33% Percoll^{TM} gradient

Cells were washed twice in 50 ml liver wash buffer (PBS/2% FCS) by centrifugation at 443 *g* for 6 min, maximum break and accelerator. The pellet was resuspended in a room-temperature 33% Percoll gradient (25 ml per sample) and spun at 693 *g* for 12 min, with minimum break and accelerator. The cell pellet was washed in 30 ml liver wash buffer at 300 *g* for 5 min. RBC lysis buffer (5 ml) was added for 5 min, then 30 ml liver wash buffer and cells spun at 300 *g* for 5 min.

2.7 | 50 *g* centrifugation

Cells were washed in 15 ml RPMI containing 10% FCS and centrifuged at 50 *g* for 10 min with minimum break. The supernatant was collected and spun at 340 *g* for 10 min, minimum break. The pellet was lysed for 5 min in 2 ml RBC lysis buffer on ice, topped up with RPMI + 10% FCS and spun at 340 *g* for 10 min, minimum break.

2.8 | Collection of discarded fractions

For the 300 *g* spin and Percoll gradient methods, the supernatant or both the hepatocyte layer, and the supernatant between the hepatocyte layer and the leukocyte pellet, respectively, was collected into a fresh tube and centrifuged at 400 *g* for 5 min. The resultant pellets were counted and stained. For the 50 *g* slow-spin method, the pellet generated following the 50 g spin was counted and stained.

2.9 | Isolation of leukocytes from lung

Perfused lungs were collected into RPMI, homogenized using scissors and digested in 2 ml of the enzyme mix detailed above, for 45 min at 37°C. Digests were filtered through a 100 μm strainer, washed with FACS buffer and RBC lysed in 3 ml RBC lysis buffer (Sigma) for 3 min. After washing, cells were passed through a 40 μm strainer and counted.

2.10 | Flow cytometry

2 $\times$ 10^{6} liver cells, or 20 μl of whole blood was incubated with Zombie Aqua fixable viability dye (Biolegend, London, UK) for 10 min at RT and

then with 0.025 μg anti-CD16/32 (2.4G2; Biolegend) in 10% normal mouse serum (Life Technologies, Paisley, UK). Cells were then incubated with antibodies (Supplemental Table 1). Cells were washed, spun at 300 *g* for 5 min and, where necessary, incubated with fluorescently labeled streptavidin. 7-AAD solution (Biolegend) was added to samples 10 min before acquisition when comparing isolation protocols. DAPI was used as a viability marker for FACS. Liver cells were gated as shown, whereas alveolar and interstitial mϕ were identified as $CD45^+CD11c^+SiglecF^+$ and $CD45^+CD11c^+SiglecF^-MHCII^+CD64^+$ cells, respectively.

For BrdU and Ki67 staining, cells were fixed and permeabilized overnight in FoxP3/Transcription Factor Staining Buffer (eBioscience). Cells were washed in PermWash (eBioscience) and stained with anti-Ki67 and anti-BrdU antibodies.

Cells were acquired on a LSRFortessa (BD Biosciences, Wokingham, UK) or FACSAriaII (BD) at the QMRI Flow Cytometry and Cell Sorting Facility, University of Edinburgh, and data analyzed in FlowJo software (Tree Star, Ashland, Oregon). Fluorescence-minus-one controls were used to set gates.

2.11 | Immunofluorescence

The median lobe from perfused liver of *Cdh5*-Cre-ERT2:mTmG mice was fixed in 4% methanol-free PFA (Thermo Scientific, Paisley, UK) at 4°C for 2–3 h then washed in PBS and resuspended in 15% sucrose gradient for 1 h at room temperature followed by 30% sucrose at 4°C overnight. Tissue was then flash frozen in optimal cutting temperature (OCT) embedding matrix (Fisher Scientific, Loughborough, UK) and stored at −80°C. Seven-micrometer sections were cut using a cryostat.

Following blocking with 20% normal goat serum, sections were stained with rat anti-mouse F4/80 (Abcam, Cambridge, UK; CI:A3-1) then AlexaFluor-594 goat anti-Rat IgG secondary (Abcam). Total number of $F4/80^+$ KCs were enumerated per liver slice and GFP and F4/80 coexpression assessed. Immunofluorescent analysis of single cells was performed on FACS-purified cells. Ten microliters of sorted cells was plated on a perfusion open and closed chamber for analysis at 20× magnification and images acquired using a Leica confocal SP5 microscope.

2.12 | Statistical analysis

Data were analyzed in Prism 6 or 7 (GraphPad), with statistics detailed in relevant figure legends. $^*P < 0.05$, $^{**}P < 0.01$, $^{***}P < 0.001$, $^{****}P < 0.0001$.

3 | RESULTS

3.1 | $F4/80^{hi}CD11b^{lo}$ KCs identified by flow cytometry contain a subset of $Cdh5^{hi}CD31^{hi}$ cells

KCs have been traditionally defined by their $F4/80^{hi}CD11b^{lo}$ phenotype, which distinguishes them from $F4/80^{lo}CD11b^+$ bone-marrow-derived myeloid cells.[19] Global transcriptomic analyses have demonstrated that, like all tissue mϕ, KCs have a unique transcriptional signature,[11–13] with CLEC4F and Tim4 emerging as markers that aid their discrimination from other hepatic monocytes and mϕ.[12,20] However, these same analyses also identified *Cdh5* (which encodes cadherin-5), a gene strongly associated with endothelial cells,[10] as part of the KC-specific signature.[11–13] Interrogation of the publically available ImmGen resource (www.immgen.org) revealed a similarly high enrichment of *Cdh5* transcripts in KCs compared with other tissue mϕ (data not shown). To establish whether KCs expressed *Cdh5*, we used a transgenic mouse strain that expresses tamoxifen-inducible Cre recombinase under the control of the *Cdh5* promoter (*Cdh5*-Cre-ERT2)[15] crossed to mTmG reporter mice.[16] While all cells in *Cdh5*-Cre-ERT2:mTmG mice express tdTomato, tamoxifen administration results in Cre recombinase activity, excision of the tdTomato cassette, and an irreversible switch to EGFP expression in *Cdh5* expressing cells and their progeny. Flow cytometric analysis of whole liver isolates gated on live, $CD45^+$ $lineage^-$ leukocytes (Fig. 1A) revealed a clear bimodal expression of GFP in $F4/80^{hi}CD11b^{lo}$ KCs, suggesting higher expression of *Cdh5* by a fraction of these cells (Fig. 1B). Bimodal expression of the endothelial marker CD31 was also evident (Fig. 1B), and simultaneous analysis of GFP and CD31 revealed a bright double positive population (Fig. 1C) that accounted for ∼10% of the $F4/80^{hi}CD11b^{lo}$ population (Fig. 1D). In comparison, less than 0.52% of lung interstitial mϕ and 0.53% of alveolar mϕ were $CD31^{hi}GFP^{hi}$ suggesting this phenomenon was not common to all mϕ populations (Fig. 1D). Back-gating of the $CD31^{hi}GFP^{hi}$ and $CD31^{lo}GFP^{lo}$ populations revealed they could not be discriminated based on size, granularity, and expression of other leukocyte markers such as CD45, Ly6C, and MHCII (data not shown). However, whereas tdTomato expression was significantly diminished in the $CD31^{hi}GFP^{hi}$ fraction of KCs (Fig. 1E), the $CD31^{lo}$ GFP^{lo} cells retained identical levels to untreated control mice, indicating that Cre-mediated excision of the tdTomato cassette had not occurred (Fig. 1F). A similar minor increase in GFP fluorescence without loss of tdTomato expression was also observed in B cells, T cells, neutrophils, and monocytes following tamoxifen treatment (data not shown). Hence, although $F4/80^{hi}CD11b^{lo}$-defined KCs contain a subset of $CD31^{hi}$ Cre-expressing cells, it seems likely that the low GFP fluorescence of $CD31^{lo}$ KC from tamoxifen-treated mice does not represent meaningful expression of *Cdh5*-driven Cre.

3.2 | Endothelial cells contaminate the traditional $F4/80^{hi}$ $CD11b^{lo}$ KC gate

We further investigated the identity of the $CD31^{hi}GFP^+$ fraction of $F4/80^{hi}CD11b^{lo}$ cells. Analysis of all $CD31^{hi}$ cells within the liver preparations revealed binding of CD45 and F4/80 antibodies to be specific when compared with their respective isotype controls (Fig. 2A). Unlike $CD31^{lo}$ KCs, the $CD31^{hi}$ $F4/80^{hi}CD11b^{lo}$ cells also expressed high levels of ICAM-2 and Lyve-1 (Fig. 2B), consistent with a lymphatic or liver sinusoidal endothelial phenotype. However, tissue sections from *Cdh5*-Cre-ERT2:mTmG mice suggested little true colocalization of F4/80 with GFP (Figs. 2C and 2D). Indeed, FACS sorting followed by confocal microscopy revealed some $CD45^+F4/80^{hi}CD31^{hi}$ cells to be doublets of $F4/80^{hi}$ KC and $CD31^{hi}$ endothelium (Fig. 2E),

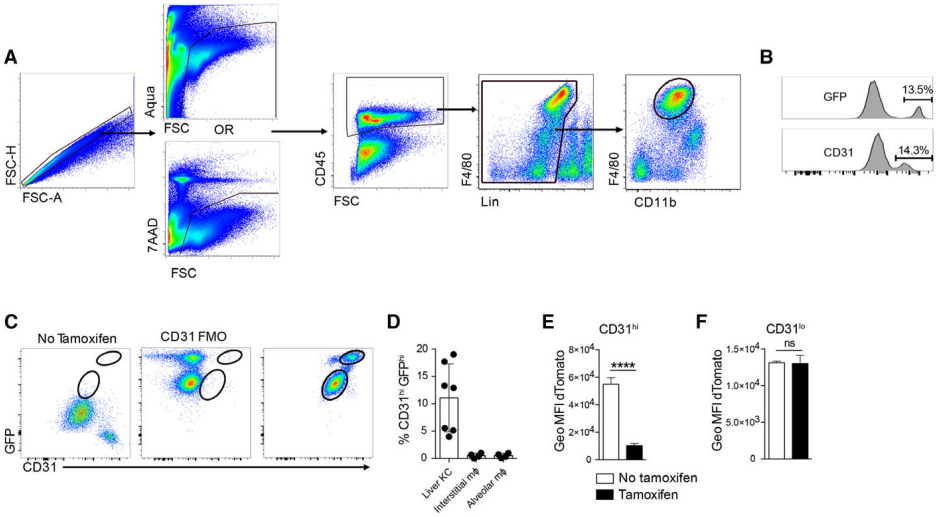

FIGURE 1 **(A) Identification of F4/80^{hi}CD11b^{lo} KCs in murine liver**. Lineage = CD3, CD19, Ly6G, and Siglec F. (B) Representative GFP and CD31 expression by F4/80^{hi}CD11b^{lo} liver cells from *Cdh5*-Cre-ERT2;mTmG mice. Proportion of GFP^{+} and CD31^{hi} cells shown (mean, $n = 7$, 3 experiments). (C) Representative GFP and CD31 expression by F4/80^{hi}CD11b^{lo} liver cells from *Cdh5*-Cre-ERT2;mTmG mice ± tamoxifen. (D) The frequency of CD31^{hi}GFP^{+} cells amongst KCs, lung interstitial and alveolar mϕ. Liver ($n = 7$, 3 experiments) and lung ($n = 4$, 2 experiments). (E and F) Geometric mean fluorescence intensity (GeoMFI) of dTomato expression by CD31^{lo}GFP^{-} KCs (E) and CD31^{hi}GFP^{+} cells (F) ($n = 3$/group, representative of 3 experiments)

whereas the majority of CD31^{hi} cells exhibited punctate colocalized surface staining of CD45 and F4/80 indicative of endothelial cells to which surface membrane from KC was tightly adhered (Fig. 2E). Consistent with this, staining for other KC-specific surface markers, such as Tim4 or CLEC4f,[12] could not differentiate the CD31^{hi} and CD31^{lo} populations despite a very marginal difference in expression intensity (Fig. 2F). In contrast, expression of a *Csf1r*-driven mApple transgene, a cytoplasmic marker of myeloid cells,[14] distinguished mApple^{hi}CD31^{lo} KCs from mApple^{-}CD31^{hi} contaminants (Fig. 2G). Furthermore, CD31^{hi}F4/80^{hi}CD11b^{lo} cells did not proliferate in response to the mϕ mitogen CSF1 (Fig. 2H).[18,21] Thus, it would seem most likely that CD45^{+}F4/80^{hi}CD31^{hi} cells identified by flow cytometry represent endothelial cells with remnants of KC membranes that are largely devoid of the intracellular components of these cells. Hence, although transgenic or intranuclear markers of KCs can aid their discrimination, surface staining for CD31 would seem the most technically simple method for excluding these cells during flow cytometry or FACS.

Of note, unbiased analysis of all CD31^{hi} cells expressing the hematopoietic marker CD45 revealed them to comprise both F4/80^{hi}CD11b^{lo} cells as described above but also other hematopoietic cells (Fig. 2I). Rather than bona fide CD45^{+} endothelial cells, FACS and imaging of CD45^{+}F4/80^{-}CD31^{hi} cells revealed a population of endothelial cells that appeared to envelop small CD45^{+} cells (Fig. 2J). Although these could be simple doublets, they may also represent transmigrating hematopoietic cells described in human liver sinusoidal endothelial cells (LSECs) in vitro.[22] Either way, we find no evidence that CD45^{+}CD31^{hi} cells represent single cells with both hematopoietic and endothelial characteristics akin to those described in rat liver.[23]

3.3 | Endothelial cell contamination is present irrespective of liver digestion protocol

Multiple methods for generating single cell preparations of murine liver leukocytes have been published and while most protocols involve enzymatic digestion, the separation of leukocytes from hepatocyte debris is more inconsistent. Hence, to exclude the possibility that the observed endothelial cell contamination was an artifact specific to our protocol for isolation of leukocytes from the liver, we compared the frequency of CD31^{hi} cells in the KCs population retrieved using 3 methods representative of commonly published protocols. In brief, all methods used the same enzymatic digestion step but employed either two 300 *g* centrifugation steps (as used for Figs. 1 and 2),[17] an initial 50 *g* prespin to first pellet and discard hepatocytes,[24,25] or a 33% Percoll gradient to remove the majority of hepatic debris.[26,27] The relative frequency of all CD31^{hi} endothelial cells recovered as a proportion of all live cells was equivalent between the 300 *g* and the Percoll gradient methods, though reduced with the 50 *g* prespin method, suggesting a proportion of endothelial cells are removed by this step (Fig 3A). However, there was a clear population of CD31^{hi}

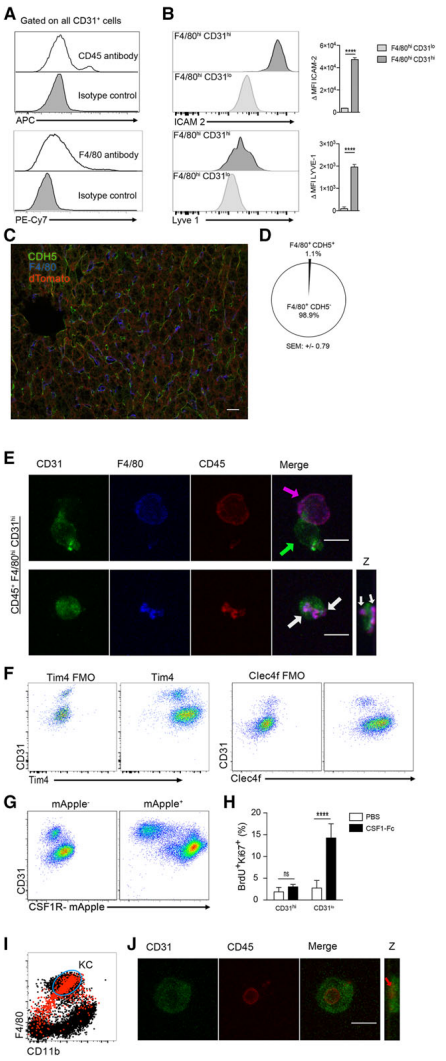

FIGURE 2 **(A) Representative expression of CD45 and F4/80 by total CD31^{hi} liver cells (n = 6, 2 experiments).** (B) Representative histograms (n = 6, 2 experiments) and delta MFI (n = 3/group, representative of 3 experiments) of ICAM-2 and LYVE-1 expression by F4/80^{hi}CD31^{hi} cells and F4/80^{hi}CD31^{lo} KCs. Significance determined by t-test. (C) Confocal image of liver from *Cdh5*-Cre-ERT2;mTmG mice (dTomato = nonrecombined cells; GFP = recombined cells) stained with F4/80 (blue). Scale bar, 20 μm. (D) Proportion of F4/80^{+}*Cdh5*$^{+}$ cells from (C) (10 FoV at 40× magnification of 4 livers). (E) Representative maximal projections of confocal z-stacks of FACS-purified

(continued on the next column)

cells within the F4/80^{hi}CD11b^{lo} KC gate using all 3 protocols (Figs. 3B and 3C), and most pronounced with the 50 g method. Notably, KC-specific *Cdh5* expression was observed in microarray datasets generated with[11,13] or without[12] Percoll gradient purification and low-speed centrifugation. Hence, although it remains possible that KC express *Cdh5* at higher levels than other resident tissue mϕ, it is highly likely that contaminating endothelial cells contributed significantly to the high expression of this gene by KCs. The exclusion of CD31^{hi} cells (Fig. 3D) is therefore a critical step for the faithful identification of KCs in mouse liver irrespective of isolation protocol.

3.4 | Isolation method can lead to selective loss of KCs

After removal of CD31^{hi} endothelial cells, we observed clear differences in the relative abundance of KCs amongst live CD45^{+} cells between isolation methods, with much lower frequencies using both the Percoll and 50 g prespin methods, whereas the frequency of F4/80^{lo}CD11b^{hi} cells was more consistent (Fig. 4A). To determine whether the difference in relative abundance in KCs between methods was due to selective loss of these cells with the Percoll gradient and 50 g prespin methods or enrichment with the 300 g method, we analyzed the hepatocyte pellet from the 50 g prespin, the supernatant from the first 300 g spin, and the hepatocyte layer from the Percoll gradient alongside the normal isolates. KCs were clearly identifiable in the discards from all protocols but at an elevated frequency in the Percoll and 50 g spin methods (Fig. 4B). Comparison of the frequency of KCs of total CD45^{+}CD31^{-} cells within the isolate compared directly with the frequency of KCs in the discard for each sample showed that KCs were significantly enriched in the discard of both the Percoll and 50 g spin methods, but not in the 300 g spin method (Figs. 4C–4E). Thus, KCs were selectively lost using both the Percoll and the 50 g spin methods, whereas the ratio of all leukocytes including KCs was not altered in the discard versus the isolate with the 300 g spin method. The Percoll method also yielded far fewer CD45^{+} cells compared with the 300 g method (Fig. 4F), that together with the lower abundance of KCs, corresponded to over a 7-fold reduction in yield of KCs using this method (Fig. 4G). It was not possible to obtain accurate cell counts from the 50 g method due to large amount of debris seemingly retained with this method, nor were many KCs present in the pellet extracted from the discarded Percoll (Fig. 4G), suggesting most remained within the

F4/80^{hi}CD31^{hi}. CD31 (green), F4/80 (blue), CD45 (red), and merge (purple). White arrows indicate areas of punctate surface F4/80 and CD45 staining by CD31^{+} cells (n = 5 from 2 separate experiments). Scale bar, 10 μm. (F) Representative Tim4, Clec4f, and CD31 expression by F4/80^{hi}CD11b^{lo} cells. (G) Representative mApple and CD31 expression by F4/80^{hi}CD11b^{lo} cells from *Csf1r*-mApple transgenic mice or their negative littermate controls (n = 9, 3 experiments). (H) Proportion of BrdU^{+}Ki67^{+} cells amongst CD31^{hi} and CD31^{lo} F4/80^{hi}CD11b^{lo} cells after administration of CSF1-Fc or PBS (n = 4, 1 experiment). Significance determined by 1-way ANOVA. (I) Overlay of all CD45^{+}CD31^{hi} cells (red) onto CD45^{+}CD31^{lo} cells. (J) Representative maximal projections of confocal z-stacks of FACS sorted CD45^{+}F4/80^{-}CD31^{hi} cells, demonstrating a CD45^{+} cell (red) enveloped in an endothelial cell (green)

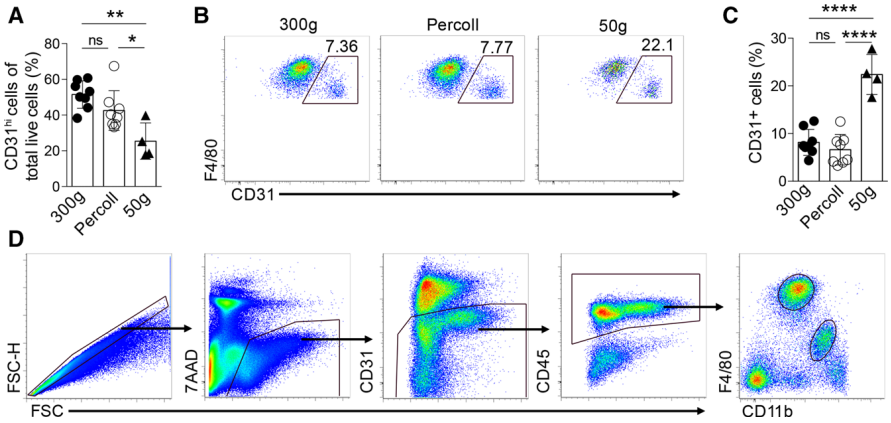

FIGURE 3 **(A) The frequency of CD31^{hi} cells of all live, single cells.** (B and C) Representative flow plots (B) and replicate data (C) of the proportion of CD31^{hi} cells amongst F4/80^{hi}CD11b^{lo} cells obtained with different protocols (300 g, Percoll, 50 g) ($n = 4–8$/group, 2 experiments). (D) Improved gating strategy incorporating CD31 to identify endothelial contaminants from the F4/80^{hi}CD11b^{lo} KCs population. Significance determined by 1-way ANOVA

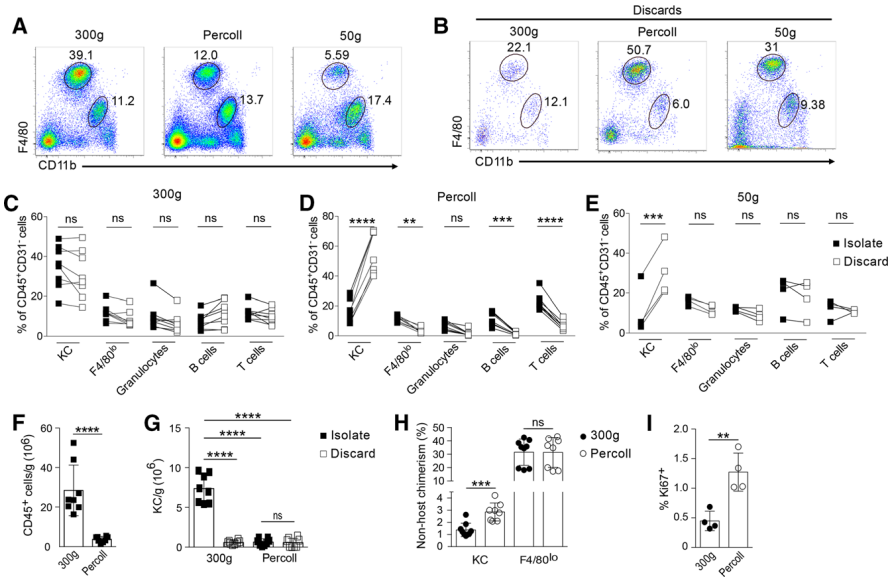

FIGURE 4 **(A and B) Representative flow plots of all isolated (A) and discarded (B) live CD45^{+}CD31^{lo} cells showing proportions of F4/80^{hi}CD11b^{lo} and F4/80^{lo}CD11b^{hi} populations from livers prepared for flow cytometry by 1 of 3 different protocols.** (C–E) The relative frequency of F4/80^{hi}CD11b^{lo} KCs, F4/80^{lo} cells granulocytes, B cells and T cells as a proportion of all CD45^{+}CD31^{lo} leukocytes in the cell isolate linked to the frequency in the discard for the various protocols ($n = 4–8$/group, 2 experiments). Significance determined by multiple *t*-test (Holm-Sidak correction). (F and G) Number of CD45^{+} cells or CD45^{+}F4/80^{hi}CD31^{lo} KCs isolated by either 300 g or Percoll method ($n = 8$/group, 2 experiments). Significance determined by t-test and 1-way ANOVA respectively. (H) Nonhost chimerism amongst KCs and F4/80^{lo} cells from liver of WT > WT tissue-protected BM chimeric mice isolated by 300 g or Percoll protocol ($n = 8$/group, 2 experiments). (I) Proportion of Ki67^{+} KCs isolated from liver by 300 g or Percoll protocol ($n = 4$/group, representative of 2 experiments). Significance determined by *t*-test

Percoll. Importantly, the loss of a large fraction of KCs using the Percoll method also led to different interpretation of important aspects of KCs biology. Specifically, KCs turnover in CD45.1/CD45.2 congenic BM chimeras was exaggerated in Percoll preparations compared with the 300 *g* method, as was the frequency of KCs positive for the cell cycle marker, Ki67 (Figs. 4H–4I). Hence, the choice of isolation method also significantly affected readouts of KCs origin and function. Two 300 *g* centrifugation steps would appear to give the most accurate, unbiased assessment of the frequency of KCs within liver leukocytes, the greatest yield of leukocytes, and hence the most representative portrayal of the characteristics of KCs in vivo.

For simplicity, only 1 slow prespin (50 *g*) and 1 density gradient (33% Percoll) method were compared in our study. However, we acknowledge that there is considerable variation reported in number and speed of centrifugations, as well as gradient concentrations used in protocols to isolate liver leukocytes.[11,13,28,29] Nevertheless, our data suggest that careful optimization of these methods will be required for studies where KCs are the major cell of interest.

4 | SUMMARY

It is imperative that populations isolated for flow cytometric, gene comparison, and functional analyses are representative of those in vivo. We have demonstrated that the established $CD45^+F4/80^{hi}CD11b^{lo}$ gating strategy used to identify KCs in liver preparations also contains a population of endothelial cells. These cells could not be excluded using antibodies to KCs surface antigens and because endothelial cells were also found to form aggregates with other $CD45^+$ cell types, we propose the simplest method to exclude them from analysis is by inclusion of antibodies to CD31 or other endothelial markers. We suggest that this strategy be adopted universally (Fig. 3D), particularly as endothelial contamination was apparent using all commonly used methods for the preparation of hepatic leukocytes for flow cytometric analysis. Cell conjugates identified by flow cytometry can reveal functionally important in vivo cell interactions[30] and hence, endothelial cells to which KC membrane is tightly bound may well represent those LSECs intimately interacting with KCs at the point of necropsy. Since KCs remain largely static in the steady state[31] further investigation of this subset of LSECs may identify factors controlling the turnover and function of KCs.[32]

AUTHORSHIP

R.W.L. and C.A.H. designed, performed, and analyzed the experiments and wrote the manuscript. A.P. performed the experiments. C.C.B. performed the experiments and edited the manuscript. J.P.I. obtained funding and reviewed the manuscript. S.J.J. conceived the experiments, wrote the manuscript, and obtained funding. R.W.L. and C.A.H. contributed equally to this work.

ACKNOWLEDGMENTS

This work was supported by a MRC grant (MR/L008076/1), a University of Edinburgh PhD studentship to C.A.H., and a Wellcome Trust Clinical PhD studentship (109889/Z/15/Z) to R.L. We thank Prof. N. Henderson for provision of *Cdh5*-Cre-ERT2:mTmG mice, Prof. R. Adams for permission to use the *Cdh5*-Cre-ERT2 mice, and Prof. D. Hume (Roslin Institute, Edinburgh, UK) for providing CSF1-Fc. We thank Trudi Gillespie for help with confocal microscopy.

DISCLOSURE

The authors declare no conflicts of interest.

REFERENCES

1. Terpstra V, van Berkel TJC. Scavenger receptors on liver Kupffer cells mediate the in vivo uptake of oxidatively damaged red blood cells. *Blood*. 2000;95:2157–2163.
2. Heymann F, Peusquens J, Ludwig-Portugall I, et al. Liver inflammation abrogates immunological tolerance induced by Kupffer cells. *Hepatology*. 2015;62:279–291.
3. Balmer ML, Slack E, de Gottardi A, et al. The liver may act as a firewall mediating mutualism between the host and its gut commensal microbiota. *Science Transl Med*. 2014;6:237ra66.
4. Crofton RW, Diesselhoff-Den Dulk MMC, Furth RV. The origin, kinetics, and characteristics of the Kupffer cells in the normal steady state. *J Exp Med*. 1978;148:1–17.
5. Perdiguero EG, Klapproth K, Schulz C, et al. Tissue-resident macrophages originate from yolk-sac-derived erythro-myeloid progenitors. *Nature*. 2014;518:547–551.
6. Yona S, Kim K-W, Wolf Y, et al. Fate mapping reveals origins and dynamics of monocytes and tissue macrophages under homeostasis. *Immunity*. 2013;38:79–91.
7. Dixon LJ, Barnes M, Tang H, Pritchard MT, Nagy LE. Kupffer Cells in the liver. *Compr Physiol*. 2013;3:785–797.
8. Ju C, Tacke F. Hepatic macrophages in homeostasis and liver diseases: from pathogenesis to novel therapeutic strategies. *Cell Mol Immunol*. 2016;13:316–327.
9. Zigmond E, Samia-Grinberg S, Pasmanik-Chor M, et al. Infiltrating monocyte-derived macrophages and resident kupffer cells display different ontogeny and functions in acute liver injury. *J Immunol*. 2014. https://doi.org/10.4049/jimmunol.1400574.
10. Zhang H, Pu W, Tian X, et al. Genetic lineage tracing identifies endocardial origin of liver vasculature. *Nat Genet*. 2016;48:537–543.
11. Okabe Y, Medzhitov R. Tissue-specific signals control reversible program of localization and functional polarization of macrophages. *Cell*. 2014;157:832–844.
12. Scott CL, Zheng F, De Baetselier P, et al. Bone marrow-derived monocytes give rise to self-renewing and fully differentiated Kupffer cells. *Nat Commun*. 2016;7:10321.
13. Lavin Y, Winter D, Belcher-Gonen R, et al. Tissue-resident macrophage enhancer landscapes are shaped by the local microenvironment. *Cell*. 2014;159:1312–1326.
14. Hawley HA, Rojo R, Raper A et al. Csf1r-mApple transgene expression and ligand binding in vivo reveal dynamics of CSF1R expression within the mononuclear phagocyte system. *J Immunol*. 2018;200:2209–2223.
15. Wang Y, Nakayama M, Pitulescu ME, et al. Ephrin-B2 controls VEGF-induced angiogenesis and lymphangiogenesis. *Nature*. 2010;465:483–486.
16. Muzudmar MD, Tasic B, Miyamichi K, Li L, Luo L. A global double-fluorescent Cre reporter mouse. *Genesis*. 2007;45:593–605.
17. Bain CC, Hawley CA, Garner H, et al. Long-lived self-renewing bone marrow-derived macrophages displace embryo-derived cells

to inhabit adult serous cavities. *Nat Commun*. 2016. https://doi.org/10.1038/ncomms11852.

18. Gow DJ, Sauter KA, Pridans C, et al. Characterisation of a novel Fc conjugate of macrophage colony-stimulating factor. *Mol Therapy*. 2014;22:1580–1592.
19. Schulz C, Perdiguero EG, Chorro L, et al. A lineage of myeloid cells independent of Myb and hematopoietic stem cells. *Science*. 2012;336:86–90.
20. Yang CY, Chen JB, Tsai TF, et al. CLEC4F is an inducible C-type lectin in F4/80-positive cells and is involved in alpha-galactosylceramide presentation in liver. *PLoS One*. 2013;8:e65070.
21. Jenkins SJ, Ruckerl D, Thomas GD, et al. IL-4 directly signals to tissue-resident macrophages to proliferate beyond homeostatic levels controlled by CSF-1. *J Exp Med*. 2013;210:2477–2491.
22. Patten Daniel A, Wilson Garrick K, Bailey Dala, et al. The Human liver sinusoidal endothelial cells promote intracellular crawling of lymphocytes during recruitment- a new step in migration. *Hepatology*. 2017;65:294–309.
23. Wang Li, Wang Xiangdon, Xie Guanhu, et al. Liver sinusoidal endothelial cell progenitor cells promote liver regeneration in rats. *J Clin Invest*. 2012;122:1567–1573.
24. Ramachandran P, Pellicoro A, Vernon MA, et al. Differential Ly-6C expression identifies the recruited macrophage phenotype, which orchestrates the regression of murine liver fibrosis. *Proc Natl Acad Sci USA*. 2012;109:E3186–3195.
25. Blom KG, Qazi MR, Noronha Matos JB, Nelson BD, DePierres JW, Abedi-Valugerdi M. Isolation of murine intrahepatic immune cells employing a modified prodecure for mechanical disruption and function characterization of the B, T and natural killer T cells obtained. *Clin Exp Immunol*. 2009;155:320–329.
26. Ikarashi M, Nakashma H, Kinoshita M, et al. Distinct development and functions of resident and recruited liver Kupffer cells/macrophages. *J Leuk Biol*. 2013;94:1325–1336.
27. Pythian-Adams AT, Cook PC, Lundie RJ, et al. CD11c depletion severely disrupts Th2 induction and development in vivo. *J Exp Med*. 2010;207:2089–2096.
28. Girgis NM, Gundra UM, Ward LN, Cabrera M, Frevert U, Loke P. Ly6C(high) monocytes become alternatively activated macrophages in schistosome granulomas with help from CD4+ cells. *PLoS Pathog*. 2014;10.
29. Yepes E, Varela-M RE, López-Abán J, Rojas-Caraballo J, Muro A, Mollinedo F. Inhibition of granulomatous inflammation and prophylactic treatment of schistosomiasis with a combination of edelfosine and praziquantel. *PLoS Negl Trop Dis*. 2015;9.
30. Reinhardt RL, Liang HE, Locksley RM. Cytokine-secreting follicular T cells shape the antibody repertoire. *Nat Immunol*. 2009;10:385–393.
31. Wang J, Kubes P. A reservoir of mature cavity macrophages that can rapidly invade visceral organs to affect tissue repair. *Cell*. 2016;165:668–678.
32. Guilliams M, Scott CL. Does niche competition determine the origin of tissue-resident macrophages? *Nat Rev Immunol*. 2017;17:451–460.

SUPPORTING INFORMATION

Additional information may be found online in the supporting information tab for this article.

How to cite this article: Lynch RW, Hawley CA, Pellicoro A, Bain CC, Iredale JP, Jenkins SJ. An efficient method to isolate Kupffer cells eliminating endothelial cell contamination and selective bias. *J Leukoc Biol*. 2018;104:579–586. https://doi.org/10.1002/JLB.1TA0517-169R